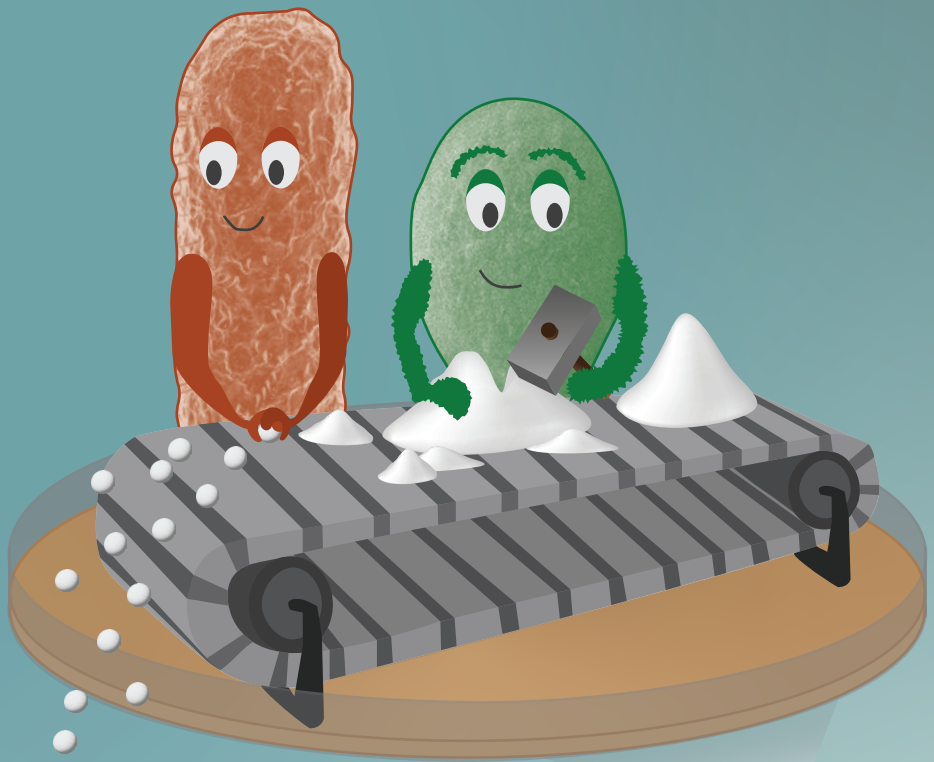# β-lactoglobulin by precision fermentation

Application-driven design and processing

Loes Hoppenreijs

Propositions

1. Beta-sheets are as much tertiary and quaternary structural elements of proteins, as they are secondary structural elements.
(this thesis)

2. Proteins show a butterfly effect, wherein minor sequential changes significantly affect macroscopic behaviour.
(this thesis)

3. Science is like Wonderland: full of distractions, but persistence leads to discovery.

4. Social skills are undervalued for scientific progress.

5. Academic research paves the way to sustainability, but consumers ultimately dictate the course.

6. The spread of misinformation by politicians or content creators is as problematic as that by scientists.

Propositions belonging to the thesis, entitled

β-lactoglobulin by precision fermentation
Application-driven design and processing

Loes J. G. Hoppenreijs

Wageningen, 28th of May 2024

β-lactoglobulin by precision fermentation

Application-driven design and processing

Loes J. G. Hoppenreijs

β-lactoglobulin by precision fermentation

Application-driven design and processing

Loes J. G. Hoppenreijs

Thesis

Submitted in fulfilment of the requirements for the degree of doctor
at Wageningen University
by the authority of the Rector Magnificus,
Prof. Dr C. Kroeze,
in the presence of the
Thesis Committee appointed by the Academic Board
to be defended in public
on Tuesday 28 May 2024
at 4 p.m. in the Omnia Auditorium.

Table of contents

1

Introduction and thesis outline

1.1. The animal in the room: unsustainable food production

Our natural environment cannot keep up with the amount of resources that are needed to feed the (still growing) global population, while also providing for overconsumption and food waste. Our food system attributes to about 21–37% of the total greenhouse gas emission, which is expected to further rise (Intergovernmental Panel on Climate Change, 2019). It is clear that we need to adapt our food system for a more sustainable future. Producers need to transition towards more sustainable practices and products, but also consumers need to shift towards more sustainable and healthy choices (United Nations Environment Programme, 2016).

Scarce arable land is often used for grazing or for growing crops for livestock: up to 40% of the arable land was used for livestock in 2017 (Mottet et al., 2017). Re-allocation of this land from feed to direct food production is generally regarded more sustainable, as the indirect food production by livestock leads to metabolic losses (Karlsson & Röös, 2019). The global decrease in production of animal-based products can only be achieved when we start consuming less of them. Van Zanten et al. (2023) reported that we could achieve a reduction in greenhouse gas emission by 25–40% and arable land use by 23% in the European Union, when lowering the consumption (and production) of animal-based produce by 25–50%. The remaining livestock can transform residual waste streams and/or marginal lands that cannot be used to grow crops into valuable food products, thereby contributing to a circular food system. In that sense, animals should be recyclers and not the main source of our food, requiring a shift towards more plant-based diets. This is not that simple: animal-based protein make up at least a quarter of the global protein intake, while it even accounts for approximately 50% of the intake in high-income countries (FAO, 2017).

1.2. Animal proteins in food formulations

Simply eliminating the consumption of animal-based products is challenging for many consumers that are used to a Western diet. To support the transition from meat to a more plant-based diet, a broad range of alternative plant-based substitutes are currently available, such as milk and egg substitutes (for direct consumption or as food ingredients in food formulations), as well as meat replacers. Particularly the substitution of milk and egg protein ingredients in food formulations is challenging, due to their high nutritional quality and techno-functional properties.

1.2.1. Nutritional quality

Being the only food that is biologically designed for being nourishing, milk is of considerably high nutritional quality. Bovine milk is by far the most consumed type of milk. In particular the protein fraction is regarded valuable, since the market

value of milk depends on its protein content. Milk contains all nine essential amino acids, which cannot be anabolized by the human body and are thereby required to be included in the diet (Guetouache et al., 2009). Besides, dietary milk proteins are rich in biologically active peptides. Those peptides are released upon digestion and can fulfil a large range of bio-functional roles in the human body, or even have beneficial effects on target diseases (Mohanty et al., 2016). Furthermore, dietary milk is an important source of vitamins and minerals, including calcium, iodine, zinc, and vitamins B2 B12, A and D (Scholtz-Ahrens et al., 2020), as well as unsaturated fatty acids (Månsson, 2008).

Dietary milk also contains components that can cause adverse reactions: a large part of the population is lactose-intolerant, while milk proteins (in particular β-lactoglobulin and α-lactalbumin) can cause allergic reactions (Villa et al., 2017). Lastly, bovine milk lipids are rich in saturated fat (~ 70 wt%; Lindmark Månsson, 2008), which is associated with the development of cardiovascular diseases (Perna & Hewlings, 2023).

1.2.2. Techno-functionality

Besides the nutritional value, isolates and concentrates of whey protein are often used as functional ingredients (Jovanovic & Barac, 2005). They are suitable ingredients for a broad range of food applications, such as ice creams, baked goods, sauces, mayonnaises, processed dairy, dressings, soups, sport drinks and many more, due to their excellent functional properties (Onwulata & Huth, 2008). The techno-functional properties of proteins is evident on different scales (Foegeding, 2015) (***Figure 1.1***):

1. The molecular scale (nanometres): individual molecules
2. The mesoscale (micrometres): higher order arrangement of the molecules
3. The macroscale (millimetres): substructures within the food
4. The food matrix (centimetres): scale at which the consumer perceives the product

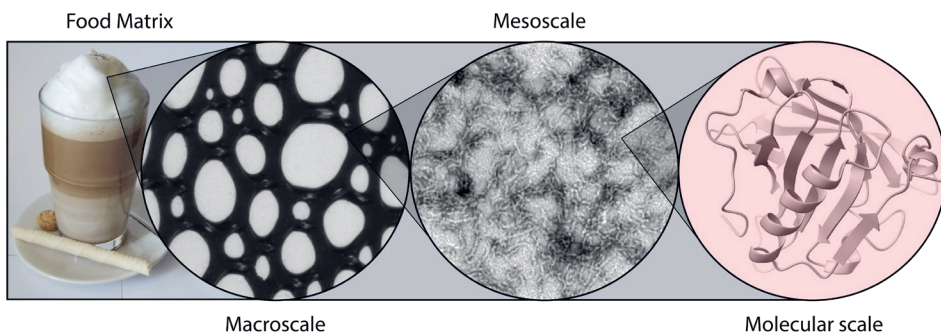***Figure 1.1.*** *Example of the structures on different scales that can exist within a milk foam (food structure), existing of bubbles (macroscale), stabilized by protein aggregates (mesoscale), formed from destabilized protein (molecular scale).*

For example, proteins can unfold (molecular scale) and form aggregates (mesoscale), which in turn are able to stabilize bubbles (macroscale), and finally avoid the collapse of foams (food matrix). The ability to exhibit these functional properties on different scales depends on the nature of the protein. Furthermore, proteins can be modified due to its processing history (e.g. conditions applied during isolation or further downstream processing), the formulation (i.e. interactions with other ingredients) and physical conditions applied to obtain the food structure (Avelar et al., 2021; Foegeding et al., 2002).

The excellent functional properties of whey protein are to a large extent attributed to β-lactoglobulin (BLG), being the most abundant whey protein (~ 55%). For example, enriched fractions of BLG demonstrate enhanced emulsion stability, viscosity and gelling properties (Tomasula et al., 2001). Therefore, the case of BLG was studied in the current work. Farrell et al. (2004) described 11 different isoforms of BLG, of which isoforms A and B are the most abundant in cow's milk. These differ in two amino acids (out of 162 total amino acids; ~ 18.3 kDa), but are structurally similar (Dong et al., 1996). The globular structure of BLG is depicted in *Figure 1.2*. It is stabilized through two disulfide (SS) bonds: one at the surface of the protein (Cys66–Cys160) and the other in its interior (Cys106–Cys119). One cysteine remains as a free thiol (SH; Cys121), which can form non-native disulfide bonds via SH/SS exchange reactions during processing.
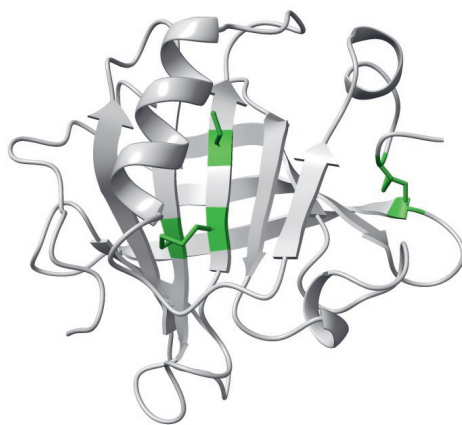
Figure 1.2. Structure of β-lactoglobulin isoform B (PDB; 3npo). Cysteine residues are highlighted in green.

Plant-based proteins are widely studied to replace milk or egg proteins in food formulations. However, until now plant-based protein have not yielded the exact same product properties, as their molecular properties are inherently different (*Figure 1.1*). Day et al. (2022) recently reviewed the major differences between animal-and

plant-based proteins. Generally, plant-based proteins are mostly storage proteins, which are large and compact structures that are more hydrophobic, less soluble and less flexible (Day et al., 2022). Using plant-based proteins to substitute animal-based proteins, such as casein or whey, generally leads to instable products with inferior protein quality and poor digestibility (Day et al., 2022). For example, plant-based proteins can sediment in beverages (Bonke et al., 2020) and poorly stabilize interfaces of foams and emulsions (Sagis & Yang, 2022).

1.3. Precision fermentation

Producing animal proteins by micro-organisms, instead of animals, could combine the best of both worlds; obtaining most optimal protein properties without slaughtering animals. Cellular agriculture allows the production of animal-based food ingredients through cell cultures instead of livestock (Mattick, 2018). These cell cultures could potentially even grow on waste streams, do not require fertile lands and take up less space. Cellular agriculture includes two major technologies: (1) cultured meat technology and (2) precision fermentation (Dupuis et al., 2023). Cultured meat technology enables the production of animal meat *in vitro*, using stem cell biology and tissue engineering principles. Precision fermentation allows the production of only a targeted protein within a cellular host, after which this protein can be harvested for consumption.

1.3.1. General principle

The manufacturing of a recombinant protein starts with its upstream production (Ratledge & Kristiansen, 2006). The expression host (e.g., yeast, bacteria or fungi) is first modified with a so-called expression vector. This expression vector includes the 'instructions' to allow the expression (and secretion) of the target protein, containing the foreign DNA that encodes the target protein. Upon cultivation of the modified host in a bioreactor, the target protein is produced and either secreted from the host or accumulated within the host. Downstream processing (DSP) is then applied to remove remaining impurities (after cell disruption, in case of accumulation within the host), such as the growth media, non-protein fermentation products, or other cellular material. Relatively simple centrifugation and filtration steps are usually applied to clarify the cell broth. Those methods are generally not suited for extensive purification of recombinant proteins and thus chromatographic methods are used instead (Gupta & Shukla, 2017). Multiple chromatographic purifications steps are usually required to obtain pharmaceutical-grade purity (Gupta & Shukla, 2017; Seetharam & Sharma, 1991). The protein is often concentrated and dried after purification.

1.3.2. New application: bottlenecks and opportunities

Precision fermentation is in fact not a new technique to be applied in food application; it has been used to produce enzymes for decades, as these are generally expensive to naturally obtain and isolate (Dupuis et al., 2023; Ratledge & Kristiansen, 2001). Now that we want to use the same technique to produce high amounts of relatively inexpensive food proteins, such as dairy or egg proteins, additional challenges but also opportunities arise. These are discussed in the following.

BLG naturally exists in milk, which contains a mixture of proteins. In contrast, the production of this particular protein is targeted when using precision fermentation. One of the major bottlenecks for the production of affordable recombinant proteins is the production yield. While the production yield can be optimized through several biotechnological approaches, the solutions to this problem are highly dependent on the molecular properties of the protein (Ratledge & Kristiansen, 2001). However, the expression offers almost unlimited freedom to produce the most optimal protein for application. For example, one may select a specific amino acid sequence; choosing the most optimal natural isoform or even substituting amino acids to enhance functionality (further referred to as **Intervention A**). Thus, precision fermentation allows us to control the molecular structure of the target protein, which then gives rise to structures on other scales that consumers perceive (***Figure 1.1***).

> **Knowledge gap 1**
>
> *Functionalization through molecular modification (Intervention A)*
>
> The production of recombinant proteins through precision
> fermentation allows substitution of specific amino acids
> in a given protein to optimize its properties for particular
> applications, but it is currently unknown which substitutions in
> BLG would improve its techno-functional properties.

Besides the upstream production, DSP of recombinant proteins to obtain high-purity proteins is typically expensive. The costs can reach up to 50–80% of the total production costs (Vermasvuori & Raisa Vermasvuori, 2006). In turn, more than 70% of these expenses emerge from chromatographic purification (Azevedo et al., 2009). Biopharmaceuticals often require this elaborate purification, while the purification is cost-effective due to the high value of the target protein. While generally striving for high purity, the typical DSP methods required are costly and challenging to scale for food purposes. Furthermore, extensive purification is usually at the expense of the

production yield, but the functional properties of the protein ingredient is probably not linearly dependent on the purity. Therefore, the DSP steps needs to be balanced with the most optimal functionality that one strives for in the ultimate food product (further referred to as **intervention B**).

Knowledge gap 2

Simplification of purification process (Intervention B)

Traditional purification of recombinant proteins usually includes chromatographic methods, which can be relatively expensive and challenging to scale. Purification generally improves functional properties of recombinant protein ingredients but at the cost of production yield. Thus, simple and scalable purification methods are required for the production of affordable recombinant food proteins. It is currently not clear to what extent purification is required to obtain a functional ingredient.

While the upstream production determines the intrinsic molecular properties of the recombinant protein to a large extent, it might not yet have its most functional form for food application. Post-processing can further alter the molecular properties, aiming to enhance the functional properties for a particular application (further referred to as **intervention C**). We refer to this as 'protein functionalization'. Lower amounts of protein may be required after functionalization to achieve the same final techno-functional characteristics in food formulations. As mentioned earlier, low production yields are a major bottleneck for the production of affordable food proteins. Functionalization of those particular proteins would thus be desired.

Knowledge gap 3

Functionalization (Interventions A, B and C)

Several interventions in the production and processing of recombinant protein are expected to affect the techno-functional properties of recombinant protein. Yet, it is unclear how far the functionality range of recombinant BLG could be extended by such interventions.

1.3.3. Functionalizing (recombinant) BLG through post-processing

Protein modification on a molecular level has been widely studied to functionalize proteins, by using chemical, enzymatic or physical modification (i.e., processing; Mirmoghtadaie et al., 2016). As the hierarchy of scales in **Figure 1.1** demonstrates, such modifications have consequences for the food structure that the consumer perceives. Besides molecular modifications, aggregation of individual proteins to form functional higher order structures (mesoscale; **Figure 1.1**) can also be a functionalization strategy. Protein destabilization can be induced to trigger BLG aggregation through extrinsic features (e.g. high temperature, chaotropic agents, solvent), as well as intrinsic features (i.e., direct protein modifications; Cao & Mezzenga, 2019). In particular, amyloid aggregates (**Figure 1.3**) have gained interest to improve functional properties of proteins. Amyloid aggregates are linear aggregates that are specifically stabilized through a cross-β-sheet conformation.
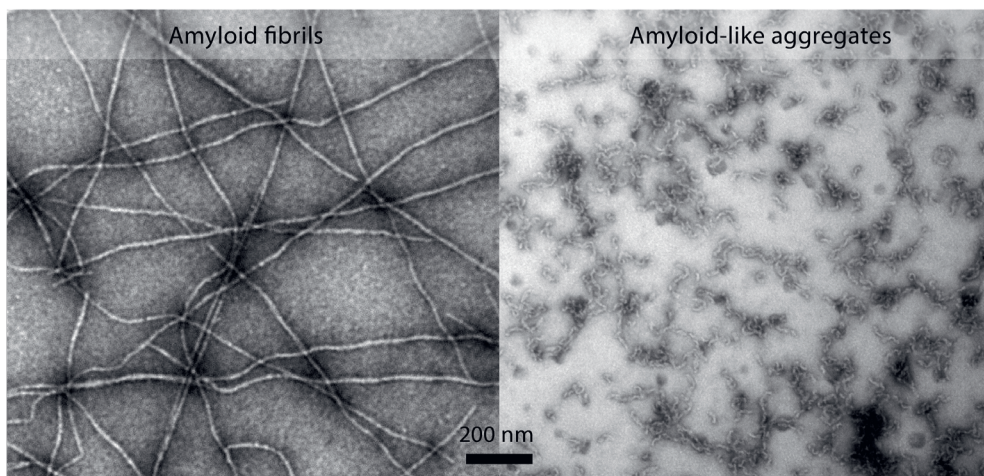
Figure 1.3. *Appearance of amyloid fibrils and amyloid-like aggregates, shown by transmission electron microscopy.*

Classical amyloid fibrils are thin (1–4 nm), long (0.1–10 µm), semi-flexible aggregates that consist of assembled peptides that are highly ordered. The high aspect ratio (length vs. thickness) of these fibrils make them exceptionally suitable to form space-filling networks. For example, Veerman et al., (2003) demonstrated that a gel can be obtained at extremely low concentrations of BLG fibrils (0.07%), as induced by $CaCl_2$. In contrast, at least 20 times more protein was needed to induce heat-set gelation of BLG. Besides being suitable gelling agents, fibrils effectively slow down drainage in foams, and may counteract de-mixing (i.e., creaming or sedimentation) in emulsions or dispersions (Jansens et al., 2019; Kroes-Nijboer et al., 2012). A major drawback of BLG amyloid fibrils is the extreme conditions necessary to induce their formation; the

standard procedure is heating (80–90 °C) of low protein concentration solutions (~ 10–25 mg mL) at pH 2.0 for several hours (5–24 h) (Cao & Mezzenga, 2019). Besides, their application range is limited since they are instable upon processing (e.g., pH adjustment, shearing and drying; Loveday et al., 2012; Heyn et al., 2021).

Alternatively, longer BLG peptides or even intact BLG can assemble through a relatively less dense cross-β conformation, forming amyloid-*like* aggregates (**Figure 1.3**). Some regions are not involved in the core aggregate structure and subsequently strain instead of stabilize it (Housmans et al., 2022). This causes amyloid-like aggregates to be shorter and more flexible than fibrils. Due to their lower aspect ratio, one might expect an inferior ability to form space-spanning networks, as reported for amyloid fibrils (Kroes-Nijboer et al., 2012). However, they are reported to be more stable against processing, for example, pH adjustments, shear or drying (Loveday et al., 2012; Heyn et al., 2021). This processing stability allows a broader application range for amyloid-like aggregates than amyloid fibrils.

The particular aggregate structure and morphology is a result of a combination of intrinsic and extrinsic features. With precision fermentation, the intrinsic features of BLG can be adapted to stimulate its tendency for fibrillization by inducing mutations, while post-processing conditions can induce fibrillization.

Knowledge gap 4
Functionalization through mesoscale modification
(Interventions A and C)

Classical fibrillization of BLG is a functionalization route that requires extensive processing. Intrinsic protein characteristics and extrinsic conditions can stimulate fibrillization. In turn, these intrinsic and extrinsic features can be controlled through upstream protein modification, DSP and post-processing. It is currently unknown which particular amino acid exchanges (in upstream production) and/or processing conditions (applied during DSP and/or post-processing) can stimulate fibrillization of recombinant proteins.

1.4. This thesis

1.4.1. Aim

Precision fermentation has gained attention to produce large amounts of affordable BLG for their application in food formulations. The production process of recombinant food proteins should be re-designed for this new application in food. This thesis aims to develop design strategies to enable efficient production and application of recombinant BLG. These strategies involve interventions during several stages of the production process, including the upstream production, DSP or post-processing (**Figure 1.5**).
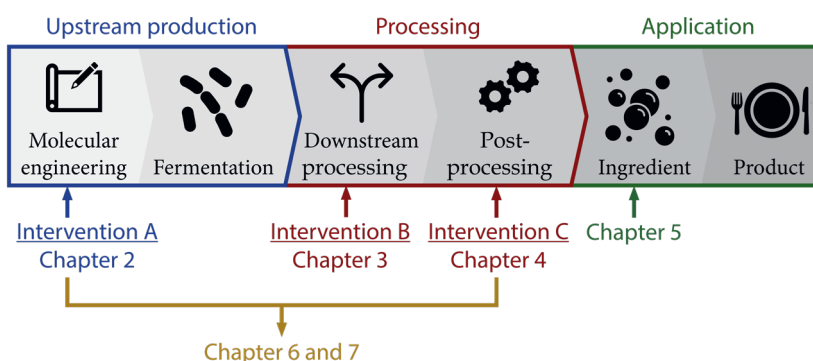
Figure 1.5. *Schematic overview of the production and processing steps towards efficient application of recombinant proteins in food, and the specific steps that will be discussed in the chapters.*

1.4.2. Approach

In upstream production of recombinant BLG, one of the major challenges is that production yields are currently low. Efficient application in food formulations is required to make the best use of the protein that is produced. A hypothesis is that (partial) destabilization of BLG via cysteine mutations could functionalize BLG for particular applications (addressing knowledge gap 1 of **intervention A**). Therefore, step-wise substitution of the cysteines in BLG was performed and the resulting structures were characterized in **Chapter 2**. This extensive characterization provided a solid base for follow-up studies on the resulting functional properties.

During downstream processing (DSP) of recombinant proteins, current purification processes (i.e., based on chromatography) are relatively expensive. Therefore, an alternative purification process was established in **Chapter 3**, being able to concentrate the protein up to ~ 70 wt% through simple precipitation and filtrations steps (addressing knowledge gap 2 of **intervention B**).

Post-processing was considered after DSP to functionalize BLG by aggregating BLG into linear amyloid(-like) aggregates. **Chapter 4** reviews the conditions that are reported to induce such aggregation, demonstrating different post-processing conditions that can be applied (addressing knowledge gap 4 of **intervention C**).

The above-mentioned interventions A, B and C are hypothesized contribute to efficient processing or application of recombinant BLG. In **Chapter 5**, we exemplify how far such interventions can extent the techno-functional range of BLG, in terms of foaming and gelling (addressing knowledge gap 3).

Conventional post-processing into amyloid fibrils necessitates extreme formation conditions, typically including heating at pH 2.0 for 5–24 h. Since disulfide bonds restrain the molecular structure of BLG, they could hinder exposure of amyloidogenic sequences and counteract rearrangements necessary to form fibrils. Thus, **Chapter 6** evaluates whether step-wise substitution of cysteines during upstream production of recombinant BLG is a suitable tool to accelerate fibrillization (upon heating at pH 2.0). To further extend the application range in terms of pH, **Chapter 7** evaluates whether this cysteine elimination can also stimulate linear growth of amyloid-like aggregates (formed upon heating at pH 3.5 and 7.0). Those chapters both address knowledge gap 4.

Finally, several interventions in the production and processing of recombinant BLG are suggested in the individual chapters. **Chapter 8** summarizes the potential of these process design strategies and discusses other food-related challenges that arise from a technical, functional and nutritional point of view.

Precision fermentation as a route to modify β-lactoglobulin structure through substitution of specific cysteines
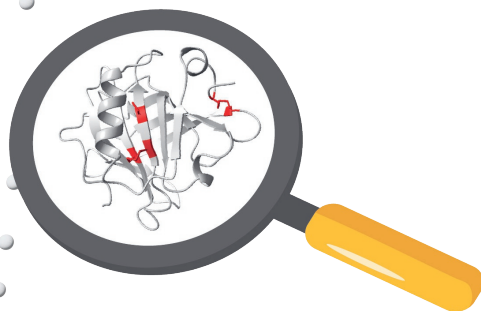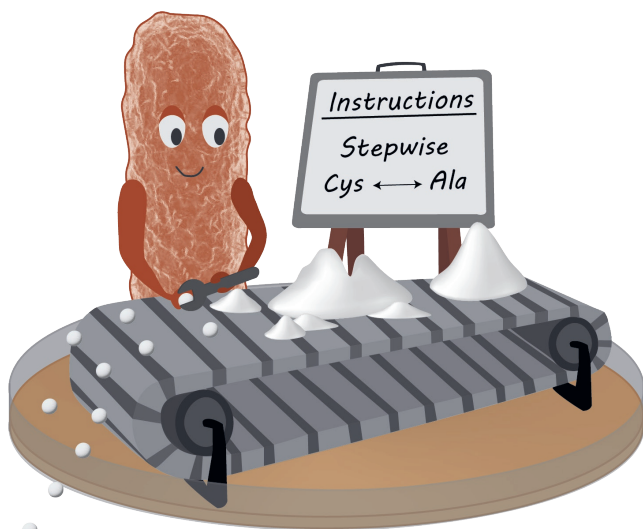
Loes Hoppenreijs, Sarah Brune, Toni Kühl, Vanessa Lautenbach, Johannes Walter, Wolfgang Peukert, Karin Schwarz, Diana Imhof, Remko Boom, Rainer Krull, Julia Keppler & Rebekka Biedendieck

Precision fermentation is a promising route to develop recombinant proteins with improved functionality. Protein functionality is highly influenced by protein structure, which can be significantly affected by conformational restraints induced by cysteines. Here, we study the impact of individual cysteines on β-lactoglobulin structure, by stepwise substituting them with alanine. Structural characterization was performed from secondary to quaternary level. The findings demonstrated that the free Cys121 played no role in the folding and dimerization of BLG. The β-barrel usually includes one disulfide bond (Cys106-Cys119), which was found to be crucial for its formation. The usually exposed disulfide bond (Cys66-Cys160) played no major role in folding of the β-barrel, but mainly modulated its accessibility and mediated dimerization. Thereby, cysteine mutations can be used as a tool to modify protein structures. These different structures can now be used to further understand the impact on protein behavior and their functionality.

Abstract

Abbreviations: BLG, β-lactoglobulin; bBLG R1, β-lactoglobulin partially reduced; bBLG R2, β-lactoglobulin completely reduced; CD, circular dichroism; DM ratio, dimer/monomer ratio; f/f0, frictional ratio; FTIR, Fourier-transform infrared spectroscopy; (RP-)HPLC, (reversed-phase) high performance liquid chromatography; IBs, inclusion bodies; IEX, ion exchange chromatography; MS, mass spectrometry; ncIBs, non-classical inclusion bodies; NEM, n-ethylmaleimide; PAGE, polyacrylamide gel electrophoresis; rBLG, recombinant β-lactoglobulin; rBLG-C, β-lactoglobulin without cysteines; rBLG-SH, β-lactoglobulin without free thiol; rBLG-SS, β-lactoglobulin without outer disulfide bond; SH, free thiol group; disulfide bond, SS bond; TCEP, tris(2-carboxyethyl)phosphine; TFA, trifluoroacetic acid

2.1. Introduction

The emerging interest of using precision fermentation as a route to produce food proteins opens new possibilities. Besides the ability to produce animal protein alternatives with similar functionality, precision fermentation can also be employed to induce targeted mutations to achieve desired protein structures that might even lead to superior functionality. Cysteine residues can form covalent inter- and intramolecular disulfide (SS) bonds, which ensure the thermodynamic stability of globular proteins, but can also form a stabilizing network between proteins (Wiedemann, Kumar, Lang, & Ohlenschläger, 2020). Therefore, the aim of this current study is to target cysteine residues to modulate the structure of β-lactoglobulin (BLG).

BLG has five cysteine residues forming two SS bonds (Creamer, Loveday & Sawyer, 2011). One SS bond is located near the surface of the protein ('outer SS bond'; Cys66-Cys160), while the other is located inside the protein ('inner SS bond'; Cys106–Cys119) (**Figure S2.1**). The fifth cysteine residue (Cys121) remains as a free thiol (SH) group and can shuffle to form intermolecular SS bonds upon exposure and deprotonation. Recombinant production of BLG through precision fermentation allows the elimination of specific SS bonds, while keeping others intact (Yamada et al., 2006). However, correct folding of the modified protein might not be achieved. So far, studies focused on substitution of the SH group in bovine BLG (Invernizzi, Annoni, Natalello, Doglia, & Lotti, 2008; Jayat et al., 2004; Yagi, Sakurai, Kalidas, Batt, & Goto, 2003), or substitution of the outer SS bond in equine BLG (Yamada et al., 2006). Studies on recombinantly produced bovine BLG variants targeting both SS bonds are currently still missing.

The working hypothesis is that exchanges of cysteine residues at different locations in BLG can differentially affect its secondary to quaternary structure and thus its behavior. By screening the effects of the position of a removed cysteine on the overall protein structure, valuable insights are obtained into how the structure of the protein can be specifically modulated. Furthermore, we expect that removal of SS bonds in recombinant BLG variants using precision fermentation will have a different structural impact as compared to chemical reduction of SS bonds in bovine BLG. Recombinant variants will lack SS bonds before folding, while chemical reduction only removes SS bonds after folding. If the final structures are more or less similar, chemically reduced bovine BLG can be used as an easier and more accessible tool to screen for the potential application of recombinant cysteine-modified variants.

Thereby, we describe the production and structural characterization of BLG variants recombinantly produced by *Escherichia coli*: either the cysteine residue containing the free SH group (rBLG-SH), the cysteines residues engaged in the outer SS bond (rBLG-SS) or all cysteine residues (rBLG-C) were substituted with alanine residues. For

comparison, disulfides in bovine BLG variants were partially (bBLG R1) or completely (bBLG R2) cleaved through chemical reduction. A complete structural characterization from secondary to quaternary level was performed for all variants. Besides, the SS bond connectivity of the variants was confirmed by mass spectrometry combined with Edman degradation.

The presented characterization provides a suitable basis for further future studies: The cysteine-modified variants can be used to elucidate the direct role of SS bonds or the indirect role of BLG structure in food systems (e.g., films, emulsions or gels), during processing (e.g., aggregation, oxidation), or digestion (e.g., hydrolysis, allergenicity). Using this knowledge, protein characteristics can be identified that show superior functionality, which in turn could contribute to more efficient use of recombinant proteins. Cysteine (or possibly other amino acid) exchanges can be then used as a suitable tool to achieve these structural characteristics, making more efficient use of the recombinant protein as a food ingredient.

2

2.2. Experimental section

2.2.1. Recombinant β-lactoglobulin variants

2.2.1.1. Bacterial strains and plasmids

E. coli DH10B (Life Technologies, Carlsbad, CA, USA) was used For all cloning experiments. For recombinant production of soluble BLG variants rBLG, rBLG-SH and rBLG-SS (Table 1), *E. coli* Origami B (DE3) (Novagen, Darmstadt, Germany) was chosen, while *E. coli* BL21 (DE3)* (ThermoFisher Scientific, Waltham, MA, USA) was used for the recombinant production of rBLG-C (***Table 2.1***). Cells were transformed with plasmid pETDuet-1/DsbC/L1A/I2S-BLGB (encoding recombinant bovine BLG B with a modified N-terminus L1A/I2S) (Loch et al., 2016) for the recombinant production of rBLG. pETDuet-1/DsbC/L1A/I2S-BLG-B also served as template for site-directed mutagenesis as described previously (Loch et al., 2016). Cysteine-encoding codons were stepwise replaced against alanine-encoding codons resulting in pRBEc9 (encoding rBLG-SH), pRBEc23 (encoding rBLG-SS), and pSBEc2 (encoding rBLG-C), respectively. Mutagenesis primers and corresponding plasmids are listed in ***Table S2.1***.

Table 2.1. *Different cysteine-modified β-lactoglobulin variants produced in this study.*

Abbreviation	Description	Mutation/modification conditions
bBLG B	Bovine BLG genetic variant B	
bBLG AB	bBLG genetic variants A and B	
bBLG R1	bBLG partially reduced	Chemically reduced at pH 3.5
bBLG R2	bBLG completely reduced	Chemically reduced at pH < 3.5
rBLG	Recombinant BLG	Leu1Ala/Ile2Ala
rBLG-SH	rBLG without SH	Leu1Ala/Ile2Ala + Cys121Ala
rBLG-SS	rBLG without outer SS bond	Leu1Ala/Ile2Ala+ Cys66Ala + Cys160Ala
rBLG-C	rBLG without any cysteine	Leu1Ala/Ile2Ala + all Cys (66, 106, 119, 121, 160) with Ala

2.2.1.2. Production and purification of recombinant β-lactoglobulin variants

BLG B protein variants rBLG (Origami B (DE3) transformed with pETDuet-1/DsbC/L1A/ I2S-BLGB), rBLG-SH (Origami B (DE3) transformed with pRBEc9), and rBLG-SS (Origami B (DE3) transformed with pRBEc23) were produced in a soluble form in recombinant *E. coli*. The production and purification was performed according to Keppler et al. (2021).

For the production of rBLG-C, *E. coli* BL21 (DE3) was transformed with pSBEc2 and cultivated overnight in a 300 mL shake flask (filling volume 50 mL with four baffles)

in LB-medium with 100 µg mL^{-1} carbenicillin (Carl Roth, Karlsruhe, Germany) at 37 °C and shaken at 150 rpm (deflection 25 mm). One liter LB-medium with 100 µg mL^{-1} carbenicillin and 2.0 g L^{-1} glucose was inoculated with 44 mL of the overnight culture and cultivated aerobically at 37 °C in a 2 L shake flask at 200 rpm (deflection 50 mm). At an optical density of 1.0–1.2, the recombinant protein production was induced with 500 µM iso-propyl-β-D-thiogalactopyranoside (IPTG, Sigma-Aldrich, Steinheim, Germany) and further incubated at 25 °C and 200 rpm (deflection 50 mm). After 24 h, cells were harvested and suspended in 10 mL of 20 mM sodium phosphate buffer (pH 6.0) supplemented with 5 µL phenylmethylsulfonyl fluoride (200 mM) (PMSF, Sigma Aldrich) and 0.5 µL Benzonase (25 U µL^{-1}, Merck, Darmstadt, Germany). All subsequent steps were performed on ice or at 4 °C. Cells were disrupted using sonication for 4 x 5 min with 2 min gaps in-between (95% power, 5 x 10% cycles). After centrifugation at 18,000 g for 30 min at 4 °C, the precipitate was washed in 10 mL sodium phosphate buffer (20 mM, pH 6.0) containing 2% (v/v) triton (Sigma Aldrich). After a centrifugation for 30 min at 10,000 g the corresponding sediment was washed in 10 mL sodium phosphate buffer (20 mM, pH 6.0) to remove remaining triton. The sediments obtained from 4 L of bacterial culture were suspended and combined in 50 mL of sodium phosphate buffer (20 mM, pH 6.0) containing 8 M urea (Carl Roth). The suspension was stirred on ice for 4 h and then centrifuged at 4 °C and 8,000 g for 30 min, followed by a next centrifugation of the supernatant for 60 min at 13,000 g and 4°C and a filtration (pore size of 0.2 µm, Sarstedt, Numbrecht, Germany).

Purification of rBLG-C was conducted manually via gravity flow using anion exchange (IEX) column. 100 mg of solubilized protein was loaded onto a Q Sepharose column (5 mL resin, Cytivia, Freiburg, Germany) equilibrated with sodium phosphate buffer (20 mM, pH 6.0). The column was washed with 2 column volumes (CV) ice cold sodium phosphate buffer (20 mM, pH 6.0) to remove urea and large protein aggregates. Proteins with proper folding were eluted with 8 CV of cold 300 mM NaCl. This fraction was then dialyzed in 100 µM NaCl at 4 °C. Finally, proteins were freeze-dried (Beta 2–8 LSCplus, Martin Christ, Osterode am Harz, Germany). Vials containing lyophilized rBLG-C were closed under dry nitrogen atmosphere and stored at 4 °C. Throughout the whole purification process, protein fractions were analyzed by SDS-PAGE and native PAGE (15% (w/v) of acrylamide).

2.2.2.   Purification and production of chemically reduced bovine β-lactoglobulin

A mixture of bovine BLG variant A and B (bBLG AB; *Table 2.1*) was isolated from whey protein isolate (BiPRO, Davisco, Eden Prairie, MN, USA), as described in ***Supporting information 2.6.3***. The obtained purified BLG AB was subsequently chemically reduced at acidic pH to avoid potential re-oxidation of reduced thiols. For complete reduction, bovine BLG AB was solubilized in ultra-pure water (2.5 wt%), the pH

was adjusted to 3.5, and afterwards the reducing agent 10 mM tris(2-carboxyethyl) phosphine (TCEP) hydrochloride was added (Sigma Aldrich). For partial reduction, TCEP was first added and afterwards the pH was adjusted to 3.5. Samples were then stored overnight and afterwards the reducing agent was removed through dialysis (3.5 kDa cut-off, SnakeSkin™ Dialysis Tubing, ThermoFisher Scientific). To ensure complete removal, the water was analyzed for the absence of TCEP using Fourier-transform infrared spectroscopy (FTIR) after each dialysis step (data not shown). After completion of TCEP removal, the retentate was freeze-dried (2-6D, Christ Epsilon, Osterode am Harz, Germany).

Pure bovine BLG genetic variant B (bBLG B; *Table 2.1*) was purified and characterized as well, to verify the direct comparison of the chemically reduced (genetic variants A and B) and recombinantly mutated BLG (genetic variant B). Bovine BLG B was isolated from the milk from a Holstein cow, that only carried the genotype for BLG B (provided by Maatschap Hoppenreijs, Bronkhorst, The Netherlands), as described in *Supporting information 2.6.3*.

2.2.3. Protein characterization

2.2.3.1. Thiol groups - Ellman's assay under denaturing conditions

The number of SH groups was determined by performing an Ellman's assay under denaturing conditions using the protocol from Ellman et al. (1959) with modifications. Ellman's reagent was prepared freshly by dissolving 5,5-dithio-bis-(2-nitrobenzoic acid) in a 100 mM sodium phosphate buffer (pH 8.0) containing 6 M guanidine hydrochloride (all obtained from Sigma Aldrich) to a concentration of 0.2% (m/v). Protein solutions of 10 mg mL^{-1} were prepared and further diluted with the denaturing buffer to reach protein concentrations of 1 mg mL^{-1}. The Ellman's reagent was then added (30 µL reagent to 1.65 mL protein solution). The mixture was incubated for 15 min in an Eppendorf shaker at room temperature, while mixed at 350 rpm, after which the absorbance was measured at 412 nm using a UV spectrophotometer (DR6000, Hach, Germany). To quantify the concentration of SH groups, the molar extinction coefficient was determined from a calibration curve using *L*-cysteine (Sigma Aldrich) in the range of 0–500 µM in 1 mM HCl. To determine the amount of SH per monomer, the concentration of SH groups was divided by the protein concentration (calculated using the weight and protein purities; *Supporting information 2.6.4*). The samples were analyzed in triplicate.

2.3.2. Determination of disulfide bond connectivity – tandem mass spectrometry (MS/MS) analysis combined with Edman sequencing

Trypsin (TPCK-treated) was purchased from Merck (Darmstadt, Germany) and stock solutions (50 mg mL[1], 1 mM HCl) were prepared and stored at -80 °C. Prior to application trypsin stocks were diluted in 50 mM ammonium bicarbonate (pH 7.8). Free cysteines were modified and detected as follows. Proteins (30-50 µM in 10 mM sodium phosphate buffer, pH 7.8 or preincubated in 80% trifluoroethanol in 10 mM sodium phosphate buffer, pH 7.8) were mixed in a 2:1 ratio with iodoacetamide (Applichem, Darmstadt, Germany) in 10 mM sodium phosphate buffer (pH 7.8) to yield a 40-fold excess of iodoacetamide and incubated for 2 h at room temperature for carbamidomethylation of reduced cysteines. After incubation, samples were desalted (ZipTip C4, Merck, Germany) and spotted with 2,5-dihydroxyacetophenone or sinapic acid for MALDI-TOF/TOF mass spectrometry analysis on an ultrafleXtreme mass spectrometer (Bruker Daltonics GmbH, Bremen, Germany). For the bottom-up analysis of BLG and BLG mutants, a 50-fold excess of each protein (800 µg mL^{-1} in 50 mM ammonium bicarbonate, pH 7.8) was incubated with trypsin for 12 h at 37 °C. Reactions were stopped by adding trifluoroacetic acid (TFA) to a final concentration of 10% (v/v). The samples were immediately subjected to separation by analytical reversed-phase high performance liquid chromatography (RP-HPLC) on a Shimadzu LC-10 system equipped with a Vydac 218TP54 column (C18, 250 × 4.6 mm, 5 µm particle size, 300 Å pore size) with a gradient system of 0.1 % TFA in water (eluent A) and 0.1% TFA in acetonitrile (eluent B) at a flow rate of 1 mL min^{-1} and 220 nm detection. The following gradient was applied for the approaches: 0–60% eluent B in eluent A in 60 min. The collected fractions were freeze-dried and redissolved in 0.1% TFA prior to measurement by mass spectrometry on a LC-ESI micrOTOF-Q III mass spectrometer (Bruker Daltonics GmbH, Bremen, Germany) or by N-terminal Edman sequencing on a PPSQ-53A (Shimadzu, Kyoto, Japan).

2.2.3.3. Secondary structure – Circular dichroism (CD) spectroscopy

Proteins were solubilized in a 10 mM sodium phosphate buffer (pH 7.0) at a concentration of 0.1 mg mL^{-1}. Changes in the secondary structure were measured in far UV (190-260 nm) recorded in a cuvette with path length 1 mm using a Jasco J-810 spectro-polarimeter (Jasco, Tokyo, Japan). The spectra were averaged over three scans and corrected by baseline subtracting. Quantification of secondary structure elements (i.e., α-helix, β-sheet, random coil and β-turn) was performed through a non-linear Levenberg-Marquardt fitting routine, using the software package CD-fit (V1.1, Wageningen Centre for Food Sciences: Structure and Functionality, The Netherlands). Spectra were fitted between 190 and 260 nm using five iterations. An independent sample t-test was performed in SPSS statistics (V28.0.1.1, IBM, New York, NY, USA) to test for significant differences with bBLG B.

2.2.3.4. Tertiary structure – intrinsic tryptophan fluorescence

Protein solutions with concentrations of 0.2 mg mL^{-1} in 10 mM sodium phosphate buffer (pH 7) were measured with Jasco Spectrofluorometer FP-8500 (Jasco, Tokyo, Japan) by excitation at 290 nm. An emission scan between 300 and 400 nm was taken to follow wavelength and intensity shifts in the fluorescence.

2.2.3.5. Quaternary structure - analytical ultracentrifugation (AUC)

Sedimentation velocity (SV) AUC experiments were performed using an Optima (Beckmann Coulter, Palo Alto, CA, USA). The samples were measured in 12 mm titania centrepieces (Nanolytics Instruments, Potsdam, Germany) at 50,000 rpm which is equivalent to 200,000 g, and a wavelength of 280 nm. The protein samples were dissolved in 10 mM sodium phosphate buffer (pH 7) and diluted accordingly (the respective absorbance at 280 nm can be taken from **Table S2.8**). The measured intensity data were converted into absorbance data by calculating the pseudo-absorbance data of each sample, as described by Kar, Kingsbury, Lewis, Laue, & Schuck (2000). SV-AUC data were analyzed with the continuous c(s) model with a sedimentation coefficient resolution of 100, which is implemented in the SEDFIT program (Version 16-1c) (Schuck, 2000). The partial specific volume of 751 µL g^{-1} was set for all samples and the solvent density and viscosity were equivalent to the properties of water at 20 °C for all analysis steps. Samples were analyzed in both independent and dependent duplicates.

2.3. Results

2.3.1. Production and purification of recombinant BLG variants

The recombinant variants rBLG (recombinant BLG), rBLG-SH (rBLG without SH), and rBLG-SS (rBLG without inner SS bond while keeping the free SH-group) were produced in *E. coli* Origami B (DE3) and purified according to Keppler et al. (2021) (purity > 90 wt%; **Table S2.2**). After purification of the variants, about 120 mg of pure protein L^{-1} of cell culture was obtained for rBLG and rBLG-SH, while about 60 mg L^{-1} of cell culture was achieved for rBLG-SS. The production of recombinant BLG in *E. coli* Origami B (DE3) without the inner SS bond, while retaining the outer SS bond and the free SH-group, resulted in the accumulation of classical inclusion bodies (**Figure S2.6**). The reduction and subsequent reconstruction of the outer disulfide bond would result in undesirable inter- and intramolecular disulfide bonds, massively reducing the yield of the appropriately folded protein variant. Therefore, the production of this variant was unsatisfying for further analyses (data not shown).

BLG lacking all cysteines (rBLG-C) also accumulated in form of inclusion bodies (IBs; **Figure S2.2**) when recombinantly produced in *E. coli* BL21 (DE3). Preliminary results showed that the rBLG-C IBs solubilize under mild conditions (e.g., at pH 10;

data not shown). Therefore, the rBLG-C inclusion bodies were referred to as non-classical inclusion bodies (ncIBs). Nevertheless, to ensure a complete solubilization of the proteins, the ncIBs were treated with 8 M urea. With gravity flow ion exchange chromatography (IEX), separation of the resolved rBLG-C from the remaining protein aggregates and contaminating proteins was achieved, as confirmed by SDS- and native PAGE analysis (*Figure S2.3* and *Figure S2.4*). The production and purification processes yielded 400 mg of pure rBLG-C per litre of cell culture. SDS-PAGE and FTIR analysis confirmed a purity of > 90 wt% (*Figure S2.3* and *Table S2.2*).

2.3.2. Validity of thiol groups and disulfide bond connectivity

2.3.2.1. Quantification of thiol groups

Bovine BLG B in pure form and a mixture of BLG A and B (bBLG B and bBLG AB) were successfully isolated from milk and whey protein isolate, respectively, with a protein purity of ~ 95 wt% (*Supporting information 2.6.4*). The reduction of the SS bonds in bBLG AB was verified by measuring the number of SH groups, as shown in *Figure 2.1*. As expected from the amino acid sequences of both variants, bBLG AB and bBLG B contained about one SH. Chemical reduction of SS bonds in bBLG AB at pH 3.5 (bBLG R1) almost doubled the SH count, indicating that only partial reduction was achieved. Reduction of BLG AB at pH < 3.5 (bBLG R2) led to a SH content of 5.44 ± 0.29, indicating complete reduction of both SS bonds. Besides, the SH content of recombinant variants was confirmed: rBLG and rBLG-SS had an SH content of about one, while substitution of Cys121 in rBLG-C and rBLG-SH led to an SH content of about zero. The SH content was also analyzed by employing carbamidomethylation of SH groups and subsequent analysis by tandem mass spectrometry (MS/MS) (*Figure S2.7* and *Table S2.4*). These results confirmed the presence of up to one SH for bBLG AB, rBLG, and rBLG-SS and none for rBLG-SH and rBLG-C. Upon chemical reduction for the aforementioned approaches, either up to 3 (bBLG R1) or up to 5 (bBLG R2) SH groups were detected (*Table S2.4*).
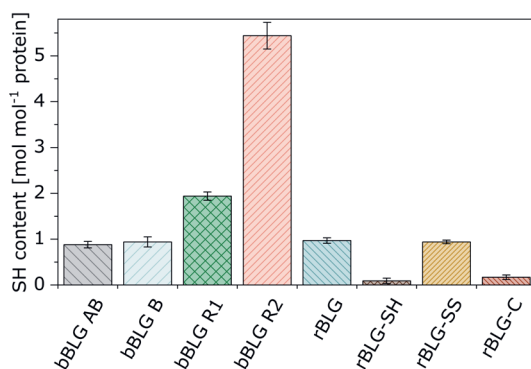

Figure 2.1. *Amount of free thiol (SH) groups in β-lactoglobulin (BLG) variants.*

2.3.2.2. Cysteine connectivity

Besides analysing the SH content, the position of the SS bonds was identified using a bottom-up analysis of the recombinant variants and reduced bovine BLG variants, using bBLG AB as a reference. Therefore, proteins were proteolytically digested with trypsin and the obtained peptide fragments were separated by RP-HPLC and subjected to analysis with tandem mass spectrometry (MS/MS). As the signal intensity of some peptide fragments bound by SS bonds decreases strongly (Creamer et al., 2004), N-terminal Edman sequencing was applied to identify these peptides without a doubt. This resulted in a 100% sequence coverage for the respective protein sequence. A detailed overview of these experiments can be found in **Supporting information 2.6.6**, while the major findings will be highlighted in the following.

For bBLG AB, the results correlate to earlier findings of Creamer et al. (2004), who detected similar fragments in a comparable order after tryptic digestion and chromatographic separation. In their study, as well as our study, a SS linkage for bBLG AB was observed for fragments 61-70 carrying Cys66 (and Asp64 in variant A or Gly64 in variant B) and 149-162 with Cys160 (**Figure 2.2B**, **Figure 2.2C** and **Table S2.5**; Creamer et al., 2004). In MS/MS analysis (**Figure 2.2C**), the assignment of a y_3 ion of fragment 149-162 (Cys160) showed an additional mass of fragment 61-70, which indicates a SS bond between Cys66 and Cys160. Similar results were obtained for all BLG variants in this study containing these two cysteines. Due to the removal of this SS bond in rBLG-SS and rBLG-C, peaks were detected for fragments 61-70 and 149-162. In addition, a concomitant complete loss of the peak for the SS-bonded fragments 61-70 and 149-162 as well as 61-69 and 149-162 was detected (**Figure S2.8** and **Table S2.6**). Similarly, for chemically reduced bBLG AB, a significant decrease (in case of bBLG R1) or a complete disappearance (in case of bBLG R2) of the same peak was observed indicating an opening of the outer bridge (**Figure S2.9**).

The investigation of the SS bond within fragment 102-124 containing Cys106, Cys119, and Cys121 with a described SS bond between Cys106 and Cys119 was found to be more challenging. The oxidized fragment 102-124 did not occur in the chromatogram. However, the peak did appear upon reduction of the protein, as was the case for bBLG R1 in low levels and for bBLG R2 in considerably increased amounts (**Figure S2.9**). These observations for oxidized and reduced BLG are in agreement with the result of Creamer et al. (2004). In addition, a clear peak was also observed when standard peptides were used that covered the corresponding sequence stretch with a distinct SS linkage (**Figure S2.10**–**S2.12** and **Table S2.7**; Creamer et al., 2004). However, for non-reduced bBLG AB, minor fractions of differentially linked fragments could be identified by both MS/MS analysis and N-terminal Edman degradation: such as a link between fragment 102-124 (Cys106, Cys119, Cys121) and 61-70 (Cys66), as well as dimers of fragment 102-124 (**Figure 2.2D** and **Table S2.5**). N-terminal Edman sequencing was a suitable method to determine these fragments without any doubt.
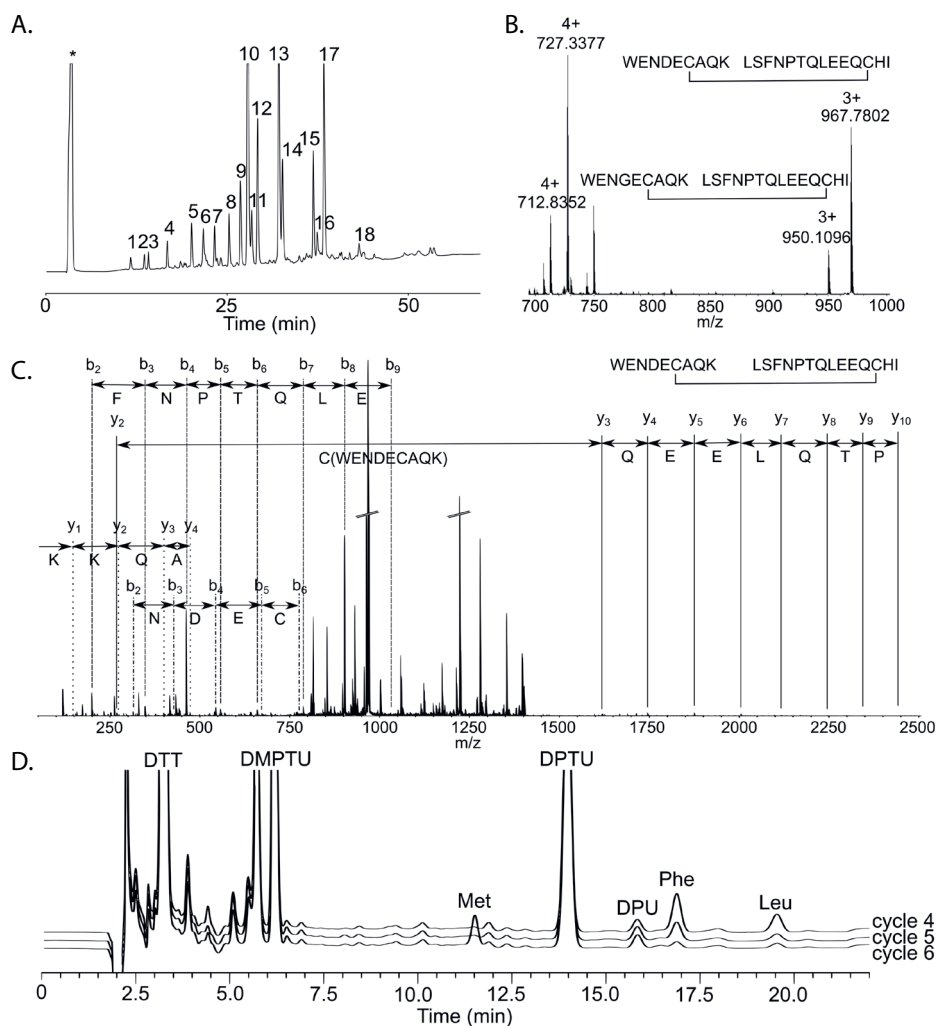
Figure 2.2. *Analysis of the tryptic digest of BLG AB. (**A**) Reverse phase (RP-) HPLC profiles of bBLG AB after tryptic digest. Corresponding peaks that were collected and selected for further analysis by mass spectrometry (MS) and tandem mass spectrometry (MS/MS) are labelled with numbers (description of corresponding fragments that were detected are given in **Table S2.5**). Asterisk marks the injection peak. (**B**) Liquid chromatography and electrospray ionization quadrupole time-of-flight mass spectrometry (LC-ESI-QTOF-MS) spectrum of peak No. 13. (**C**) LC-ESI-QTOF-MS/MS spectrum of m/z 967.7802 from the MS spectrum of peak No. 13 representing the SS-connected fragments 61-70 and 149-162. (**D**) Cycle runs of N-terminal sequencing covering amino acid positions 4-6 of peak 18 showing an increase in the intensity of the correlating phenylthiohydantoin (PTH)-derivatives that are representative for the occurrence of amino acids phenylalanine, cysteine (no peak increase) and methionine, respectively. Occurrence of residual PTH-leucine from cycle 3 that*

*was not cleaved in that cycle can be still detected in cycle 4. The total run for this peptide was performed for 10 cycles confirming the existence of peptide sequence YLLFCMENSA that allowed for further determination in combination with the observed mass detected by MS and MS/MS analysis (**Table S2.5**).*

Interestingly, when Cys121 was substituted with Ala (fragment 102-124 of rBLG-SH), a major peak in the chromatogram appeared (**Table S2.5** and **Table S2.6**). Based on the obtained molecular weight of the fragment ion, this peak was assigned to be an internal SS bond between Cys106 and Cys119 (**Figure S2.8** and **Table S2.6**). For rBLG, a linked peptide consisting of fragments 102-124 and 149-162 occurred, which was not present in the isolated BLG AB. The formation of a SS bond between these fragments indicates the formation of a minor fraction of differently folded protein upon bacterial expression. This is further supported by the occurrence of the reduced fragment 61-69 or heterodimers of fragments 61-69 and 61-70 potentially because of the missing SS bond between Cys66 and Cys160.

2.3.3. Structure analysis

2.3.3.1. Secondary structure

Secondary structure elements (i.e., α-helices, β-sheets, random coil, and β-turn) of the BLG variants are shown in **Figure 2.3**. There were no significant differences found in the structural elements of bBLG AB and B ($p > 0.05$). A minor decrease in all structured elements (α-helix, β-sheets, and β-turn) was observed for bBLG R1, while random coil structures slightly increased (**Figure 2.3A**). This trend was more evident for the completely reduced bBLG R2, leading to an increase of 12% and 16% in random coil structures, respectively. Lastly, a slight decrease (4-6%) in β-turn content in these variants was observed as compared to bBLG AB.

Recombinant BLG had a similar secondary structure to bovine BLG (**Figure 2.3**). The substitution of cysteines in the different variants had significant impact on their structures ($p \leq 0.01$), when compared to the recombinant wild-type. The exchange of Cys121 to Ala led to a minor decrease in the random coil structure (-8%), while increasing the α-helical content (+6%). Removal of the outer SS bond in rBLG-SS resulted in a loss in β-sheet content (-12%), while forming more random coil (+10%) and α-helical (+5%) structures instead. Additional removal of the inner SS bond (and Cys121Ala) in rBLG-C resulted in a further decrease in the β-sheet content (-39%), as well as an increase in random coil (+31%) and α-helical (+13%) structures. The β-turn content was slightly decreased by 3 and 5% for rBLG-SS and rBLG-C ($p \leq 0.05$), while it was unaffected for rBLG-SH.
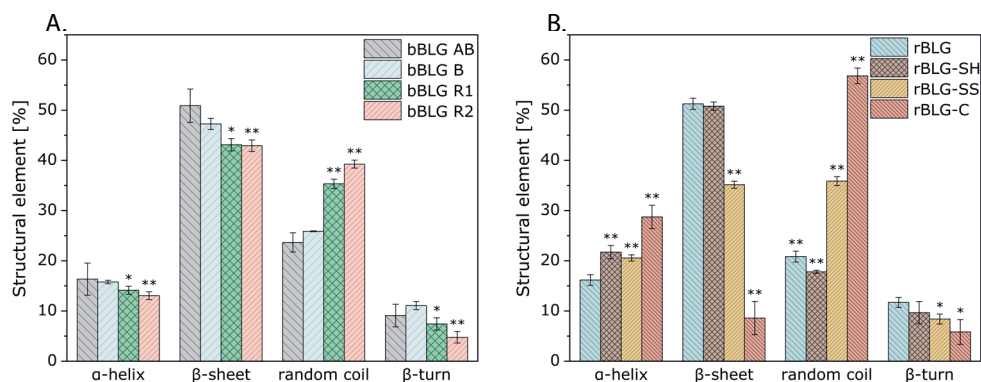
Figure 2.3. *Secondary structure element distribution of (**A**) bovine BLG variants and (**B**) recombinant BLG variants, derived from circular dichroism (CD) analyses. Values significantly different from bBLG B at p ≤ 0.05 (*) or p ≤ 0.01 (**) are labelled, accordingly.*

2.3.3.2. Tertiary structure

Tryptophan fluorescence is a widely used tool to analyse the tertiary protein structure (Vivian & Callis, 2001). The fluorescence spectra are shown in **Figure 2.4**. Bovine BLG A and AB both have emission maxima at 331 nm (denoted as 'fluorescence wavelength') after excitation at 290 nm, indicating similar tertiary structure. Also, rBLG and rBLG-SH showed a similar fluorescence wavelength, while the fluorescence intensity was slightly lower. The removal of the outer SS bond by chemical reduction or recombinant substitution enhanced the fluorescence intensity, as shown for bBLG R1/R2, rBLG-SS, and rBLG-C, respectively. Additionally, these variants showed a higher emission wavelength at 336–337 nm, as compared to bBLG and rBLG. Further reduction of bBLG R2, as compared to bBLG R1, only led to a further minor increase in fluorescence intensity and no change in fluorescence wavelength maximum. Substitution of all cysteine (rBLG-C) showed the highest fluorescence intensity and biggest wavelength shift (to 338 nm).
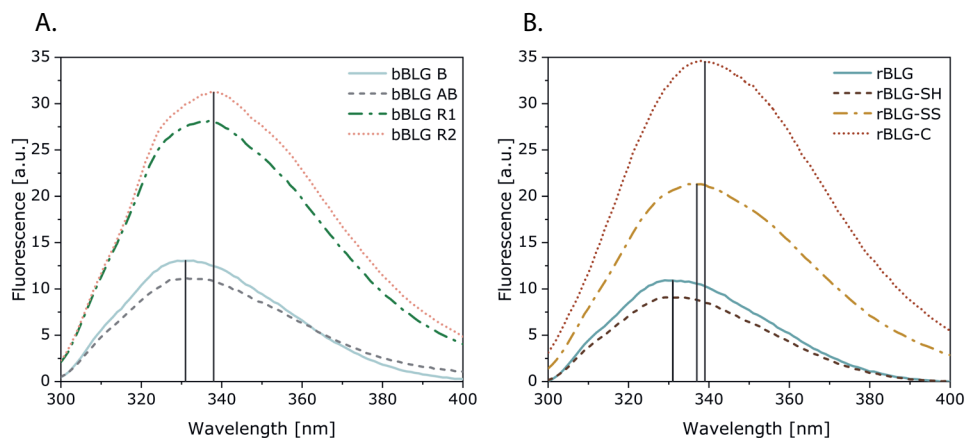
Figure 2.4. *Fluorescence emission spectra of (**A**) bovine BLG variants and (**B**) recombinant BLG variants. Fluorescence excitation was at 290 nm and emission spectra were recorded from 300–400 nm.*

2.3.3.3. Quaternary structure

Analytical ultracentrifugation (AUC) was performed to get insights into the dimerization state of the BLG variants. All analyzed BLG variants showed the presence of two differently sedimenting species: a smaller (~ 1.9 S) and a larger species (~ 2.6 S; **Figure 2.5**). This behavior was observed earlier and indicates the simultaneous presence of monomers and dimers at neutral pH values (Keppler et al., 2021; Zhang, Wright, & Zhong, 2013). To compare quaternary structures, the dimer/monomer signal ratio (DM-ratio) was derived from the integrated sedimentation coefficient distributions of the two corresponding species (**Table S2.8**), while keeping the overall loading concentration constant. Additionally, an alternative method for characterizing the dimerization state is shown in the **Supporting information 2.6.8**. Based on the comparison between DM-ratio and the weight-signal average, both yielded same results.

The native bovine BLG variants bBLG AB and bBLG B appeared in an equilibrium between monomer and dimer, with the dimers dominating (DM-ratio of 1.85 ± 0.23 and 3.40 ± 0.56, respectively). A decreased DM-ratio of 0.06 ± 0.01 was observed for bBLG R2. The variant bBLG R1 gave contradicting results, which were confirmed in repeated experiments (**Table S2.8**): either with dominating monomer or dimer fraction. An increased number of dimers (DM-ratio of 5.53 ± 0.80) was obtained for rBLG, as compared to the bBLG variants, while rBLG-SH showed almost congruent behavior to the native bBLG B sample with a similar DM-ratio of 3.92 ± 1.12. In contrast, rBLG-SS predominantly assumed the monomeric configuration (DM-ratio of 0.20 ± 0.04). The variant without cysteine residues (rBLG-C) showed excess of dimers, similar to bBLG AB (DM-ratio 2.21 ± 0.11). Furthermore, a strong additional peak near a sedimentation coefficient of zero in rBLG-C indicates the presence of not sedimenting, small molecules.

Furthermore, the frictional ratio (f/f_0) gives information on the particle's solvatization and shape anisotropy, as described by Smith (1988). Spherical particles have an f/f_0 ratio close to one, while the f/f_0 ratio of particles with increasing asymmetry and/or hydration deviates (Smith, 1988). All considered variants had f/f_0 values between 1.11–1.16 (**Figure 2.5**), which indicates a globular protein structure, except when both SS bonds were removed: bBLG R2 and rBLG-C revealed a significantly higher frictional coefficient of 1.18 ± 0.01 and 1.25 ± 0.04 ($p \leq 0.05$), compared to native bBLG and rBLG, respectively.
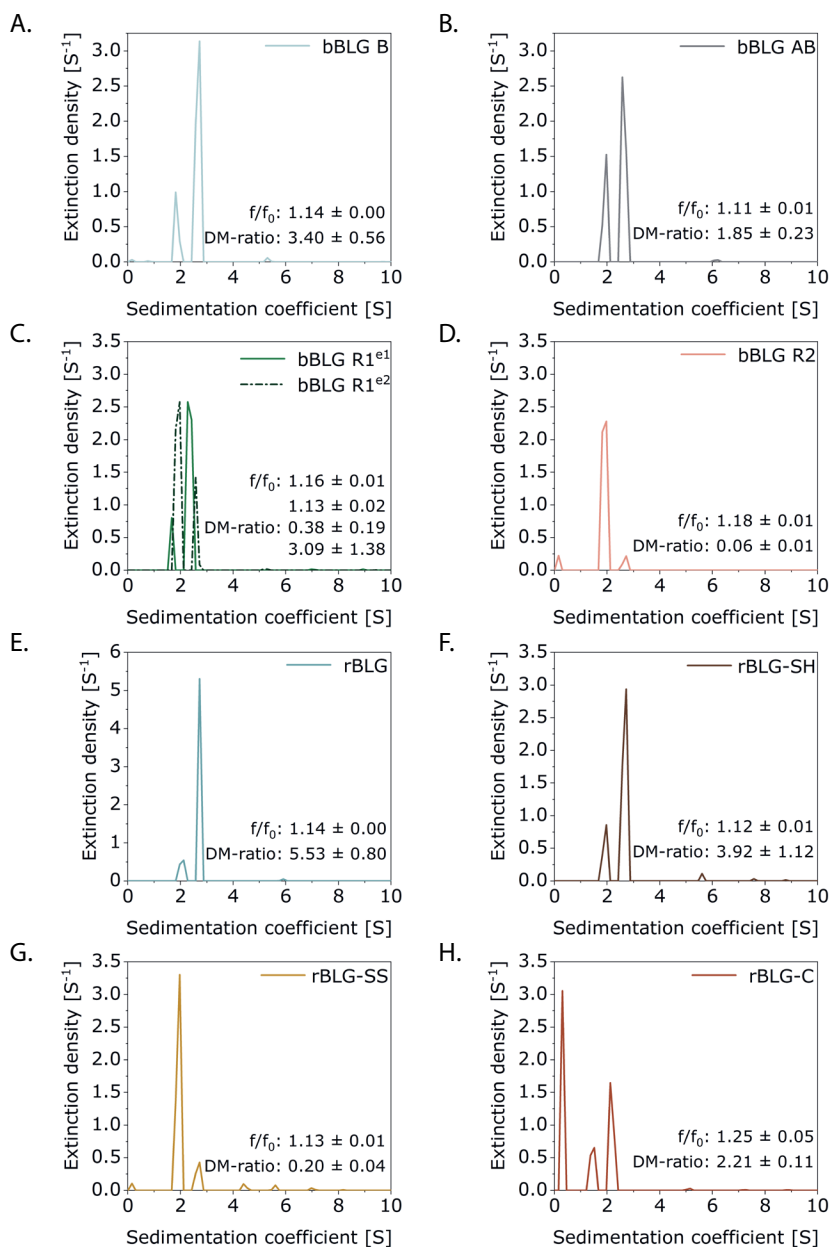
Figure 2.5. *Sedimentation coefficient distributions of (**A-D**) bovine BLG variants and (**E-H**) recombinant BLG variants at pH 7.0 with respective frictional ratio (f/f$_0$) and dimer/monomer signal ratio (DM-ratio) calculated from integrated peaks. The two curves in diagram C demonstrates contradicting results for partially reduced BLG (**Table S2.8**), which are exemplarily represented as experiment 1 (e1) and 2 (e2). The BLG concentration was constant for all experiments (**Table S2.8**).*

Chapter 2

2.4. Discussion

The characteristics of the prepared variants are summarized in **Table 2.2** and are first shortly discussed individually in **Section 2.4.1**. **Section 2.4.2** then compares the structural implications of the two approaches to remove SS bonds to provide fundamental insights in the role of (specific) SS bonds for BLG folding (particularly the calyx and its accessibility), stability, and dimerization behavior.

2.4.1. Characterization of the cysteine-modified β-lactoglobulin variants

2.4.1.1. Bovine β-lactoglobulin and its chemical reduction

Bovine BLG AB was treated with TCEP at pH 3.5 or < 3.5, which resulted in either partial (R1; 2–3 SH groups) or complete (R2; 5 SH groups) reduction (**Figure 2.1**; **Figure S2.7** and **Table S2.4**). Partial reduction of BLG primarily resulted in opening of the outer SS bond, but also minor reduction of the inner SS bond. Due to its accessibility, the outer SS bond is often also reported to participate in SH/SS exchange reactions during early stages of heat-induced aggregation (Surroca, Haverkamp, & Heck, 2002). In turn, this led to a slight decrease in structured elements and a concomitant increase of random coil structures (+12% and +16% for bBLG R1 and R2, respectively; **Figure 2.3A**) resulting in an opened globular fold (**Figure 2.4A** and **Figure S2.5**). Both

Table 2.2. *Overview of the characteristics of the β-lactoglobulin (BLG) variants as compared to bovine BLG (bBLG B). Similar behavior to bBLG is indicated with ✓. Differences in terms of SS bond connectivity and the structure are described. Green color indicates increase and red colour indicates decrease in secondary structure elements compared to bBLG B.*

Variant	Cysteine connectivity
bBLG B	Cys106-Cys119, Cys66-Cys160, Cys121
bBLG AB	Same as bBLG B
bBLG R1	Partial cleavage (SH ≈ 2-3) of mostly Cys66-Cys160
bBLG R2	All bonds cleaved (SH ≈ 5)
rBLG	Same as bBLG B
rBLG-SH	Free Cys121
rBLG-SS	Cys106-Cys119, Free Cys121
rBLG-C	No cysteine

[1]At pH 7.0; * Significant at $p \leq 0.05$; ** Significant at $p \leq 0.01$.

observations have been reported before (Mohan Reddy, Kella, & Kinsella, 1988; Sakai, Sakurai, Sakai, Hoshino, & Goto, 2000; Wu & Narsimhan, 2008) and result from the lifted conformational restraint upon reduction of the SS bond(s). In turn this causes dimers to dissociate, as is further discussed in **Section 2.4.2**.

To our knowledge, partial or complete reduction of SS bonds and subsequent removal of the reducing agent was not reported before, unless released SH groups were blocked by modifying groups, such as iodoacetamide or NEM (Hoffmann & van Mil, 1997; Liu, Chen, & Mao, 2007). Removal of the reducing agent is often desired as it may induce side reactions during exposure for an extended period, such as backbone cleavage (Liu et al., 2010). Blocking SH by modifying groups on the other hand can have a destabilizing effect (Jayat et al., 2004; Sakai et al., 2000). In our study, oxidation of SH seemed to be mostly avoided by applying acidic conditions. It should be noted that these chemically reduced variants might form non-native SS bonds under different conditions, due to an increased reactivity of the SH groups after deprotonation (e.g., alkaline pH) and/or through exposure (e.g., unfolding during heating) (Surroca et al., 2002). This was for example observed in our study during alkaline conditions applied in native PAGE analysis (pH 8.8) leading to faded bonds at higher MW (**Figure S2.5**). These aggregates were evident only during this analysis and only included minor amounts of BLG. Since analysis of the fully reduced BLG variant by AUC (pH 7.0) and Ellman's assay (pH 8.0) indicated a monomeric conformation and almost complete reduction, it can be assumed that no reformation of the disulfide bonds occurred under these conditions.

Table 2.2. Continued.

Secondary structure				Tertiary structure	Quaternary structure[1]
α-helix	β-sheet	Random coil	β-turn		
~16	~47	~26	~11	Globular	Mostly dimers
✓	✓	✓	✓	✓	✓
✓	-8*	+12**	-4*	Opened	Inconsistent
✓	-8*	+16**	-6*	Opened further	Mostly monomers
✓	✓	-5**	✓	✓	Mostly dimers
+6%**	✓	-8**	✓	✓	✓
+5**	-12**	+10**	-3*	Slightly opened	Mostly monomers
+13**	-39**	+31**	-5*	Disordered	Monomers and dimers

2.4.1.2. Recombinant substitution of the free thiol group (rBLG-SH)

Recombinant variants rBLG and rBLG-SH were successfully produced with *E. coli* in similar amounts reported before for the wild-type (~ 120 mg protein L^{-1} of cell culture Keppler et al., 2021). Here, the removal of the free SH group had no effect on the production yield. The SS bonds and cleavage patterns of rBLG after tryptic digestion strongly resembled those of the native bBLG (***Figure 2.2***; ***Figure S2.8***, ***Table S2.5*** and ***Table S2.6***). Only a few minor impurities of other differently-folded isomers were detected for rBLG. Furthermore, the Cys121Ala substitution in rBLG-SH did not lead to major changes in the secondary structure of rBLG-SH compared to the wild-type (***Figure 2.3***; ***Table 2.2***), which was also already shown for the mutation Cys121Ser in BLG (Jayat et al., 2004). Cys121 is located within the β-barrel of BLG (***Figure S2.1***). Thereby, the introduction of alanine, which is somewhat more hydrophobic compared to cysteine, can induce slight destabilization of the β-sheets (Monera, Sereda, Zhou, Kay, & Hodges, 1995). The tertiary structure of rBLG-SH remained mostly similar to the wild-type, as shown by tryptophan fluorescence (***Figure 2.4***). The tertiary structure is not directly stabilized by Cys121, as it is too distant to form hydrogen bonds with neighbouring groups (Burova, Choiset, Tran, & Haertlé, 1998). Since the tertiary structure remained similar and Cys121 is not located at the dimer interface (***Figure S2.1***), the dimerization behavior was also unaffected (***Figure 2.5***). This was also reported by Yagi et al. (2003). In contrast, chemical modification of Cys121 is often reported to dissociate dimers, as shown for several reagents including 2-mercaptoethanol and mercaptopropionic acid (Burova et al., 1998), and 5-thio-2-nitrobenzoic acid (Sakai et al., 2000). This has been attributed to the denaturing conditions used during chemical treatment and/or the bulkiness of the modifying agent (Jayat et al., 2004; Sakai et al., 2000).

2.4.1.3. Recombinant substitution of the outer disulfide bond (rBLG-SS)

About half the yield of purified recombinant rBLG-SS (~ 60 mg L^{-1}) could be obtained compared to rBLG and rBLG-SH, probably due to minor destabilization induced by removal of the outer SS bond (Cys66–Cys160). The removal of this bond had no impact on the SS bond connectivity of the inner SS bond (Cys106–Cys119) (***Figure S2.8*** and ***Table S2.6***). Similarly to partial or completely reduced bBLG AB, a slight increase in random structure was observed (+10%) as compared to native bBLG B (***Figure 2.3B***). In contrast to chemical reduction, the increased random coil structure was only at the expense of the β-sheets (-12%) and seemed to slightly increase the α-helical content (+5%). Thus, the removal of the outer SS bond might hinder a small fraction of the β-sheet structure to fold, while its removal after folding does not completely destabilize this β-sheet structure. Probably the β-sheet involving β-strand D was affected, as it contains Cys66 (***Figure S2.1***). Similarly to reduced bBLG, the tertiary structure opened slightly, as shown by a red shift in the fluorescence wavelength and a minor shift in the native PAGE (***Figure 2.5***, ***Figure S2.5***; Albani, Vogelaer, Bretesche,

& Kmiecik, 2014). Besides, the variant remained mostly monomeric (**Figure 2.5**; further discussed in **Section 2.4.2**). In general, even without the outer SS bond, bovine BLG was able to fold to a native-like structure. This has also been shown before for equine BLG under physiological conditions, which contains a SS bond in the same location (Yamada et al., 2006).

2.4.1.4. Recombinant substitution of all cysteines (rBLG-C)

Besides the specific elimination of the SH group or the outer SS bond, variant rBLG-C lacks all cysteine residues, including the inner SS bond. As the far-UV CD spectrum of rBLG-C was comparable to the spectrum of denatured BLG, a molten globule-like structure was assumed (Qi et al., 1997). Besides the random coil structure, it also assumed α-helical structure (+13%). Based on the sequence of BLG, it is expected to mainly form α-helices, but these α-helices are reported to transform into β-sheets during folding due to non-local interactions in the tertiary structure (Hamada & Goto, 1996). Thereby, the recombinant removal of the inner SS bond opened the structure and could avoid these non-local interactions, hindering the transition of α-helices to β-sheets. The additional increase in random coil conformation indicates that in bBLG not all β-sheets are formed through α-helical structures. Consequently, the globular tertiary structure of rBLG-C was further opened, as compared to other variants (**Figure 2.4** and **Figure S2.5**). Although the characteristic tertiary structure of BLG is no longer present (as indicated by near-UV CD), some tertiary structure elements still existed, as complete denaturation of rBLG-C in 8 M urea led to a further increase in tryptophan fluorescence (**Figure S2.12**).

For the quaternary structure analyzed by AUC, rBLG-C assumed both the monomeric and dimeric states, comparable to bBLG (**Figure 2.5**). The presence of two species was also observed during RP-HPLC as two distinct peaks (**Figure S2.14**). Dimeric species could form through hydrophobic interactions of the exposed regions, which are usually hidden in the globular structure of bBLG. The AUC analysis showed a large slow-sedimenting fraction, which may be due to the presence of completely unfolded protein with higher frictional coefficients, or smaller compounds, such as tightly bound RNA and/or DNA. This was confirmed by agarose gel-electrophoresis and a shift in absorbance maximum towards lower wavelengths (**Figure S2.4**, **Table S2.8** and **Figure S2.13**). Krachmarova, Ivanov, & Nacheva (2020) suggested that RNA may influence protein aggregation behavior due to electrostatic interactions. Since no major change in the isoelectric point of recombinant variants was observed (**Table S2.9**), the impact is expected to be limited.

Due to the lack of structure, rBLG-C accumulated mostly as ncIBs (Peternel, Grdadolnik, Gaberc-Porekar, & Komel, 2008) during its recombinant production in *E. coli*. After solubilization of the ncIBs, rBLG-C was purified using an IEX column without a time-consuming and elaborate refolding process. Thereby, a relatively large amount (400

mg L^{-1} cell culture) of highly pure and soluble rBLG-C protein was obtained after one single step. Trinh, Thuoc, & Thao (2021) described the production of G-CSF as ncIBs, from which correctly folded protein was obtained via a chromatography step without prior refolding.

2.4.2. Fundamental insights in role of disulfide bonds in β-lactoglobulin structure

The removal of both SS bonds in rBLG-C resulted in a disordered structure, while most of the β-sheet structure was folded when only the inner SS bond remained in rBLG-SS. Besides, removal of the inner SS bond, while preserving the outer SS bond, caused misfolding and subsequent formation of inclusion bodies. We therefore assume that the inner SS bond is crucial for the folding of the calyx. In native bBLG, the inner SS bond connects β-strands G and H, forming the core β-sheet during early stages of folding. This then extends to form the hydrophobic core E-F-G-H β-sheet (Forge et al., 2000). The inability of rBLG-C to fold demonstrates that the correct connectivity of the SS bonds can be essential for folding when producing proteins recombinantly (Qin, Zhang, & Wang, 2006). Although the production of BLG in micro-organisms is a useful approach to study folding processes in more detail, it might not fully represent the *in vivo* folding process of BLG in ruminants.

The chemically reduced variants did not reveal a disordered structure. Thereby, it is assumed that the inner SS bond is crucial to fold the calyx, but not to maintain it once it is folded. Chemical reduction of the SS bonds thereby led to destabilization, but not complete unfolding. Lastly, cleaving the outer SS bond (Cys66–Cys160) led to an opened structure in both rBLG-SS and the reduced variants bBLG R1 and R2. Thereby, the outer disulfide can modulate the accessibility of the calyx. Similar findings have been reported for other lipocalins, such as human tear lipocalins. Recombinant removal of the SS bond Cys61–Cys153 also resulted in proper calyx formation and concomitantly increased structural flexibility, which in turn increased ligand binding. It was suggested that this SS bond regulates the structural flexibility and accessibility of the calyx and thus plays a role in controlling receptor-ligand interactions in human tear lipocalins (Gasymov, Abduragimov, & Glasgow, 2011). Interestingly, even though the structures of the cysteine-modified variants varied, their isoelectric points were found to be similar (4.9–5.1; *Table S2.9*). This indicates that different folds did not impact the surface charge of BLG, as suggested before by Lautenbach, Hosseinpour & Peukert (2021).

Removal of the outer SS bond in rBLG-SS made it unable to associate into dimers at pH 7.0. Since this was also the case for the chemically reduced bBLG, the dissociation of the dimer was related to the cleavage of the outer SS bond and not to the introduction of the alanine residues in rBLG-SS. To the best of our knowledge, it has not yet been reported that cleavage of the outer SS bond hinders BLG dimerization. The dimerization motifs are located within the AB-loop (amino acids 33, 34, 40) and I-strand (amino acids 145–153) (Ohtomo, Fujiwara, & Ikeguchi, 2012). From the 3D structure, one can observe that the outer SS bond is closely located and indirectly

bridges these two dimerization motifs (***Figure S2.1***). Thereby, a hypothesis is that removal or cleavage of this bond (for example, via protein oxidation) could lead to distancing of the two motifs, which might prevent dimer formation. Further research should be conducted to confirm this.

2.5. Conclusions

For more efficient use of proteins produced by precision fermentation, amino acid substitution could be used as a tool to modify protein structures for enhanced functionality. Therefore, the aim of this study was to target cysteine residues to modulate the structure of BLG. We confirmed that due to the different positions and connectivity of cysteine residues in BLG, the removal of specific cysteines resulted in different structures.

The recombinant substitution of only the SH group had no major consequences for BLG structure, compared to bovine and wild-type BLG. As this variant is unable to participate in SH/SS exchange reactions, it is potentially more robust during processing and can be used to further elucidate on the role of intermolecular SS bonds in protein functionality. Furthermore, recombinant removal of the outer SS bond did not affect folding of the calyx of BLG, while the globular tertiary structure was more opened. This made the calyx more accessible and hindered dimerization. This could potentially lead to better binding of ligands. Due to the lifted conformational restraint by SS removal, these variants are expected to unfold more easily and be more flexible. These destabilized variants can in turn be used to study, for example, the absorption at interfaces of foams and emulsions. Additional removal of the inner SS bond in the recombinant variant disabled folding and led to a disordered structure. Thereby, it has been demonstrated that the location of the cysteine residues removed is crucial for its impact on BLG structure.

A second outcome of this study was that chemical reduction of bovine BLG does not always result in similar behavior to recombinant cysteine substitution: chemical removal of both SS bonds resulted in a folded structure, while recombinant removal of all cysteines did not. In contrast, both partial and complete reduction led to a similar, opened structure as rBLG-SS, although to another extent (***Table 2***). Thereby, chemical reduction can be used to screen for the potential behavior and functionality of rBLG-SS and not rBLG-C. However, a drawback of the reduced variants is that released SH groups are highly reactive when further exposed and/or deprotonated. Hence, the applicability of reduced BLG is limited towards lower pH ranges or requires further SH-blocking modification.

In summary, the characterization of the presented variants provides a solid base for follow-up studies, which can screen for protein behavior that result in enhanced functionality. For example, the unfolded and flexible rBLG-C is able to form functional fibrillar structures upon heating at pH 7.0, which cannot be achieved using bovine BLG due to its constraint conformation (***Chapter 7***).

2.6. Supporting information

2.6.1. 3D structure of BLG
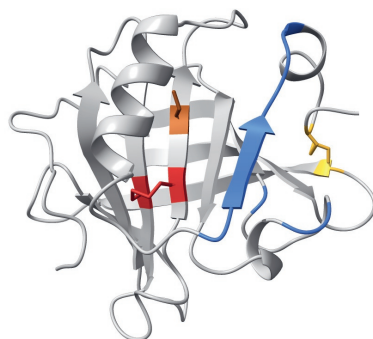
Figure S2.1. *3D structure of rBLG with free thiol (Cys121) in* **brown***, the inner (Cys106-119) disulfide bond in* **red** *and outer disulfide bond (Cys66-160) in* **yellow***. The dimerization motifs are highlighted in* **blue***. 3D structure was created with ChimeraX based on alphafold model of rBLG (Pettersen et al., 2021).*

2.6.2. Mutagenesis primers

Table S2.1. *Mutagenesis primers of site directed mutagenesis.*

Amino acid exchange	Forward primer	Reverse primer
Cys66Ala	GGGAAAATGGTGAAGCTG CCCAGAAAAAAATCATTGCC	GGCAATGATTTTTTTCTGG GCAGCTTCACCATTTTCCC
Cys106Ala	CAAAAAATACCTGCTGTTC GCCATGGAAAATAGCGCAG	CTGCGCTATTTTCCATGGC GAACAGCAGGTATTTTTTG
Cys119Ala	GTACGAACCAGACACTGA GCTGCCAGGCTCTGTTCC	GTACGAACCAGACACTGA GCTGCCAGGCTCTGTTCC
Cys121Ala	CAGAGCCTGGCATGTCAG GCTCTGGTTCGTACACCGG	CCGGTGTACGAACCAGAG CCTGACATGCCAGGCTCTG
Cys160Ala	CCCAGCTGGAAGAACAGG CCCATATCTAATAAGGTAC	GGTACCTTATTAGATATGG GCCTGTTCTTCCAGCTGGG

2.6.3. Methods for isolation of bovine BLG

2.6.3.1. Isolation of BLG mixed genetic variants A and B

A mixture of bovine BLG variant A and B (bBLG AB) was isolated from whey protein isolate (BioPro, Davisco, USA), according to Mailliart & Ribadeau-dumas (1988). The powder was dissolved at a concentration of 10 wt%, the pH was adjusted to 2.0 and sodium chloride (Sigma Aldrich) was added (14 wt%). The mixture was stirred for 30 min and 2-fold diluted. It was then centrifuged (20 min x 10,000 g) to remove precipitated protein. More NaCl (16 wt%) was added to precipitate BLG, after which the pH was adjusted to 7 and dialysis was performed using dialysis tubing with a MWCO of 3.5 kDa (SnakeSkin™ Dialysis Tubing, ThermoFisher Scientific). The dialysate was frozen and freeze-dried. The final protein purities of bBLG AB was 95.9 ± 0.6 wt%, respectively, as shown by Dumas analysis (protein conversion factor of 6.38).

2.6.3.2. Isolation of BLG genetic variant B

Pure bovine BLG genetic variant B was produced and characterized as well, to verify the direct comparison of the chemically reduced (genetic variants A and B) and recombinantly mutated BLG (genetic variant B). Bovine BLG B was isolated from milk containing only the B variant. About 10 mL of milk was collected from 86 Holstein cows (Maatschap Hoppenreijs, Bronkhorst, the Netherlands) to screen for the presence of BLG A or B, or both. The samples were centrifuged (4,800 g x 10 min; Sorvall legend XFR centrifuge, ThermoScientific) and the upper fat layer was removed with a spatula. The pH was adjusted to 4.6. After centrifugation (4,800 g x 10 min), the supernatant was analyzed with reversed phase high-performance liquid chromatography to see whether only BLG B was present, which was the case for six cows.

Five liters of milk was taken from a cow that only carried the gene for the B isoform, centrifuged (20,000 g x 5 min; Sorvall Lynx 4000, Thermo Fisher Scientific) and the fat was removed with a spatula. The pH was adjusted to 4.6, heated at 30 °C and centrifuged at 7,000 g for 30 min to remove the casein. The supernatant was collected and the pH was adjusted to 3.8. It was heated to 57 °C and kept at this temperature for 30 min, after which it was filtered (Whatmann 695 ½). The supernatant was adjusted to pH 7.0 and dialyzed (4 °C; 8 kDa cut-off, BioDesignDialysis tubing D108, Thermo Fisher, Scientific). Afterwards, the dialysate was frozen and freeze-dried (2-6D, Christ Epsilon, Osterode am Harz, Germany). Fourier transform infrared spectroscopy analysis showed that still some lactose was present and therefore further purification was performed as described above for the isolation of BLG from whey protein isolate. The final protein purities of bBLG B was 94.7 ± 1.1 wt%, respectively, as shown by Dumas analysis (protein conversion factor of 6.38).

2.6.4. Protein purities

The protein samples were weighed and analyzed by Fourier-transform infrared (FTIR) spectroscopy for their protein content, to determine the protein purity (**Table S2.2**). The protein purity was subsequently used to calculate the amount of free thiol groups per BLG monomer.

Table S2.2. *Protein purities of BLG variants.*

Protein variant	Protein purity [wt%]
bBLG B	87.9 ± 9.4
bBLG AB	95.8 ± 6.6
bBLG R1	96.7 ± 2.9
bBLG R2	93.7 ± 3.2
rBLG	93.2 ± 4.5
rBLG-SH	91.8 ± 0.5
rBLG-SS	96.8 ± 4.0
rBLG-C	91.3 ± 1.7

FTIR analysis was performed using a Confocheck Tensor 2 system (Bruker Optics, Ettlingen, Germany) equipped with a thermally controlled Aquaspec unit (Bruker Optics, Ettlingen, Germany) at 25 °C (Ministat 125, Huber, Kirchheim, Germany). The system was continuously flushed with nitrogen and the sensor was cooled with liquid nitrogen. Samples were solubilized to a final concentration of 50 mg mL^{-1}. Spectra were then obtained between 3,000 and 1,000 cm^{-1} against ultrapure water, using 64 scans and a resolution of 4 cm^{-1}. The protein purity of the samples was determined from the absorbance spectra (not manipulated), analyzed with a quantification package from Bruker. All analyses were performed in the OPUS software 8.5.29 (Bruker Optics) and all measurements were performed in triplicate.

2.6.5. Electrophoresis

Throughout the purification process, polyacrylamide gel electrophoresis (PAGE) was performed to locate the proteins (**Figure S2.2** and **Figure S2.3**). In addition, recombinant variants were analyzed on an agarose PAGE to observe nucleic acids before and after purification, as shown in **Figure S2.4**. The concentration of the nucleic acids in the recombinant variants was determined with NanodropTM, and are listed in **Table S2.3**. After production and purification, native page was performed as shown in **Figure S2.5**. Lastly, **Figure S2.6** shows an attempt to produce a recombinant variant with removed inner SS bond, while keeping the outer SS bond and free thiol.

Methods: PAGE analysis was performed with the BIO-RAD Mini-PROTEAN Tetra System (Bio-Rad Laboratories, Hercules, Canada). SDS-PAGE was carried out according to a

modified protocol of Righetti et al. (2004). Native PAGE was also performed in a similar manner, except that the SDS was omitted. 15% separating gels and 6% stacking gels were used. Electrophoretic separation was performed at a constant voltage of 150 V. Subsequently, the gels were stained with Coomassie Brilliant Blue staining solution (Coomassie Brilliant Blue R-250, 30% ethanol, 10% acetic acid) and then de-stained (30% ethanol, 10% acetic acid).
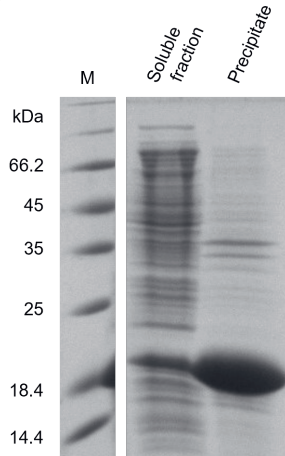
Figure S2.2. SDS-PAGE analysis of supernatant with soluble proteins and cell precipitate with rBLG-C inclusion bodies after sonication of BL21 cells.
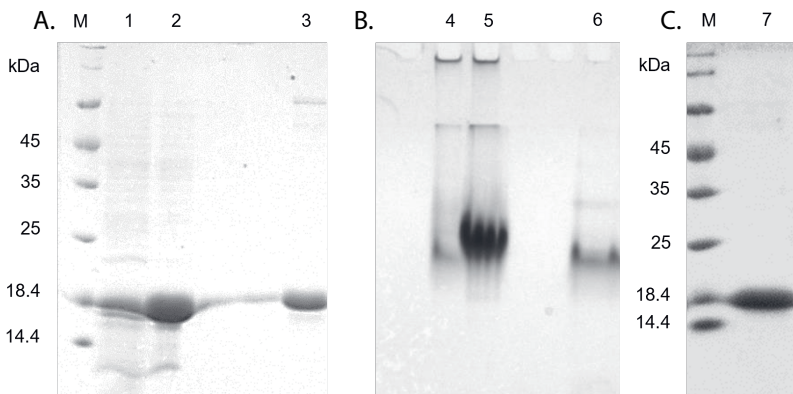
Figure S2.3. (*A* and *C*) SDS-PAGE and (*B*) native PAGE analysis of IEX purification process of rBLG-C. Inclusion bodies were solubilized in 8 M urea and loaded onto a Q Sepharose column. Flow through, washing fraction and elution fraction were collected. Lane M: MW marker. Lane 1,4: flow through fraction. Lane 2,5: washing fraction with 20 mM sodium phosphate buffer pH 6. Lane 3,6: Elution fraction with 300 mM NaCl. Lane 7: purified rBLG-C (10 µg).
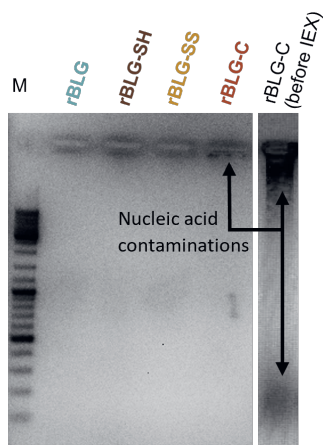
Figure S2.4. Agarose gel-electrophoresis of recombinant protein samples (freeze-dried samples,10 mg mL^{-1}) and rBLG-C IBs solubilized in 8 M urea before IEX purification.

Table S2.3. Nucleic acid concentration in protein samples measured with NanodropTM. The nucleic acid concentration was calculated from the absorbance at 260 nm, while the protein concentration was measured at 280 nm.

Protein variant	Nucleic acid concentration [µg mg^{-1} protein]
rBLG	22.6
rBLG-SH	26.3
rBLG-SS	24.4
rBLG-C	36.9
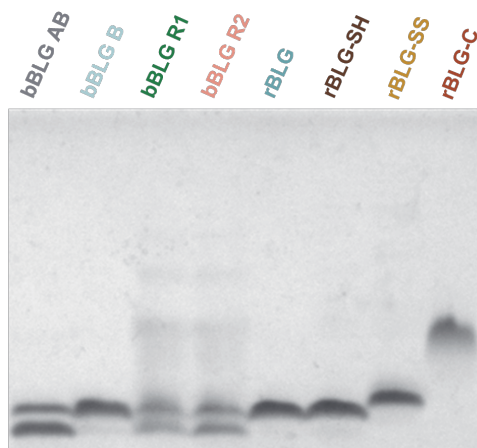
Figure S2.5. Native PAGE analysis of bovine BLG variants and recombinant BLG variants. 5 µg of freeze-dried BLG were applied per lane.
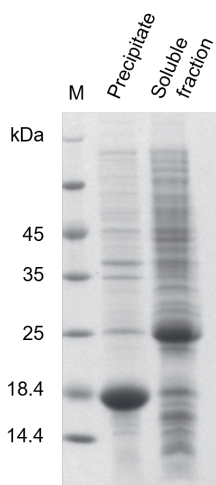
Figure S2.6. *SDS-PAGE analysis of supernatant with soluble proteins (most abundant band belongs to DsbC which acts as folding mediator) and cell precipitate with inclusion bodies formed during the production of a recombinant variant that lacks inner disulfide bond (Cys106-Cys119), while retaining the outer disulfide bond and free SH-group, after sonication of Origami B cells.*

2.6.6. Details on MS/MS analysis combined with Edman sequencing

2.6.6.1. Detection of reduced cysteines in BLG variants and mutants

Untreated bBLG AB could not be modified by iodoacetamide, which is in line with earlier observations concerning the difficult accessibility of the reduced cysteine (***Figure S2.7A***) (Yagi et al., 2003; Jayat et al., 2004). In these cases, the induction of structural reorganization, for example, initiated by application of denaturing (urea, guanidine hydrochloride) or refolding agents (hexafluoroisopropanol or trifluoroethanol, TFE) that do not affect the disulfide connectivity is required. As earlier reported, application of approx. 50% TFE induces a structural change from the β-sheet structure to an α-helical structure in BLG (Shiraki et al., 1995). We utilized this change to allow for better accessibility to refold tightly-folded protein regions and were able to detect a distinct fraction of carbamidomethylated proteins (***Figure S2.7B***). Interestingly, when applying the same protocol for carbamidomethylation and refolding to sBLG and its mutants, different results were obtained (***Table S2.4***). Exchange Cys121Ala as well as substitution of all cysteines did not show any increase of the molecular weight after incubation with iodoacetamide (***Table S2.4***) and, thus, no modification of cysteines was observed, i.e., no reduced cysteines appear in these BLG mutants (BLG-SH, BLG-C). All other variants and mutants containing non-mutated Cys121 (bBLG AB, rBLG, rBLG-SS) revealed the existence of one reduced cysteine (***Table S2.4***). In addition, for bBLG

AB a mass increase for variants A and B to 18,604 and 18,690 m/z was detected (***Figure S2.7A***) that could be attributed to lactosylation of the protein. The latter is known to potentially occur by the Maillard reaction upon heat treatment of milk (Imre et al., 2003).

A.
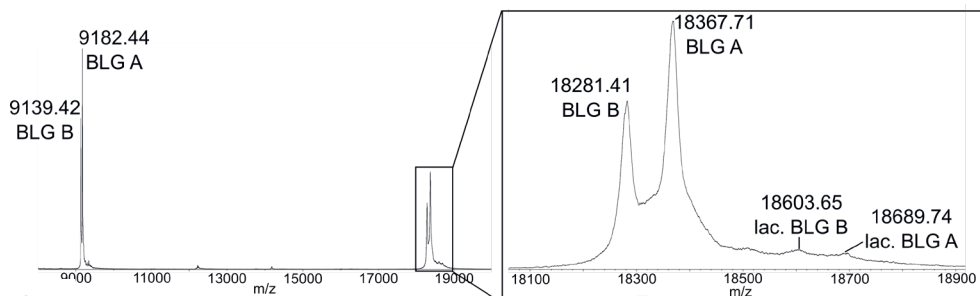
B.
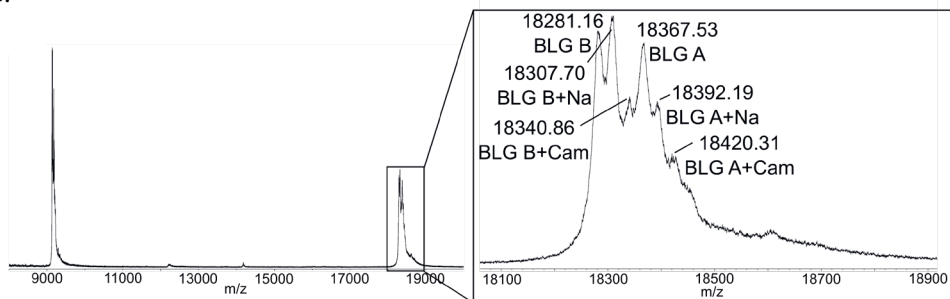
Figure S2.7. *MALDI-TOF-MS spectra for the detection of reduced cysteines of carbamido-methylated BLG AB. BLG AB was treated with iodoacetamide for carbamidomethylation (**A**) without and (**B**) with addition of 53% TFE to the reaction mixture. lac., lactosylated.*

Table S2.4. *Detected masses after carbamidomethylation of bBLG AB, chemically treated bBLG AB, rBLG and its mutants. MS peaks were detected as [M+H]+. Proteins were detected with MALDI-TOF-MS. Proteins were treated with 53% TFE before addition of iodoacetamide.*

Variant	Non-alkylated M_w (M_w obs.) [g mol^{-1}]	Non-alkylated M_w (M_w calc.) [g mol^{-1}]	Alkylated M_w (M_w obs.) [g mol^{-1}]	Alkylated M_w (M_w calc.) [g mol^{-1}]
bBLG AB	18367.71 18281.41	18363.13 (variant A) 18277.01 (variant B)	18420.31 18340.86	18420.15 (variant A + 1 Cam) 18334.06 (variant B + 1 Cam)
bBLG R1	18366.14	18363.13-18367.30 (variant A)	18423.60 18478.13 - - -	18420.15 (variant A + 1 Cam) 18479.21 (variant A + 2 Cam) 18536.27 (variant A + 3 Cam) 18595.33 (variant A + 4 Cam) 18652.39 (variant A + 5 Cam)
	18280.22	18277.01-18281.21 (variant B)	18338.12 18390.89 18448.34 - -	18334.06 (variant B + 1 Cam) 18393.12 (variant B + 2 Cam) 18450.18 (variant B + 3 Cam) 18509.24 (variant B + 4 Cam) 18566.29 (variant B + 5 Cam)
bBLG R2	18366.50	18367.30 (variant A)	18425.80 18481.18 18541.42 - 18654.31	18420.15 (variant A + 1 Cam) 18479.21 (variant A + 2 Cam) 18536.27 (variant A + 3 Cam) 18595.33 (variant A + 4 Cam) 18652.39 (variant A + 5 Cam)
	18282.05	18281.21 (variant B)	18341.18 18396.38 18452.19 18504.94 18562.82	18334.06 (variant B + 1 Cam) 18393.12 (variant B + 2 Cam) 18450.18 (variant B + 3 Cam) 18509.24 (variant B + 4 Cam) 18566.29 (variant B + 5 Cam)
rBLG	18211.04	18208.85	18264.32	18265.90 (+ 1 Cam)
rBLG-SH	18178.42	18176.78	18180.14	18176.78
rBLG-SS	18147.20	18146.73	18207.41 - -	18203.78 (+ 1 Cam) 18262.85 (+ 2 Cam) 18319.90 (+ 3 Cam)
rBLG-C	18059.69	18052.55	18055.79	18052.55

a - WENGEA$_{66}$AQK; WENGEAA$_{66}$QKK

b - WENGEC$_{66}$AQK[#,†] (also ASVTQTMK except bBLG AB)

c - WENGEC$_{66}$AQK   WENGEC$_{66}$AQK[#]; WENGEC$_{66}$AQK   WENGEC$_{66}$AQKK[#]

d - C$_{106}$MENSAEPEQSLAC$_{119}$QA$_{121}$LVR

e - WEND/GEC$_{66}$AQK   LSFNPTQLEEQC$_{160}$HI; WEND/GEC$_{66}$AQKK   LSFNPTQLEEQC$_{160}$HI

f - LSFNPTQLEEQA$_{160}$HI

g - WENGEC$_{66}$AQKK   YLLFC$_{106}$MENSAEPEQSLAC$_{119}$QC$_{121}$LVR

h - YLLFA$_{106}$MENSAEPEQSLAA$_{119}$QA$_{121}$LVR (only rBLG-C)

i - YLLFC$_{106}$MENSAEPEQSLAC$_{119}$QA$_{121}$LVR

j - YLLFC$_{106}$MENSAEPEQSLAC$_{119}$QC$_{121}$LVR   YLLFC$_{106}$MENSAEPEQSLAC$_{119}$QC$_{121}$LVR
    YLLFC$_{106}$MENSAEPEQSLAC$_{119}$QC$_{121}$LVR   LSFNPTQLEEQC$_{160}$HI

k - YLLFC$_{106}$MENSAEPEQSLAC$_{119}$QC$_{121}$LVR   YLLFC$_{106}$MENSAEPEQSLAC$_{119}$QC$_{121}$LVR

Figure S2.8. *Disulfide connectivity's in bBLG AB, rBLG and its cysteine mutants. RP-HPLC profiles are shown after tryptic digestion. Peaks were collected and selected for further analysis by MS and MS/MS (description of corresponding fragments that were detected are given in **Table S2.5**; fragments in peaks that did not occur in bBLG AB or peaks that changed their composition are given in **Table S2.6**). Grey bars are covering peaks that contain fragments with cysteines and the corresponding disulfide connectivity's or mutated cysteines as could be determined by MS/MS analysis. Fragments are given below the chromatograms. Dashed lines between cysteines for fragment 102-124 indicate that the disulfide connectivity could not be unambiguously determined due to low signal intensities and low fragment concentrations. Asterisk marks the injection peak.*

*#Fragments that did not occur in bBLG AB although a peak was detected but attributed to other fragments of this protein (**Figure 2.2**, **Table S2.6**). †Fragments that did not occur in rBLG-SH although a peak was detected but attributed to other fragments of this protein (**Figure 2.2**, **Table S2.6**).*

2.6.6.2. Analysis of disulfide connectivity

For the chemically reduced approaches of bBLG R1 and bBLG R2, carbamidomethylation was performed as described for bBLG AB. For bBLG R1, our results indicated existence of up to 2 (variant A) or 3 (variant B) reduced cysteines, while for bBLG R2 up to 5 reduced cysteines (both variants) could be detected (**Table S2.5**).

Table S2.5. *Identified sequences of peptides from a tryptic digest of bBLG AB.*

Peak	Retention time [min]	M_w (M_w obs.) [g mol^{-1}]	M_w (M_w calc.) [g mol^{-1}]	Peptide sequence[e]
1	11.7	331.24[a]	330.23	ALK [139-141]
2	13.6	425.26[a]	424.25	HIR [146-148]
3	14.2	409.21[a]	408.20	FDK [136-138]
4	16.8	573.36[a]	572.35	IIAEK [71-75]
5	20.1	916.47[a]	915.47	IDALNENK [84-91]
6	21.7	503.29[a]	502.28	DIQK [11-14]
		673.39[a]	672.38	GLDIQK [9-14]
7	23.3	623.30[b]	1244.58	TPEVDDEALEK [125-135]
8	25.3	933.55[a]	932.54	LIVTQTMK [1-8]
9	26.9	653.35[a]	652.35	PMHIR [144-148]
		837.48[a]	836.47	ALPMHIR [142-148]
10	28.0	674.43[a]	673.42	IPAVFK [78-83]
		696.35[a]	695.33	VAGTWY [15-20]
		597.35[b]	1192.67	VLVLDTDYKK [92-101]
11	28.4	903.57[a]	902.56	TKIPAVFK [76-83]
12	29.2	1065.59[a]	1064.58	VLVLDTDYK [92-100]
		623.30[b]	1244.58	TPEVDDEALEK [125-135]
		818.39[b]	1634.77	TPEVDDEALEKFDK [125-138]
13	32.2	969.45[c]	2847.30	WENGECAQKK : LSFNPTQLEEQCHI [61-70]S-S[149-162], variant B
		950.11[c]	2905.30	WENDECAQKK : LSFNPTQLEEQCHI [61-70]S-S[149-162], variant A
14	32.7	1360.61[b]	2719.20	WENGECAQK : LSFNPTQLEEQCHI [61-69]S-S [149-162], variant B
		695.31[d]	2777.21	WENDECAQK : LSFNPTQLEEQCHI [61-69]S-S[149-162], variant A

Peak	Retention time [min]	M_w (M_w obs.) [g mol⁻¹]	M_w (M_w calc.) [g mol⁻¹]	Peptide sequence[e]
15	36.9	857.46[a]	856.44	DAQSAPLR [33-40]
		1015.54[b]	2029.05	SLAMAASDISLLDAQSAPLR [21-40]
		959.43[d]	3833.70	WENGECAQKK : YLLFCMENSAEPEQSLACQCLVR [61-70]S-S[102-124], variant B
16	37.5	555.32[a]	554.31	YLLF [102-105]
		829.90[b]	1657.78	LSFNPTQLEEQCHI [149-162]
		1191.63[a]	1190.62	SLAMAASDISLL [21-32]
		1015.53[b]	2029.05	SLAMAASDISLLDAQSAPLR [21-40]
17	38.4	1157.14[b]	2312.25	VYVEELKPTPEGDLEILLQK [41-60]
18	43.2, 43.9	1322.60[d]	5286.34	YLLFCMENSEPEQSLACQCLVR- YLLFCMENSEPEQSLACQCLVR [102-124]S-S[102-124], variant B

MS peaks were detected as [a][M+H]⁺, [b][M+2H]²⁺, [c][M+3H]³⁺, [d][M+4H]⁴⁺. Peptides were detected with LC-ESI-QTOF-MS. [e]Peptide sequences were determined by LC-ESI-QTOF-MS/MS or N-terminal sequencing when ion counts in LC-ESI-QTOF-MS were too low for an unambiguous determination of the peptide sequence. Amino acid positions in the protein are given in brackets.

Table S2.6. *Identified sequences of peptides from a tryptic digest of rBLG and mutants thereof that differ with bBLG AB.*

Peak	Retention time [min]	M_w (M_w obs.) [g mol⁻¹]	M_w (M_w calc.) [g mol⁻¹]	Peptide sequence[e]
rBLG				
19	18.6	865.45[a]	864.44	ASVTQTMK [1-8]
		701.46[a]	700.45	KIIAEK [70-75]
		532.73[b]	1063.44	WENGECAQK [61-69]
6	21.7	503.29[a]	502.28	DIQK [11-14]
		673.40[a]	672.38	GLDIQK [9-14]
		751.99[c]	2252.96	WENGECAQKK-WENGECAQK [61-70]S-S[61-69]
20	40.8	1075.99[d]	4299.94	YLLFCMENSEPEQSLACQCLVR- LSFNPTQLEEQCHI [102-124]S-S[149-162]
21	52.5	1322.60[d]	5286.34	Y L L F C M E N S E P E Q S L A C Q C L V R- YLLFCMENSEPEQSLACQCLVR [102-124]S-S[102-124]

Peak No. 8 (25.3 min) disappeared. Peak No. 19 containing a fragment covering sequence ASVTQMTK [1-8] was detected instead.

Table S2.6. *Continued.*

Peak	Retention time [min]	M_w (M_w obs.) [g mol^{-1}]	M_w (M_w calc.) [g mol^{-1}]	Peptide sequence[e]
			rBLG-SH	
19	18.6	865.45[a]	864.44	ASVTQTMK [1-8]
		701.46[a]	700.45	KIIAEK [70-75]
6	21.7	503.29[a]	502.28	DIQK [11-14]
		673.39[a]	672.38	GLDIQK [9-14]
		564.25[d]	2252.96	WENGECAQKK-WENGECAQK [61-70]S-S[61-69]
22	31.2	1038.96[b]	2075.91	CMENSAEPEQSLACQALVR [106-124]
23	40.4	1307.12[b]	2612.21	YLLFCMENSAEPEQSLACQALVR [102-124]

Peak No. 8 (25.3 min) disappeared. Peak No. 19 containing a fragment covering sequence ASVTQMTK [1-8] was detected instead. Peak No. 18 (43.2 and 43.9 min) disappeared and no fragment covering dimer sequence of YLLFCMENSEPEQSLACQALVR was detected.

Peak	Retention time [min]	M_w (M_w obs.) [g mol^{-1}]	M_w (M_w calc.) [g mol^{-1}]	Peptide sequence[e]
			rBLG-SS	
25	17.0	516.75[b]	1031.47	WENGEAAQK [61-69]
		580.79[b]	1159.56	WENGEAAQKK [61-70]
26	17.5	517.23[b]	1032.45	WEDGECAQK [61-69]#
19	18.0	776.32[a]	775.31	WENGEAA [61-67]
		597.30[a]	596.29	EQAHI [158-162]
		865.45[a]	864.44	ASVTQTMK [1-8]
		701.46[a]	700.45	KIIAEK [70-75]
6	21.3	673.38[a]	672.38	GLDIQK [9-14]
27	25.4	469.21[a]	468.20	TWY [18-20]
		806.41[a]	805.40	LSFNPTQ [149-155]
28	25.9	597.26[a]	596.26	AGTWY [16-20]
		678.35[a]	677.34	LSFNPT [149-154]
29	31.7	814.44[b]	1626.86	AASDISLLDAQSAPLR [25-40]
		1048.54[a]	1047.52	LSFNPTQLE [149-157]
		1177.59[a]	1176.57	LSFNPTQLEE [149-158]
30	35.5	813.91[b]	1625.80	LSFNPTQLEEQAHI [149-162]
17	43.1	1322.56[d]	5286.34	YLLFCMENSEPEQSLACQCLV-YLLFCMENSEPEQSLACQCLVR [102-124]S-S[102-124]

Peak No. 8 (25.3 min) disappeared. Peak No. 19 containing a fragment covering sequence ASVTQMTK [1-8] was detected instead. Peaks No. 13 (32.2 min) and 14 (32.7 min) disappeared and no fragments covering connected sequences WENGECAQKK-LSFNPTQLEEQCHI [61-70] S-S[149-162] and WENGECAQK-LSFNPTQLEEQCHI [61-69]S-S[149-162] were detected.

Table S2.6. *Continued.*

Peak	Retention time [min]	Mw (Mw obs.) [g mol-1]	Mw (Mw calc.) [g mol-1]	Peptide sequence[e]
rBLG-C				
25	17.0	516.75[b]	1031.47	WENGEAAQK [61-69]
		580.79[b]	1159.56	WENGEAAQKK [61-70]
26	17.5	517.23[b]	1032.45	WEDGECAQK [61-69]#
19	18.0	865.45[a]	864.44	ASVTQTMK [1-8]
6	21.3	503.29[a]	502.28	DIQK [11-14]
		673.39[a]	672.38	GLDIQK [9-14]
30	35.5	813.91[b]	1625.80	LSFNPTQLEEQAHI [149-162]
31	39.7	851.11[c]	2550.28	YLLFAMENSAEPEQSLAAQALVR [102-124]

Peak No. 8 (25.3 min) disappeared. Peak No. 19 containing a fragment covering sequence ASVTQMTK [1-8] was detected instead. Peaks No. 13 (32.2 min) and 14 (32.7 min) disappeared and no fragments covering connected sequences WENGECAQKK-LSFNPTQLEEQCHI [61-70]S-S[149-162] and WENGECAQK-LSFNPTQLEEQCHI [61-69]S-S[149-162] were detected. Peak No. 18 (43.2 and 43.9 min) disappeared and no fragment covering dimer sequence of YLLFCMENSEPEQSLACQALVR was detected.

Only those peaks are given for each protein that differ from bBLG AB as depicted in Figure S8. MS peaks were detected as [a][M+H]+, [b][M+2H]2+, [c][M+3H]3+, [d][M+4H]4+. Peptides were detected with LC-ESI-QTOF-MS. [e]Peptide sequences were determined by LC-ESI-QTOF-MS/MS or N-terminal sequencing when ion counts in LC-ESI-QTOF-MS were too low for an unambiguous determination of the peptide sequence. Amino acid positions in the protein are given in brackets. #Occurrence of Asp instead of Asn in position 63 is attributed to deamidation during treatment with trypsin as described earlier (Hao et al, 2011).

Table S2.7. *Analytical data of peptides.*

Peptide	Peptide sequence	M_w [a] (M_w calc.) [g mol^{-1}]	Prep. HPLC t_r [min]	Analytical HPLC t_r [min]*
1	YLLF**C**MENSAEPEQSLA**C**QCLVR	2645.27 (2644.18)	66.3[b]	21.2
2	YLLF**C**MENSAEPEQSLACQ**C**LVR	2645.23 (2644.18)	65.3[b]	20.3
3	YLLF**S**MENSAEPEQSLACQCLVR	2629.24 (2628.20)	98.7[c]	19.3
4	YLLFCMENSAEPEQSLA**S**QCLVR	2629.21 (2628.20)	99.2[c]	19.3
5	YLLFCMENSAEPEQSLACQ**S**LVR	2629.21 (2628.20)	94.4 [c]	19.4

[a] MS-peaks were detected as [M+H]⁺. Peptides were detected with MALDI-TOF-MS. Purification was performed using semi-preparative RP-HPLC: [b]15-65% eluent B in 120 min and [c] 0-50% eluent B in 120 min. [d] For analytical RP-HPLC the following gradient was used: 20–60% eluent B in 40 min. *All peptides were >95% HPLC pure.

Bottom-up analysis of the disulfide connectivity showed significant differences between bBLG AB, bBLG R1, and bBLG R2 in the positions of the expected fragments of Cys-containing fragments in the HPLC chromatograms (**Figure S2.9**). In both TCEP-treated BLGs a strong decrease for the peak that contained the disulfide-linked fragments 61-70 (or 61-69) and 149-162 (Cys66-Cys160) was observed compared to bBLG AB. Concomitantly, an increase for the respective reduced single fragments could be detected. The peak for fragment 102-124 (Cys106, Cys119, Cys121) showed a different behavior. While no peak was observed for the oxidized single fragment in bBLG AB, a minor increase for the reduced fragment could be detected for bBLG R1. This indicated reduction of the SS bond in this fragment in a minor amount and was confirmed by MS/MS analysis in agreement with earlier findings by Creamer et al. (2004). Finally, for bBLG R2 a strong peak for the reduced fragment 102-124 was observed. Along with the results from the reduction approach, in which an SH content of 5.44 ± 0.29 was found, a complete reduction of both bridges can thus be concluded for bBLG R2.
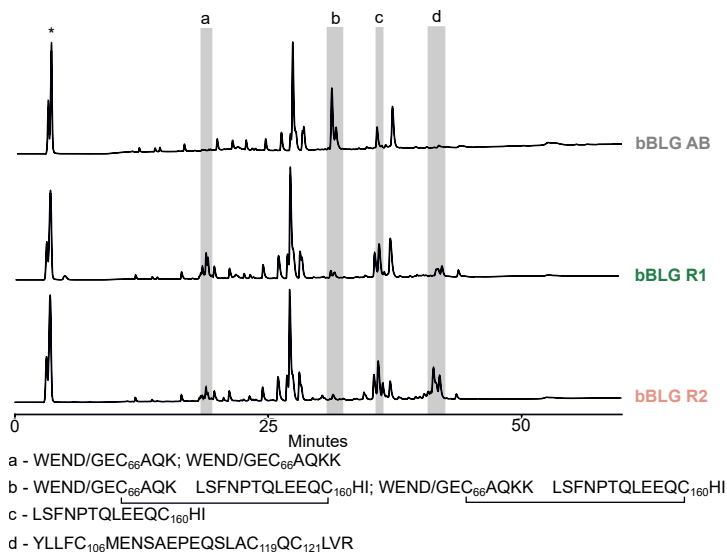
a - WEND/GEC$_{66}$AQK; WEND/GEC$_{66}$AQKK

b - WEND/GEC$_{66}$AQK LSFNPTQLEEQC$_{160}$HI; WEND/GEC$_{66}$AQKK LSFNPTQLEEQC$_{160}$HI

c - LSFNPTQLEEQC$_{160}$HI

d - YLLFC$_{106}$MENSAEPEQSLAC$_{119}$QC$_{121}$LVR

Figure S2.9. *Disulfide connectivity's in bBLG AB and chemically reduced bBLG R1 and R2. RP-HPLC profiles of bBLG AB, bBLG R1, and bBLG R2 after tryptic digest. Peaks were collected and selected for further analysis by MS and MS/MS. Grey bars are covering peaks that contain fragments with cysteines and the corresponding disulfide connectivity's as could be determined by MS/MS analysis. Fragments are given below the chromatograms. Asterisk marks the injection peak.*

2.6.6.3. Study of disulfide shuffling using peptide fragment 102-124 as standard

The disappearance of fragment 102-124 containing cysteines 106, 119 and 121 triggered us to synthesize a control peptide for comparison and to identify the position of the oxidized fragment in the chromatogram. An oxidative self-folding approach of the linear precursor molecule yielded 2 of 3 of the expected disulfide-bonded isomers with disulfide links between Cys106 and Cys119 (**peptide 1**) and Cys106 and Cys121 (**peptide 2**). Again, disulfide bonds were confirmed by the loss of signal intensity at the corresponding positions of the oxidized cysteines (***Figure S10***). A comparison of the obtained retention times for 1 and 2 with the chromatograms of the tryptic digest of bBLG AB, rBLG, and rBLG-SS was surprising as no peak was detected at the expected positions for these proteins. For rBLG-SH, a retention time of fragment 102-124 possessing the disulfide bridge between Cys106 and Cys119 was obtained that was eluting close to 1 with the same bond. As a consequence, we designed an approach to imitate the conditions during the tryptic digest and dissolved 1 and 2 in buffer at pH 8.0 and incubated those samples for approx. 5-10 min before subsequent analysis by RP-HPLC (***Figure S2.11***). An immediate decrease of the peak intensity of the expected isomer and, thus, a conversion into a mixture of further compounds primarily covering isomers 1 and 2 due to disulfide shuffling could be

observed. This disulfide shuffling effect was even stronger for 2 than for 1. This led us to conclude that fragment 102-124 that contains at least one reduced cysteine has a strong tendency to form immediately a mixture of differentially connected isomers as soon as it is released upon cleavage by trypsin. The occurrence of a mixture of potential fragments subsequently will lead to a reduction of the total intensity of the potential main fragment and, consequently, results in a significant signal reduction and formation of several differently connected variant of fragment 102-124. However, it cannot be excluded that alternative connectivity's are already preformed in the protein due to the close proximity of Cys121 to Cys119 and the disulfide bridge between Cys106 and Cys119.
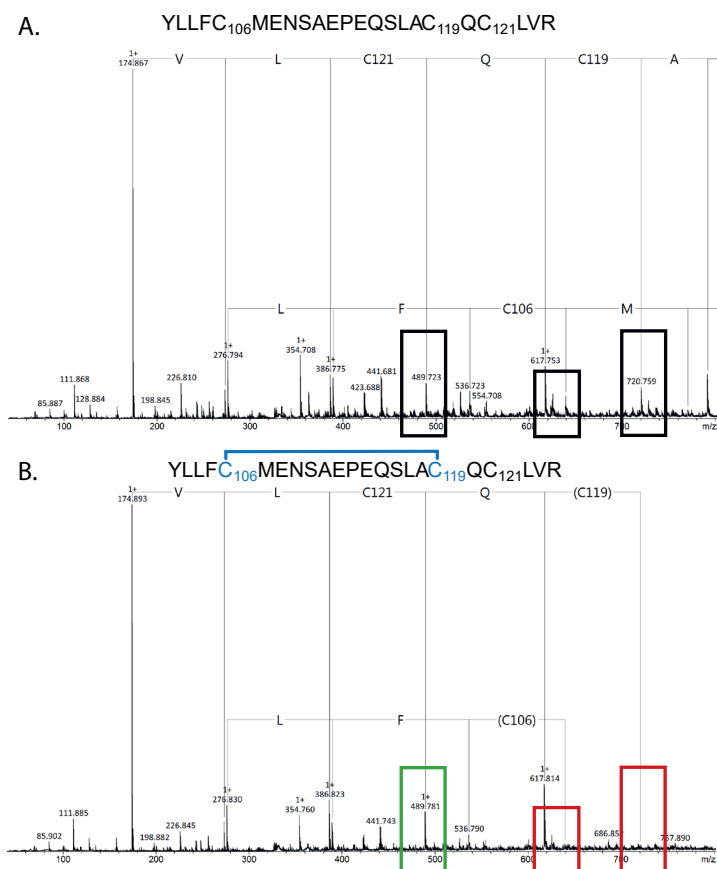

Figure S2.10. *Determination of disulfide connectivity's in (**A**) reduced fragment 102-124, (**B**) isomer 1 and (**C**) isomer 2 by MS/MS analysis. Relevant peaks for the determination of cysteine oxidation states are encircled. Color of the circle indicates either loss (red) or similar (green) signal intensity compared to the fully reduced fragment 102-124. A loss in signal intensity for fragment ions that contain Cys106, Cys119 or Cys121 indicated formation of a disulfide bond by the corresponding cysteine and confirmed the shown structure.*
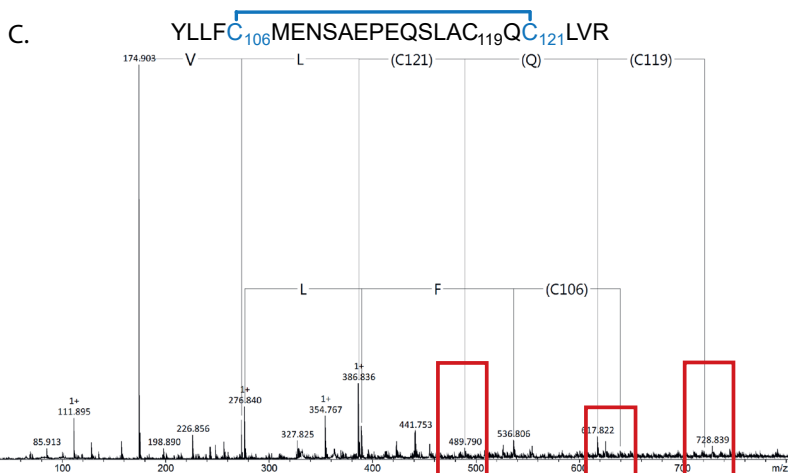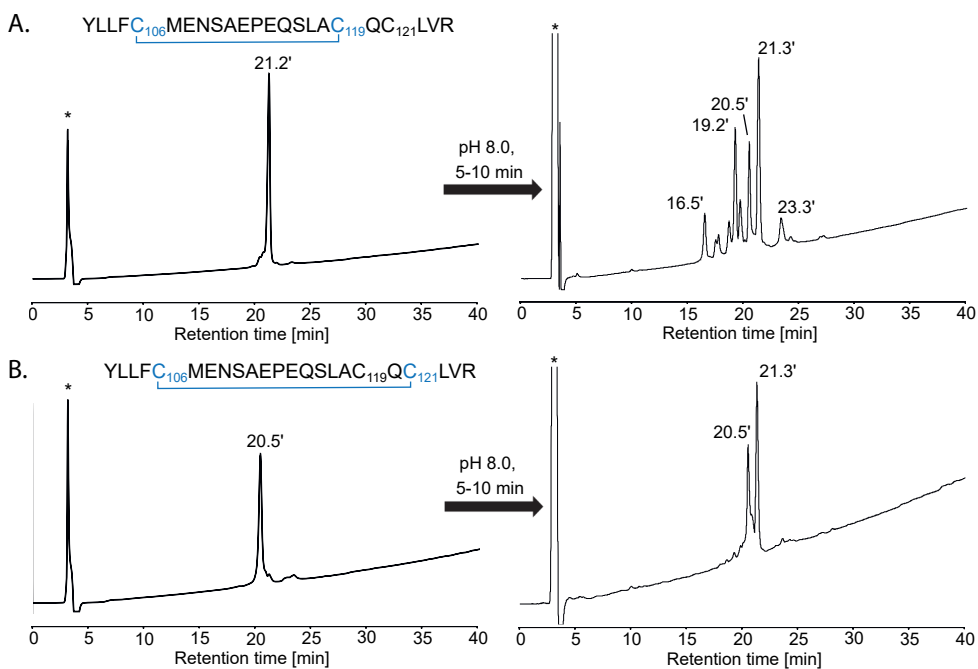
C.

Figure S2.10. Continued.

A.

B.

Figure S2.11. *Disulfide shuffling of pure isomers of fragment 102-124 (peptides 1 and 2) under mild basic conditions. RP-HPLC profiles of pure isomer 1 (A) and 2 (B) before (left) and after (right) incubation in buffer at pH 8.0. For analytical RP-HPLC the following gradient was used: 20–60% eluent B (0.1% TFA in acetonitrile) in eluent A (0.1% TFA in water) in 40 min. Asterisk marks the injection peak.*

To prevent disulfide shuffling during the analysis of the standard peptides a set of serine-substituted peptides was prepared in which either Cys106 (**peptide 3**, Cys119 linked to Cys121), Cys119 (**peptide 4**, Cys106 linked to Cys121), or Cys121 (**peptide 5**, Cys106 linked to Cys119) was replaced (**Table S2.7**). Unfortunately, in a co-elution experiment applying equimolar amounts of peptides 3-5, only one main peak was observed, in contrast to peptide isomers 1 and 2 with distinct separated peaks in the chromatograms of their mixtures (**Table S2.7**). As the behavior of the serine-substituted compounds 3-5 differs significantly from that of the non-substituted isomers 1 and 2 they do not qualify as standard controls.

2.6.6.4. Detailed methodology

Peptides were synthesized on an automated peptide synthesizer EPS 221 (Intavis Bioanalytical Instruments AG, Cologne, Germany) according to a standard Fmoc-protocol. Synthesis was performed on Rink amide MBHA resin with a loading capacity of 0.53 mmol/g (Iris Biotech GmbH, marktredwitz, Germany). Coupling reactions were performed as double couplings using Fmoc-amino acid derivatives activated with 2-(1H-benzotriazole-1-yl)-1,1,3,3-tetramethyluronium hexafluorophosphonate (HBTU) in the presence of DMF, and N-methylmorpholine. Fmoc removal was carried out by treating the resin twice with 20 % piperidine in N,N-dimethylformamide (DMF). All deprotection and coupling steps were followed by intensive washings using DMF. Peptide cleavage was initiated upon addition of 1 mL/100 mg resin reagent K (75 mg phenol, 25 µL ethandithiol, 50 µL thioanisol, 50 µL water in 1 mL TFA). After 3 h, crude peptides were filtered and precipitated in ice-cold diethyl ether, centrifuged and pellets were washed for several times with diethyl ether. Compound purity and identity were determined by analytical RP-HPLC analysis as mentioned above and MALDI-TOF or LC-ESI mass spectrometry (**Table S2.7**).

Peptide oxidation was performed as described earlier (Böhm et al, 2014). The linear precursor molecules (10 µM) were dissolved in Tris-buffer (0.1 M Tris-HCl, 1 mM EDTA, pH 8.7) and stirred on air for 19–72 h. Reaction monitoring was performed by RP-HPLC on a Shimadzu LC-10A system as mentioned above and the collected fractions were identified by MALDI-TOF or LC-ESI mass spectrometry. After completion of the reaction, the mixture was separated by semi-preparative HPLC using a Knauer Eurospher 100 column (C18, 250 x 32 mm, 5 µm particle size, 100 Å pore size) on a Shimadzu LC-8A system. A gradient was used with the elution system of 0.1 % TFA in water and 0.1% TFA in 90 % acetonitrile/water (**Table S2.7**). Fractions were frozen and freeze-dried for further analysis by tandem mass spectrometry (**Table S2.7**) on a ultrafleXtreme MALDI-TOF/TOF mass spectrometer (Bruker Daltonics GmbH, Bremen, Germany). Peptides were dissolved in alkaline buffer (0.2 M Tris-acetate buffer, 2 mM EDTA, pH 8.0). After sample preparation (app. 5-10 min) samples were injected into a Shimadzu LC-10A system as described above.

2.6.7. Tryptophan fluorescence of urea-denatured rBLG-C

To test whether rBLG-C has a fully unfolded conformation, it was checked whether further unfolding occurred in 8 M urea. In **Figure S2.12**, the tryptophan fluorescence of rBLG-C solubilized in a phosphate buffer or urea is shown. The urea fully unfolds the protein and thereby both tryptophan residues are exposed to the solvent, causing a red shift up to 355 nm. The shift between rBLG-C and rBLG-C in urea indicates a specific fold for rBLG-C, in which tryptophan residue W61 is only partially exposed.
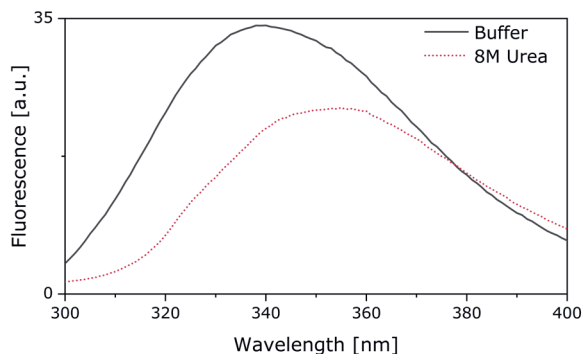

Figure S2.12. *Fluorescence emission spectra of rBLG-C solubilized in 10 mM sodium phosphate buffer (pH 6) and rBLG-C solubilized in 8 M of urea. Fluorescence was excited at 290 nm and emission spectra were recorded from 300 – 400 nm.*

2.6.8. Analytical ultracentrifugation

Prior to the analytical ultracentrifugation (AUC) experiments, the absorbance of the samples at 280 nm was measured to check whether the protein concentrations were similar. The exact measurements can be found in **Table S2.8**, as well as the calculated DM-ratio from the respective integrated sedimentation distribution peaks and the best-fit frictional ratio (f/f_0) of the protein samples. All variants were measured in triplicate; the first repetition was done with the same sample stored in the fridge and the third replicate was measured with a fresh sample.

Typically, the AUC results are highly reproducible. However partly reduced native BLG AB (sample 3) showed contradicting results even within repeated measurements. This sample was eight times freshly prepared and showed sometimes a monomer-dimer equilibrium with dominating dimers and another time with predominating monomeric species. This indicates that sample bBLG R1 is unstable and/or not homogenously reduced. Repetitions 3A und 3B as well as 4A and 4B were done with the exact same sample solution two demonstrate the flawless reproducibility within an AUC experiment.

Table S2.8. *Absorbances prior to AUC analysis, the dimer-to-monomer (DM) ratio and the fitted frictional ratios (f/f₀).*

Variant	Replicate	Abs @ 280 nm	DM ratio	Weight signal average sw / 10^{-13} s	f/f_0
bBLG B		0.80	3.58	2.48	1.138
		0.80	3.98	2.50	1.147
		0.77	2.65	2.46	1.138
bBLG AB		0.77	1.98	2.36	1.104
		0.78	2.05	2.41	1.127
		0.78	1.52	2.36	1.108
bBLG R1	3.1	0.71	6.09	2.25	1.123
	3.2	0.80	0.32	2.07	1.167
	3.3A	0.77	0.27	2.04	1.145
	3.3B	0.77	0.23	2.02	1.172
	3.4A	0.70	2.23	2.25	1.100
	3.4B	0.70	2.09	2.33	1.108
	3.5	0.76	2.65	2.21	1.148
	3.6	0.78	3.10	2.35	1.115
	3.7	0.77	2.37	2.38	1.156
	3.8	0.79	0.71	2.14	1.150
bBLG R2		0.57	0.07	1.94	1.194
		0.57	0.05	1.91	1.163
		0.79	0.07	1.93	1.172
rBLG		0.80	6.57	2.60	1.139
		0.80	5.43	2.62	1.142
		0.73	4.60	2.58	1.142
rBLG-SH		0.77	3.77	2.52	1.129
		0.77	5.37	2.53	1.112
		0.68	2.63	2.46	1.104
rBLG-SS		0.66	0.22	2.04	1.146
		0.78	0.25	2.03	1.122
		0.78	0.15	2.03	1.123
rBLG-C		0.69	2.08	1.98	1.296
		0.69	2.34	1.89	1.258
		0.59	2.22	2.03	1.181

2

The interpretation of the degree of dimerization via the evaluation of the integration of the peak areas depends on several factors. For example, the shape of the sedimentation coefficient distribution itself depends on the analysis procedure of the measured data as well as experimental parameters such as random and stochastic noise, rotor speed or measurement time. In addition, the dissociation rate will determine whether only one or two peaks are observed for monomer and dimer equilibrium. A more robust method for assessment of the dimerization is the consideration of the signal average sedimentation coefficient. To support our findings, this factor was evaluated for all our measurements and shown in *Table S2.8*. Both strategies follow the same trend, confirming that both approaches are valid and can be applied to observe relative differences between the samples. Furthermore, exact quantification of the dissociation constant would give more information about the exact quantities, but this is beyond the scope of the current work.

rBLG-C also contained a slow-sedimenting fraction, which might be attributed to be residuals of free DNA in the sample (see absorbance shift towards 260 nm in *Figure S2.13*). This might also have been caused by the unfolding of the protein, resulting in slower sedimentation due to loss in shape and therefore higher frictional coefficient. The large proportion of this fraction can also contribute to the fact that the supposed monomer-dimer equilibrium was shifted to the monomer fraction, as the overall concentration was adjusted based on the absorbance of the sample.
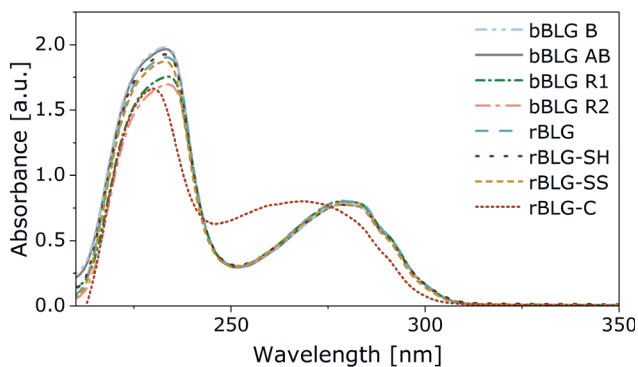

Figure S2.13. *Absorbance spectra of the respective BLG variants.*

2.6.9. Reversed-phase high performance liquid chromatography (RP-HPLC) analysis

Protein variants were eluted on a reversed-phase high-performance liquid chromatography column to observe differences in their binding affinity. The chromatograms are shown in *Figure S2.14*. For bovine BLG, variant B elutes earlier than variant A which is in accordance with literature (Keppler et al., 2021). The later elution of the relatively more hydrophilic BLG A is opposite to what is expected based on its surface hydrophobicity. This demonstrates the surface hydrophobicity does not dominate in determining the characteristic retention time in this case. Partial and complete reduction only led to a change in retention time for BLG A, as changes in the folding can alter the affinity for the column. The chromatogram of the recombinant variants is shown in *Figure S2.14B*. Substitution of cysteine residues with alanine residues in rBLG-SH and rBLG-SS resulted in earlier elution, possibly due to the lower hydrophobicity of the introduced alanine residues. Although the opened structure of rBLG-SS might also have an impact. Interestingly, substitution of all cysteine residues (rBLG-C) resulted in two distinct peaks, containing variants with similar or longer retention as compared to rBLG. As rBLG-C is mostly unfolded, hydrophobic amino acid sequences that are usually buried in the hydrophobic core are exposed to the surface. This could cause a higher affinity with the hydrophobic column and will thereby result in a later elution as compared to folded BLG. The second earlier peak might be due to association of rBLG-C through intermolecular hydrophobic interactions, which subsequently could lower the interaction of these sequences with the column, resulting in an earlier elution (more similar to bovine BLG).
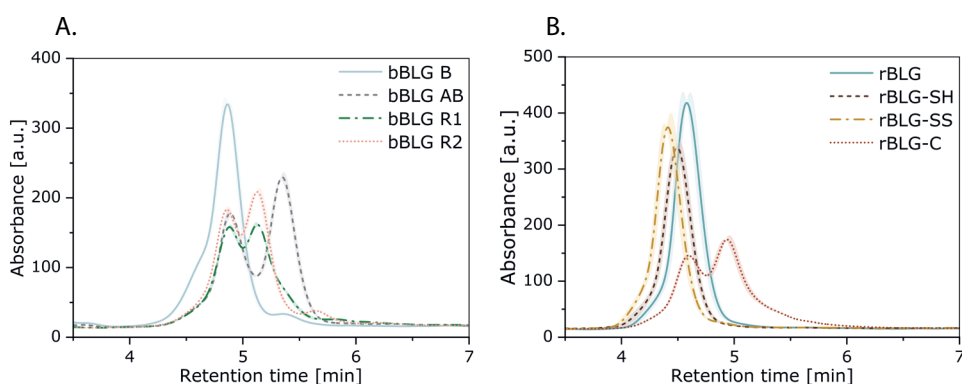

Figure S2.14. Chromatogram for (A) bovine and (B) recombinant BLG variants. Standard deviation is based on independent duplicates.

Method: Samples were solubilized in concentrations of 1 mg mL^{-1}. The samples were analyzed with a UltiMate 3000 HPLC system equipped with a UV detector at 214 nm

(Thermo Fisher Scientific) and a VDSpher Optibio PUR 300 C4-SE column (150 mm Length, 4.6 mm inner diameter, 5 µm particle size; VDS optilab, Berlin, Germany). Mobile phase A contained Milli-Q water and mobile phase B contained acetonitrile, both with 0.1% TFA. A gradient elution was performed at a flow rate of 1 mL min^{-1}, from 40 to 50% mobile phase B (v/v) in 9 min. The column temperature was maintained at 30 °C.

2.6.10. Isoelectric point analysis

The surface charge (i.e., zeta potential) of the variants was measured as a function of pH (6 to 4) to find the isoelectric point (pI). For bovine BLG, values are in line with literature, which reports values between 4.7–5.4 (Haug et al., 2009). Both chemical reduction and recombinant substitution were not found to impact the isoelectric point.

Table S2.9. *Isoelectric point of BLG variants. Average and standard deviation is based on dependent triplicates.*

Protein variant	Isoelectric point [-]
bBLG B	4.58 ± 0.16
bBLG AB	4.88 ± 0.08
bBLG R1	5.03 ± 0.03
bBLG R2	5.05 ± 0.03
rBLG	4.94 ± 0.02
rBLG-SH	4.88 ± 0.07
rBLG-SS	5.02 ± 0.02
rBLG-C	4.87 ± 0.03

Method: protein solutions were prepared in a concentration of 1 mg mL^{-1}. The zeta potential was then measured as a function of pH, using the zetasizer (Zetasizer nano, Malvern Panalytical, Almelo, The Netherlands) attached to a MPT-2 Multi-purpose Titrator (Malvern Panalytical). About 10 mL was loaded into the titrator and the disposable folded capillary zeta cell (Malvern Panalytical) was filled. The titrator was set to change the pH from 6 to 4 with steps of 0.5, using titrants of 0.1 M HCl, 0.025 M HCl and 0.1 M NaOH. The sample settings were set using the refractive index of protein (1.45) and using water as a dispersant. The sample was left to equilibrate 60 s prior to each measurement, and was measured three times. Each measurement had a minimum of 10 and a maximum of 100 runs. Each protein was analyzed in independent triplicates.

2

3

Simple purification of recombinant β-lactoglobulin using polyphosphate
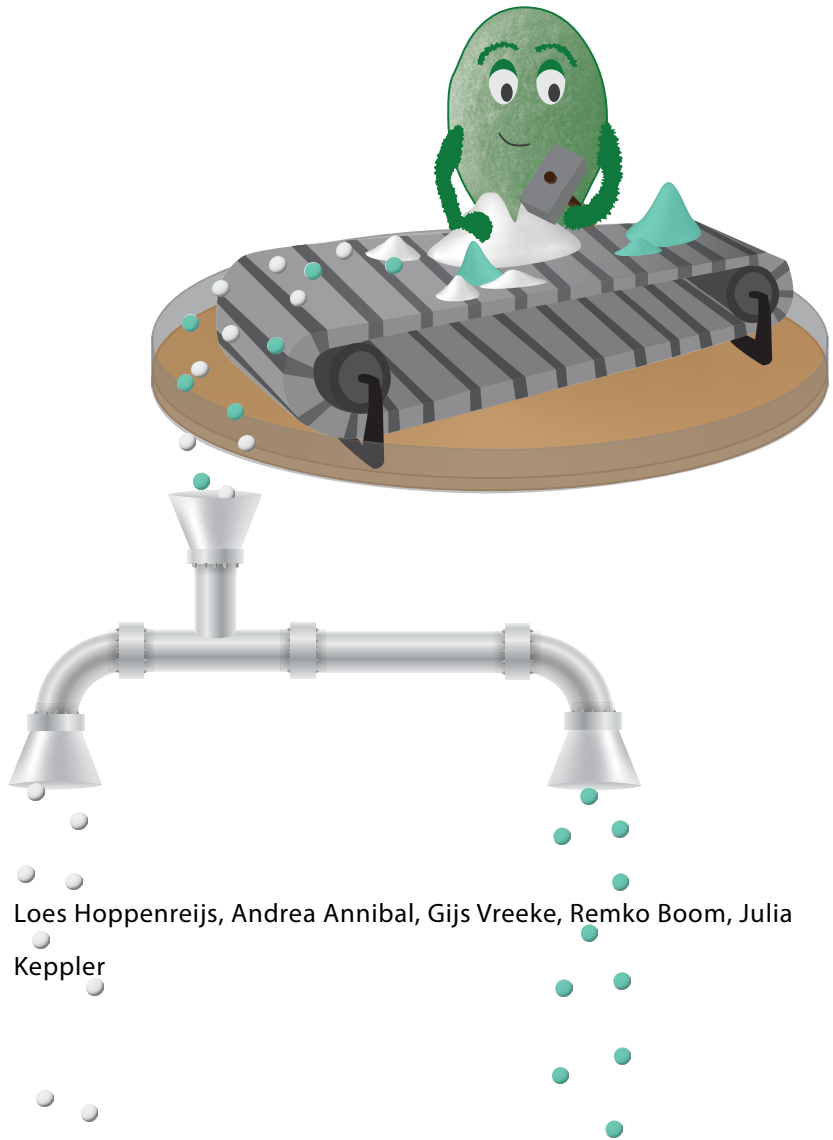
Loes Hoppenreijs, Andrea Annibal, Gijs Vreeke, Remko Boom, Julia Keppler

Proteins produced through precision fermentation are often purified through chromatographic methods, while scalable and cost-effective purification methods are desired for food application. Here, we present a relatively simple method for purification of protein produced from yeast, using BLG secreted from *Pichia pastoris* as an example. The food-grade salt hexametaphosphate (HMP) was used to precipitate the protein at acidic pH, while the impurities (extracellular polysaccharides; mainly mannan) remained soluble. After re-solubilization of the protein-HMP complex by neutralization, excess HMP was selectively precipitated using calcium chloride. Finally, the protein content of the crude sample increased from 24 to 72 wt% (comparable to purification with anion exchange chromatography), containing residual polysaccharides (9 wt%) and HMP (1 wt%). The established method had no significant impact on the structural and functional properties (i.e., emulsification) of the protein. The presented method shows potential for cost-effective purification of recombinant proteins produced through yeast-based expression systems.

Abstract

Abbreviations: Bicinchoninic acid assay, BCA assay; extracellular polysaccharides, EPS; fourier transform infrared spectroscopy, FTIR; hexametaphosphate, HMP; high performance anion-exchange chromatography with pulsed amperometric detection, HPAEC-PAD; isoelectric point, IEP; recombinant β-lactoglobulin produced from yeast, yBLG; sodium dodecyl sulfate-polyacrylamide gel electrophoresis, SDS-PAGE; ultra-performance liquid chromatography coupled with a photodiode array detector and mass spectrometry, UPLC-PDA-MS; whey protein isolate, WPI; β-lactoglobulin, BLG.

3.1. Introduction

Precision fermentation is gaining attention to produce animal proteins on an industrial scale without the need of livestock. These so-called 'recombinant' or 'heterologous' proteins are produced through modified micro-organisms, such as bacteria, fungi or yeasts (Linder, 2023). Recombinant proteins can closely resemble the natural protein in terms of sequence and structure, and thereby also its nutritional value and functionality (Keppler et al., 2021). In addition, controlled modifications can be applied through gene mutations to design protein structures for superior functionality, for example, to alter protein stability (**Chapter 2**), modulate protein-protein interactions (**Chapter 6** and **Chapter 7**; Sakurai & Goto, 2002), improve digestibility (Yagi et al., 2003) or decrease allergenicity (Kazem-Farzandi et al., 2015).

The use of precision fermentation for recombinant food proteins has made significant progress in recent years, especially for egg and milk proteins. The major whey protein β-lactoglobulin (BLG) has been commercialized already since it has no intricate post-translational modifications, such as glycation or phosphorylation (Linder, 2023). In addition, BLG is interesting from a functionality point of view, showing excellent gelling and surface activity (Tomadoni et al., 2020). It has been successfully produced and secreted in soluble form from the yeast *Pichia pastoris* (also called *Komagataella phaffii*) in many studies (Denton et al., 1998; Jayat et al., 2004; Wilson et al., 1999; Yagi et al., 2003). Denton et al. (1998) reported the presence of soluble polysaccharide impurities after production of BLG by *P. pastoris*, but not their identity. For *Saccharomyces cerevisiae*, mannan in particular is released into the growth medium, due to damaging of the outer cell wall (Chlup et al., 2007) or its release upon growth and autolysis (Giovani et al., 2010). In contrast, Krátký et al. (1975) found that the released mannan does not originate from the cell wall, but is mostly secreted. To separate the target protein from such soluble cellular impurities, as well as the growth medium, extensive purification of recombinant proteins is often achieved through chromatography. Especially ion-exchange chromatography, as this technique is well-established and yields high purity products (Saraswat et al., 2013). Application of these methods on the scales necessary for commercial production of food proteins is challenging, as they require high investment, have low throughput (while being difficult to adapt for continuous operations), and dilute the product (thus necessitate re-concentration) (Agyei et al., 2016; Rudge & Ladisch, 2019). Thereby, we aim to explore a method that promises to be better suited for food production, in terms of costs and sustainability.

Precipitation of proteins using the food-grade salt sodium hexametaphosphate (HMP), also called 'Graham's salt', at acidic pH is a relatively old purification method. For example, it has been used to purify rapeseed protein (Thompson et al., 1976) and

fish protein (Pelroy & Spinelli, 1971), and to recover protein from whey (Hidalgo et al., 1973). We hypothesize that we can use a similar method to separate yeast-based recombinant proteins from polysaccharide impurities, due to their opposite charge at acidic conditions. The precipitation allows separation of the target protein, but also concentration, which is an advantage over conventional chromatographic methods.

In the current study, we therefore evaluate whether we can purify recombinant BLG (genetic variant A) produced from *P. pastoris*, using protein precipitation induced by HMP. We present a possible mechanism for the precipitation, an optimization of the method, and give an outlook for future application. To understand how (i) the recombinant expression and (ii) the purification method affects the protein, we also investigate their impact on BLG sequence, (secondary) structure and functionality (i.e., emulsification).

3

3.2.   Materials & methods

3.2.1.   Materials

Crude recombinant BLG produced by the yeast *P. pastoris* (crude yBLG) was provided by Formo (Berlin, Germany). Fermentation was based on a standard protocol from Invitrogen (USA) for the fermentation of *P. pastoris*, similar to Wilson et al. (1999). *P. pastoris* cells were transformed with a plasmid that encoded BLG isoform A: The sequence was retrieved from Uniprot (P02754) and cloned in an already described optimized expression plasmid pAaZBgl (Ahmad et al., 2014), under a methanol inducible promotor AOX1 (Kielkopf et al., 2021). In addition, an α-mating factor signal peptide (from *Saccharomyces cerevisiae*) was included in the sequence to allow secretion of the expressed protein (Lin-Cereghino et al., 2013). After production, the cell broth was harvested and micro-filtrated using 0.2 μm cassettes (Hydrosart Slice, Sartorius, Germany) and subsequently filtered using 10 kDa cassettes (Hydrosart Slice) to obtain the filtered cell broth (crude yBLG). Bovine BLG (mix of genetic A and B variants; bBLG) was isolated from whey protein isolate (WPI; BioPro, Davisco, USA) according to **Chapter 2** and was used as reference.

3.2.2.   Purification method

Approximately 10 mg mL^{-1} protein solution was prepared and sodium HMP (Sigma Aldrich, USA) was added (HMP:BLG molar ratio of 10:1). The solution was hydrated for one hour, while slowly rotated in a carrousel. The pH was then adjusted to 4.0 using 1 M HCl and the solution was rotated for another hour at room temperature. The (protein-rich) precipitate was separated from the soluble fraction using centrifugation (4,816 g for 1 h; Legend XFR, Sorvall™, ThermoFisher Scientific, USA), after which the supernatant was removed by decanting. The precipitate was then re-solubilized by first adding 100 μL of ultrapure water, mixing and then slowly adding 1 M sodium hydroxide to adjust the pH to 7.0. Thereafter, calcium chloride (CaCl$_2$) was added (to a final concentration of 150 mM) and the sample was incubated by rotating for 1 h at room temperature to selectively precipitate HMP. The insoluble fraction was removed by centrifugation (maximum speed of 4,816 g for 1 h). The (protein-rich) supernatant was collected by decanting and was then dialyzed (Slide-A-Lyzer MINI Dialysis Devices, 10K MWCO, 2 mL; ThermoFisher Scientific) and subsequently freeze-dried (Beta 2–8 LSCplus, Martin Christ, Osterode am Harz, Germany). An overview of the purification method is shown in **Figure 3.1**.
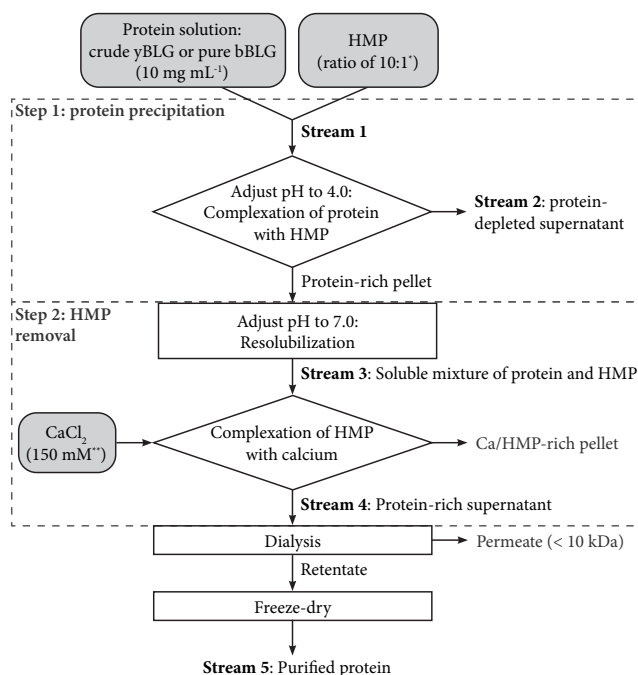
Figure 3.1. *Flow chart of the purification process with optimal conditions. *For bovine BLG, a HMP:BLG molar ratio of 2:1 was optimal. **The indicated concentration was obtained after adding CaCl$_2$ to stream 3.*

3.2.2.1. Establishing the purification method

The purification method depicted in **Figure 3.1** includes two major steps: (1) the precipitation of protein by HMP and (2) the removal of HMP. Several conditions were tested to optimize these steps for both bBLG and yBLG, as listed in **Table S3.1**, in independent duplicates. To optimize step (1), the protein-rich pellet was dried and weighed, and the protein-depleted supernatant was analyzed for its protein content using a bicinchoninic acid (BCA) assay. To confirm the presence and size of residual protein in the supernatant, the protein-depleted supernatant was also analyzed with SDS page (without any further dilution; **Figure S3.3**). For evaluation of step (2), different amounts of CaCl$_2$ were added (50–200 mM; **Table S3.1**) to stream 3 (i.e., resolubilized protein solution with HMP; **Figure 3.1**) to induce precipitation of HMP, while keeping the protein solubilized. Subsequently, the HMP-rich pellet was dried and weighed, and the protein-rich supernatant was analyzed with FTIR and an assay for total phosphorus content.

3.2.3. Mass balance of the streams throughout purification

The final purification method (**Figure 3.1**) was applied to the filtered cell broth in independent duplicate. Pure bBLG was treated with the same method, as a control. The volumes of the streams were estimated by weighing and converting the weight using the density of water (0.997 g mL^{-1}). Samples were taken throughout the purification process (for all the streams indicated in **Figure 3.1**) and lyophilized (Beta 2–8 LSCplus) to obtain the dry matter content. The carbohydrate, protein and HMP content of the powders was determined as explained the following section. A mass balance was made using these contents, the dry matter content and approximate volumes of the streams. The software e!Sankey calc (Version 5.2.1) to make a Sankey diagram.

3.2.3.1. Composition

3.2.3.1.1. Protein analysis by BCA assay

The protein content was determined using the bicinchoninic acid (BCA) method (Pierce BCA Protein Assay Kit; Thermo Fisher Scientific). Bovine Serum Albumin that was used for calibration in the range of 20 to 2,000 µg mL^{-1}. The absorbance was measured using DR6000 UV/VIS Spectrophotometer (Hach, Loveland, USA) at 562 nm. All measurements were performed in independent duplicates.

3.2.3.1.2. Protein composition by Gel electrophoresis

After precipitation of protein by HMP, supernatants were analyzed with sodium dodecyl sulfate-polyacrylamide gel electrophoresis (SDS-PAGE). Materials were used from Bio-Rad Laboratories Inc when not specified further. A reducing sample buffer was prepared by mixing the Laemlli sample buffer with 2-mercaptoethanol (9:1 v/v; Sigma Aldrich, USA). Samples were diluted with the reducing sample buffer (1:1 v/v) and heated at 100 °C for 10 minutes. The running buffer (10x Tris/Glycine/SDS) was prepared by a ten times dilution with ultrapure water. A 12% pre-cast gel (Mini-PROTEIN TGX™) was placed in the gasket, which was subsequently filled with the running buffer. Per well, 20 µL of sample or 5 µL of marker (Precision Plus Protein™ Dual Color) was added. Also untreated crude yBLG (0.5 mg mL^{-1}) was added as a reference. The buffer tank was completely filled with running buffer and the page was ran at 200 V until the marker reached the bottom of the gel. Gels were washed twice using water, stained for about one hour using a Coomassie staining solution (Bio-Safe™) and washed with water. Gels were scanned using a densitometer (GS-900). For crude yBLG, also the protein purity was determined by comparing the intensity of the band to bBLG (0.5 mg mL^{1}; protein content of 98% by Dumas), both obtained through Image Lab Software (version 6.1.0).

3.2.3.1.3. Composition by Fourier-Transform Infrared spectroscopy

Fourier-Transform Infrared spectroscopy (FTIR) was used to screen for changes in the protein content, while observing relative decreases in (carbohydrate) impurities and/or HMP. Protein powders were solubilized at a concentration of 50 mg mL^{-1} in ultrapure water, while liquid samples were analyzed without further dilution. An Invenio-S system (Bruker, USA) with a liquid nitrogen cooled MCT detector was used with the OPUS software (Bruker). Samples (20 µL) were loaded on the surface of attenuated total reflection crystal (Bio-ATR; Bruker) and left to equilibrate for two minutes before starting the measurement. Measurements were performed at 25°C using ultrapure water as the background and averaged over 64 scans at a resolution of 4 cm^{-1}.

Also the protein content was determined using FTIR through integration of the amide I region (1600-1700 cm^{-1}) of the spectra without manipulation. A calibration was performed using standard solutions of bBLG (5–100 mg mL^{-1}) and values were determined based on independent duplicates. Finally, to observe differences in protein conformation; spectra were vector normalized in the amide I region using nine smoothing points and subsequently the second derivative was determined. All data manipulation was performed in the software OPUS (version 8.5; Bruker).

3.2.3.2. Assay for total phosphorus

To determine the HMP content of the sample, an assay was used to quantify the total phosphorus in the samples, based on the manual of the Total Phosphorus Kit (Megazyme, Ireland). First, solution A was prepared by solubilizing 10 wt% ascorbic acid in 1 M HCl. Besides, solution B was prepared by solubilizing 5 wt% ammonium molybdate in ultrapure water. The reagent was made by mixing solutions A and B in a volume ratio of 5:1. For calibration, HMP standards were prepared in the range of 17–171 µM. One mL of sample or standard was then added to 0.5 mL reagent and incubated for 1 h at 40 °C, while mixing in an Eppendorf shaker. The absorbance was measured at 655 nm. Ultrapure water was used as a blank and measurements were performed as independent triplicates.

3.2.3.3. Carbohydrate analysis (HPAEC-PAD)

The carbohydrate content and composition were determined after extensive hydrolysis, according to Pandeirada et al. (2021). First, 10 mg of the material was transferred to Kimax tubes. Pre-hydrolysis was performed with 72 wt% sulfuric acid (H_2SO_4) for 1 h at 30 °C, followed by further hydrolysis with 1 M H_2SO_4 for 3 h at 100 °C. After cooling, the hydrolysates were diluted and analyzed with High Performance Anion-Exchange Chromatography using Pulsed Amperometric Detection (HPAEC-PAD). In short, an HPLC system (ICS5000, Dionex, USA) was equipped with a guard column (2 mm ID x 50 mm) and HPAEC column (2 mm ID x 250 mm; both CarboPac

PA1, Dionex) at 20 °C. Ten µL was injected and eluted using a flow rate of 0.4 µL min^{-1}, using the following eluents: 0.1 M sodium hydroxide (NaOH; eluent A) and 1.0 M NaOAc in 0.1 M NaOH (eluent B). The elution gradient can be found in Pandeirada et al. (2021). Identification and quantification was performed using standards of glucose, mannose and glucosamine (all Sigma Aldrich) in the range of 5–50 µg mL^{-1}.

3.2.4. Detailed protein analysis

After purification with the established method (**Figure 3.1**), purified yBLG was analyzed for its sequence according to **Section 3.2.4.1**. Besides, both bBLG and yBLG were further characterized in terms of structure (**Section 3.2.2.1.3**) and functionality (**Section 3.2.4.2**), before and after treatment with the established purification method.

3.2.4.1. Protein sequence and purity (UPLC-PDA-MS)

The protein purities of bBLG and crude yBLG were determined with ultra-performance liquid chromatography coupled with a photodiode detector and mass spectrometry (UPLC-PDA-MS). Chemically reduced and diluted protein solutions (0.5 mg mL^{-1}) were injected (4 µL) on the Acquity Premier UPLC equipped with PDA and the Select Series Cyclic IMS (Waters, USA). Separation was performed on the Acquity Premier peptide column (BEH C18, 2.1 mm x 150 mm, 300 Å, 1.7 µm) with a gradient of 1% ACN with 0.1% TFA in UPLC-MS grade water (mobile phase A) and 1% UPLC-MS grade water with 0.1% TFA in ACN (mobile phase B). The gradient, sample preparation and mass spectrometer settings were similar as described previously by Vreeke et al. (2023). To evaluate whether BLG was modified upon recombinant expression, the mass of the each peak was analyzed by deconvolution of the charge state envelope using the Maxent function in the Masslynx software (version 4.2). The absolute protein concentrations (µM) were calculated using the UV peak areas at 214 nm and the molar extinction coefficients of bBLG A (293,351 L mol^{-1} cm^{-1}) and bBLG B (293,373 L mol^{-1} cm^{-1}) and yBLG (303,151 L mol^{-1} cm^{-1}), according to:

$$[BLG] = (A_{214}\,Q)/(\varepsilon_{214}\,l\,V_{inj}\,k_{cell})$$

where A_{214} (µAU min) is the UV peak area at 214 nm, V_{inj} (µL) is the volume of sample injected, Q (µL min^{-1}) is the flow rate (350 µL min^{-1}), ε_{214} (L mol^{-1} cm^{-1}) the molar extinction coefficient and l (cm) is the path length of the UV cell (according to the manufacturer). The cell constant, k_{cell} for the UV detector was 0.78, as previously determined (Vreeke et al., 2022).

The sequence of yBLG was analyzed according to Vreeke et al. (2022), using bBLG as a control. Both yBLG and bBLG (after purification) were hydrolysed with bovine trypsin (enzyme to substrate molar ratio of 1:25; at 37 ºC) in a 50 mM TRIS-HCl buffer pH 8.0 for 2 h. The obtained hydrolysates were mixed (1:1, v/v) with 50 mM TRIS-HCl buffer containing 20 mM dithiothreitol and incubated for 2 h to reduce the disulfide bonds.

Afterward, the hydrolysates were diluted five times with mobile phase A, acidified to pH 2.0, and subsequently centrifuged for 10 min at 14,000 g. The supernatant was injected on the UPLC-PDA-MS. The mass spectra were matched to peptide sequences with UNIFI software (version 1.8), according to the guideline and criteria for MS/MS fragments listed in Vreeke et al. (2022).

3.2.4.2. Emulsifying properties

To test the influence of the recombinant expression and the impact of the purification method on the protein functionality, both bBLG (before and after treatment) and yBLG (crude and purified) were used to prepare emulsions. Sunflower oil (local supermarket Jumbo) was stripped from surface active compounds by overnight incubation with alumina powder (1:3 v%), while rotating (Berton et al., 2011). Most alumina was removed again by centrifugation (2,000 g at 20 °C for 20 min); Residual alumina was removed with additional centrifugation at 10,000 g at 20 °C for 30 min. Besides, protein solutions were prepared (0.1 wt%) in a 10 mM phosphate buffer (pH 7.0). Coarse emulsions were produced by mixing the stripped sunflower oil (10 wt%) and protein solution, using a high-speed blender (UltraTurrax, IKA-Werke GmbH & Co., Germany) at 11,000 rpm for one min. The final emulsion was obtained by passing the coarse emulsion five consecutive times through a high-pressure M-110Y Microfluidizer (Microfluidics, USA) at 300 bars, while cooled with ice water. Emulsions were prepared in independent duplicates.

The droplet size distribution was measured on the same day, using a Mastersizer 3000 (Malvern Instruments, United Kingdom). For the material properties, the refractive index was set at 1.47 (sunflower oil) and 1.33 (water), the absorption index at 0.001 and density at 0.92 g cm^{-3}. Measurements were averaged over three runs, and a general-purpose analysis model was applied to obtain the mean diameter of the volume-weighted distribution ($d_{4,3}$) (Malvern Panalytical, United Kingdom). The emulsions were analyzed in dependent duplicates.

3.3. Results and discussion

The composition of recombinant BLG produced from yeast, prior to any further treatment (referred to as 'crude yBLG'), is discussed in **Section 3.3.1**. Subsequently, the establishment of the purification method is described in **Section 3.3.2**, demonstrating the possible mechanism and suitable conditions. The established purification method was then applied to crude yBLG, using bBLG as a control, and the major components throughout the process were quantified in **Section 3.3.3**. Lastly, an outlook is presented in **Section 3.3.4**, discussing future application of the proposed purification method for downstream processing of the cell broth. The latter includes an evaluation of the impact of the recombinant expression and downstream processing on the structure and functionality of the recombinant BLG, as well as suggested improvements for upscaling and the application range.

3.3.1. Sample composition prior to treatment

3.3.1.1. Quick first impression of the composition by ATR-FTIR

Fourier-transform infrared spectroscopy (FTIR) was performed as a first indication of the impurities present in the samples prior to treatment, as shown in **Figure 3.2**. Bovine BLG has characteristic peaks in the amide I (1700-1600 cm^{-1}) and amide II (1600-1500 cm^{-1}) regions, primarily due to stretching vibrations of C=O and bending of N-H/C-N in the peptide bonds, respectively (Barth, 2007). Absorption in these regions was lower in the crude yBLG as compared to bBLG, indicating lower protein content. Besides, major bands around 1200–900 cm^{1} were observed that are indicative for the presence of polysaccharides, due absorption of C-O-C and C-O-H linkages (Baca-Bocanegra et al., 2022). Denton et al. (1998) also reported the presence of polysaccharides in isolates of recombinant BLG produced by *P. pastoris*.
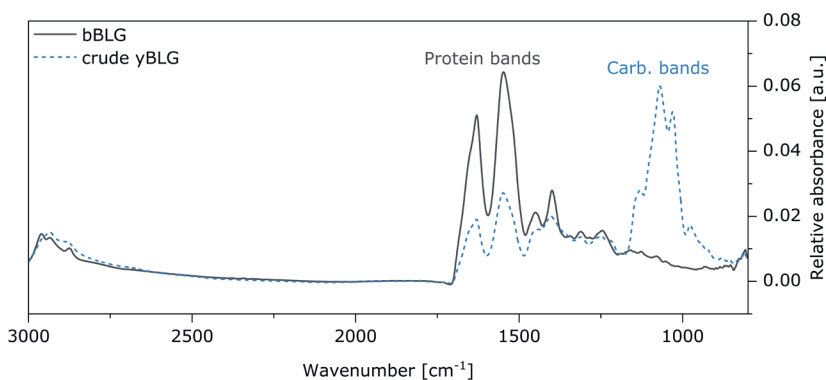

Figure 3.2. *FTIR spectra of bovine BLG (bBLG) and crude recombinant BLG (yBLG) without manipulation. Characteristic bands for both protein and carbohydrates are indicated.*

3.3.1.2. Further analysis of extracellular polysaccharides

After hydrolysis of the polysaccharides, the sugar content was 53 ± 1 wt%. Further identification of the sugar building blocks in the crude yBLG sample revealed that the polysaccharides consisted of mannose (91.2 ± 0.7 mol%) and minor amounts of glucose (3.8 ± 0.3 mol%) and glucosamine (5.0 ± 0.4 mol%). Similarly, Farinha et al. (2022) showed that the building blocks of water-soluble polysaccharides from *P. pastoris* were mainly mannose, which originate from mannan, with minor traces of glucose and glucosamine (2–5%). Vinogradov et al. (2000) had isolated and characterized the mannans from *P. pastoris* and found that a fraction of the oligosaccharide side chains was substituted with glucose or glucosamine through a phosphodiester linkage, resulting in a charged acidic mannan.

3.3.1.3. Protein quantification: impact of impurities

The presence of impurities in the crude yBLG sample could further interfere with protein quantification, depending on the method used. Therefore, several protein quantification methods were compared: UPLC, BCA assay, SDS-PAGE, FTIR, and Dumas. The protein purities of bBLG and crude yBLG based on these methods are listed in ***Table 3.1***. The total protein content of the crude yBLG was overestimated by the Dumas method, suggesting the presence of non-protein nitrogen containing impurities. These impurities include, for example, host-cell related compounds (such as glucosamine in mannan), or residual process-related impurities (such as ammonium), although the latter are expected to be mostly removed during ultrafiltration (cut-off value of 10 kDa). As polysaccharides impurities also contain a carbonyl group that can absorb in the amide I region of the FTIR spectra, their presence can also lead to overestimation of the protein content as determined by FTIR.

Table 3.1. *Purity of the materials (amount of protein on dry weight basis) determined with several methods. [1]Quantification with UPLC-PDA was performed using the extinction coefficient calculated based on amino acid sequence. Standard deviation based on the integration of the UV area. [2]For Dumas, a protein factor of 6.29 assumed for quantification. [3]Protein content was not applicable, as bBLG was used for quantification.*

Variant	UPLC-PDA[1]	BCA	SDS-Page	FTIR	Dumas[2]
bBLG	91 ± 6	93 ± 3	n.a.[3]	n.a.[3]	98 ± 0
Crude yBLG	17 ± 6	26 ± 0	25 ± 2	30 ± 0	35 ± 0

The protein content obtained from analysis using the BCA assay and SDS-PAGE were found to be in a similar range (25-26%), while the protein content obtained by UPLC-PDA was slightly lower (17%). Due to separation before (protein specific) detection, the protein content determined by UPLC-PDA is expected to be the least affected

by the impurities. The BCA assay is based on the reduction of copper ions by the peptide chain, which results in colour formation. Reducing sugars might also have interfered with this reaction, but according to Noyes et al. (2014), the absorptivity of polysaccharides is limited because of the localization of reducing groups, as well as the low number of reducing groups per polysaccharide. To verify this, mannan (from the yeast *Saccharomyces cerevisiae*; Sigma Aldrich) was subjected to the BCA assay and the absorbance response of this material was only about 1%, as compared to the response of BLG in the same concentration range (0.5–2 mg mL^{-1}; data not shown). Since the BCA assay is simple and found to be reliable, further protein quantification was performed using this method.

3.3.1.4. Checking for protein degradation

In general, secreted proteins can potentially be degraded in the cell broth by secreted proteases or intracellular proteases that are released upon cell death (Jahic et al., 2006). Thereby, the amount of BLG in the crude yBLG was further analyzed with UPLC-PDA-MS to check for other protein impurities. This showed a single peak in the chromatogram (***Figure S3.1***) with several masses around 18–19 kDa (***Figure S3.2***). Also, a single band was observed in SDS page (***Figure S3.3***). These different masses were annotated as BLG variants, as further discussed in ***Section 3.2.4.2***. Smaller peptides were not observed, indicating minimum protease presence and/or activity (***Figure S3.2***). The occurrence of cell lysis was monitored by the manufacturer and was not found throughout the production. Thereby, we conclude that potential protein impurities were either produced in low amounts and/or might have been removed prior due to the filtration step (< 10 kDa).

3.3.2. Establishing the purification method

Precipitation of proteins around the isoelectric point (IEP) has been previously used, for example, to enrich BLG from whey (Amundson et al., 1982). Thereby, the pH of a solution with crude yBLG solution (10 mg mL^{-1}) was adjusted to the IEP of BLG (pH 5.0; ***Table S3.2***), but the solution remained clear (data not shown). This indicated that the carbohydrate impurities counteracted the protein precipitation. Precipitation at pH 3.6 was also tested (measured IEP of the crude BLG material; ***Table S3.2***), but only little amount of the material precipitated (~ 8 wt%) and the protein purity in the precipitated material only increased to ~ 57 wt% (data not shown). Thereby, the use of the precipitation agent HMP was further evaluated to stimulate protein precipitation for purification. This method is shown in ***Figure 3.1*** and includes two major steps: the precipitation of protein by hexametaphosphate (HMP; ***Section 3.3.2.1*** and ***Section 3.3.2.2***) and the removal of HMP (***Section 3.3.2.3***).

3.3.2.1. Precipitation of bBLG using HMP: Suitable conditions and mechanism

The protein precipitation induced by HMP was first investigated for the bovine BLG to screen for suitable conditions with highly abundant material. Different pH values and HMP concentrations were investigated (**Table S3.1**). The precipitated weight fraction upon addition of different HMP concentrations at pH 3.0 and 4.0 is shown in **Figure 3.3A**.
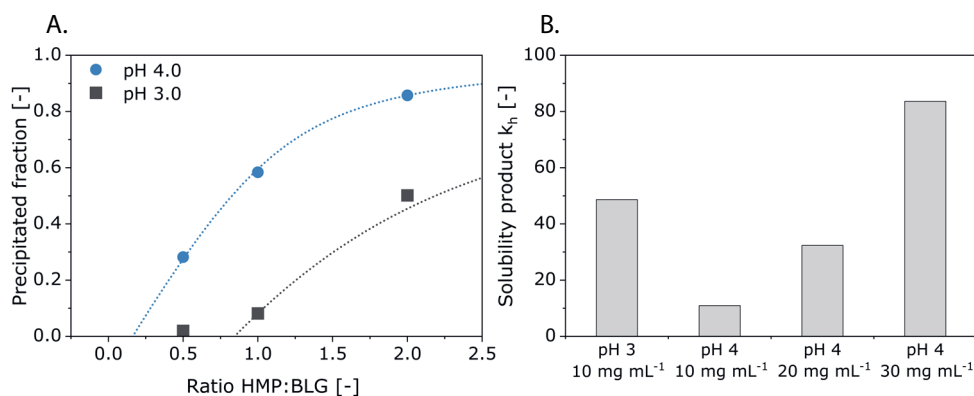

Figure 3.3. (**A**) The precipitated sample fraction (based on weight) for precipitation of bBLG at pH 3.0 and 4.0 (10 mg protein mL^{-1}). The dotted line indicates the fitted complexation model (**Equation S3.6E**). (**B**) The solubility constants derived from the complexation model established at pH 3.0 and 4.0 (10 mg protein mL^{-1}), as well as different protein concentrations (20 and 30 mg protein mL^{-1}; **Figure S3.4**). A smaller solubility constant implies poorer solubility and therefore a higher tendency for precipitation.

Precipitation of bBLG occurred both at pH 3.0 and pH 4.0, but relatively more precipitation was observed at pH 4.0 (**Figure 3.3**). At acidic pH, BLG has a positive net surface charge (IEP ~ 5.0), while HMP is negatively charged (**Supporting information 3.5.4.1**). These opposite charges induce attractive ionic interaction, which can result in cross-linking between proteins by HMP, when HMP interacts with at least two protein molecules. Subsequent cross-linking between protein and HMP ions can ultimately lead to the formation of sufficiently large flocs that precipitate. The attractive force between HMP and BLG was calculated to be more favourable at pH 4.0, as compared to pH 3.0 (about 1.2 times higher; calculation can be found in **Supporting information 3.5.4**).

Since more protein is precipitated when using a polyphosphate with an increased chain length (**Figure S3.5**; Melachouris, 1972), the precipitation was most likely induced by ionic cross-linking and not salting-out. Salting-out of BLG requires a much higher salt concentration, as compared to the HMP concentration applied here. For example, no BLG precipitation was observed at pH 4.0 upon addition of NaCl up to a NaCl:BLG

molar ratio of 1000:1 (data not shown). Furthermore, HMP can be hydrolysed into its shorter chains tri- and orthophosphate, and this reaction is acid-catalysed (Watanabe et al., 1975). The lower efficiency of precipitation at pH 3.0 (**Figure 3.3**) could therefore be related to enhanced HMP hydrolysis, as compared to pH 4.0. However, this effect is probably limited as this reaction is relatively slow; for example, the half-time of the degradation of polyphosphate at 30 °C is about 17 days at pH 3.0 (calculation can be found in **Supporting information 3.5.6**). HMP could cross-link and precipitate not only the globular protein BLG, but also the unstructured (dephosphorylated) caseinate (**Figure S3.6**). A similar mechanism also allows the negatively charged polyphosphate to cross-link positively charged amino groups in chitosan to form and cross-link nanoparticles (Antoniou et al., 2015).

If indeed the precipitation was induced by cross-linking through ionic interactions, the precipitation of the ionic compounds in a saturated solution can be simply described by a solubility product. Using this principle, a simple model for complexation was established (**Equation S3.6E**). It was assumed that the stoichiometry in the precipitation is approximately 1 to 1; a lower value would indicate that insufficient amounts of HMP is present to form a percolating aggregate with multiple proteins. On the contrary, a higher number would render a protein-HMP complex too negatively charged, inhibiting further cross-linking with other proteins. Indeed, compositional analysis of the precipitate showed that the molar ratio between BLG and HMP was approximately 1 (results not shown). The solubility constant was therefore described according to:

$$k_h = [HMP][BLG]$$

When not using the absolute molar *concentrations* of HMP and BLG, but the molar *fractions* (φ_{HMP} and φ_{BLG}, respectively) that are precipitated, this converts into:

$$k_h = P_0(1 - \phi_{HMP})(1 - \phi_{BLG})$$

This model indeed adequately described the measured precipitation (**Figure 3.3A; Figure S3.4A**), confirming that the precipitation was due to simple complexation. The solubility constants were derived from the fit, as shown in **Figure 3.3B**. The solubility constant was about four times higher at pH 4.0, as compared to pH 3.0, confirming more efficient precipitation at pH 4.0. The model indicates increased complexation when applying higher protein concentrations. One may expect that at very high concentrations, changes in the ionic strength may also influence the value of the overall solubility product (k_h/P_0) but with the current concentrations (10–30 mg protein mL^{-1}), it remained quite stable (**Figure S3.4A**). As the targeted cell broth is relatively dilute, all further experiments were conducted with 10 mg mL^{-1} protein solutions.

3.3.2.2.　　　Precipitation of rBLG using HMP: impact of cellular impurities

Next, the precipitation of recombinant protein from the cell broth (i.e., crude yBLG) was investigated. Due to the low purity of the crude yBLG and possible interferences with the protein precipitation, different HMP:BLG molar ratios of 2:1, 5:1, 10:1 and 100:1 were used for screening, as shown in *Figure 3.4*. A molar ratio of 10:1 was found to induce the highest amount of protein precipitation from the crude yBLG material. This optimal molar ratio was higher compared to a ratio of 2:1 that was found for bBLG (*Figure 3.3*), confirming that cellular impurities in the crude yBLG material interfered with the HMP-protein complexation. Non-covalent interactions between proteins and polysaccharides include electrostatic interactions, steric exclusion, hydrophobic interactions and hydrogen bonding (McClements, 2006) and can affect protein structure, behaviour and functionality (Kong et al., 2022). Thereby, non-covalent interactions between polysaccharide impurities and BLG lower the availability of potential binding sites at the protein surface for complexation with HMP.
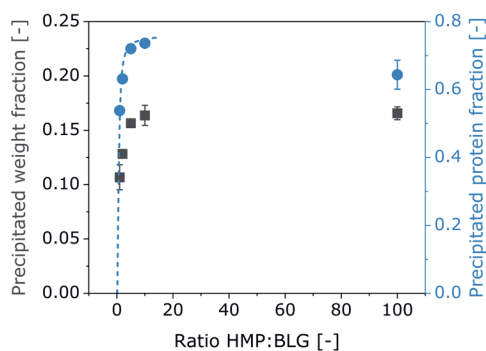

*Figure 3.4. The impact of different amounts of HMP on the precipitation induced at pH 4.0 for solutions of crude yBLG (10 mg mL^{-1}). Both the fraction of material precipitated (by dry weight of the pellet) and the fraction of protein precipitated (by decrease in soluble protein using the BCA assay) are shown. The dotted line indicates the fitted complexation model with values $R_C = 0.237$ and $k_c = 0$, as further explained in **Supporting information 3.5.5.2**.*

The complexation of the positively charged BLG with the negatively charged HMP will not completely neutralize it. Thus, the complex remains positively charged, allowing complexation with a second HMP molecule. This negatively charged HMP$_2$BLG complex allows further complexation with another positively charged BLG molecule, rendering the HMP$_2$BLG$_2$ complex to be positive again. This results in a chain reaction ultimately leading to the formation of large aggregates that precipitate. The negatively charged mannan could have neutralized the charge of the positively charged protein, lowering its electrostatic interaction with HMP. The charged state of the mannan was calculated to be in the same range as BLG (-8.9 and +10.0 respectively, at pH 4.0; *Equation S3.4*),

indicating that a molar interaction of 1:1 would be sufficient to neutralize the overall charge almost completely. When mannan binds with the protein and neutralizes the charge, further charge-driven complexation with HMP will be hindered. In turn, this would break the chain reaction that propagates aggregation (described above). Recently, Shang et al. (2023) also reported that fungal extracellular polysaccharides can associate to WPI through non-covalent interactions, resulting in a decreased surface charge of the complex. The complexation of BLG with polysaccharide impurities would lower the availability of potential binding sites for its complexation with HMP, subsequently hindering the protein precipitation. This impact was included in our simple model for complexation by assuming a second, parallel complexation between BLG and polysaccharide (PS) impurities:

$$\begin{cases} k_h = [HMP][BLG] \\ k_c = [PS][BLG] \end{cases}$$

BLG indeed shows a decreased complexation with HMP in the presence of polysaccharide impurities (*Equation S3.14*). Increases in HMP concentration did improve the protein precipitation under these circumstances (*Figure 3.4*) by shifting the equilibrium towards the complexation of protein with HMP (*Equation S3.5*). However, a residual amount of protein (about 26 wt%) was left in the supernatant of the crude yBLG, in contrast to the complete precipitation observed for bBLG, even when adding high amounts of HMP (up to a HMP:BLG molar ratio of 100; *Figure 3.4*).

Using the HMP-BLG solubility constant from the earlier experiments with pure BLG, the best fit was obtained with the association constant of the interaction between carbohydrates and BLG (k_c) being (close to) zero. This means that the complexation between polysaccharides and BLG is very strong, essentially rendering the protein that is associated with polysaccharides completely resistant against complexation with HMP. Further analysis of the supernatant revealed that the residual soluble protein was actually present in the form of aggregates (*Figure S3.3*). Thus, small complexes of BLG with HMP formed, but resisted precipitation upon centrifugation. The large voluminosity of the polysaccharides could induce steric hindrance, and its charge could dominate that of BLG, making these small complexes electrostatically stable against further flocculation. Thus, the model was consistent for the complexation of bovine BLG and recombinant BLG in the cell broth, yielding information about the nature of the interaction between the polysaccharides impurities and BLG.

Addition of more HMP (molar ratio of 100:1) resulted in a slightly less precipitated protein. The ionic strength at these high HMP concentrations probably affected the complexation between HMP and BLG (*Figure 3.4*). Some residual smaller soluble aggregates and even unaggregated protein remained in the supernatant (*Figure S3.3*), as saturation of the protein (aggregate) surface with polysaccharides and HMP could have caused repulsion instead of cross-linking. As a HMP:BLG molar ratio of 10:1 resulted in optimal precipitation, this condition was chosen for further experiments.

3.2.3. Solubilization of precipitated protein and removal of HMP

The second major step in the purification process was the removal of HMP. After precipitation of pure bBLG with HMP at a pH value of 4.0, the protein was re-solubilized by increasing the pH to 7.0, which converted the precipitate into a clear solution (data not shown). This is in line with results of Hidalgo et al. (1973), who also demonstrated the solubilization of WPI-HMP complexes upon neutralization. Both HMP and BLG carried an overall negative surface charge at this neutral pH (***Supporting information 3.5.4.1***). Thereby, their interaction was weakened, allowing for decomplexation and subsequent solubilization. Dialysis was not effective to subsequently remove HMP (***Supporting information 3.5.7***), even though dialysis of a pure HMP solution (10 mg mL^{-1}) confirmed that HMP could pass the membrane. Similarly, Alomirah & Alli (2004) reported that extensive dialysis of a supernatant containing BLG-HMP complexes did not reduce the ash content. Thus, residual interactions of HMP with BLG hindered its removal by dialysis, and we thereby hypothesize that some residual HMP remained bound to local positively charged patches on the protein.

The free HMP could be removed by addition of CaCl$_2$. HMP is known to chelate calcium ions and thereby used to remove calcium ions from, for example, water (also called softening of hard water; Rashchi & Finch, 2000), or micelles to destabilize them (de Kort et al., 2011). CaCl$_2$ was added to solutions containing pure bBLG or crude yBLG (i.e., stream 3 in ***Figure 3.1***) to remove HMP. The amount of CaCl$_2$ was varied between 50 and 200 mM. The amount of HMP precipitated was determined with an assay and is shown in ***Figure 3.5A***.
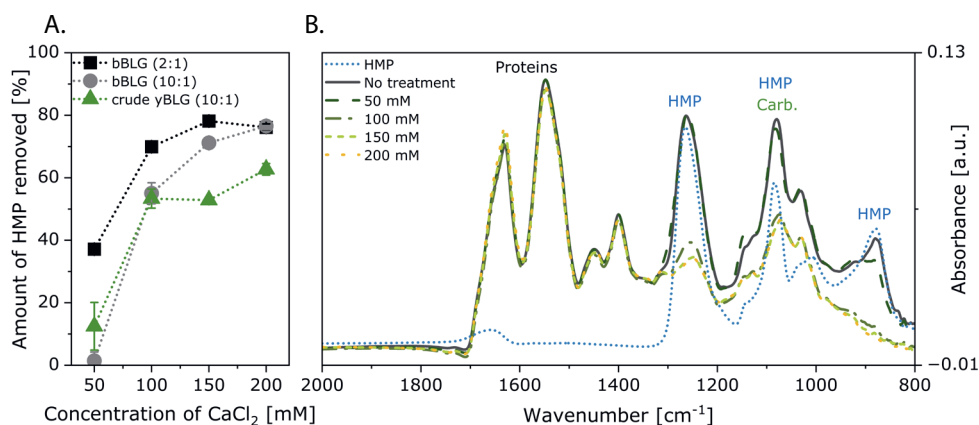

Figure 3.5. (***A***) Fraction of HMP that was precipitated by CaCl$_2$ from a solution of pure bBLG or crude yBLG with HMP (i.e., stream 3 in ***Figure 3.1***). (***B***) FTIR spectra of crude yBLG with HMP (i.e., stream 3 in ***Figure 3.1***) upon addition of different amounts of CaCl$_2$. A HMP stock solution (~ 54 mM) as added as a reference.

In the presence of both yBLG or bBLG, about 150 mM $CaCl_2$ was necessary to reach a maximal precipitation of HMP, while 100 mM $CaCl_2$ was sufficient in the absence of protein (**Table S3.3**). Thereby, BLG-HMP interactions probably compete with the Ca-HMP complexation. In both cases, a residual amount of HMP remained in solution, and thereby we hypothesize that small HMP-calcium complexes have appreciable solubility. Also, FTIR analysis of the supernatant confirmed that 150 mM $CaCl_2$ was sufficient to induce maximal precipitation (FTIR analysis of yBLG and bBLG shown in **Figure 3.5B** and **Figure S3.8**, respectively): a maximal decrease in the absorption peaks corresponding to HMP was observed upon addition of 150 mM $CaCl_2$. Besides, the absorption region that corresponds to the protein fraction (i.e., amide 1 and 2 region) mostly remained constant upon $CaCl_2$ addition, indicating that $CaCl_2$ selectively precipitated HMP, while BLG was kept in solution. For the removal of excess HMP from the protein solutions in further experiments, a concentration of 150 mM $CaCl_2$ was chosen.

3.3.3. Optimized purification process: composition

Both pure bBLG and crude yBLG were treated with the established purification process (**Figure 3.1**) and samples were taken to determine the protein and HMP content throughout the process. For yBLG, also the carbohydrate content was determined. The purities and mass balance throughout the process are depicted in **Figure 3.6**.

After addition of the same amount of HMP to pure bBLG or crude yBLG, the measured HMP content in the presence of crude yBLG (10%) was overestimated by approximately 0.8 wt%. This overestimation can be due to presence of mannan, containing side chains that were linked through phosphodiesters, as explained in **Section 3.2.1.2**.

After adjusting the pH to 4.0 (step 1), most of the protein from both bBLG and the crude yBLG precipitated; about 2 and 21 wt% of the protein was lost to the supernatant, respectively. For the crude yBLG, most of the carbohydrate impurities remained in the supernatant after this precipitation step. For bBLG, the supernatant mainly contained residual HMP. The protein-rich pellet in yBLG contained a low amount of carbohydrates (13 ± 0 wt%) as compared to the carbohydrate content (48 ± 1 wt%) of the crude yBLG feed. This demonstrates that the protein fraction and not the carbohydrate fraction precipitated in the presence of HMP at acidic pH, as both carbohydrates and HMP were negatively charged (**Supporting information 3.5.4.1**). The carbohydrates present after HMP precipitation could originate from the residual supernatant in the HMP-BLG pellet, and/or carbohydrates that interacted strongly with the protein.
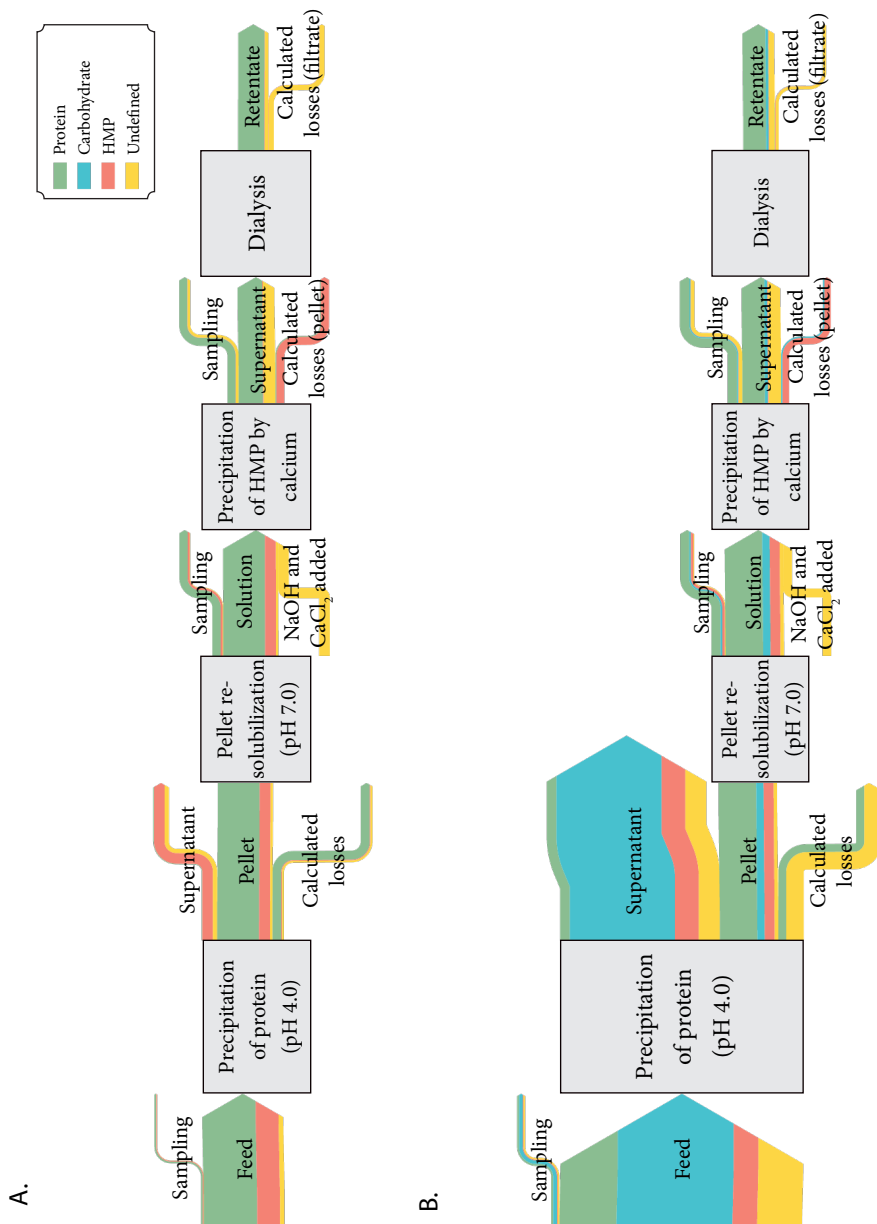
Figure 3.6. Sankey diagram of the mass balance throughout the treatment (**Figure 3.1**) of (**A**) bBLG and (**B**) crude yBLG. Before and after treatment, the composition sample (wt%) of the separate streams is shown. The undefined fraction was calculated by subtracting the measured protein, carbohydrate and HMP content from the total dry weight of the sample. The calculated losses were calculated by the mass difference of the incoming and outgoing streams.

After HMP precipitation and re-solubilization of bBLG and yBLG, the HMP content decreased significantly upon addition of $CaCl_2$ (from about 17–20 wt% to 2 wt%). Dialysis led to a slight increase in protein content, which was about equal to the decrease in the undefined fraction (7–8 wt% and 14–15 wt% for yBLG and bBLG, respectively). This could be attributed to the removal of residual ions, such as Ca^{2+}, Na^+ or Cl^-, that would concentrate the protein fraction. Furthermore, no considerable amount of protein was lost in the HMP removal (step 2) or dialysis step.

Eventually, the crude yBLG was successfully purified, increasing the protein content from 26 ± 0 to 72 ± 1 wt%, with minor fractions of carbohydrates (9 ± 1 wt%) and residual HMP (1 ± 0 wt%). Overall, about 38 wt% of the protein was lost throughout the purification process, of which about 26% was lost due to incomplete precipitation by HMP (step 1). The residual HMP after purification possibly remained bound to the protein. Both yBLG and bBLG showed a similar IEP of pH 4.0 ± 0.2 and pH 4.2 ± 0.2, respectively. This is lower as compared bBLG before the treatment (pH 5.0 ± 0.0), and indeed indicates that positively charged amino acids associate with residual HMP. Besides, the IEP of the crude BLG was found to be lower (pH 3.6 ± 0.2) due to the presence of acidic mannan (**Supporting information 3.5.4.1**).

To compare the established purification method to conventional purification, a similar batch of crude yBLG (33 ± 5 wt% protein) was purified using anion exchange chromatography (method in **Supporting information 3.5.9**), reaching a protein purity of 72 ± 7 wt%. Both methods rely on charge-driven adsorption of the BLG, resulting in similar purity. Using a similar expression and subsequent purification with anion exchange chromatography, Denton et al. (1998) obtained a protein purity of 78%. They achieved further purification up to 99% with size exclusion chromatography, but with major losses of about 68% (Denton et al., 1998). This indicates that a fraction of the purified BLG forms complexes with the remaining polysaccharide impurities, which might have consequences for the protein structure and functionality.

3.3.4. Towards food application

3.3.4.1. Bovine versus recombinant BLG: sequential differences and post-translational modifications

Sequential changes and post-translational modifications affect molecular and functional properties of recombinant proteins. Therefore, the protein in the purified yBLG was analyzed with UPLC-PDA-MS to identify sequential differences with bBLG. Analysis of the intact protein showed that bBLG contained two species with a mass of 18,366 and 18,280 kDa, corresponding to the genetic variants A and B, respectively. The recombinant expression of genetic variant A (yBLG) resulted in a mixture containing two major species with larger MWs of 19,280 and 19,479 kDa. Tryptic digestion of

yBLG was performed to further investigate the difference in sequence, as compared to bBLG. The peptides identified in the hydrolysate of yBLG covered the amino acid sequence for 99.4%. The N-terminus of BLG (**LIV**...) was altered in yBLG: leucine was substituted with a prolonged sequence (AKEEGVSLEKR**IV**...) and its truncated form (EKGVSLEKR**IV**...). This prolonged sequence was caused by an incomplete removal of the signal peptide (α-mating factor from *Saccharomyces cerevisiae*). Wilson et al. (1999) also reported a heterogenous mixture of BLG with higher molecular weight produced from *P. pastoris*, using a similar α-factor signal peptide, and attributed this to incomplete cleavage of the signal peptide. Lastly, the distribution of the different yBLG exact masses did not change during purification, indicating that the variants had similar affinity to HMP complexation.

P. pastoris is known for glycosylating secreted proteins (Bretthauer & Castellino, 1999). Therefore, the intact mass was compared to the calculated mass to check for covalent modifications. When considering the two major sequential differences described above, a theoretical mass difference with bBLG was calculated to be 914 and 1,114 Da. These calculated mass differences match the measured exact mass differences (913.2 and 1,112.6 Da, respectively). Thereby, it is concluded that no further covalent modifications were induced by *P. pastoris*, besides the N-terminal modification and expected intramolecular disulfide bond formation. This result was as expected, as BLG does not contain suitable glycosylation sites for the N-linked glycosylation (Kalidas et al., 2001). Besides, the evidence for O-linked glycosylation by *P. pastoris* is limited (Bretthauer & Castellino, 1999).

3.3.4.2. Impact of recombinant expression and purification on BLG structure and function

The sequential differences can result in a changed folding of the peptide chain, and in turn affect physicochemical and functional properties of yBLG. Besides, downstream processing of crude yBLG could induce unfolding. Therefore, the impact of (i) the N-terminal modification of yBLG and (ii) the purification method on BLG secondary structure was evaluated, using FTIR. For bBLG and yBLG, both before and after purification, the second derivative of amide I region in the FTIR spectra were determined and are shown in **Figure 3.7A**. The wavenumber of minima in these spectra correspond with specific secondary structure elements. All BLG variants show similar spectra with a major trough around 1628 cm^{-1}, which corresponds with the typical intramolecular β-sheet structure of BLG (**Chapter 6** and **7**). It is concluded that the recombinant expression nor the purification method significantly affect the secondary structure of BLG, since all graphs mostly overlap. Keppler et al. (2021) reported that simple N-terminal modifications (M**LIVTQ**... and AS**VTQ**, compared to **LIVTQ**) also did not impede the BLG fold or functionality to any significant extent. The

impact of the N-terminal modification is probably limited as the N-terminus is located on the outside of the globular protein. As also the interaction between BLG and HMP did not affect the secondary structure, we expect this interaction to mostly occur at the surface of the protein and thereby not to disrupt the fold considerably.
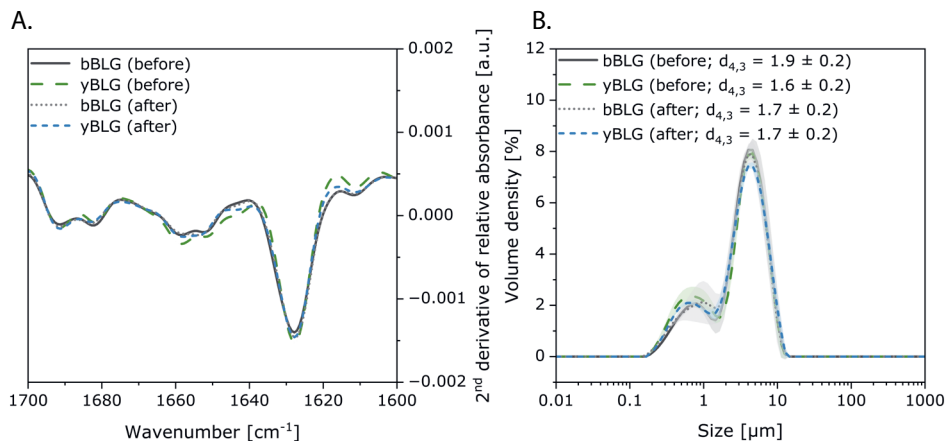

Figure 3.7. (**A**) *Second derivative of the FTIR spectra of BLG variants, and (**B**) the size distribution of the droplets in emulsions (10 wt% stripped sunflower oil, 0.1 wt% protein in 10 mM phosphate buffer, pH 7.0) stabilized by BLG variants. Besides, the mean diameter of the volume-weighted distribution ($d_{4,3}$) is shown. Bovine (bBLG) and recombinant (yBLG) BLG variants are shown before and after purification (i.e., stream 6 in **Figure 3.1**).*

Finally, an experiment was performed to obtain a first impression on the impact of recombinant expression (N-terminal modification in particular) and purification on the functionality of BLG. We chose to evaluate its use as an emulsifying, as the application in emulsions required relatively low amounts of the recombinant protein. Proteins such as WPI, caseinate and pea protein isolate show a decreasing droplet size in the concentration range 0.2–0.8 wt% protein (Hinderink et al., 2019), using the same emulsion preparation method. We applied an even lower BLG concentration of 0.1 wt% to be able to observe potential differences in the droplet size of emulsions prepared with the BLG variants. The droplet size distribution and the average volume-weighted diameters are shown in **Figure 3.7B**. The use of bovine and recombinant BLG resulted in an emulsion with similar droplet size, both before and after purification. Mannan is a poor emulsifier due to its overall hydrophilicity (Kuncheva et al., 2007). We expect therefore that the surface is mostly stabilized by the protein fraction and not by the (mannan) impurities. Since all BLG variants are highly similar in terms of sequence and structure (**Figure 3.7A**), their emulsions also yield similar droplet size distributions.

3.3.4.3. Outlook for upscaling and application range

We demonstrated that the established purification method was able to separate recombinant protein from the filtered cell-free broth, thus allowing purification of recombinant BLG. However, before it can be compared to conventional purification methods, in terms of costs and sustainability, scenarios for upscaling and for the application range need to be developed:

In the first step of the purification process, the protein is cross-linked through multivalent ionic interactions with the polyanion HMP, resulting in precipitation. This precipitation step can be transformed in a continuous process to make it more feasible for scale-up, for example, by using filtration instead of centrifugation. We observed a critical amount of smaller aggregates that remain in the HMP-supernatant after centrifugation, and we expect that these losses could be minimized in a continuous system. When such a system would be continuously fed with more of the crude yBLG material, this could potentially allow further growth and sedimentation of the BLG-HMP complexes.

To render the process at least partially circular, the HMP-supernatant (stream 2 in *Figure 3.1*) could be further utilized as it contains both valuable mannan and HMP. Mannan is valuable in food and feed applications due to its functional characteristics (e.g., increases viscosity and stabilizes emulsions), as well as its association with several health benefits (e.g., can improve gut health and the immune system) (Zhang et al., 2022; Singh et al., 2018). As the mannans are not expected to interact with HMP and are larger in size, the two can potentially be separated with ultrafiltration. The HMP fraction of the supernatant can then be re-used in the precipitation of recombinant proteins. However, desalting of the HMP-supernatant might be necessary due to accumulations of ions, which possibly could hinder the HMP-protein interaction (Hidalgo et al., 1973). This should be possible using nanofiltration, as HMP is polyanionic and thereby larger than the other simple ions present.

In the second step of the purification process, we demonstrate the possibility to partially remove HMP. The necessity of HMP removal should be evaluated in future studies, considering the protein functionality, as well as nutritional aspects. For example, HMP was reported to positively affect whey protein-based beverages, but accurate HMP concentrations were key to achieve this (Rasouli et al., 2020). If HMP removal is required, we demonstrated that excess HMP amounts can be selectively precipitated through calcium ion addition. The Ca-HMP precipitate should be further utilized, for example, by dissolving these complexes at acidic pH (Kunaschk et al., 2015) and separation of the phosphate from the calcium ions. Inspiration for the separation of calcium and HMP can be taken from waste water applications, as the selective removal of phosphate is a dominant theme here. For example, using ad- and desorption in fixed bed filters (Kunaschk et al., 2015).

Lastly, the necessity of the purification of the crude yBLG should be determined for specific applications. We have demonstrated that emulsions stabilized with crude and purified yBLG have similar droplet size distribution. In applications where protein-protein interactions are more evident, such as in aggregation or gelation, we hypothesize that larger differences in functionality may be found due to the N-terminal protein modification, and the presence of HMP and yeast-originated impurities. This is further addressed in **Chapter 5**. Besides, other impurities in the yeast cell broth could strongly affect sensorial properties (Mahadevan & Farmer, 2006). The presence of these flavour and odour compounds in the purified yBLG is yet to be determined.

3.4. Conclusions

Hexametaphosphate is an affordable and food grade polyphosphate that can selectively precipitate recombinant β-lactoglobulin secreted by *P. pastoris* (yBLG), while soluble polysaccharides impurities (i.e., identified as mainly mannan) remain in the solution. An increase in yBLG purity from 26 to 72 wt% was achieved through two major steps: (1) protein precipitation through complexation with HMP and (2) subsequent protein solubilization and HMP removal by elevation of the pH and calcium ion addition, respectively. The results indicate that the developed method will also apply to other secreted yeast-based recombinant food proteins, as first trials with more randomly coiled caseinates confirmed. It remains to be seen how far this extends to other production hosts, such as bacteria and fungi, which have different impurities than the mannans released from yeast. It is also unclear whether HMP precipitation applies for intracellularly produced proteins, because the required cell lysis introduces a broad range of different impurities.

An advantage of the presented method is that all used precipitation agents are food grade. Their complete removal from the target protein is not strictly necessary, and they might in fact contribute towards specific target functionalities, which is subject to future studies. Besides, a major advantage over conventional purification methods is that the precipitation of the dilute cell broth allows pre-concentration of the protein, simplifying subsequent processing. Thus, the precipitation method holds promise for obtaining affordable fractions for recombinantly produced yeast-based food proteins.

3.5. Supporting information

3.5.1. Conditions for optimizing purification

Table S3.1. *Precipitation conditions tested for optimal recovery of protein. Optimal conditions are shown in bold.*

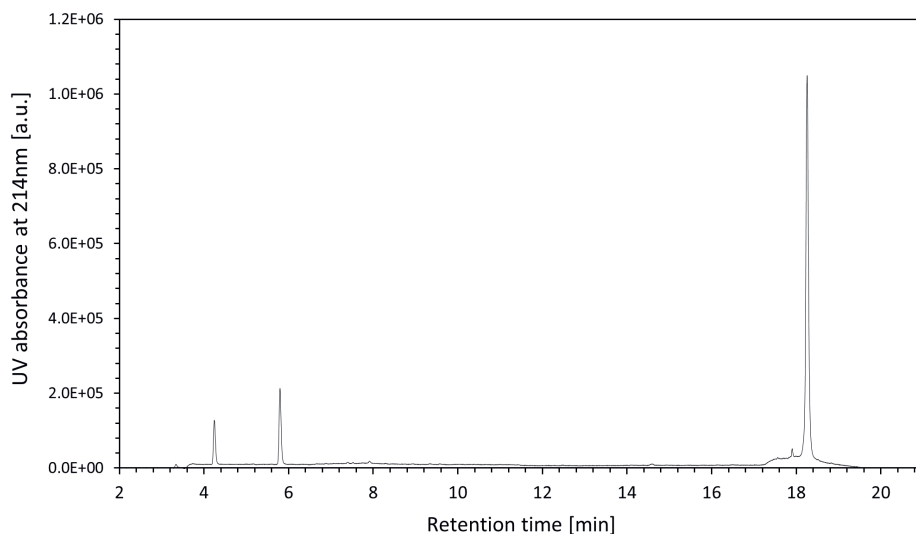| Variant	pH	HMP:BLG molar ratio	CaCl$_2$ [mM]
bBLG	3.0	0.5	
		1	
		2	
	4.0	0.5	
		1	
		2	
yBLG	4.0	4	
		5	
		10	
		100	
yBLG PP	4.0	1	
		2	
		5	
		10	
		100	
bBLG	**4.0**	2	50
			100
			150
			200
		10	50
			100
			150
			200
yBLG PP	**4.0**	**10**	50
			100
			150
			200

3.5.2. UPLC analysis

Figure S3.1. *Chromatogram at UV$_{214nm}$ of yBLG analyzed with UPLC-PDA-MS. Peaks at 4.24 and 5.80 min are due to elution of DTT.*
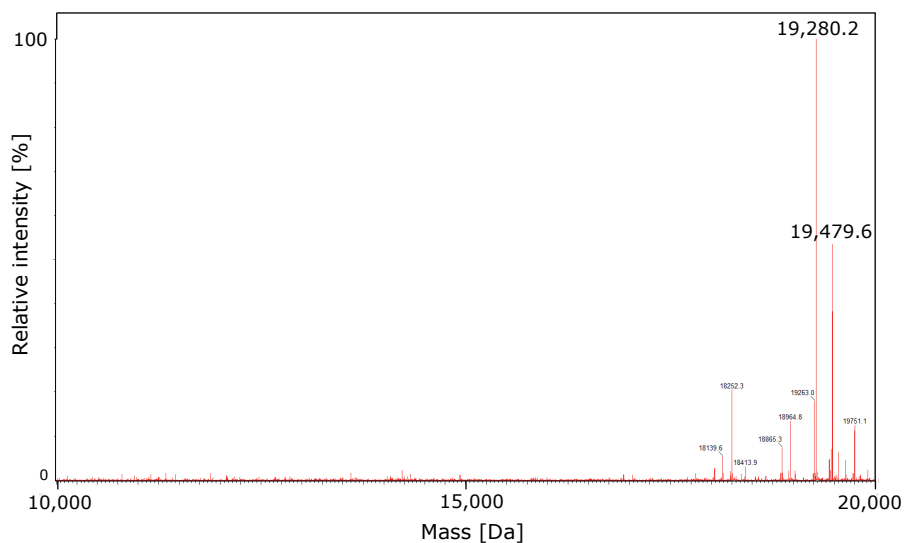

Figure S3.2. *Deconvoluted mass spectrum using Maxent of yBLG with UPLC-PDA-MS at UV retention time 18.26 min (**Figure S3.1**).*

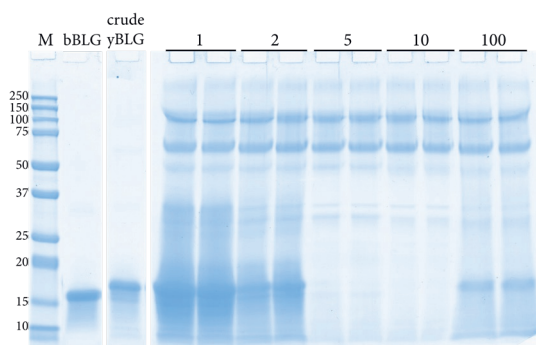### 3.5.3. Size of protein in supernatant after HMP precipitation

Figure S3.3. *HMP was added in different molar ratios (HMP:BLG ratios of 1, 2, 5, 10 or 100) to 10 mg mL^{-1} crude yBLG solutions at pH 4.0 to induce precipitation. The soluble fraction was collected and loaded on this SDS-page gel (without dilution). A molecular weight marker (Precision Plus; M) was added as a reference, as well as pure bovine BLG (bBLG; protein purity of 93 wt% by BCA) and crude yBLG (so without HMP; purity 26 wt% by BCA assay) at a protein concentration of ~ 0.5 mg mL^{-1}.*

3.5.4. Charge distribution

3.5.4.1. Measured zeta-potential

The zeta-potential was measured for 1 mg mL^{-1} protein solutions. The isoelectric point was determined as the pH where the average net charge of the sample was zero and is listed in **Table S3.2**. Solutions of pure mannan and HMP were measured to be negatively charged in range of pH 3 to pH 7.

Table S3.2. *Overview isoelectric points as the pH at which the average surface charge was found to be zero.*

Protein variant	Isoelectric point
bBLG	5.0 ± 0.0
Crude yBLG	3.6 ± 0.2
bBLG (after treatment)	4.2 ± 0.2
yBLG (after purification)	4.0 ± 0.0

3.5.4.2. Calculation of charged state of compounds

The complexation between BLG and HMP was expected to be due to ionic interaction. The difference in attractive forces between those two compounds at pH 3.0 and 4.0 was calculated. First, the charged state of BLG and HMP at the corresponding pH was calculated as follows.

The protonation state of the ionizable groups can be defined, according to:

$$R = \frac{[A^-]}{[AH]}$$

[**Eq. S3.1**]

Using the dissociation constant (*pKa*), *R* can be determined according to:

$$pH = pKa + \log(R)$$

[**Eq. S3.2**]

Using the mass balance (*AH+A⁻=1*), the concentration of (de)protonated ionizable groups can be found to be:

$$[AH] = \frac{1}{R+1}$$

[**Eq. S3.3A**]

$$[A^-] = 1 - [AH]$$

[**Eq. S3.3B**]

For BLG, the protonation state of each ionizable amino acid (R, H, K, D, E, C-terminus, N-terminus) in the protein sequence was calculated, using the dissociation constants from Martell et al. (1976). Based on the charge upon (de)protonation and corresponding amino acid count, the net charge of BLG was determined to be 10.0 at pH 4.0 and 18.5 at pH 3.0.

For HMP, the total (de)protonation was calculated using the dissociation constant and average chain length of polyphosphate in HMP from Sigma Aldrich, taken from Robinson et al. (2021). The electrostatic attraction (F_e) between two oppositely charged molecules (with charges and and distance) was then determined based on Coulomb's law (with constant):

$$F_e = \frac{kq_1q_2}{r^2}$$

[**Eq. S3.4**]

Using **Equation S3.4** and the charged state of BLG and HMP at pH 3.0 and 4.0, was found to relatively be 1.2 times bigger at pH 4.0 as compared to pH 3.0.

3.5.5. HMP precipitation

3.5.5.1. Precipitation of pure BLG by HMP

The interaction of HMP (*H*) and protein (*P*) to form a complex (*HP*) can be described:

$$H + P \rightleftharpoons HP \qquad \text{[\textit{Eq. S3.5}]}$$

Assuming the complex is partially soluble, we have a solubility product constant (k_h), according to the concentrations of the reactants:

$$k_h = [H][P] \qquad \text{[\textit{Eq. S3.6A}]}$$

The final concentrations are a result of the initial concentrations, which have been reduced by the formation of the complex. Therefore, **Equation S3.6A** can be written as:

$$k_h = ([H_0] - [HP]) \cdot ([P_0] - [HP]) \qquad \text{[\textit{Eq. S3.6B}]}$$

We do not use the absolute molar concentrations, but the fraction of the protein that is complexated with HMP and subsequently precipitates (φ_{HMP}), and as independent variable, the ratio (R_h) between the initially added HMP and protein:

$$\phi_{HMP} = [HP]/[P_0] \qquad \text{[\textit{Eq. S3.7}]}$$

$$R_h = [H_0]/[P_0] \qquad \text{[\textit{Eq. S3.8}]}$$

Substitutions of **Equation S3.7** and **Equation S3.8** into **Equation S3.6B** leads to:

$$k_h = (R_h[P_0] - \phi_{HMP}[P_0]) \cdot ([P_0] - \phi_{HMP}[P_0]) = [P_0]^2 \cdot (R_h - \phi_{HMP}) \cdot (1 - \phi_{HMP}) \qquad \text{[\textit{Eq. S3.6C}]}$$

Which can be further written as the quadric equation:

$$k_h = [P_0]^2(\phi_{HMP}{}^2 - (1 + R_h) \cdot \phi_{HMP} + R_h) \qquad \text{[\textit{Eq. S3.6D}]}$$

We see here that the fraction of precipitated protein depends on the solubility divided by the square of the initial protein concentration, and the relative amount of HMP added, R_h. Rewriting this to make φ_{HMP} explicit gives:

$$\phi_{HMP} = \frac{1}{2}\left(1 + R_h - \sqrt{(1 + R_h)^2 - 4\left(R_h - \frac{k_h}{[P_0]^2}\right)}\right) \qquad \text{[\textit{Eq. S3.6E}]}$$

Experiments were performed to precipitate bBLG at pH 3.0 and 4.0 (1 wt% protein) using different ratios of HMP:BLG (0.5:1, 1:1 and 2:1; i.e., R_h). The fraction of the material that precipitated (i.e., φ_{HMP}) was measured as the dry weight of the pellet, as compared to the initial amount of material solubilized. The established model (**Equation S3.6E**) was fitted to the data, as shown in **Figure S3.4**. From the fit, the solubility constant (k_h) was determined for the specific conditions; a higher solubility constant means lower tendency for precipitation. A similar approach was used to determine the solubility constant for precipitation at pH 4 for various protein concentrations (1, 2 and 3 wt%). Normalization of the solubility constants for the initial protein concentration yields similar solubility products at pH 4.0, as shown in **Figure S3.4**.
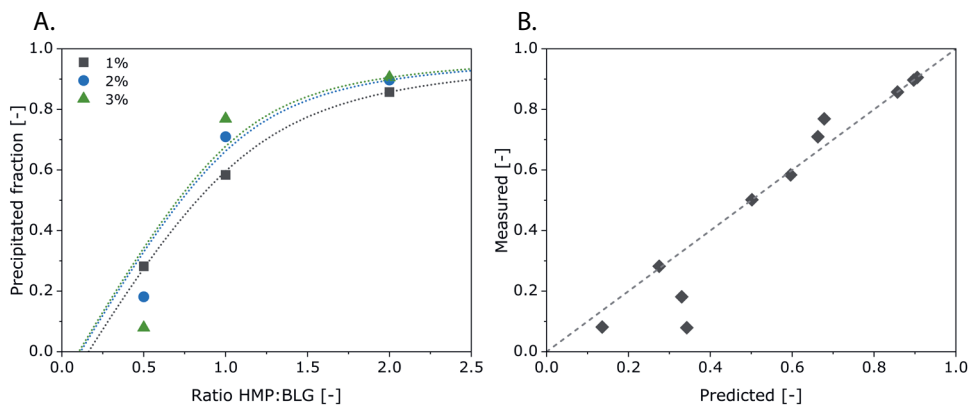
Figure S3.4. (**A**) *The precipitated fraction (φ_{HMP}) for precipitation of bBLG at pH 4.0 induced HMP for various protein concentrations (wt%). The dotted lines indicate the fitted complexation model.* (**B**) *The precipitated fraction (φ_{HMP}) as measured under various conditions (i.e., 1% protein at pH 3.0 and 4.0, and for 2 and 3% protein at pH 4.0) compared to the predicted value. The dotted line indicates when the predicted and measured values are equal.*

3.5.5.2. Precipitation of yBLG by HMP: impact of cellular impurities

For the recombinant material (crude yBLG), we suppose that there is an additional interaction between proteins and carbohydrate impurities, which competes with the complexation of proteins with HMP. We have adjusted the model as follows.

Complexation of BLG [P] with carbohydrate impurities [C] resulted in a soluble complex, and thereby an equilibrium constant (k_c) can be defined, according to:

$$k_c = \frac{[C] \cdot [P]}{[CP]} \qquad \textbf{[Eq. S3.9A]}$$

The final concentrations are again a result of the initial concentrations, which have been reduced by the formation of the complex (similar to **Equation S3.6B**). For the protein, this includes both the complexation with HMP [HP] and carbohydrates [CP]. Substitution gives:

$$k_c = \frac{([C_0]-[CP]) \cdot ([P_0]-([HP]+[CP])))}{[CP]} \qquad \textbf{[Eq. S3.9B]}$$

The fraction of the protein is *complexated* with the carbohydrates (φ_{HMP}) and the ratio of (initial) carbohydrate to (initial) protein are described in **Equation S3.10** and **Equation S3.11**, respectively;

$$\phi_c = [CP]/[P_0] \qquad \textbf{[Eq. S3.10]}$$

$$R_c = [C_0]/[P_0] \qquad \textbf{[Eq. S3.11]}$$

Using these equations, we can substitute and rewrite **Equation S3.9B** to be:

$$\phi_c = \frac{1}{2}\left(1 - \phi_{HMP} + R_c + \frac{k_c}{[P_0]} - \sqrt{\left(1 - \phi_{HMP} + R_c + \frac{k_c}{[P_0]}\right)^2 - 4R_c(1 - \phi_{HMP}))}\right)$$

[Eq. S3.12]

Since the concentration of protein that is available to make a complex with HMP, is decreased due to the interaction between carbohydrates and protein, **Equation S3.6B** was changed to be:

$$k_h = ([H_0] - [HP])([P_0] - [HP] - [CP])$$

[Eq. S3.13]

This ultimately also changes the fraction of the protein is precipitated as the complex to be:

$$\phi_{HMP} = \frac{1}{2}\left(1 - \phi_c + R_h - \sqrt{(1 - \phi_c + R_h)^2 - 4\left(R_h(1 - \phi_c) - \frac{k_h}{[P_0]^2}\right)}\right)$$ **[Eq. S3.14]**

Complexation of BLG with HMP was assumed to result in precipitation, and the solubility product of this complex (k_h) was established earlier for the model system of bovine BLG with HMP at pH 4.0 (for different protein concentrations), without outliers at low concentrations; resulting in a solubility constant of 13.397.

The two implicit **Equation S3.12** and **Equation S3.14** were then iterated using Python, using the optimize fsolve procedure from the SciPy library to find the solution to the two quadratic **Equation S3.12** and **Equation S3.14**, and then *optimize,minimize* function in the same library to fit the model in the experimental data. Using the solubility constant 13.397, the values for k_c and R_c were fitted to the data for the precipitation of protein in the crude yBLG material (**Figure 3.4**). This resulted in a fit with values R_c = 0.237 and k_c = -0.00909 (mg/mL)². Als the latter value cannot be negative, the physical realistic value of k_c is zero. The obtained fit with k_c = 0 in **Figure 3.4** is basically as good as with the numerally found value. The marginally better fit with the negative value is probably an indication of the influence of the increasing ionic strength: the degree of precipitation decreased further at much higher HMP:BLG molar ratios, again due to much higher ionic strengths (**Figure 3.4**).

3.5.5.3. Precipitation of bBLG by polyphosphate with shorter chain length

It is our hypothesis that the chain length of the phosphate polyanion determines the possibility for flocculation. Complexation of an HMP ion with BLG gives a complex that is still negatively charged, as the positive charge of BLG at the chosen pH is larger. This enables a second HMP molecule to associate with it, which then reverts the complex to a negative charge. This then enables a BLG molecule to associate, rendering it positive again, etcetera.

Using a trivalent ion STP will reduce this potential, as the positive valency of the BLG can be better matched by 1–3 STP molecules, creating a complex that does not have much charge at all, and therefore will not grow as much. Having sufficient STP may still enforce some polymerization, but the creation of larger aggregates is less likely.
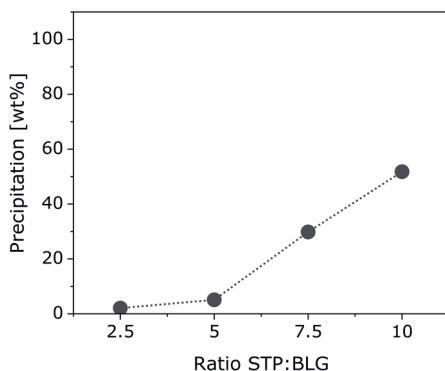
Figure S3.5. Precipitation of BLG by sodium triphosphate (STP) at pH 4.0 and a protein concentration of 1 wt%, as measured by the decrease in protein content in the supernatant (BCA assay).

3.5.5.4. Precipitation of unstructured protein by HMP

We hypothesize that also other proteins can form similar complexes with HMP, as compared to BLG. To demonstrate this, we measured the degree of precipitation with both normal and dephosphorylated caseinate (since BLG is also not naturally phosphorylated). The method for dephosphorylation is explained below. The results are depicted in **Figure S3.6**; natural caseinate indeed readily precipitated upon low additions of HMP, while higher amounts of HMP were needed to induce precipitation for dephosphorylated caseinate. Thereby, a higher amount of binding sites stimulates complexation, but not necessarily cross-linking.
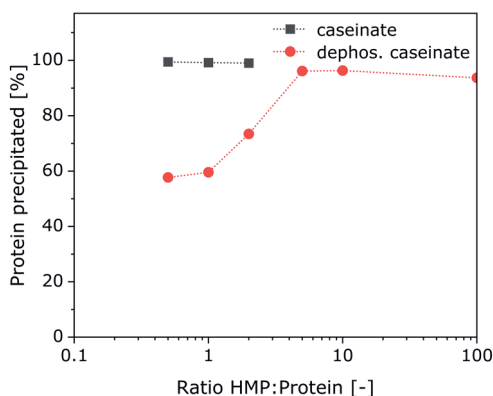

Figure S3.6. Precipitation of caseinate (90 wt% protein; Lactoprot) and dephosphorylated caseinate (96 wt% protein) in the presence of HMP at pH 4.0 and a protein concentration of 10 mg mL^{-1}.

Dephosphorylation of the caseinate was performed as follows. Sodium caseinate was hydrated for 30 min in a 10 mM TRIS buffer (10 g L⁻¹) under mild stirring and heating at 50 °C. The pH was adjusted to 8.0 by adding 1 M hydrogen chloride. Alkaline phosphatase was added (0.1 g L⁻¹) and the solution was stirred for 8 h at 37 °C, after which the enzyme was deactivated by heating at 80 °C for 10 minutes. The sample was then kept overnight in cold storage. The next day, the free phosphate was removed through ultrafiltration and the dephosphorylated casein was then spray dried.

3.5.6. Half-life of polyphosphate degradation

We assumed that degradation of HMP in water was assumed to be a first-order reaction, and thereby depends on its concentration [A] as follows:

$$\ln \frac{[A]_0}{[A]} = k_H t \qquad [\textit{Eq. S3.15}]$$

in which k_H is the rate constant of the reaction and t the incubation time.

To obtain the half-life of the reaction [A] was substituted with [A]$_0$/0.5 and t with the half-time ($t_{1/2}$), as follows:

$$\ln \frac{[A]_0}{[A]_0/2} = \ln 2 = k_H t_{1/2} \qquad [\textit{Eq. S3.16}]$$

Using *Equation S3.16*, we can derive the following expression of the half-time:

$$t_{1/2} = \frac{\ln 2}{k_H} \qquad [\textit{Eq. S3.17}]$$

The rate constants for the degradation of hexametaphosphate degradation were expected to be in a similar range as compared to polyphosphate. Using the constant reported by Watanabe et al. (1975; $2.90 \cdot 10^{-5}$ min⁻¹) and *Equation S3.17*, a half-time of about 17 days was calculated.

3.5.7. Dialysis for HMP removal

After precipitation of bBLG with HMP, it was verified whether or not we can remove the HMP with dialysis. FTIR analysis was performed before and after dialysis at either pH 7.0 or 8.0, as shown in **Figure S3.7**. It is clear that the presence of HMP increased absorbances around 1350 and 900 nm, which remained unaffected after dialysis. Thereby, it was concluded that dialysis was unable to remove HMP.
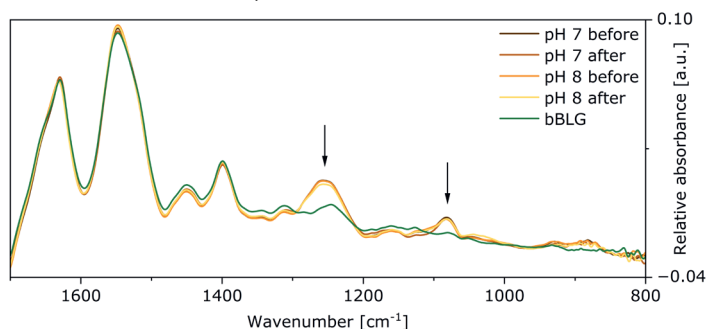

Figure S3.7. *FTIR spectra of bBLG after HMP precipitation at pH 4.0 ('before'), adjusting the pH to 7.0 or 8.0 and dialysis against MQ with the corresponding pH value ('after'). Spectra were normalized the region 800–1700 cm^{-1} to account for concentration differences. Untreated bBLG is plotted as a reference. Peaks indicative for HMP are highlighted with an arrow.*

3.5.8. Precipitation of HMP by calcium

Table S3.3. *Precipitation of HMP stock solutions by different amounts of $CaCl_2$. The amount of HMP removed was calculated after determining the concentration with an assay for total phosphorus. Standard deviations are based on independent duplicates.*

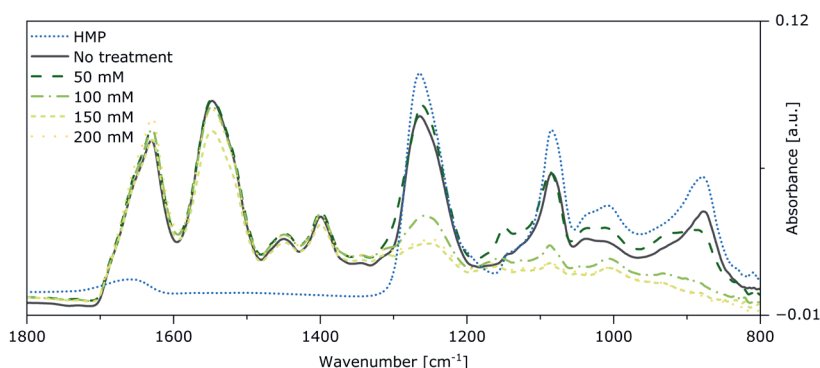| HMP [mM]	Volume [mL]	$CaCl_2$ [mM]	HMP removed [%]	Precipitate [mg]	Residual concentration [mM]
5.0	30	1	No precipitation		
		10			
		100	60 ± 0	58 ± 1	2.0 ± 0
		200	58 ± 0	57 ± 1	2.1 ± 0
15.0	10	1	No precipitation		
		10			
		100	74 ± 0	78 ± 1	3.9 ± 0
		200	75 ± 0	77 ± 0	3.8 ± 0

Figure S3.8. *FTIR spectra of bBLG with HMP (i.e., stream 3 in Figure 1) upon addition of different amounts of CaCl$_2$. A HMP stock solution (~ 54 mM) as added as a reference.*

3.5.9. Method for purification using anion exchange chromatography

For comparing the established purification method to conventional purification, anion exchange chromatography was performed, using a protocol of Keppler et al. (2021) with adjustments. An Aktä Purifier system (GE Healthcare Life Sciences, USA) was equipped with a HiTrap™ Capto™ Q ImpRes chromatography column (5mL column volume; GE Healthcare Life Sciences) for fractionation, and a HiPrep™ 26/10 desalting column (53 mL column volume, GE Healthcare Life Sciences) to remove ions. Crude yBLG (32.6 ± 5.0 wt% protein) was prepared in the phosphate buffer (4 wt% sample) and was injected in the system using a 5 mL sample loop.

Two different eluents were used for the separation: eluent A was a 20 mM phosphate buffer with pH 9.3, and eluent B was ultrapure water containing 500 mM NaCl. Protein was eluted by using a linear gradient from 0–100% eluent B (10 column volumes). The outlet was fractionated in 5 mL samples. The protein eluted between 54 and 66 minutes and was collected.

The collected protein fraction was desalted using the desalting column. Isocratic elution was achieved with ultrapure water. The desalted and purified yBLG was then freeze-dried using Epsilon 2-10D LSCplus (Martin Christ GmbH, Germany). The protein purity was determined using the BCA assay to be 72.1 ± 6.5 wt%.

4

Engineering amyloid and amyloid-like morphologies of β-lactoglobulin

Loes Hoppenreijs, Laura Fitzner, Therese Ruhmlieb, Timon Heyn, Kerstin Schild, Atze-Jan van der Goot, Remko Boom, Anja Steffen-Heins, Karin Schwarz & Julia Keppler

Almost all proteins can form amyloid and amyloid-like aggregates, depending on environmental conditions, that have unique functional properties. This opens numerous applications for designed aggregates in materials, medical and food applications. However, it is poorly understood how the amyloid(-like) aggregation and their resulting morphology is induced or influenced by various environmental and processing conditions.

We identified and summarized conditions under which amyloid(-like) aggregates are formed and their impact on aggregate morphology. The focus is on β-lactoglobulin, but generic effects on other proteins are discussed, in order to elucidate common mechanistic properties.

The flexibility of linear aggregates can be evaluated by comparing the persistence (L_p) and contour length (i.e., length when completely stretched; L_c). Shorter and more flexible amyloid-like aggregates ($L_p < L_c$) usually occur from a relatively fast assembly (e.g., low repulsion, high concentration, solvents). Longer, semi-flexible amyloid aggregates ($L_p \sim L_c$) based on fibrillization-prone peptides that are slowly formed and assembled (e.g., high repulsion, low concentration). In either case, the aggregation kinetics increases through protein destabilization (e.g., heating, zinc addition, solvent and hydrolysis effects) and decreases through stabilization (e.g., glycerol addition). Post-processing (e.g., mechanical or interfacial stress) fragments aggregates into stiffer rods ($L_p > L_c$). Semi-flexible morphologies can align in liquid crystalline phases or interact with linear polysaccharides; while flexible aggregates can entangle. This allows for various possibilities to build higher order fibril or hybrid networks for various applications, such as bundles, coatings/films, or gels. This knowledge is crucial to produce specific morphologies for applications and to draw conclusions about how morphologies will be affected during processing (e.g., shearing).

Abstract

Abbreviations: AGE, advanced glycation end-product; β2m, β2-microglobulin; BLG, β-Lactoglobulin; BSA, bovine serum albumin; CMC, critical micelle concentration; DMSO, Dimethyl sulfoxide; DTT, dithiothreitol; EGCG, epigallocatechin-3-gallate; Lc, contour length; Lp, persistence length; RCM-BLG, reduced and carboxymethylated BLG; SDS, Sodium dodecyl sulfate; TEM, transmission electron microscopy; ThT, Thioflavin-T; WPC, whey protein concentrate; WPI, whey protein isolate.

4.1. Introduction

Amyloid aggregation is a type of protein aggregation in which linear self-assemblies are formed through intermolecular stacking of β-sheets under specific circumstances. Amyloids have been mostly associated with neurodegenerative diseases, but it is increasingly accepted that all proteins can form amyloid structures, including food proteins (Cao & Mezzenga, 2019), and do this to some extent during food preparation, e.g. during boiling of egg white (Monge-Morera et al., 2020).

Amyloid structures with specialized functions are also evident in various organisms ranging from bacteria to mammals. For example, functional amyloids are involved in the attachment of mussels (Priemel, Degtyar, Dean & Harrington, 2017) and squids (Deepankumar et al., 2020) to foreign surfaces, and in the colonization of bacteria and yeast (Fowler, Koulov, Balch & Kelly, 2007), which illustrates their high (wet-resistant) surface adhesive properties. Additionally, they mechanically stabilize shells of insects and fish eggs, revealing their strong structural properties (Fowler et al., 2007). In plant seeds, amyloid-like aggregates stabilize storage proteins through their high stability, resistance to proteolysis and toxicity against fungal and mammalian cells (Antonets et al., 2020). Although there is an ongoing debate around the safety of engineered aggregates that needs to be resolved before any applications can be produced for human consumption, the outstanding properties of amyloid structures in nature is an inspiration for engineered functional amyloid aggregates from (food) proteins.

Bovine β-lactoglobulin (BLG) is the most abundant protein in whey and is extensively studied and used in the food industry. Amyloid aggregates of BLG or whey protein isolate (WPI) are reported to be, for example, efficient gelators (at 0.3 wt%; Veerman, Baptist, Sagis & Van der Linden, 2003), emulsifiers (Cao & Mezzenga, 2019), encapsulates (Humblet-Hua, Van Der Linden & Sagis, 2012), and are good carriers for iron (Shen et al., 2017) and curcumin (Mohammadian et al., 2019). In addition, films from BLG amyloid aggregates are remarkably strong, having a comparable elastic modulus to keratin and collagen (Knowles, Oppenheim, Buell, Chirgadze & Welland, 2010). Many novel materials from BLG amyloid aggregates have already been described, which could be used e.g., as biosensors, nanocomposites, or catalysts (Wei et al., 2017).

The functionality of amyloid aggregates is in particular attributed to their specific high aspect ratio (i.e., length/thickness; Knowles & Mezzenga, 2016). Besides the classical straight amyloids, BLG can form 'amyloid-like' aggregates when the β-sheets are less tightly stacked, which are shorter and more flexible. The linear BLG aggregate morphology therefore varies from short, single-stranded, worm-like and flexible aggregates to long, multi-stranded, straight and semi-flexible fibrils (Jordens, Adamcik, Amar-Yuli & Mezzenga, 2011). Semi-flexible fibrils with a high aspect ratio,

effectively increase the viscosity and form gels. Worm-like aggregates increase the viscosity much less, at comparable concentrations (Loveday, Anema & Singh, 2017). Amyloid aggregates display effective emulsifier properties through a Pickering mechanism, protecting droplets from coalescence. The binding is particularly strong for anisotropic particles. For example, in the case of fibrils, it is practically impossible to detach them once they have attached to a surface (Jordens, Isa, Usov & Mezzenga, 2013). Therefore, several morphologies with varying application potential can be produced, by adapting environmental and processing conditions.

Conditions at which BLG forms amyloid(-like) structures are high concentrations of urea (Hamada & Dobson, 2009), alcohols (Gosal, Clark & Ross-Murphy, 2004), or at a combination of elevated temperature, low pH, and low ionic strength (Heyn et al., 2020). These conditions initially destabilize the native protein and form the aggregate building blocks: partly unfolded BLG and/or its constituent peptides. During the nucleation phase, the building blocks self-assemble into weakly associated nuclei. Further addition of building blocks during the growth phase results in the formation of linear aggregates. For insulin, it has been shown that the growth is unidirectional (Heldt, Zhang & Belfort, 2011). Based on the role of specific conditions on the aggregation process, the conditions can be divided into aggregation and post-aggregation factors. Aggregation factors mainly include conditions or modifications that can affect the aggregate morphology through their impact on the balance between intra- and intermolecular interactions. Besides, the aggregation kinetics are influenced by all factors that result in a local increase of protein-protein collisions (e.g., shearing or surfaces). Post-aggregation factors affect and change the mature aggregate morphology, which includes the gradual modification of the properties, and fragmentation. The aggregate stability is important for post-processing, which is determined by the internal molecular packing density (and resulting morphology) of the aggregates. In addition to the targeted post-processing of amyloid structures, fragmentation can occur unintendedly during food processing or storage. The final aggregate morphology and flexibility then determines the further assembly into higher order networks of bundles (one dimensional), at interfaces (two dimensional), or in gels (three dimensional), which then lead to various applications. ***Figure 4.1*** describes the major steps in the formation of protein aggregates.
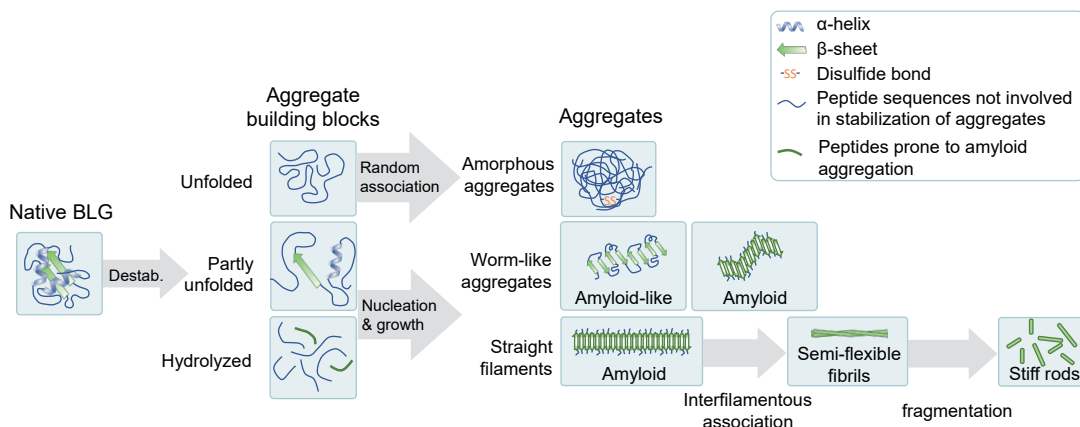
Figure 4.1. *Schematic overview of the general self-assembly of destabilized (destab.) BLG into aggregate building blocks and subsequent aggregates with amorphous, worm-like or straight morphology.*

An in-depth review on how to use physical and chemical conditions to modify BLG and subsequently tune the aggregate morphology and its assembly into multidimensional structures is currently lacking. Therefore, this review will discuss the conditions that favor the engineering of specific amyloid morphologies and will identify gaps in our knowledge. In addition, post-aggregation factors (intended or unintended) will be discussed, which are also relevant for further modification of the morphology. We will not focus on the use amyloid structures for further applications, as this has already been reported earlier (Cao & Mezzenga, 2019; Jansens et al., 2019; Lambrecht et al., 2019; Loveday et al., 2017).

We will first summarize the primary conditions that affect the aggregate morphology, namely the pH, ionic strength, temperature and protein concentration. We will then discuss the effects of the physical processing conditions, such as shearing, cavitation and pressure, that mainly affect the fragmentation of mature amyloid structures. Also, the influence of the presence of solid/liquid and liquid/liquid interfaces will be discussed. Besides physical processing, the chemical environmental conditions can be adapted to modify the structure of proteins and subsequently the aggregation behavior. Finally, we will touch upon how the individual fibrils with specific morphology can associate into higher order networks, forming fibers, films and gels with high mechanical stability.

4.2. The primary conditions: pH value, ionic strength and temperature

Amyloid aggregates are formed through the formation of building blocks from the individual proteins and the subsequent assembly of these building blocks. The building blocks of amyloid aggregates are (partly) unfolded or hydrolyzed BLG, which contain (exposed) fibrillization-prone sequences. In particular, the factors and factor combinations of pH value, ionic strength, and temperature are of crucial importance for the exposure or formation of such fibrillization-prone building blocks, their aggregation kinetics, and the resulting aggregate morphology. In the following section, an overview of the conventional fibril formation conditions for BLG is given, starting with the effect of the pH value, the ionic strength and the temperature on the resulting morphologies (***Section 4.2.1***), followed by the effect of these primary conditions to tune the morphology of mature fibrils (***Section 4.2.2***) and ending with an outlook on fibril morphology of other food proteins under these conditions (***Section 4.2.3***).

4.2.1. Aggregation

The most common environmental conditions for the formation of different amyloid(-like) aggregates from BLG are low pH (≤ 3.5), low ionic strength and elevated temperature (> 70 °C), resulting in typical semi-flexible fibrils. Random aggregation is prevented by the electrostatic repulsion induced through low pH values (≤ 3.5). At pH < 3, the association of intact BLG is unfavorable and hydrolysis is necessary to allow for amyloid aggregation. Acidic hydrolysis within the relevant time frame (several hours) can be induced by heating at > 70 °C (typically 80–90 °C), leading to the formation of peptides with increased fibrillization propensity. These peptides include mainly the N-terminal peptide sequences 1–33 and 1–53. The inclusion of these specific peptide sequences is mainly attributed to their increased hydrophobicity, capacity to form β-sheets and low charge (Akkermans, Venema, van der Goot, et al., 2008). Specific amino acid residues can stabilize the intermolecular β-sheets. For example, through hydrogen bonds by amide-containing residues (glutamine and asparagine; Heyn, 2020) or π-π stacking of aromatic groups in aromatic residues (phenylalanine and tryptophan; Porat, Abramowitz & Gazit, 2006).

Association of these fibrillization-prone peptides results in thin (~ 2.6 nm), long (contour length, L_c = 0.2–5 μm), straight and well-ordered amyloid aggregates (***Figure 4.2A***; Akkermans, Venema, van der Goot, et al., 2008; VandenAkker, Engel, Velikov, Bonn & Koenderink, 2011). The flexibility of these aggregates can be evaluated by comparing the persistence (L_p) and contour length (axial circumference), which are of the same order of magnitude for less flexible structures. VandenAkker et al. (2011) showed that this is the case for the fibrils (L_p = 3.8 ± 0.1 μm) and therefore we will refer to these structures as 'semi-flexible fibrils' (***Figure 4.2A***). Besides, their folding

density is approximately 2% higher as compared to native BLG (Uttinger et al., 2020). Since only a fraction of the total protein peptide chain is included in the fibrils, the maximum conversion factor for incorporation is only 40–50% (Bolder, Vasbinder, Sagis & van der Linden, 2007; Serfert et al., 2014). BLG is the main constituent of WPI and makes up about half of the total protein content. WPI shows similar fibrillization kinetics and fibril morphology, since only BLG is incorporated in the fibrils at pH 2 and 80 °C. Further proteins present in WPI (α-lactalbumin and bovine serum albumin) are mostly inert to fibrillization under these conditions. However, they can form small aggregates that are able to lower the gelation concentration of BLG fibrils by introducing depletion forces (Bolder, Hendrickx, Sagis & Van Der Linden, 2006).
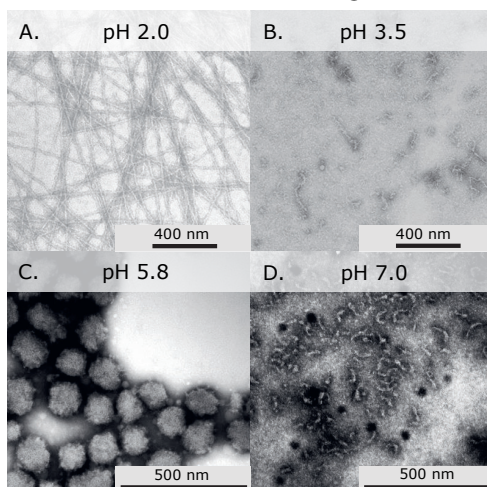

Figure 4.2. *Transmission electron microscopy images of BLG aggregates prepared at (**A**) pH 2.0 and (**B**) pH 3.5 (both 2.5% BLG at 90 °C for 5 h, from Keppler, Heyn, Meissner, Schrader & Schwarz (2019), and (**C**) pH 5.8 and (**D**) pH 7.0 (both 1.0% BLG at 85 °C for 15 min, from Jung et al. (2008).*

Another type of amyloid aggregate can can form from BLG at higher pH values. At pH 3 to 3.5 and temperatures > 70 °C (Heyn et al., 2020), partly unfolded BLG can directly associate into more randomly associated amyloid-like aggregates that are thin (1–3 nm) and short (L_c = 50–200 nm; **Figure 4.2B**). We will refer to these structures as 'worm-like aggregates'. They are more flexible ($L_p \sim$ 10 nm) than semi-flexible fibrils (Heyn et al., 2019; Jung, Savin, Pouzot, Schmitt & Mezzenga, 2008). In addition, they are less compact, which is explained by the incorporation of unstructured (random coil) peptide sequences into the aggregates (Heyn et al., 2019). Lux et al. (2021) hypothesized that rearrangements for worm-like aggregates at pH 3.5 cause outward folding of the C-terminus. Ye, Hedenqvist, Langton & Lendel (2018) demonstrated that a larger fraction of C-terminal peptides is included in the core segment of amyloid-like aggregates, due to less acidic hydrolysis at this relatively higher pH value.

At pH values near the isoelectric point, the morphology shifts toward monodisperse, compact, and randomly associated spherical aggregates (~ 150 nm, **Figure 4.2C**) (Jung et al., 2008). The electrostatic repulsion at neutral pH (being higher than the isoelectric point) allows for aggregation into unbranched, short (< 100 nm) and worm-like aggregates with a diameter of 6 ± 1 nm (**Figure 4.2D**; Da Silva Pinto et al., 2012; Jung et al., 2008). These authors was confirmed the amyloid-like nature with a Thioflavin T (ThT) assay (Da Silva Pinto et al., 2012), which is frequently used as a first indicator of amyloid aggregation.

Enzymatic hydrolysis can be applied as an alternative to acidic hydrolysis, to produce peptides with increased fibrillization propensity. Akkermans, Venema, van der Goot, et al. (2008) reported that hydrolysis of BLG with the endoproteinase AspN allows for amyloid aggregation at a lower temperature (37 °C). After hydrolysis at pH 8 and a pH adjustment to pH 2, semi-flexible fibrils (~ 1 μm) and random aggregates (~ 50 nm) were formed. The obtained heterogeneity in the morphology was confirmed by Hamada et al. (2009), who showed that the morphology depends on the peptides that are involved in nucleation. Therefore, the type of proteinase determines whether fibril formation is enhanced or suppressed. For instance, Gao, Xu, Ju & Zhao (2013) observed that the hydrolysis of whey protein concentrate (WPC) with trypsin allows fast fibril formation, while the hydrolysis with protease A, M and pepsin resulted in slower aggregation. Trypsin-treated WPC formed unbranched, long, semi-flexible fibrils, while WPC treated with the other enzymes resulted in shorter and/or branched fibrils after prolonged heating (5–10 hours). The difference was mainly attributed to the ability of trypsin to preserve the α-helix structure, which is transferred to β-strands and subsequent intermolecular β-sheets during fibrillization, while the other enzymes destroyed 51–37% of the α-helix structure. Besides, they observed a decreased free thiol content during the hydrolysis for all enzymes, except trypsin, which indicated that additional disulfide bonds were formed. Intermolecular disulfide bond formation is expected to hinder amyloid aggregation. Lastly, aggregation was also stimulated by cleavage at hydrophobic amino acids as performed by trypsin, which lead to higher surface hydrophobicity of the resulting peptides, as compared to cleavage by the other enzymes.

The initial protein concentration influences the amyloid morphology mainly through its impact on the size distribution of the peptides that result from acidic hydrolysis. A gradual increase from pH 2 to pH 3 is observed upon acidic hydrolysis, which in turn limits further hydrolysis and stimulates aggregation (Ye et al., 2018). This will occur faster at higher protein concentrations, while larger peptides are then included in the aggregates. Low initial BLG concentrations are generally used (up to 3.0–4.0 wt%), which results in semi-flexible fibrils. Higher concentrations (~ 7.5–8.0 wt%) result in shorter and worm-like aggregates (L_c = 100–500 nm, L_p ~ 90 nm) with a similar

4

diameter (~ 2.6 nm; VandenAkker et al., 2011, 2016; Ye et al., 2018). These worm-like aggregates include more random coil and α-helix structures, while the semi-flexible fibrils contain more β-sheets (VandenAkker et al., 2016; Ye et al., 2018). Ye et al. (2018) attributed the differences in secondary structure to an increased incorporation of C-terminal peptides, although VandenAkker et al. (2016) did not find differences in peptide building blocks. For worm-like aggregates that are formed at the relatively higher protein concentrations from intact BLG or longer peptides, it is hypothesized that N- and C-terminal peptides might be linked through native disulfide bonds.

In addition to the pH value and protein concentration, ions affect the BLG amyloid morphology. This is due to charge screening effects (i.e., lower electrostatic repulsion), but also to direct binding to the protein. Amyloid aggregation at acidic pH values and elevated temperatures can be accelerated by the addition of salt, which generally leads to a shift towards worm-like aggregation due to more random association (e.g., > 50 mM NaCl at pH 2.0; Arnaudov, de Vries, Ippel & van Mierlo, 2003). Similar to the worm-like aggregates at pH 3.5 or at high initial protein concentration, these aggregates are more flexible. Loveday et al. (2010) found that in the presence of ≥ 60 mM $CaCl_2$ or ≥ 33 mM NaCl, L_c is a few hundred nanometers and L_p is 38–84 nm, while in the absence of salt, L_c is 0.5–1 μm and the L_p of 1.8–4.3 μm. They reported that both monovalent (Na^+, Cl^-) and divalent (Ca^{2+}) ions accelerate the growth of fibrils to a comparable extend, leading to similar morphologies. In contrast, only divalent ions accelerated the nucleation, presumably through bridging between peptides. Similarly, Zappone, De Santo, Labate, Rizzuti & Guzzi (2013) observed a longer lag phase for BLG fibril formation in the presence of copper (Cu^{2+}) without affecting the fibril growth much. Copper destabilizes BLG, which leads to earlier unfolding upon heating (i.e., decreased denaturation temperature), and may initiate thiol oxidation and disulfide exchange reactions. An equimolar addition of copper to BLG resulted in fibrils with a larger diameter due to increased interfilamentous association. Further addition of cupper (1:10 mol/mol) resulted in the formation of additional fibrils with a smaller diameter (~ 1 nm), probably due to the stabilization and elongation of smaller nuclei that otherwise would fall apart (Zappone et al., 2013). Similarly, zinc also accelerates fibril formation through destabilization of BLG, due to unfolding prior to heating (in contrast to copper) by further opening of the disulfide bond conformation (~ 50% for Zn-BLG and ~ 25% for Cu-BLG). In addition, zinc is more effective in redistribution of charges, which led to bigger (up to 65 nm instead of 50 nm) and slightly branched fibrils during heat-induced aggregation (Navarra et al., 2014).

4.2.2. Post-aggregation

Once mature amyloids are formed, their morphology can be modified by changing the environmental or processing conditions, for example, through continued acidic hydrolysis during prolonged incubation. Even though it is assumed that worm-like aggregates consist mainly of intact BLG at pH > 3.0, Keppler et al. (2019) showed that BLG is partly hydrolyzed at pH 3.5 at 90 °C (mostly > 5–24 hours). This hydrolysis proceeded at prolonged incubation times, while the relative number of intermolecular β-sheets had already stabilized (1–2 days). This was postulated to be due to 'shaving' of aggregates. In essence, this is the removal of peptide sequences that are not involved in the intermolecular aggregation, but which were linked to peptide sequences that were involved. One could expect a morphological change towards the semi-flexible fibrils since the building blocks change towards peptides, but this was not the case, which indicates that the two types of aggregates differ in their core segments.

Extended heating times may cause individual BLG fibril filaments to associate into twisted or helical filament bundles (Adamcik & Mezzenga, 2018). For example, two or more single filaments (~ 2.6 nm diameter) associated into thicker fibrils (~ 4.0 nm diameter) after 96 hours of incubation at 80 °C and pH 2.0 (VandenAkker et al., 2011). A higher tendency for this association was observed when increasing the incubation pH from 2.0 to 4.0 (Jung, Gunes & Mezzenga, 2010). At pH 2.0 and 90 °C, maximally five filaments interacted for incubation times up to 5 hours, with up to 16 strands after 30 h of incubation (Lara, Adamcik, Jordens & Mezzenga, 2011). Interestingly, the heterogeneity of the number of filaments included in the fibrils was higher when produced with conventional heating, as compared to microwave-assisted heating. This was attributed to the need for heat transfer in conventional heating, as compared to instant heating by microwave-induced rotation of water molecules (Lee et al., 2015).

Association of the BLG filaments into bundles occurs through hydrophobic short-range attractions, while long-range electrostatic repulsions lead to a twist in the fibril that has a periodic pitch (i.e., twist frequency). Therefore, the addition of NaCl to mature fibrils leads to a longer pitch (Bolisetty, Adamcik & Mezzenga, 2011). A slightly longer pitch was also observed at higher temperatures (100–120 °C) (Loveday, Wang, Rao, Anema & Singh, 2012). Similarly, Lee et al. (2015) found amyloid aggregates with a longer pitch and a lower surface charge density when heating with a microwave at 100 °C, as compared to heating to 70–80 °C. The authors hypothesized that the stacking mechanism at higher temperature resulted in more stable aggregates.

Amyloid aggregates prepared at acidic pH are often exposed to and stored at higher pH values for application in food, which results in a morphological shift. A pH adjustment to pH 4–6 induced semi-flexible BLG fibrils to aggregate into unordered aggregates,

4

due to the lower interfibrillar electrostatic repulsion around their isoelectric point of about 5 (Jones et al., 2011; Karbasi et al., 2021; Peng, Yang, Li, Tang & Li, 2017). In addition, the fibrils became more flexible and shorter due to the progressive reduction in intrafibrillar electrostatic repulsion (Jones et al., 2011; Peng et al., 2017). In contrast, addition of NaCl to mature semi-flexible BLG fibrils did not change the morphology of the individual filaments but did increase the interfilamentous association (Adamcik & Mezzenga, 2011). Peng et al. (2017) reported that a further pH adjustment to 7.0 allowed for an increased electrostatic repulsion that opened the aggregates, resulting in alignment of the fibrils. In addition, exposed free thiol groups are more reactive at higher pH and thereby might form intermolecular disulfide bonds. Free thiol groups are less reactive due to protonation at the acidic pH, usually applied for amyloid formation, although it remains unclear whether that completely avoids intermolecular disulfide bond formation under these conditions.

4.2.3. Amyloid aggregation of other food proteins

Several food proteins possess 'core regions', i.e., specific amino acid regions that are prone to amyloid aggregation under sufficiently long aggregation times (Jansens et al., 2019). Slow aggregation is induced under particular conditions, depending on the protein sequence, folding and stability. Goldschmidt, Teng, Riek & Eisenberg (2010) showed that at least 98.7% of all proteins contain a core region that can form intermolecular β-sheets. It can therefore be assumed that amyloid aggregation is a generic protein property. In the following, a selection of proteins that show similar morphologies or interesting differences to BLG are described.

Worm-like aggregates and semi-flexible fibrils can be formed from several animal proteins under similar conditions described in ***Section 4.2.1***. Usov, Adamcik & Mezzenga (2013) reported simultaneous worm-like aggregate and semi-flexible fibril formation for bovine serum albumin (BSA; 6 wt% at 90 °C and pH 2). Short ($L_c \sim 0.5$ μm) and worm-like ($L_p = 0.15$–16 μm) aggregates were formed initially (≤ 40 hours), with long ($L_c \sim 2.2$ μm) and semi-flexible ($L_p = 1.3$–2.6 μm) fibrils being additionally formed during prolonged heating times (up to 145 hours). They proposed that worm-like BSA aggregates are converted into semi-flexible fibrils during prolonged heating, by converting the twisted filaments into nanotube-like structures. A similar aggregation behavior has been shown for ovalbumin by Lara et al. (2012). Flexible worm-like aggregates ($L_p = 63 \pm 7$ nm) were formed within the first few hours, followed by bendable ($L_p = 300 \pm 80$ nm), longer filaments formed after around 2 hours. After approx. 6 hours of incubation, filaments intertwined to form rigid ($L_p = 3,000 \pm 700$ nm) fibrils. Longer incubation times resulted in shorter contour lengths and addition of salt resulted in a shift towards longer worm-like aggregates, without any fibrils. Gosal et al. (2005) proposed that different amyloid forming pathways compete,

resulting in either the worm-like aggregate or semi-flexible fibril structures. For the human amyloid protein β2-microglobulin (β2m) they propose that fast kinetics in which no lag phase is observed result in worm-like morphology, while slow kinetics with a lag phase result in semi-flexible fibrils. Similar to BLG, β2m forms flexible, short ($L_p = 50$), and worm-like aggregates (at pH 3.5 in the presence of 200 mM NaCl). In addition, β2m forms rigid, long ($L_p = 1,740$), and semi-flexible fibrils that consist of multiple filaments, at pH < 2.5 in the absence of NaCl. A shift towards semi-flexible fibrils can be induced by removing the nucleation barrier through changes in the solution conditions (e.g., decrease in pH), addition of seeds, or agitation.

In comparison to fibrils from animal proteins, a lower resemblance to semi-flexible BLG fibrils is observed for fibrils from plant storage proteins, such as pea protein, patatin, and soy protein as those are often branched (**Figure 4.3**). Heating pea protein at pH 2.0 and 85 °C resulted in short and worm-like aggregates that present a certain degree of branching (Munialo, Martin, Van Der Linden & De Jongh, 2014), in contrast to the unbranched semi-flexible fibrils formed from BLG under these conditions. Patatin also forms short (~ 0.5 μm), worm-like aggregates at pH 2.0. Likewise, soy glycinin forms branched amyloids (20 h, pH 2.0 and 85 °C), having comparable flexibility to BLG fibrils, but being longer ($L_c = 0.1$–4 μm ≈ L_p; Akkermans et al., 2007). Amyloids from soy protein isolate (80% soy glycinin, 20% β-conglycinin) are similar to the ones from soy glycinin but show a higher degree of branching (i.e., lower birefringence signal). It remains unclear what causes this branching, but plant proteins in general contain a relatively low amount of charged residues (Day, 2013), which might increase their tendency to assemble at multiple locations at the protein or peptide. Lastly, wheat gluten is also shown to form unbranched fibrils (and amorphous aggregates) upon heating at 78 °C for 22 h or boiling for 15 min. An enzyme treatment was performed to remove the amorphous aggregates, which might have also affected the fibril morphology (Monge-Morera et al., 2021).
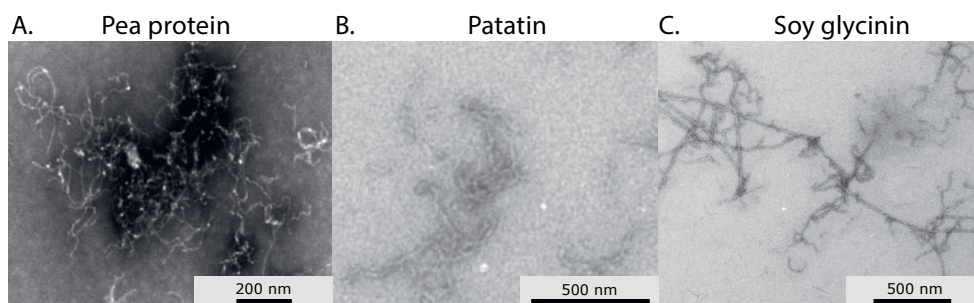
A.   Pea protein   B.   Patatin   C.   Soy glycinin

Figure 4.3. *Amyloid aggregates prepared from (**A**) 4 wt% pea protein (20 h at pH 2.0 and 85 °C, taken from Munialo et al., 2014), (**B**) patatin (prolonged heating at pH 2.0 and unknown temperature, taken from Akkermans, 2008), and (**C**) 4 wt% soy glycinin (20 h at pH 2.0 and 85 °C, taken from Akkermans et al., 2007).*

4.3. Further physical processing conditions

Processing and storage of fibrils in specific environments can lead to morphological changes. Below we will discuss studies that demonstrate the considerable influence of the mechanical energy input and change of the interfacial energy on the amyloid aggregates. These aspects destabilize the initial non-aggregated protein structure, accelerate the denaturation, and influence the morphology of the already aggregated structures.

4.3.1. Mechanical stress and shear field

Mechanical stress (e.g., shear forces, cavitation, or high- or dynamic pressure application) is both an aggregation and post-aggregation factor. Shear stress can irreversibly or reversibly change the protein conformation, and results in an increased aggregation tendency without affecting the resulting morphology (Heyn et al., 2020). Fibrillization is generally regarded to follow a nucleation-dependent polymerization mechanism, which consists of nucleation and elongation (Chatani et al., 2009). The nucleation rate is affected by the corresponding shear flow, as protein-protein collisions are either induced (turbulent flow) or prevented (laminar flow). For BLG, conformational changes were described at shear rates up to $1000\ s^{-1}$ in combination with acid pH and high temperature (Rahaman, Vasiljevic & Ramchandran, 2015). Cavitation and simultaneously generated air-water interfaces can stimulate a globular protein to unfold and to aggregate (Wang, Nema & Teagarden, 2010). They also locally affect nucleation by inducing and preventing spatial assembly of proteins, thereby having an impact on nucleation and fibril growth.

The mechanical energy input and corresponding flow plays an important role in aggregate nucleation and growth. In general, shearing of BLG solutions by shear rheometers, magnetic stirrers, or four-roller apparatus, can shorten the lag phase, accelerate subsequent growth and affect fibril yield and length (Akkermans, van der Goot, Venema, van der Linden & Boom, 2008; Akkermans et al., 2006; Bolder, Sagis, Venema & Van Der Linden, 2007; Dunstan, Hamilton-Brown, Asimakis, Ducker & Bertolini, 2009). Similarly, shear pulses have been shown to cause accelerated nucleation (Akkermans et al., 2006). Akkermans, van der Goot, Venema, et al. (2008) explained the increased kinetics by the enhanced transport of potential building blocks to the active nucleus end, due to the implemented shear field. Even though the impact of shear on the BLG fibril morphology has not been reported extensively in literature, effects were described for other proteins. For the fibrillization of the protein glucagon, a minimum mechanical stress (e.g., by agitation speed) can lead to two different fibrillar morphologies (MacChi et al., 2011). Fibrils created at low stress were mostly straight, modestly twisted and tended to associate laterally. Fibrils created

at high stress were very straight, showed a pronounced twist and did not associate laterally. The importance of mechanical stress for the occurrence of polymorphism was also noted for fibrils from Aβ-peptide (Petkova et al., 2005) and prion proteins (Makarava & Baskakov, 2008). Greving, Cai, Vollrath & Schniepp (2012) demonstrated that shear can result in the formation of self-assembled fibrils from native silk protein during spin coating, prior to drying. The fibril diameter decreased with the protein concentration (0.1 wt% compared to 10 wt%).

Mechanical stress mainly influences the fibrillization mechanism through fragmentation and secondary nucleation. Fragmentation of protofibril structures in the shear field, e.g., during stirring (Bolder, Sagis, et al., 2007; Dunstan et al., 2009; Heyn et al., 2020) or ultrasound application (Sneideris, Milto & Smirnovas, 2015), results in release of new active ends. These so-called 'seeds' are available as nuclei that can subsequently grow into fibrils (Dunstan et al., 2009). Nicoud, Lazzari, Balderas Barragán & Morbidelli (2015) reported that upon increased agitation (50–250 rpm), fragmentation reactions are accelerated about eight times more as compared to fibril growth, which therefore leads to a lower average length of fibrils. The breakage pattern remained the same, while thermal breakage shifts from an erosion (i.e., at fibril ends) to random breakage at lower temperatures, for both BLG and insulin.

The influence of mechanical stress on fibrils as a post-aggregation factor is particularly relevant in the context of the manufacturing processes of (food) products. In such processes, different mechanical stresses act on the fibrils. For example, the application of rotor-stator dispersion and high-pressure homogenization, as used to produce stable oil-in-water emulsions, strongly affects the fibril size (Serfert et al., 2014; Uttinger et al., 2020). Cavitation by ultrasound (Mantovani, de Figueiredo Furtado, Netto & Cunha, 2018) or dynamic high-pressure treatment (Serfert et al., 2014) leads to even stronger fragmentation of mature fibrils into fibers of 80 and 90 nm. Thus, such processes can also be intentionally used for post-processing of fibrils, as the resulting fragments have a homogenous length and are less flexible than intact fibrils.

The decrease in mean fibril length depends almost directly on the applied mechanical energy intake. Heyn et al. (2021) showed that semi-flexible fibrils (pH 2.0) and worm-like aggregates (pH 3.5) from BLG were only partly dissociated upon energy intakes up to 76 J mL^{-1} min^{-1}, as applied by ultra-sonication. Fragmentation of worm-like aggregates from BLG was less pronounced than for semi-flexible fibrils, when the mechanical stress was applied by rotor-stator disperser, probably due to the higher flexibility, and larger homogeneity of the stress over the fluid. Static high-pressure of lysozyme fibrils above 450 bar can lead to fibril or filament dissociation, which may be due to hydration of pressure-sensitive water-excluded cavities and hydrophobic pockets in the fibril structure (Radovan, Smirnovas & Winter, 2008).

4.3.2. Solid and liquid surfaces/interfaces

Interfaces can induce unfolding, adsorption and alignment of proteins. Therefore, a liquid or solid interface can induce aggregation of BLG. Even though it remains unclear whether it can induce amyloid aggregation of BLG, such effects were found for other proteins like insulin (Lee, Um, Park & Park, 2008) and Aß-peptide (Moores, Drolle, Attwood, Simons & Leonenko, 2011). In the latter example, exposure to a hydrophobic solid surface (beads) promoted spherical amorphous aggregates, while charged surfaces induced anisotropic fibril formation. Similar effects were observed for immunoglobulin by Zhu, Souillac, Ionescu-Zanetti, Carter & Fink (2002): the negatively charged surface of mica promoted fibril formation. Interestingly, this was not the case with mica that was positively charged or modified to have a non-polar surface. It was stated that the growth mechanism on solid surfaces accelerates fibril formation, as compared to aggregation in solution. Fibrillization of immunoglobulin at the surface can occur through bidirectional linear assembly of building blocks, or through linear growth from amorphous cores. Lastly, the deposition of a water droplet on a heated super hydrophobic surface can induce fibril formation into different morphologies, as shown for disease related proteins (Tau and PHF6 peptide) and lysozyme. Short fibrils were formed at a temperature gradient (with respect to the environment) of 20 °C, while longer fibrils formed at higher temperature gradients. The growth process and resulting fibril morphology varied with the convective flow induced by the temperature gradient, but also the de-pinning process (Zhang et al., 2020).

Surfaces and interfaces can also function as a post-processing factor to modify the fibril morphology. Heat-induced semi-flexible BLG fibrils tend to curve into rings and loops when exposed to liquid interfaces (air-water and oil-water). The stress caused by bending, high surface tension or exposure to air can result in fracturing of the fibrils (similar to mechanical fragmentation, *Section 4.3.1*). The resulting shorter fibrils can also bend and form rings at a liquid interface. In addition, they can assemble in or on existing rings, either in a parallel or perpendicular fashion (Jordens et al., 2014). It is unclear whether these rings remain stable during foaming or drying.

As discussed in *Section 4.3.1*, seeds can accelerate fibril formation. This effect could be regarded as a surface effect, because "seeds" can act as a solid surface to promote self-association. Seeds can aggregate with surrounding proteins, which favors conformational changes in the proteins and may lead to subsequent exposure of hydrophobic groups. This accelerates the ordered aggregation. In addition, the seeds act as a template for the conformational changes induced and thereby can be used to change the morphology (Vetri & Foderà, 2015).

The effects of surfaces on the self-association are also evident in the drying of fibrils. Using the Langmuir-Schaefer deposition technique, Smith, Fernandez-Rodriguez, Isa & Mezzenga (2019) describe that soft/flexible fibrils tend to de-wet at the water-air meniscus due to capillary forces. These capillary forces occur at the receding meniscus during drying. This can cause aggregation of the fibrils into higher order structures (**Section 4.5**). The surface tension influences this change in the receding meniscus. Thus, low viscosity and volatile excipients that lower the surface tension, such as hexane, are needed to prevent morphological changes when transferring fibrils from a liquid-liquid interface to a solid substrate (Smith et al., 2019).

4.4. Further chemical environmental conditions

As described in the previous section, the fibril properties can be modified by adaptation of the physical processing conditions. Likewise, the physicochemical conditions can accelerate or inhibit amyloid aggregation, and modify aggregate properties after aggregation.

4.4.1. Denaturants and surfactants

Protein unfolding is one of the critical steps observed in amyloid aggregation, which is often achieved through elevation in temperature (**Section 4.2.1**). Alternatively, denaturants (e.g., guanidine chloride or urea) can be used to reduce intra- and intermolecular interactions, through direct interaction with the protein or changing the solvent quality (Hamada & Dobson, 2009; Stumpe & Grubmüller, 2007; L. Zhang & Schmit, 2017). For example, urea can displace water at the interface of proteins, weaken hydrophobic interactions, and thereby indirectly induce unfolding. Besides, it can solvate the peptide backbone, exposing polar and aromatic residues, leading to further unfolding (Stumpe & Grubmüller, 2007). Unfolding of the protein results in exposure of aggregation-prone structures, which may increase the tendency for aggregation. However, intermolecular interactions are decreased simultaneously, which results in destabilization of the aggregates when formed. Whether these effects will result in an accelerated or decelerated fibrillization, depends on the denaturant, its concentration, and the type and stability of the protein. In the presence of 3–5 M urea, BLG can form unbranched semi-flexible fibrils (8–10 nm diameter) at neutral pH after incubation for 1 month (37 °C). Urea concentrations below 3 M and above 5 M prevent the formation of amyloid aggregates. At concentrations of < 3 M, the dimer is stabilized, and unfolding is limited. Fibrils prepared with 3 M urea contained some thicker fibrils (~ 15 nm) as compared to fibrils formed with 4 and 5 M urea (~ 8–10 nm) (Hamada & Dobson, 2009).

The surfactant sodium dodecyl sulfate (SDS) is commonly used to destabilize the native conformation of proteins by neutralizing charges and inducing hydrophobic

interactions. Khan et al. (2012) used SDS (100-fold molar excess) to induce aggregation of several proteins at a pH that was 2 units below or above the pI. Above the pI, SDS and the proteins were both negatively charged, preventing interaction of SDS with the proteins, thereby avoiding aggregation. Below the pI, amyloid aggregates were formed with different morphologies depending on the protein. They ranged from worm-like amyloids to semi-flexible fibrils, and varied in branching, size, and degree of interfibrillar aggregation. Jung et al. (2008) prepared heat-induced semi-flexible fibrils (pH 2.0) and worm-like aggregates (pH 7.0) from BLG and observed the complexation with SDS upon a pH shift to 3.0. SDS neutralized the charge of the amyloid structures, resulting in precipitation. However, upon a further increase in SDS, a double layer was formed that resulted in redispersion of the aggregates (including at the isoelectric point, as discussed in **Section 4.2.2**). Other surfactants (> 10 mM), such as fatty acids or soy lecithin, can also hydrophobically interact with peptides or proteins. Mantovani, Fattori, Michelon & Cunha (2016) found a decreased yield for heat-induced fibrillization of WPI in the presence of soy lecithin, without affecting the fibrillization rate or the resulting morphology. Fibril aggregation was stimulated above the critical micelle concentration (CMC) of lecithin, possibly through an excluded volume effect.

4.4.2. Solvents

Apart from denaturants and surfactants, solvents such as ethanol can also induce unfolding through destabilization of the protein, and thereby can indirectly promote aggregation. Solvent-induced fibrillization has a clear impact on the morphology (Kayser et al., 2020; Liu, Li, Qin & Zhong, 2021; Yoshida et al., 2012). In contrast, substances that stabilize the tertiary structure, such as glycerol (plasticizer), will likely hinder the aggregation without altering the morphology (Dave, Loveday, Anema, Jameson & Singh, 2014).

Many solvents partly denature BLG, which is then followed by a transition into a predominant β-sheet conformation via an initial stage of α-helical conformation (Kayser et al., 2020; Yoshida et al., 2012). At high protein concentrations, this mechanism can be followed by amyloid-like aggregation (Yoshida et al., 2012). Solvents that were already found to affect the amyloid aggregation of BLG at various conditions (e.g., temperature, pH value) are 2,2,2-trifluoroethanol, 3,3,3′,3′,3′-hexalfluoro-2-propanol, methanol, ethanol and propane-2-ol (Gosal, Clark, Pudney & Ross-Murphy, 2002).

Worm-like aggregates can be obtained by assembly of intact proteins instead of closely assembled β-sheet peptides in the presence of hydro-ethanolic solutions, for example, at low temperatures up to 30-50 °C (Kayser et al., 2020). Hydrophobic forces then become less relevant due to the more non-polar environment compared to purely aqueous solutions, while hydrogen bond strength increases. The polarity is determined by the solvent type (e.g., dimethyl sulfoxide [DMSO], ethanol, or methanol) and its volume,

affecting the hydrophobicity and binding mode. In addition, temperature elevations affect the polarity (i.e., through the dielectric constant), but also the protein-solvent interactions (i.e., binding) and the protein mobility. Consequently, a lower solvent concentration is required to induce amyloid aggregation at increased temperatures. The effect of solvents on the aggregate morphology is time dependent. Kayser et al. (2020) observed spherical aggregates (no amyloids) immediately after the addition of ethanol, DMSO or methanol (30%, v/v, 30 °C). Both spherical and worm-like aggregates were present after five hours of incubation. Both worm-like aggregates and semi-flexible fibrils were formed in the presence of ethanol at higher temperature (10–50%, v/v, 85 °C; Liu, Li, Qin & Zhong, 2021). Interestingly, solvent-induced aggregates vary in their morphology, which could potentially be used to shape these aggregates. For example, DMSO-induced aggregates were found to be slightly longer (100–150 nm) than ethanol-induced aggregates (20-60 nm) (Kayser et al., 2020).

Exposure to solvents can be used as a post-aggregation factor. Jordens et al. (2011) mixed heat-induced semi-flexible BLG fibrils with ethanolic solutions (10–50%, v/v) and incubated (37 °C) them for several weeks. Initially the semi-flexible fibrils (~ 2.4 µm in water) changed their morphology into worm-like aggregates (~ 29 nm in the presence of 50% ethanol for 1 week). These consisted of peptides as building blocks with an increased concentration of random coil and turn elements, and lost their multistrand character (2.5–2 nm, instead of 4–10 nm). The contour length of the worm-like aggregates increased at the expense of the semi-flexible fibrils, when incubated for longer (up to 550 nm in 8 weeks). A critical concentration of 30% was necessary for the described transformation.

4.4.3. Oxidants and reductants

Different chemical modifications of BLG can be induced through oxidation reactions. Protein oxidation is a generic term for the covalent modification of proteins through chemical reactions with reactive oxygen, nitrogen or sulfur species (Hellwig, 2019). Amino acids can be chemically modified depending on the nature of the oxidant and the oxidation mechanism, leading to the formation of carbonyls, hydroperoxides and sulfur oxides. These modifications can lead to changes in charge and hydrophobicity, crosslinking of sulfide or tyrosine, cleavage of disulfides and/or backbone cleavage (Davies, 2016). Consequently, destabilization and (partial) unfolding can lead to aggregation (Davies, 2005). Thus, protein oxidation is an aggregation factor. From a technological point of view these effects can modulate the functional properties of the proteins (Hellwig, 2019).

Oxidative stress can thus cause oxidative modifications, with structural changes as a consequence. These structural changes favour and promote amyloid aggregation *in vivo*, as is the case in the development of neurodegenerative disorders (Cheignon

et al., 2018; Gregersen, Bolund & Bross, 2003). Such oxidative effects may also occur during the extreme *in vitro* incubation conditions applied to form fibrils (e.g., urea, high temperature and low pH; see **Section 4.2**), demonstrating the potential of oxidation reactions for the targeted production of amyloid aggregation. Oxidation reactions during the aggregation process itself (90 °C, pH 2 or pH 3.5) can change the building blocks of amyloid aggregates of BLG and thus affect the resulting morphology and functionality of the aggregates (Keppler et al., 2019). Recently, Maity et al. (2021) reported that selective methionine oxidation in BLG leads to a more flexible and unfolded state, which is more prone to fibrillization. Heat-induced aggregation at physiological pH lead to worm-like aggregates (40–55 nm diameter) for native BLG, while more fibrillar aggregates were obtained for oxidized BLG (20–35 nm diameter).

Reduction reactions also affect amyloid aggregation. For BLG, Hamada & Dobson (2009) only found monomeric species in urea-induced BLG fibrils, indicating the absence of intermolecular disulfide bonds. It remains unclear whether intermolecular disulfide bonds are formed in heat-induced fibrils. However, intramolecular disulfide bonds play a major role in amyloid aggregation. Under similar conditions, Hamada et al. (2009) showed that certain BLG peptide sequences (βG, βH, and βI strands) are hindered to form amyloid structures, due to a conformational restraint induced by disulfide bonds. Reduction and carboxymethylation of BLG (RCM-BLG) therefore stimulated fibril formation. Two types of fibrils were formed for RCM-BLG, i.e., semi-flexible fibrils (~ 14.7 nm diameter) and worm-like aggregates (~ 10.2 nm diameter), while intact BLG showed a uniform semi-flexible fibril morphology (~ 16.9 nm diameter). The difference in morphology was explained by the exposure of further regions in RCM-BLG that could initiate nucleation. Seeding experiments with peptides from the different region of BLG confirm that this results in a shift in the morphology.

4.4.4. Ligands: phenolic compounds and sugars

BLG can be modified by association or reaction with other compounds (mainly by phenolic compounds and sugars), which will change the amyloid building blocks and subsequently influence the amyloid formation kinetics and resulting morphology. In addition, phenolic compounds can inhibit protein oxidation (**Section 4.4.3**) through their antioxidative property, and is also shown to inhibit *in vitro* aggregation of the pathogenic Aβ peptide (Hamaguchi, Ono, Murase & Yamada, 2009).

Interaction of proteins with phenolic compounds generally inhibits amyloid aggregation. The flavanoid rutin binds in the hydrophobic core of BLG, decreasing the solvent accessibility and thereby decelerating (but not completely preventing) amyloid aggregation (Al-Shabib et al., 2019). Curcumin and its derivatives can also bind with BLG monomers, destabilizing them or blocking potential aggregation sites (Maity et al., 2018). Resveratrol hydrophobically binds with BLG, inducing a

slight opening of the hydrophobic cavity (Ghorbani Gorji et al., 2015). This structural change increases the surface hydrophobicity led to the formation of amorphous BLG aggregates instead of amyloid aggregates (pH 2.0 and 70 °C; Ma, Zhang, Liu, Xie & Wang, 2018). The effect of the fibrillization of ovotransferrin by phenolic compounds depends on whether it is covalently bound or not. Wei & Huang (2020) reported that fibrillization of ovotransferrin was inhibited in the presence of (covalently and non-covalently bound) epigallocatechin-3-gallate (EGCG). Interestingly, the fibril length was further reduced when EGCG was covalently bound (from 327 to 78–102 nm) instead of non-covalently bound (from 327 to 322–312 nm). Non-covalently bound EGCG led to thicker fibrils, while covalently bound EGCG had no impact. Wei & Huang (2019) also demonstrated different effects for covalent and non-covalently bound gallic acid: Covalently bound gallic acid reduced the L_c (327 to 92–127 nm), while non-covalently bound gallic acid did not affect the L_c. The fibril diameter increased with covalently bound gallic acid (6-filament instead of 2- and 4-filament from native protein), as compared to non-covalently bound gallic acid (3-filament). The zeta-potential, surface hydrophobicity, rheological properties, antioxidant activity and digestion of the fibrils was affected differently as well. Moreover, the addition of phenolic compounds can also act as a post-aggregation factor: Maity et al. (2018) reported the disruption of amyloid-like aggregates (prepared at 75 °C and pH 7.4) into smaller oligomers (< 120–130 nm compared to ~ 140–150 nm) upon incubation with curcumin and its derivatives for 24 hours.

BLG functional side groups (i.e., sulfhydryl, amino, carboxylic acid, and hydroxyl groups) can also be covalently modified with other compounds. For example, citraconylation of amino groups in lysine residues neutralizes the electrostatic repulsion between BLG monomers, which reduces the BLG stability and enhances fibrillization (Ghadami, Khodarahmi, Ghobadi, Ghasemi & Pirmoradi, 2011). Similarly, glycosylation (glucosylation and lactosylation) neutralizes charges and accelerates protein unfolding. Yet, the positive impact of the charge neutralization on fibrillization is often outweighed by the steric hindrance and introduction of hydrophilic side groups, which hinders amyloid structure formation. Glycosylation thus decreased fibrillization kinetics (Zhao et al., 2020), but did not affect the aggregate morphology (Dave, Loveday, Anema, Jameson & Singh, 2014). In contrast, *in vivo* glycation of proteins has been often reported to stimulate fibrillization, most likely through the formation of advanced glycation end-products (AGEs) that are prone to cross-linking. Da Silva Pinto et al. (2012) and Zhao et al., (2020) reported disulfide bond formation within and between fibrils from glycated BLG. This was accompanied by a morphological shift from amorphous to worm-like amyloid aggregates. For lactosylation of WPI, Liu & Zhong (2013) reported that the fibrillization rate remained unaffected, while the fibril yield was reduced.

Interestingly, glycated WPI fibril solutions remained transparent upon changes in pH (3.0–7.0) and salt addition (0–150 mM NaCl), and the fibrils were heat stable. Sugars can be added to fibrils post-aggregation to enhance fibril functionality: Karbasi et al. (2021) showed that modification of BLG fibrils with maltodextrin leads to an increased colloidal stability at pH 4.0 by inducing steric hindrance, while maintaining the fibril morphology.

4.5. Multidimensional amyloid networks formed as a function of the morphological diversity

During application, fibrils will spatially arrange in one-dimensional alignment (1D) or two- or three- dimensional networks (2 and 3D). For example, they are entangled into higher order bundles (1D), deposited onto surface coatings or form films (2D), or form gels (3D networks) (Schleeger et al., 2013; Wei et al., 2017). The mechanical stability of these systems depends on the ability of the fibrils to align or interlock with each other, depending mostly on the fibril morphology (i.e, their flexibility and length). Further properties such as their surface hydrophobicity, the intermolecular interactions, and their surface charge can be changed and will affect the rheological behavior of the fibrillar matrix (Schleeger et al., 2013). Thus, modification of fibril properties allows for a range of textural options (***Figure 4.4***).
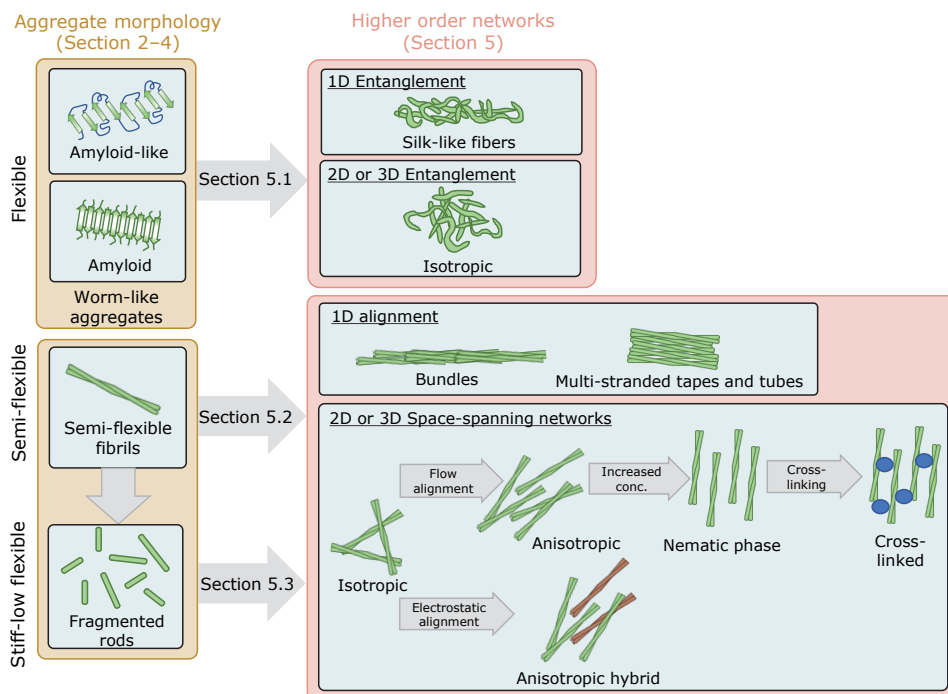

Figure 4.4. *Modification and assembly of amyloid(-like) aggregates into higher order networks.*

4.5.1. Networks made of flexible worm-like aggregates ($L_p < L_c$)

Aggregates have a highly flexible nature when their persistence length (L_p) is much lower than their contour length (L_c). Most worm-like BLG aggregates belong to that category (usually L_p ~ 10-40 nm) (**Table 4.1**). Kamada et al. (2017) demonstrated the flow-induced formation of hydrogel fibers of aggregates in a microfluidics setup. In this 1D orientation, purified short and flexible aggregates prepared at high protein concentration > 6 wt% (L_p ~ 41 nm, L_c = 100-1,000 nm; **Section 4.2.1**) show poor alignment with flow. Instead, they showed superior entanglement with increased mechanical strength than those observed for aligned semi-flexible fibrils. Besides, they suggested a similar association mechanism for worm-like amyloid aggregates and recombinant spider silk proteins.

In 2D applications, amyloid(-like) structures arrange in planar orientation and can result in (Pickering type) stabilization. Besides, highly flexible ethanol-induced worm-like BLG aggregates (**Section 4.4.2**) were found to have a high surface adsorption rate and packing density on the oil droplet surface, which increased the thermal stability of emulsions (Liu et al., 2021). Interfaces stabilized by worm-like aggregates have a higher surface shear modulus than those stabilized by semi-flexible fibrils, although the complex shear modulus of worm-like aggregates was significantly lower (Humblet-Hua, Van Der Linden & Sagis, 2013; **Section 4.5.2.1**).

In 3D orientation, highly flexible, curly pea protein amyloids yielded a lower gel strength than semi-flexible WPI fibrils, which was attributed to the higher flexibility of the pea protein amyloid aggregates and thus their lower degree of alignment (Munialo et al., 2014). Short and flexible salt-induced worm-like WPI aggregates (**Section 4.2.1**) were likewise reported to have a lower capacity to enhance the bulk viscosity than semi-flexible fibrils at pH 2.0, because of their short and irregular morphology. Fibrils made in the presence of $MgCl_2$ and $BaCl_2$ could create networks at somewhat lower concentrations than those prepared in the presence of LiCl and KCl. Although all aggregates were worm-like and flexible, it was hypothesized that $MgCl_2$ and $BaCl_2$ fibrils could be slightly longer and thus show better alignment capacity. Difference in the surface properties are also likely (Loveday, Su, Rao, Anema & Singh, 2012).

4.5.2. Networks made of straight amyloid aggregates ($L_p \approx L_c$)

4.5.2.1. Semi-flexible fibrils

For long, straight and semi-flexible fibrils L_p usually equals L_c or is close to it (**Table 4.1**). During 1D orientation (i.e., fibril bundles), flow alignment of semi-flexible fibrils was observed by Kamada et al. (2017). Semi-flexible BLG fibrils align to fibers of high mechanical stability during electrospinning in the presence of poly(ethylene oxide). The elastic modulus of these fibers was superior to those made from silk, collagen or

gelatin. The fibrils were, however, already mechanically fragmented during mechanical mixing of the solution (L_c of approx. 1 μm), and the electrospinning process further reduced the size to ~ 97 nm (Chen, Narayanan, et al., 2020). Thus, the flexibility of the fibrils likely decreased during processing, due to the size reduction.

Fibril bundles with increasing rupture stability and length can be prepared through association with other fibrous macromolecules, such as pectin. Because of weak interactions, the fibrils can slide within the hybrid-bundle into a more stable configuration. A wide range of structures and functionalities could be possible by varying the ratio of protein fibrils and carbohydrate fibrils (Loveday & Gunning, 2018). Likewise, the self-association of hen egg-white lysozyme and insulin in the presence of carbohydrate fibrils from gum arabic or pectin can already result in higher order fibrillar aggregates (Ow, Bekard & Dunstan, 2018). Similarly, BLG can create ordered fibril structures that assemble into tapes (of 180 nm width) in the presence of pectin with a high degree of methyl esterification. These tapes are stabilized through electrostatic interactions (Hettiarachchi et al., 2016). Thus, hybrid materials are a promising route towards optimization of the functionality of semi-flexible fibrils.

Likewise, in 2D networks BLG fibrils align longitudinally in the film plane during the casting process, while they stack with nematic order in the presence of plasticizers (Knowles et al., 2010). Characterization of the mechanical properties of the films reveal, among other things, a Young's modulus that is similar to the rigid proteinaceous materials collagen and keratin. Semi-flexible straight fibrils align at an interface or surface which increases the complex shear modulus by an order of magnitude compared to short rigid fibrils (Humblet-Hua et al., 2013). In foams, fibrils generally anchor to the air-water interface. The comparatively lower foam stability of semi-flexible fibrils (pH 2; versus amorphous aggregates at pH 5) is explained by uneven attachment without forming a densely packed layer against coalescence (Peng et al., 2017), destabilizing the liquid film between bubbles. Oboroceanu, Wang, Magner & Auty (2014) reported that polydisperse fibril systems that still incorporate unconverted material are most effective in stabilizing liquid interfaces. For the presence of longer fibrils, it is important to induce steric hindrance (Peng et al., 2017). Unconverted material is required to increase the viscosity of the liquid film. A similar synergy between fibrils and unconverted material is found for surface coatings of microcapsules and emulsions (Serfert et al., 2014).

In 3D networks, an increase in the concentration of semi-flexible fibrils induces a phase transition from an isotropic to a nematic phase above 0.4 wt% fibril, which is quantified by a 2D order parameter (Bolisetty et al., 2011). The addition of EGCG to semi-flexible fibrils that are already stacked in a nematic phase results in self-assembled hybrid supramolecular hydrogels through the well-known cross-linking capacity of the

phenolic compounds via hydrogen bonds and hydrophobic interactions (Hu et al., 2018; *Figure 4.4*). Associative interactions between semi-flexible whey protein fibrils and starch contributes to a synergistic increase in gel elasticity at low pH, but not at neutral pH conditions at which starch and protein are poorly compatible and may phase separate (Chen, Fang, Federici, Campanella & Jones, 2020). Another example for hybrid materials is the composite gel created by BLG fibrils in combination with bacterial cellulose microfibrils (Peng et al., 2019).

4.5.2.2. Branched fibrils

Although branched fibrils are usually not observed with BLG (except in the presence of zinc or with specific proteases, as discussed in *Section 4.2.1*), they occur with some other proteins (*Section 4.2.3*). Generally, a higher degree of branching counteracts fibril alignment and lowers the bulk viscosity, as shown for highly branched soy protein isolate fibrils compared to slightly branched glycinin fibrils (Akkermans et al., 2007).

4.5.3. Networks made of stiff aggregates ($L_p > L_c$)

The post-aggregation modification of semi-flexible fibrils into smaller aggregates though mechanical treatment (*Section 4.3.1*) and pH shift (*Section 4.2.1*, *Table 4.2*) results in stiff and rod-like fragments if the persistence length L_p is much bigger than the contour length L_c (Storm, Pastore, MacKintosh, Lubensky & Janmey, 2005). Thus, when semi-flexible fibrils are fragmented, L_c is reduced, but not L_p (leading to $L_p > L_c$). One can generalize that the flexibility of the fragments therefore usually decreases as a function of the size reduction, although this entails a heterogenous group of fragments varying from low flexible to rod-like.

In 1D orientation, stiff fibrils are unlikely to entangle but rather align with flow, when the concentration is high enough. The fibril concentration at which the nematic regime is reached correlates with the fibril thickness (d) and length (~ $1/dL^2$; Kroes-Nijboer, Venema & Linden, 2012). Therefore, fragmented fibrils align at higher concentrations than intact fibrils. Besides, a high strength is reported for electrosprayed hierarchical fibers that are made from BLG fibrils in the presence poly(ethylene oxide), which is likely to be caused by stiff fibril elements that were produced through fracture of intact semi-flexible fibrils during the electrospraying process (Chen, Narayanan, et al., 2020; *Section 4.5.2.1*). However, it could be difficult to trace the final material properties back to a particular size and flexibility.

In 2D networks stiff fibril fragments (< 500 nm) result in reduced emulsion stability due to a decrease in viscosity in the bulk phase and incomplete surface coverage, as compared to semi-flexible fibrils (Mantovani et al., 2018). Different emulsion processes will affect the fibril fragment size differently and therefore the resulting emulsifying capacity will vary (*Section 4.3.1*, Serfert et al., 2014).

In 2- and 3D networks, stiff fibrils form isotropic viscoelastic multilayers at surfaces and interfaces, which are disordered instead of nematic (Humblet-Hua et al., 2013). However, medium-sized rods of 100-200 nm length generated through high-pressure homogenization of semi-flexible fibrils can still have an anisotropic-nematic phase transition, albeit at approx. 10 times higher concentration than observed for semi-flexible fibrils (Jung et al., 2010). Adaption of the length of amyloid fibrils through shear stress (**Section 4.3.1**) thus allows for a modulation of the phase behavior, from highly elongated nematic tactoids formed with larger fibril fragments, to cholesteric droplets made from shorter fibril fragments (Bagnani, Nyström, De Michele & Mezzenga, 2019).

4.6. Conclusions and outlook

This presented review and categorization provides crucial insights into the production and application of specific BLG amyloid(-like) morphologies. These can be the basis of a variety of higher order structures and networks that can be used for numerous interesting applications in materials, medicine, and food. In addition, conclusions can also be drawn as to how the morphologies change further during processing (e.g., shearing), either specifically or unintentionally.

In view of reviewing BLG fibrillization:

- Amyloid(-like) aggregates can be categorized based on their size and flexibility. Shorter and more flexible amyloid-like aggregation results from a relatively fast and less specific assembly, for example, caused by low repulsion, high concentration, or when using solvents.

- The aggregation is generally accelerated by factors that destabilize the native protein structure (e.g., high temperature, zinc, solvent, hydrolysis, interfaces, oxidation) and decellerated by stabilizing factors (e.g., glycerol) or steric hindrance (e.g., protein binding with phenolic compounds or sugars).

- Mechanic post-processing (e.g., shearing, or interfacial stress) fragmentates aggregates into rods that are usually stiffer than their initial morphology.

- Chemical post-processing factors, such as addition of salts or modification with phenolic compounds (e.g. EGCG or gallic acid) can induce self-association of fibrils into tapes and sheets, while pH changes may fragment the aggregates into thinner or shorter aggregates.

- Different environmental conditions applied will affect not only the morphology-based effects but also the aggregate surface properties (i.e. surface charge and hydrophobicity). Therefore, each modification condition should be evaluated for additional chemical changes that could be beneficial for a particular application.

- When assembling into higher order structures or networks, semi-flexible morphologies can align into liquid crystalline phases or interact with linear polysaccharides (hybrid networks), while flexible aggregates have a high capacity to entangle.

The collective literature presented shows that amyloid(-like) aggregation of proteins is subject to numerous generic effects. For example, phenolic compounds prevent amyloid aggregation in both pathogenic and various food proteins. Other generic effects that accelerate the association kinetics are mechanical stress (e.g., shear and surfaces) and protein oxidation. In particular, the role of amino acid oxidation on amyloid aggregation has until now been specifically studied in pathogenic aggregation, while not much information is available for functional proteins. In addition, any safety evaluation should take various morphologies and any morphological changes caused during process modifications and digestion into account. Zhang, Zhao & Zheng (2014) already reported the different cytotoxicity of large mature amyloids and smaller amyloid oligomers. On the whole, generic effects of natural and engineered amyloid(-like) aggregates should be further explored in the future, as this is one way to identify favorable conditions for the formation of engineered amyloid aggregates and at the same time a possibility to prevent or circumvent undesirable health effects by protein alteration.

4

Table 4.1. *Overview of aggregation conditions and resulting morphology, in terms of contour and persistance length (Lc and Lp, respectively) and thickness (d), and the corresponding section discussing it further.*

Main type	Morphology			Section
	Described morphology	L_c (nm)	d (nm)	
Amorphous aggregates	Monodisperse, compact and spherical	n.a.	150	2.1
	Smaller		10-20	4.1
			20-50	4.4
		n.a.	n.d.	
	Larger		150-400	4.3
			400-600	
			1000	2.1
Worm-like aggregates	Thin, short, worm-like and flexible ($L_p \sim$ 10 nm)	50-200	1 - 3	2.1
	Less flexible ($L_p \sim$ 90 nm)	100-500	2.6	2.1
	Flexible ($L_p \sim$ 41 nm)	100-1,000	2.5 ± 0.5	5.1
	More flexible	15-500	n.d.	4.2
		100-500	2.7	
	Thicker	< 100	6 ± 1	2.1
		100-300	thicker	4.4
Altered worm-like aggregates	Fragmented	100-110	n.d.	4.4
	Aggregated and fragmented	n.d.	n.d.	4.3
	Aggregated	100	20	4.4
Semi-flexible/ straight fibrils	Thin, long, straight and semi-flexible (L_p = 3,818 ± 164 nm)	200-5,000	2.6	2.1 / 4.4 / 4.1
	L_p (~1960 nm)	100-1,100	4.1 ± 1.1	5.1
	More curved and branched		n.d.	2.1
	More flexible	n.d.	thicker	4.4
	Thicker		thicker	4.4
Association of filaments	Homogeneous distribution	n.d.	~ 4	
			increase with wavelength	2.2
	1-2 filaments		1-5	
	2-3 filaments	n.d.	4-6	2.1
	Longer pitch		n.d.	2.2
Altered straight fibrils	Aggregated	n.d.	n.d.	4.4
				4.1
	Fragmented and aggregated			4.3
Mixture of morphologies	Both straight and worm-like structures	n.d.	1.02-1.47	4.3
			n.d.	2.1
		1000	50	2.1
	Shift towards more straight (self-seeded) or thinner fibrils (peptide seeded)	n.d.	1.46	2.1
	straight and amorphous	120-130		4.4

Table 4.1. *Continued.*

Aggregation conditions			Reference
pH	T (°C)	Aggregation factor	
5.8	85 - 90	n.a.	Jung et al., 2008
2	30-50	Solvent (30% ethanol)	Kayser et al., 2020
7	98	Ligands (maillard products)	Zhao et al., 2020
7.4	75	Ligands (isoaxole) Ligands (pyrazole)	Maity et al., 2018
7 8/9	RT	Oxidation (Ascorbic acid & H_2O_2)	Alavi et al., 2018
8	37	Enzyme (endoproteinase AspN)	Akkermans et al., 2008
3.5	90	n.a.	Heyn et al., 2019
2	80	Concentration (7.5% BLG)	VandenAkker et al., 2011
2	90	Concentration (> 6.0% BLG)	Kamada et al., 2017
2.0	30-50	Solvents	Kayser et al., 2020
2/7	RT		Gosal et al., 2004
7	90	pH	Jung et al., 2008
	98	Glycation	Zhao et al., 2020
7.4	75	Ligands (curcumin diacetate)	Maity et al., 2018
3.5	90	Prolonged heating (72 hours)	Keppler et al., 2019
7		Glycation	Da Silva Pinto et al., 2012
2	80	Concentration (3% BLG)	VandenAkker et al., 2011
		Glycation	Dave et al., 2014 Liu & Zhong, 2013
		Surfactant (lecithin, < CMC)	Mantovani et al., 2016
2	90	concentration (< 4% BLG)	Kamada et al., 2017
2	90	Enzyme (Protease A, pepsin, protease M) Enzyme (Trypsin)	Gao et al., 2013
4.6	80	Citraonylation	Ghadami et al., 2011
3.5	RT	Allura red (0.5-1 mM)	Al-Shabib et al., 2018
2	80	Prolonged heating (72 hours)	VandenAkker et al., 2011
	varied	Heating technique (conventional vs. microwave heating)	G. Lee et al., 2015
	80	Copper (1:10, mole BLG/cupper) Copper (Equimolar addition)	Zappone et al., 2013
2	100	Temperature (microwave-assisted heating)	G. Lee et al., 2015
2	85	Rutin (30 µM)	Al-Shabib et al., 2019
	80	Surfactant (lecithin, > CMC)	Mantovani et al., 2016
	90	Prolonged heating (72 hours)	Keppler et al., 2019
7	37	Denaturant (5 M urea, 3 months)	Hamada & Dobson, 2009
2	80	Salt (≥ 60 mM CaCl2 or ≥ 33 mM NaCl)	Loveday et al., 2010
8	80	Enzyme (AspN endoproteinase, pH shift to 2)	Akkermans et al. 2008
7	37	Seeding (βA, βG and βH seeds) in 5M urea (3 months)	Hamada et al., 2009
7.4	75	Ligands (curcumin diacetate)	Maity et al., 2018

4

Table 4.2. *Overview of the effect of post-aggregation factors on specific morphologies, the morphological shift that occurs (diameter, d; persistence length, L_p; contour length, L_C) and the corresponding sections where it is discussed further. All aggregates were prepared at 80–90°C and a BLG concentration of 1–4% (w/v).*

Main type	Morphological shift	Section
Amorphous aggregates	SDS double layer prevents aggregation	4.1
Worm-like aggregates	Slightly fragmented (L_c from 74 to 50 nm) Fragmented (L_c from 102 to 50 nm)	3.1.2
	SDS double layer prevents aggregation	4.1
Semi-flexible fibrils	Unaffected	4.1
	Curve into rings (500-2,000 nm diameter) and loops Assembly of fragmented fibrils at edge of the rings	3.2
	SDS double layer prevents aggregation	4.1
Interfilament association	Thicker (d = 12 ± 3.1, for control d = 5.2 ± 1.1)	4.1
		4.4
	Thicker, longer pitch Twisting filaments suppressed	2.2
	Loss of multi-stranded fibrils (d = 2-2.5 nm, for control d = 4-10 nm) Shift to worm-like aggregates (L_p from 2,369 to 29 nm)	4.2
Aggregated and/or fragmented	Aggregated	4.1
	Fragmented and aggregated Fragmented (n.d.)	2.2
	Fragmented (L_c from 290-480 nm to 80-90 nm)	
	Fragmented (n.d.) Fragmented (L_c from 7,043 to 107 nm) Fragmented (L_c from 161 to 17.2 nm)	3.1.2

Table 4.2. Continued.

Post-aggregation factor	Aggregation pH	Reference
Complexation with SDS (> 1 mM), pH adjustment to isoelectric point	5.8	Jung et al., 2008
Rotor-stator dispersion (up to 43 J mL^{-1}) Ultra-sonication (up to 76 J mL^{-1} min^{-1})	3.5	Heyn et al., 2021
Complexation with SDS (> 1 mM) and pH adjustment to isoelectric point	7.0	Jung et al., 2008
pH shift to 3.0		Mantovani et al., 2016
Liquid-liquid interfaces (air-water & oil-water)	2.0	Jordens et al., 2014
Complexation with SDS (> 1 mM) and pH adjustment to isoelectric point		Jung et al., 2008
Complexation with SDS (> 1 mM)		Jung et al., 2008
Complexation with maltodextrin (pH 9, 90 °C)		Karbasi et al., 2021
Low ionic strength (undefined) High ionic strength (undefined)	2.0	Bolisetty et al., 2011
40 - 50% ethanol		Jordens et al., 2011
pH shift to 5.0 - 7.0		Mantovani et al., 2016
pH shift to 4.0 - 6.0 pH 7.0 - 8.0		D. Peng et al., 2017
Dynamic high-pressure treatment (40 MPa, three cycles)	2.0	Serfert et al., 2014
Ultrasound (6.8*10^5 kJ m^{-3})		Mantovani et al., 2018
Rotor-stator dispersion (up to 43 J mL^{-1}) Ultra-sonication (up to 76 J mL^{-1})		Heyn et al., 2021

4

Towards affordable recombinant β-lactoglobulin:

5

Exploring functionality gain through production and processing interventions
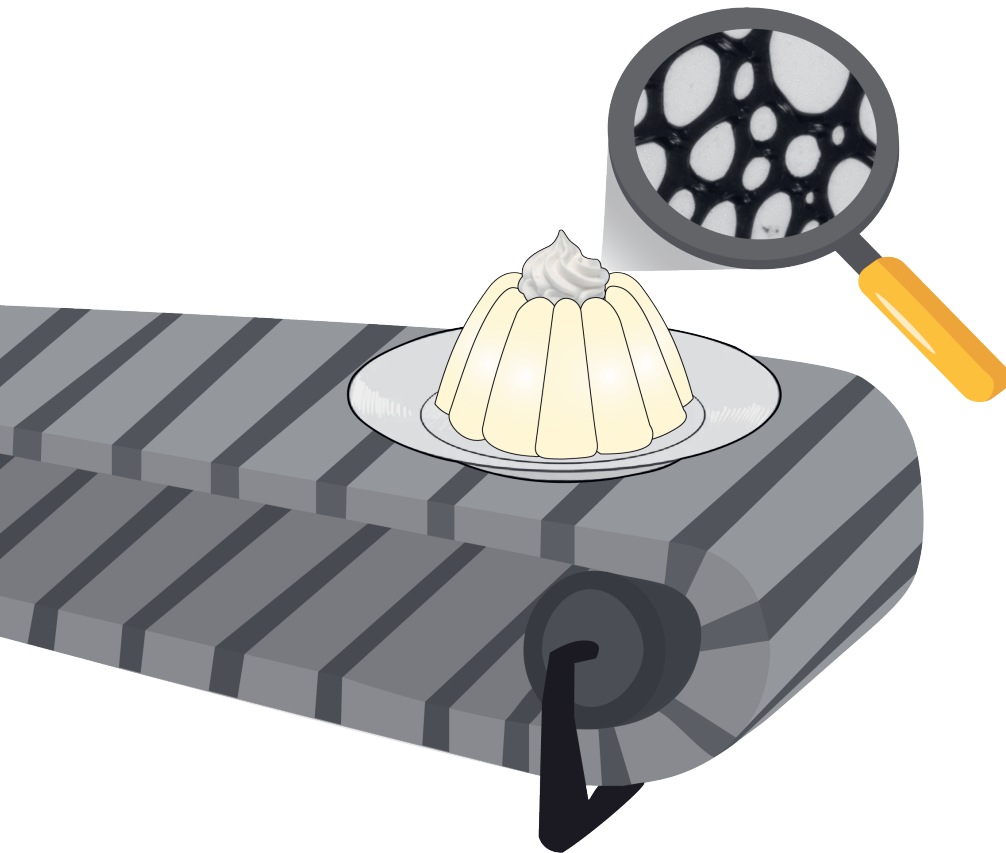
Loes Hoppenreijs, Sarah Brune, Rebekka Biedendieck, Rainer Krull,

Remko Boom & Julia Keppler

Interventions in the upstream production and further processing of recombinant food proteins affect its properties when used for food application. Often the efficiency of particular interventions is evaluated based on molecular purity and yield rather than final functional properties. Yet, the formulation of foods, including the amount of protein required, can be affected when the functional properties have changed. In this explorative study, we exemplify how far we can extend the functionality range of the major whey protein β-lactoglobulin (BLG), in terms of foaming and (heat-set) gelling, through various interventions.

Slight changes in the amino acid sequence of BLG (intervention A) affected its functional properties significantly. Foams were up to ten times more stable, when selecting different natural isoforms of BLG (isoform A instead of B) or when inducing targeted cysteine mutations. The isoform B yielded stronger thermally induced gels (+ 40%) compared to isoform A. During downstream processing of recombinantly secreted BLG, limited purification (intervention B) of up to ~ 67 wt% enabled reasonable foaming properties and superior gelation, while a lower purity of ~ 22 wt% resulted in poor performance in both cases. Post-processing allowed conversion of native whey protein into soluble amyloid-like aggregates (intervention C). These aggregates resulted in better foam stability (i.e. approximately four times longer than non-aggregated protein), but did not improve heat-set gelation.

The presented study demonstrates that one should not only consider protein yield and purity, but also functional properties when developing recombinant proteins for food application. In turn, these functional properties are a result of the complete upstream and downstream chain.

Abstract

Abbreviations: β-lactoglobulin, BLG; BLG recombinantly produced by *Escherichia coli*, rBLG; BLG recombinantly produced by *Pichia pastoris*, yBLG; BLG from bovine milk, bBLG; downstream processing, DSP; hexametaphosphate, HMP; Loss modulus, G″; Storage modulus, G′; whey protein isolate, WPI.

5.1. Introduction

Livestock-based production of proteins for food formulations requires at least partial replacement, due to sustainability and animal welfare issues. Precision fermentation has gained attention as an alternative production route for those proteins, as it allows production of the same high-quality proteins without requiring livestock. Precision fermentation has been used for decades to produce specific proteins, such as enzymes and pharmaceuticals (Dupuis et al., 2023), but not yet for large-scale production of animal-based food protein ingredients. The overall production costs have to be reduced substantially for this new application. Interventions can be made in both the upstream production and further processing for this purpose. The consequences of such interventions are often evaluated in terms of relative changes in protein yield or purity. Yet, the molecular design, the production, and the further processes applied can alter the protein structure, its stability, as well as the association behaviour. In turn, such changes will influence the techno-functional properties of the final protein ingredient. Positive effects may allow efficient application in food formulations, thus necessitating less protein. In contrast, negative effects above a certain degree may be unacceptability for food application. It is currently unclear how strongly the functionality range of one protein can be modulated based on such interventions.

The aim of this study is to demonstrate how the choice on production and processing may influence the technical functionalities for food formulations. We aim to exemplify how the functionality range of recombinant proteins can be altered, rather than aspiring to a full coverage of the effects. A range of interventions in different stages of the production process was applied (**Figure 5.1**). The functionality was evaluated based on foaming and gelling properties; screening for the ability to stabilize interfaces, as well as the ability to form space-spanning networks.
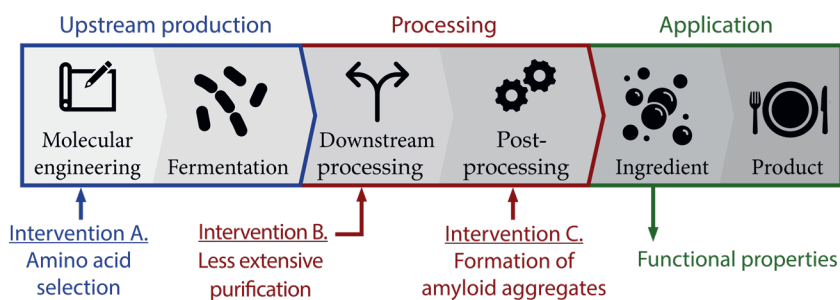

Figure 5.1. *Overview of the production process of recombinant proteins for food application. Interventions in several stages of the production process are highlighted in the following.*

The major whey protein β-lactoglobulin (BLG) was used as an example, being a common animal-based protein ingredient in food application. Besides, its recombinant production has already been demonstrated in previous studies for research purposes (for example, Denton et al., 1998; Keppler et al., 2021; Kim et al., 1997). We intentionally selected (recombinant) BLG from several sources (i.e., bovine, yeast, bacteria) to capture a broad range of functional properties that can be achieved. As a result, BLG ingredients differ in the protein amino acid sequence (with structural consequences) and purities, as summarized in **Table 5.1**.

Table 5.1. *BLG ingredients that are investigated in this study to evaluate the impact of particular interventions during upstream production, downstream processing (DSP) or post-processing.*

	Intervention		Abbrev.	Description
Upstream production	A. Amino acid selection	Natural isoforms	bBLG A	Bovine BLG isoform A (bBLG A)
			bBLG B	Bovine BLG isoform B (bBLG B)
		Cysteine mutations (*E. coli*)	rBLG	Recombinant BLG B (Leu1Ser/Ile2Ala)
			rBLG-SH	rBLG lacking free thiol (Cys121Ala)
			rBLG-SS	rBLG lacking exposed disulfide (Cys66Ala/Cys160Ala)
			rBLG-C	rBLG lacking all cysteines (Cys66Ala/Cys106Ala/Cys119Ala/Cys121Ala/Cys160Ala)
DSP	B. Mild purification		Crude yBLG	~ 26 wt% recombinant BLG[1]
			Purified yBLG	~ 72 wt% recombinant BLG[1] + 1 wt% HMP
Post-processing	C. Transformation		WPI (control)	Whey protein isolate (73 ± 1 wt% BLG)
			WPI amyloid-like aggregates	Prepared by heating at pH 3.5 for 5 h
			WPI amyloid fibrils	Prepared by heating at pH 2.0 for 5 h

[1]*N-terminal modification AKEEGVSLEKR and truncated forms (**Chapter 3**).*

5.1.1. Intervention A: choices in upstream production

A first intervention includes the selection of a specific primary protein structure during upstream production (Intervention A). Here, the two major natural isoforms BLG A and B (isolated from milk) were investigated. BLG B was recombinantly produced by *Escherichia coli* (rBLG) and had slightly modified N-terminus compared to the bovine protein (Keppler et al., 2021; **Table 5.1**). In addition to the production of the natural isoform, it has already been shown that additional step-wise substitution of different

cysteines in rBLG by alanine (rBLG-SH, rBLG-SS, rBLG-C) can alter the structure of BLG from secondary to quaternary level (**Chapter 2**). We further explore the consequences for their functional properties in this study. All these BLG variants still show a sequence homology of > 96% and have comparable purity (> 90 wt%; **Chapter 2**). *E. coli* was used for producing recombinant variants, due to the ease of genetic manipulation, relatively low cost and rapid growth (Francis & Page, 2010). A major drawback for industrial application is its inability to secrete proteins (Kleiner-Grote et al., 2018). Nevertheless, the recombinant production of BLG by *E. coli* still serves our purpose here, as it demonstrates the influence of the primary structure on the functional properties.

5.1.2. Interventions B and C: processing

A second intervention focused on the purity of the BLG ingredients that is achieved through DSP. Any DSP configuration typically needs to find a balance between purity and yield (Intervention B). Extensive purification usually comes at the expense of yield, but the functional properties are probably not linearly dependent on the protein purity; lower purity may even result in better functionality. Therefore, we investigate the impacts of impurities on the functional properties of recombinant BLG. In this case, *Pichia pastoris* was used for the production of recombinant BLG (yBLG). *P. pastoris* is an attractive host for food application, as it has GRAS (generally regarded as safe) status, can secrete the recombinant protein and is able to grow to relatively high cell densities (Dupuis et al., 2023). After removal of the yeast cells and low molecular weight impurities by filtration, the yBLG purity is about 26 wt% ('crude yBLG', main impurity mannans; **Chapter 3**). Further purification up to ~ 72 wt% can be achieved by selective and reversible precipitation of protein by the food-grade salt hexametaphosphate (HMP; **Chapter 3**). In this procedure, excess HMP is removed from the purified material ('purified yBLG') but a residual amount of ~ 1 wt% remains, probably ionically associated with the protein. This relatively simple purification process could potentially replace large-scale expensive chromatographic processes, if the resulting less pure ingredients still exhibit functional properties.

After DSP, proteins can be functionalized through specific post-processing. This would enhance the value of the food ingredient. Therefore, a third intervention considers additional processing to aggregate whey protein isolate (WPI) into amyloid aggregates (Intervention C), which has been reported to improve functionality in some cases (Jansens et al., 2019). For this demonstration we use WPI instead of BLG, since it is more widely available and has been reported to form aggregates with a similar internal structure to BLG (Mahmoudi et al., 2007).

5.2. Experimental Section

5.2.1. Preparation protein ingredients

5.2.1.1. Intervention A: variants in the amino acid sequence

To obtain pure forms of BLG with natural mutations, bovine BLG natural isoforms A and B (bBLG A and B, respectively) were purified from milk of cows that was homozygous for the corresponding variants, according to **Chapter 2**. Recombinant BLG (rBLG; natural isoform B) was produced in *E. coli*. Recombinant cysteine mutants were produced through substitution of cysteine residues with alanine residues; including the BLG variant without free thiol (Cys121; rBLG-SH), the outer disulfide bond (Cys66, Cys160; rBLG-SS) or any cysteines (Cys66, Cys106, Cys119, Cys121, Cys160; rBLG-C). Details about the production and purification can be found in **Chapter 2**.

5.2.1.2. Intervention B: less extensive purification

Recombinant BLG was produced from *Pichia pastoris* (yBLG; natural isoform A). Production and purification were performed as described in **Chapter 3**. In short, production, filtration (> 10 kDa) and spray drying were performed to obtain 'crude yBLG' (obtained from Formo; Germany). Crude yBLG was solubilized, further purified using subsequent precipitation and solubilization steps, and lyophilized (Beta 2-8 LSCplus, Martin Christ, Germany) to obtain 'purified yBLG'. The BCA assay kit (Pierce™, ThermoFisher Scientific, USA) was used to determine the protein content of the samples.

5.2.1.3. Intervention C: transformation into amyloid aggregates

Whey protein isolate (WPI; BiPro, USA) was used to prepare two types of amyloid aggregates: (1) amyloid fibrils and (2) amyloid-like aggregates. About 300 mL of 10 mg mL^{-1} WPI was prepared in a 500 mL volume Schott bottle, and the pH was adjusted to pH 2.0 (for amyloid fibrils) or pH 3.5 (for amyloid-like aggregates) using 1 M hydrochloric acid (HCl). The solution was heated in a water bath at 90 °C, while stirred at 350 rpm using a heat- and water-resistant magnetic stirring plate (MIXdrive 15 HT, 2Mag AG, Germany). After incubation for 5 h, the solution was cooled on ice and the pH was quickly adjusted to 7.0 using 1 M sodium hydroxide (NaOH). The protein solution was dialyzed for three days in a cooled room (4 °C), using a dialysis membrane with 8 kDa cut-off value (BioDesign Inc., USA). For dialysis, demi-water was used in a volume that was approximately 100 times larger than the protein solution and was refreshed twice a day. Finally, the solutions were frozen and lyophilized to obtain dried amyloid-like aggregates. Analysis with Transmission Electron Microscopy (TEM) was performed throughout processing of the aggregates to check whether the morphology was affected, according to **Chapter 7**.

5.2.2. Functionality experiments

5.2.2.1. Foaming

The foaming properties of protein solutions were determined at different concentrations by analysis with the Foamscan™ (Teclis, France). Protein solutions were prepared a day before the measurement in a concentration of 1 mg mL^{-1} in a 10 mM phosphate buffer (pH 7.0) in independent triplicates. Subsequent dilution with the buffer was performed to obtain solutions with different protein concentrations. All solutions were analyzed at 1, 0.5, 0.25 and 0.1 mg mL^{-1}, except for WPI amyloid-like aggregates (1, 0.5, 0.15, 0.1, 0.05 mg mL^{-1}) due to its relative high foam stability. For the recombinant cysteine mutants, the solution at 1 mg mL^{-1} was re-used after analysis to prepare the subsequent solutions with lower protein concentrations. The absorbance was measured before and after analysis (diluted to 0.5 mg mL^{-1}) in a quartz cuvette at 280 nm (DR6000; Hach, USA) to check whether the protein content decreased due to the analysis.

The protein solution (31 mL) was stepwise injected into the Foamscan to calibrate the vertical electrodes: first 16 mL (i.e., approximately 15 mL detected and 1 mL to fill the dead space in the injection tube) and then three subsequent steps of 5 mL. Foaming was induced through sparging air through a glass frit (P3; porosity of 16 – 20 µm; Teclis, France) at 250 mL min^{-1}, until a total foam volume of 160 mL was reached.

The time to reach 160 mL of foam was recorded by a camera to note the foamability. The foam stability was derived as the half-life time ($t_{1/2}$) of the foam collapse. A second camera captured the foam structure for 1 mg mL^{-1} solutions. Pictures were taken directly after sparging ended and were analyzed using Matlab (R2022B; Version 9.13.0.2166757) and the toolbox DIPimage (Luengo Hendriks & van Vliet, 2000; Version 2.8). The script is available upon request. The minimum size of bubbles included in the analysis was set to 50 pixels^2 to avoid the interference of artifacts, such as reflections. Finally, the Sauter mean diameter ($d_{3,2}$) of the bubbles in the foam and air fraction of the foam were determined.

5.2.2.2. Gelation

Protein samples were solubilized in ultrapure water (1.5 mL) in a concentration of 15 wt% protein. The pH was adjusted to 7.0 when necessary, using 1 M NaOH or HCl, and the solution was stored overnight the fridge to ensure complete hydration. The next day, the solution was degassed: it was placed in a desiccator (used as vacuum chamber) connected to a vacuum pump. A vacuum ($^1/_4$ of total power) was applied to the chamber of the desiccator for 20 min, while the solution was slowly stirred with a magnetic stirrer. Afterwards, the degassed solution was analyzed for its heat-set gelation. A rheometer (MCR502; Anton Paar GmbH, Austria) was equipped with

a small volume concentric cylinder (CC10/T200/SS; Anton Paar GmbH). The cup was filled with 900 μL of sample. After lowering the cylinder into the sample, 100 μL of paraffin oil (Supelco; Merck, Germany) was transferred onto the sample to prevent evaporation during heating. First, the temperature was stabilized at 20 °C and the sample was equilibrated for 5 min. Then, a heating cycle was applied to induce gelation: the temperature was increased from 20 to 90 °C in 20 min, then held at 90 °C for 30 min, then cooled back to 20 °C in 20 min, and kept at 20 °C for another 5 min. The shear strain and shear frequency were kept constant at 1% and 1 Hz, respectively, during the heating cycle. The gel point was determined as the point at which the storage modulus (G′) became higher than the loss modulus (G″) and the torque was above the threshold value (i.e., 0.0005 m · Nm).

After gel formation, deformation was applied by increasing the shear strain amplitude from 0.01 to 1000% at a constant frequency of 1 Hz. The initial strengths of the gels were determined as the average storage modulus at low shear strain (0–1%; linear viscoelastic region), i.e., when the G′ was independent of the shear strain. The critical strain was determined as the strain at which the initial gel strength decreased by 5%. Lissajous plots were prepared by plotting the intracycle shear stress and shear strain response at a shear strain amplitude of 2.4, 23.8, 101, 318 and 1010%.

5

5.3. Results and discussion

First, the impact of slight changes in BLG amino acid sequence (intervention A) on the functional properties is discussed in **Section 5.3.1**, considering both natural isoforms and the cysteine mutations. **Section 5.3.2** then describes to what extent simplified purification of expressed BLG (intervention B) affects the functionality of the protein. In **Section 5.3.3**, additional post-processing is considered to transform WPI into amyloid aggregates (intervention C) to improve functional properties. Finally, a summary and comparison of the performance of all BLG ingredients is given in **Section 5.3.4**.

5.3.1. Intervention A: variations in the amino acid sequence

Bovine milk containing only bBLG isoforms A or B was collected and these proteins were purified. Highly pure protein powders were obtained after purification, containing 94.6 ± 1.2 and 94.0 ± 1.1 wt% bBLG A and B, respectively (by Dumas; nitrogen conversion factor of 6.33; Kosters et al., 2010). Besides, production of wild-type BLG B and cysteine mutants in *E. coli* and subsequent purification also resulted in high purity (> 90 wt%; **Chapter 2**). The complete structural characterization of these variants, as well as the bovine control, can be found in **Chapter 2**. The main structural elements are summarized in **Table 5.2**.

Table 5.2. *Overview of the structure of the cysteine mutants, according to **Chapter 2**. Main differences are highlighted in bold.*

Variant	Secondary structure element [%]				Tertiary structure	Quaternary structure
	α-helix	β-sheet	Random coil	β-turn		
bBLG B	16 ± 0	47 ± 1	26 ± 0	11 ± 1	Globular	Mostly dimers
rBLG	16 ± 1	51 ± 1	21 ± 1	12 ± 1	Globular	Mostly dimers
rBLG-SH	22 ± 1	51 ± 1	18 ± 0	10 ± 2	Globular	Mostly dimers
rBLG-SS	21 ± 1	**35 ± 1**	**36 ± 1**	8 ± 1	**Opened**	**Mostly monomers**
rBLG-C	29 ± 2	**9 ± 3**	**57 ± 2**	6 ± 2	**Disordered**	**'Dimers'**

5.3.1.1. Impact of intervention A on foaming properties

Figure 5.2 depicts the formation of foam from bBLG A and B solutions, the foam structure, and foam collapse. The foams from bBLG A were formed more quickly (**Figure 5.2A**), and thus contained relatively less air and more liquid, as compared to bBLG B (**Figure 5.2C**). Smaller average bubble sizes were also noted (**Figure 5.2C**). Likewise, Euston et al. (1999) observed smaller droplet size in emulsions stabilized by bBLG A, as compared to bBLG B.

Foams from bBLG A were stable for almost 10 times as long, as from bBLG B. Ipsen et al. (2001) reported accelerated adsorption of partially hydrolysed bBLG A, which did not affect interfacial properties but improved the resulting foam stability (Ipsen et al., 2001). Thus, the faster adsorption and smaller average bubble size of bBLG A foams are expected to have improved the foam stability.
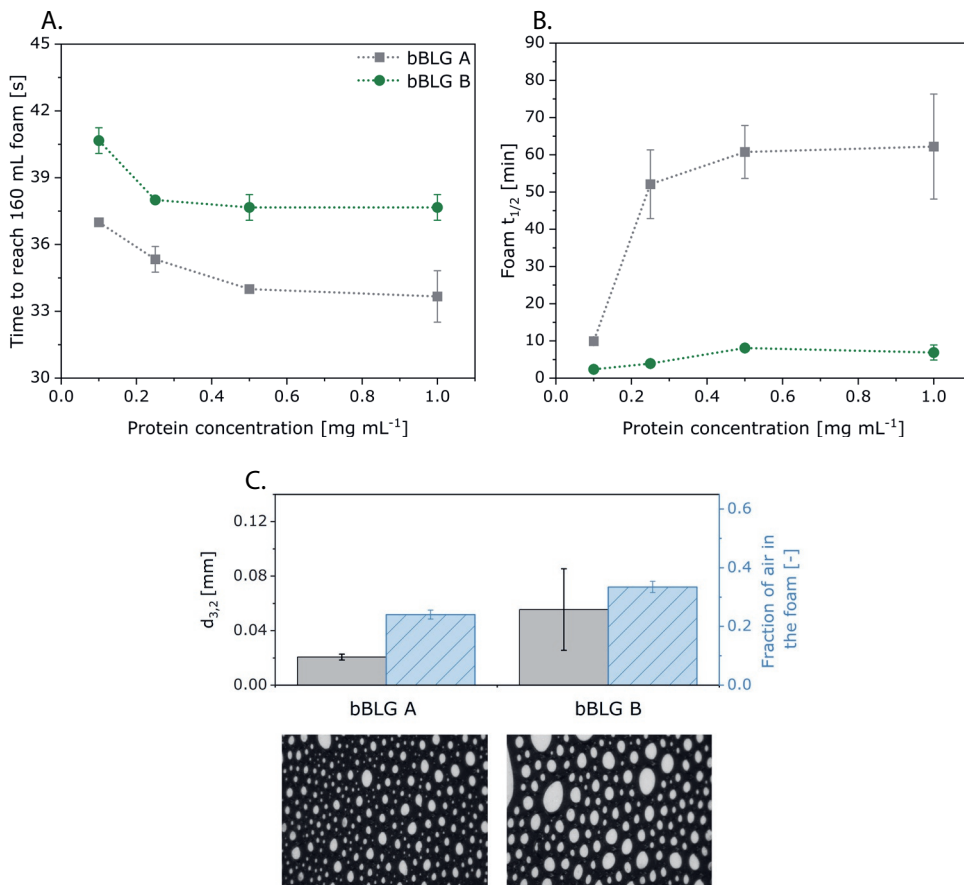

Figure 5.2. (A) Time to reach 160 mL of foam volume when sparging (250 mL min^{-1}) solutions of bovine BLG natural isoforms A and B, and (B) the corresponding foam half-life time (t$_{1/2}$). (C) Immediately after formation of the foam from 1 mg mL^{-1} solutions, the Sauter mean diameter (d$_{3,2}$) of the bubbles and the fraction of air in the foam is shown, with corresponding pictures.

The better foamability of bBLG A is probably not directly related to its higher surface charge (surface charge given in Table S5.1), as this is generally expected to increase the energy barrier for adsorption to the interface (Foegeding et al., 2006). Instead, the monomeric configuration and structural flexibility of bBLG A may have enhanced its foaming properties, as compared to the dimeric configuration and tighter structure

of bBLG B. Perriman et al. (2007) reported a preferential adsorption of BLG monomers over dimers. They describe that the hydrophobic residues involved in the adsorption to the air-water interface, are also involved in the dimer interface. Thereby, dimers have to dissociate into monomers before adsorption to the interface.

Besides to the different monomer-dimer equilibrium, BLG A exhibits a higher conformational flexibility: it has been reported to be more sensitive to unfolding upon pressurizing (Olsen et al., 2022), to tryptic hydrolysis (Creamer et al., 2004), and to exchange of the hydrogen atoms within its structure (Dong et al., 1996). Thus, bBLG A is likely to anchor more easily to the air-water interface and/or structural rearrangements occur to a larger extent, as compared to bBLG B. This is in line with Ipsen & Otte (2004), who demonstrated faster adsorption of bBLG A to the air-water interface (< 0.1 mg mL^{-1} BLG in a 20 mM imidazole buffer; pH 7.0). However, the same authors also found that bBLG B yielded a more stable foam (10 mg mL^{-1} in a 20 mM imidazole buffer), when the foam was prepared under high-shear whipping conditions. Mackie et al. (1999) reported faster adsorption of bBLG B to the air-water interface and attributed this to its higher surface hydrophobicity in its native state (< 0.02 mg mL^{-1} BLG in a 10 mM phosphate buffer; pH 7.0). This opposite conclusion regarding the relative performance of these natural isoforms might be due to different conditions that were applied, including the protein concentration and the procedure used to prepare the foams. A low protein concentration was applied in the study of Mackie et al. (1999), which could alter the monomer-dimer equilibrium (Euston et al., 1999). In case of Ipsen & Otte (2004), the high shear may have facilitated destabilization of the variants. The impact of the stability of the native structures on the foamability and resulting foam stability will then be reduced.

Figure 5.3 summarizes the formation of foam, the structure of the foam, and foam collapse for the produced recombinant BLG variants: the wild-type (rBLG), the variant lacking free thiol (Cys121; rBLG-SH), the variant lacking the outer disulfide bond (Cys66–Cys160; rBLG-SS) and the variant lacking all cysteines (rBLG-C). The variant bBLG B is depicted as a control. The sample at 1 mg mL^{-1} after measuring was re-used to prepare the further dilutions, as only low amounts of recombinant protein material were available. Re-use of the sample was not expected to affect the results, as conformation changes upon foaming are expected to be reversible (Phillips et al., 1995). The measurement resulted in a slight dilution caused by residual water in the device after cleaning. This dilution was in the range of 5.0 to 8.8 wt% and was similar for the different samples ($p > 0.05$). The protein concentrations depicted for these samples (*Figure 5.3*) were corrected for this dilution.
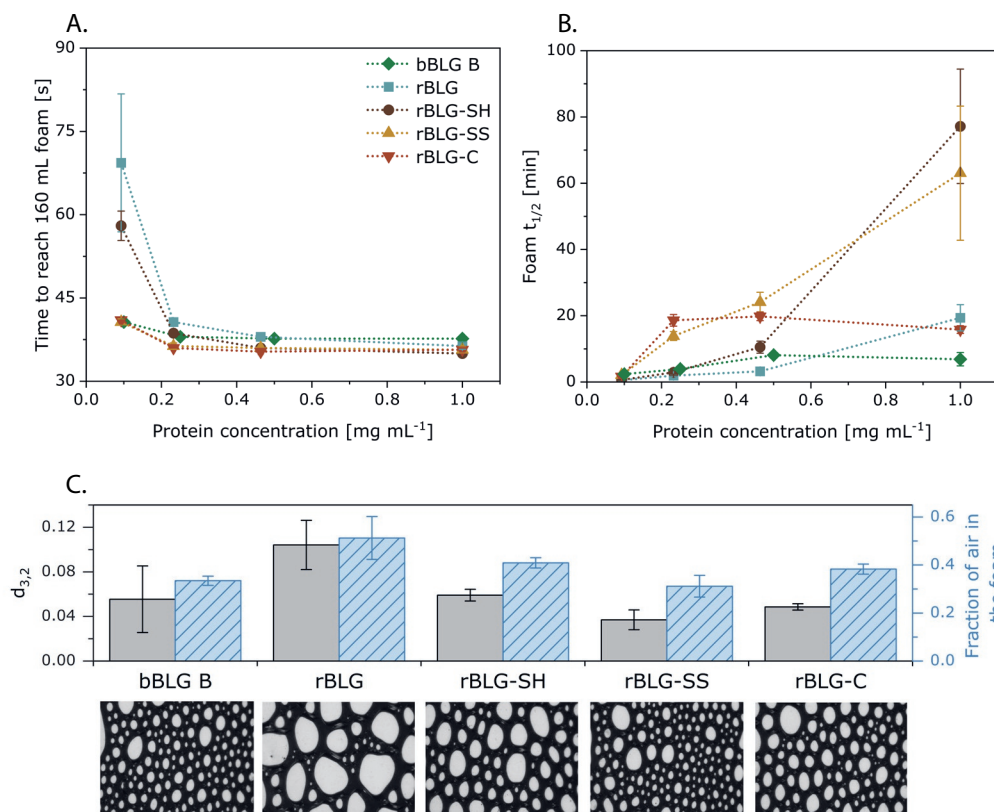
Figure 5.3. (**A**) Time to reach 160 mL of foam volume when sparging (250 mL min^{-1}) solutions of recombinant BLG variants: rBLG, rBLG-SH, rBLG-SS, rBLG-C, and (**B**) the foam half-life time ($t_{1/2}$). (**C**) Immediately after formation of the foam from 1 mg mL^{-1} solutions, the Sauter mean diameter ($d_{3,2}$) of the bubbles and the fraction of air in the foam is shown, with corresponding pictures.

The foaming behaviour was different between bovine BLG B and the wild-type rBLG. bBLG B demonstrated slightly better foamability and stability at concentrations < 1 mg mL^{-1} (**Figure 5.3C**). The wild-type rBLG contains two mutations at the N-terminus: Leu1Ala and Ile2Ser. Both Leu and Ile in bovine BLG are more hydrophobic than Ala and Ser in the wild-type (Wilce et al., 1995). Increased hydrophobicity can accelerate protein adsorption, especially in the protein-poor regime (Delahaije & Wierenga, 2022). The faster adsorption of bBLG B to the interface might also explain the smaller bubble size, as compared to rBLG (**Figure 5.3C**). The foam stability of bBLG B was not improved when increasing the protein concentration from 0.5 to 1 mg mL^{-1}. Surprisingly, the foam of rBLG had a higher stability at 1 mg mL^{-1} than that of bBLG B (**Figure 5.3B**), even though its bubbles were larger (**Figure 5.3C**). To explain these differences, further investigation of the interfacial properties is recommended.

Removal of the free thiol (Cys121Ala) slightly increased the foamability, especially at relatively 'higher' concentrations (1 mg mL^{-1}; **Figure 5.3A**). In addition to the improved foamability of rBLG-SH, as compared to rBLG, the foam stability was also enhanced (**Figure 5.3C**). Croguennec et al. (2006) reported improved foaming properties of BLG when blocking the free thiol, which was attributed to the destabilizing impact of the modification. Similarly, our induced mutation also destabilized BLG: the onset temperature for denaturation was decreased by approximately 5 °C (Brune et al., 2023). Destabilization could facilitate rearrangements at the interface, potentially improving the surface coverage. If so, this could in turn explain the formation smaller bubbles (**Figure 5.3C**). Finally, some studies suggest that intermolecular disulfide bonds might form upon adsorption to the interface, which in turn would contribute to the foam stability (Bos & Van Vliet, 2001; Martin et al., 2002; Nicorescu et al., 2009). However, our current results do not support this hypothesis.

Removal of the intramolecular disulfide bond in rBLG-SS and rBLG-C also improved the foamability, especially in the protein-depleted regime (< 0.5 mg mL^{-1}; **Figure 5.3A**). Kella et al. (1989) observed increased adsorption of whey proteins when 50% of the disulfide bonds were cleaved, due the increased unfolding ability. Recombinant removal of the intramolecular disulfide(s) is expected to increase the tendency to unfold at the air-water interface, but also the extent of this unfolding. Interestingly, rBLG-SS and rBLG-C demonstrated similar foamability (**Figure 5.3A**). This indicates that the improved behaviour is related to removal of the outer SS bond (Cys66-Cys160), and not necessarily by the removal of the inner disulfide bond (Cys106-Cys119).

Removal of all cysteines in rBLG-C led to a similar foam stability at concentrations < 1 mg mL^{-1}, but lower foam stability at a concentration of 1 mg mL^{-1}, as compared to rBLG-SS (**Figure 5.3B**). At higher concentrations, the denser packing at the interface could allow a thicker interface for the partially destabilized rBLG-SS, as compared to the more disordered rBLG-C (**Table 5.2**). Similarly, Ipsen et al (2001) reported a lower viscoelastic modulus of interfaces stabilized by completely hydrolysed bBLG A, compared to those stabilized by partially hydrolysed bBLG A. Interfaces stabilized by disordered caseinate exhibit a lower viscoelastic modulus, compared to globular proteins (Lajnaf et al., 2022). Thereby, we hypothesize that while completely destabilizing BLG by substituting all cysteines leads to better foam formation, partial preservation of the structure allows the formation of a stronger interface.

We earlier hypothesized that the better foaming functionality of bBLG A is mostly related to its destabilized and monomeric configuration, as compared to bBLG B, under the conditions applied. This is consistent with our hypothesis that protein destabilization improves foam formation. Removal of the outer disulfide bond in recombinant BLG B (variant rBLG-SS) transforms the genetic B variant into a monomeric configuration

that is partially destabilized (**Table 5.2**). This variant demonstrated similar foaming properties at 1 mg mL^{-1}, as compared to BLG A, while the foaming properties at lower concentrations were inferior to those of bBLG A (**Figure 5.2**; **Figure 5.3**). This indicates that the improved properties of bBLG A in the protein-depleted regime under the applied conditions are not only due to structural destabilization and/or its monomeric configuration, but are (also) related to other physicochemical properties that are changed due to one or both mutation(s).

Overall, it is clear that the foaming properties can be highly influenced by the substitution of only a few amino acids, as shown for the natural isoforms of induced cysteine mutations. We hypothesize that foam formation is mostly facilitated by structural destabilization (on secondary to quaternary level), while the residual structure (stabilized by the inner disulfide bond) contributes to foam stability. In addition, other changes in the physicochemical properties can also play a role.

5.3.1.2. Impact of intervention A on heat-set gelation

The heat-induced gelation of solutions of bBLG A and bBLG B is shown in **Figure 5.4**, while the main parameters are listed in **Table 5.3**. Gelation occurred for both variants when 15 wt% protein solutions were heated for approximately half an hour (**Table 5.3**). Variant bBLG A gelled slightly earlier (~ 0.4 min) and showed a steeper increase in the storage modulus (G′; **Figure 5.4**), as compared to bBLG B. Huang et al. (1994) and McSwiney et al (1994) also observed earlier gelation and more rapid initial gelation of bBLG A than bBLG B solutions, and attributed this to its lower heat stability. We also observed earlier unfolding of bBLG A under the applied conditions (onset temperature for unfolding is listed in **Table S5.3**). Thus, we hypothesize that the free thiol is exposed more rapidly and then formed intermolecular disulfide bonds more easily. This is in line with Elofsson et al. (1996), who also reported earlier disulfide bond formation for bBLG A, as compared to bBLG B (determined at ~ 48 mg mL^{-1}). Disulfide bond formation in BLG B could also be slightly delayed due to the necessity to first dissociate the dimeric configuration prior to unfolding. In contrast, Manderson (1998) reported a slower aggregation of bBLG A than bBLG B in dilute systems (2–5 mg protein per mL). They argued that the opposite might be true at high protein concentrations (> 50 mg mL^{-1}) or at temperatures < 95 °C, as also suggested by Nielsen et al. (1996).
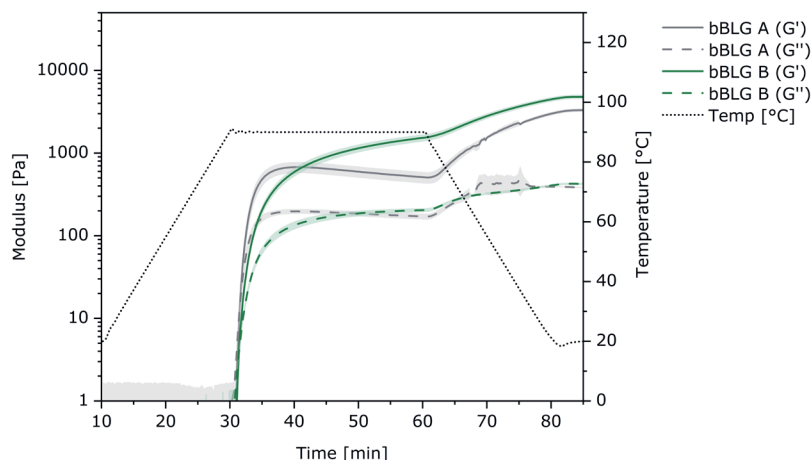
5

Figure 5.4. *Storage (G') and loss (G") moduli upon heating 15 wt% protein solutions of bovine BLG natural isoforms A and B.*

Table 5.3. *Gelation properties of various protein solutions (15 wt% total protein).*

	Gel point [min]	Final G' [Pa]	Critical strain [%]
bBLG A	31.7 ± 0.1	3,442 ± 146	5.2 ± 0.8
bBLG B	32.1 ± 0.1	4,831 ± 336	8.4 ± 1.5

bBLG B showed a more gradual initial increase in G', but eventually yielded a stronger gel than bBLG A during longer heating times (***Figure 5.4***, ***Table 5.3***). The final G' for bBLG B was about 40% higher as compared to bBLG A. The subsequent deformation showed that the bBLG A gel was less elastic upon small deformation, as it showed a lower critical strain (***Table 5.3***). The behaviour upon large deformation is depicted in the Lissajous plots, shown in ***Figure 5.5***. Only the Lissajous plots for the bBLG B gels exhibit inverted sigmoidal shape at 101% and 318%. This so-called strain stiffening behaviour indicates a high resistance of the gel against larger deformation (i.e., when the strain increases). This may indicate a higher cross-link density within the gel (Groot et al., 1996). Besides, the shear stresses obtained are relatively higher, while irreversible deformation (i.e. opening of the Lissajous plot; ***Figure 5.5***) is delayed for bBLG B gels, confirming these are stronger than bBLG A gels.

The stronger and more ductile gel that was obtained with BLG B, as compared to BLG A, has not been previously reported. Huang et al. (1994) and McSwiney et al. (1994) obtained a higher G' for bBLG A, instead of bBLG B, when heating BLG in a buffer at 80 to 85 °C. Yet, Huang et al. (1995) noted that the G' values became more similar for the two variants during longer heating times. This is in line with our results, indicating different aggregation mechanisms with bBLG A and bBLG B, when comparing the

initial and the extended gelation phases. Complete destabilization of the monomeric BLG is expected when the variants are heated for a longer period of time (> 40 min) at sufficiently high temperature (90 °C). Disulfide bond formation can then be maximized and the extent of disulfide bond formation in bBLG B gels may exceed that in bBLG A gels. This increased density of disulfide cross-links could explain the higher G' (**Figure 5.4**), as well as the strain stiffening behaviour of the gel (**Figure 5.5**). Qin et al. (1999) reported higher accessibility (and resulting reactivity) of Cys121 in bBLG B, due to a greater mobility of this region. Manderson (1998) mentioned that the different amino acid at position 64 between bBLG A and B is close to the disulfide bonds Cys66-Cys160. The charged Asp64 in bBLG A could have caused increased electrostatic repulsion, as compared to the neutral Gly64 in bBLG B, and subsequent decreased the reactivity of the thiol to participate in thiol-disulfide interchange reactions. This electrostatic repulsion might be suppressed in both the studies of Huang et al. (1994) and McSwiney et al. (1994), because of the buffers used. In those cases, the reactivity of Cys66-Cys160 towards disulfide bond formation can be more similar for BLG A and B, while the structural flexibility of BLG A could enhance intermolecular interactions to form a stronger gel. Thus, specific isoforms can be selected to improve gelation, while the preferred isoform can differ when the gelation conditions are changed.
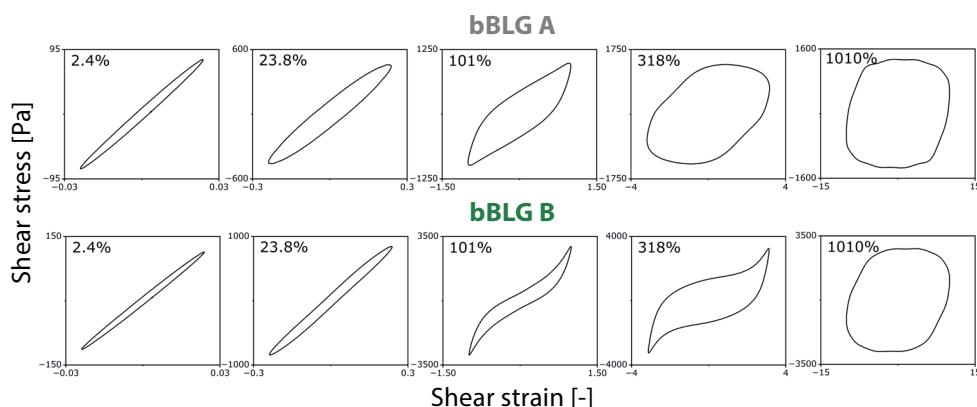
Figure 5.5. *Lissajous plots of heat-set bBLG A and bBLG B gels (15 wt% protein; average of triplicate), plotting the shear stress and shear strain (for sinusoidal strain). The maximum strain amplitude is depicted in the upper left corner of the graphs.*

5.3.2. Intervention B: less extensive purification

Recombinant BLG (natural isoform A) was produced with *P. pastoris*. Crude yBLG is the material that we refer to after production and secretion of recombinant BLG, and removal of insoluble and small molecular weight (< 8 kDa) material (e.g., salts, nutrients and released small cellular impurities). After further purification with the method described in **Chapter 3**, we obtained the material we refer to as 'purified yBLG'.

This material had a comparable protein content to that reported in **Chapter 3** (**Table 5.4**). We assume that also the carbohydrate content (i.e., mostly mannan impurities) and HMP content were also in comparable range, while a fraction of ~ 20 wt% of impurities remained unidentified. Finally, we do not have a suitable control that has the same sequence as yBLG (i.e., with modified N-terminus; **Table 5.1**) without any impurities. Thereby, we depict the results of bBLG A, being the bovine isomer that resembles yBLG most (**Table 5.1**), for comparison.

Table 5.4. *Expected composition of crude yBLG and purified yBLG, as reported in* **Chapter 3**. *The protein content in this current research is given in* **bold**.

Material	Content (DM%)		
	Protein	Carbohydrate	Hexametaphosphate
Crude yBLG	26 ± 0 **22.4 ± 0.2**	53 ± 1	n.a.
Purified yBLG	72 ± 0 **67.1 ± 0.7**	9 ± 1	1 ± 0

5.3.2.1.   Impact of intervention B on foaming properties

Figure 5.6 shows the formation of foam from crude and purified yBLG solutions, the resulting structure of the foam, and the foam collapse. An instable foam was formed for crude yBLG at the highest concentration of 1 mg mL^{-1} and therefore no further dilutions were tested. The foam already collapsed during its formation (i.e., 43–164% of the sparged gas was released), causing the time to reach 160 mL of foam to be almost twice as long as for other BLG variants (**Figure 5.6A**). Due to the early collapse of the bigger bubbles, the mean bubble size in the final foam and the fraction of air in the foam were relatively small (**Figure 5.6C**). The poor foaming properties of the crude yBLG seem to be related to specific impurities and not necessarily the N-terminal modification, as the foaming properties improved significantly after purification (**Figure 5.6**). Mannan impurities are not expected to cause the poor foamability of crude yBLG, because both crude and purified yBLG contain a considerable amount of mannan (**Table 5.4**). Further identification of the unknown fraction in crude yBLG and investigations of model systems is suggested to determine the cause of the poor functionality of crude yBLG.

The purified yBLG demonstrated better foaming properties than crude yBLG, but inferior than bBLG A (**Figure 5.6**). Purified yBLG formed larger bubbles and the foam was about 10 times less stable, as compared to bBLG A. Similar to crude yBLG, but to a lesser extent, the inferior foaming could have been caused by unknown impurities. Furthermore, the extended N-terminus could have also influenced the foaming properties of the purified yBLG, for example, by enhancing electrostatic repulsion.
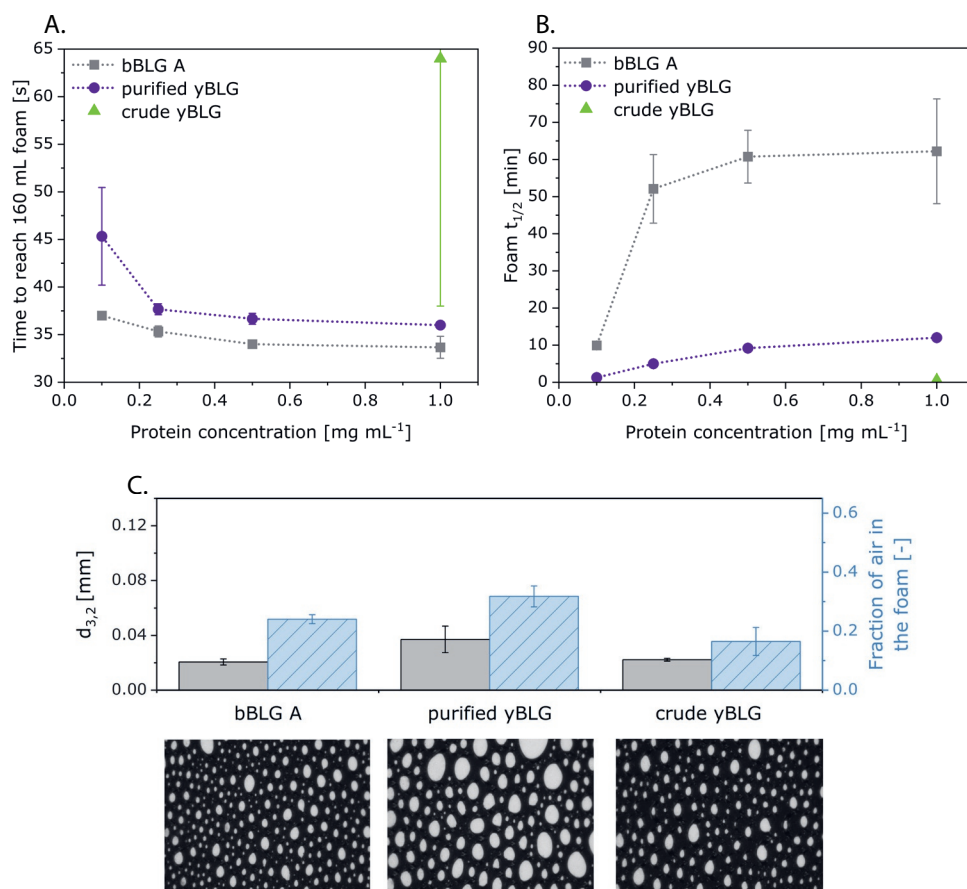
Figure 5.6. (**A**) Time to reach 160 mL of foam volume when sparging (250 mL min⁻¹) solutions of recombinant BLG before and after purification, and bovine BLG A for comparison, and (**B**) the foam half-life time ($t_{1/2}$). (**C**) Immediately after formation of the foam from 1 mg mL⁻¹ solutions, the Sauter mean diameter ($d_{3,2}$) of the bubbles and the fraction of air in the foam is shown, with corresponding pictures.

5.3.2.2. Impact of intervention B on heat-set gelation

The heat-set gelation of crude and purified yBLG is depicted in **Figure 5.7**, while the main parameters are listed in **Table 5.5**. The crude yBLG (~ 22 wt% protein) showed extremely poor gelling properties. Compared to pure bBLG A at the same protein concentration, twice as long heating time was required to reach gelation, while the formed gel was very weak (**Table 5.5**). Although crude yBLG was slightly more thermostable, it starts to unfold at 72 °C (**Table S5.1**) and is thereby expected to aggregate under the applied conditions. The gelation properties of yBLG clearly improved after purification (purified yBLG; **Figure 5.7**) and even exceeded those of bBLG A. This indicates that impurities prior to purification had counteracted the gelation, while the intrinsic functionality of purified yBLG is very good.
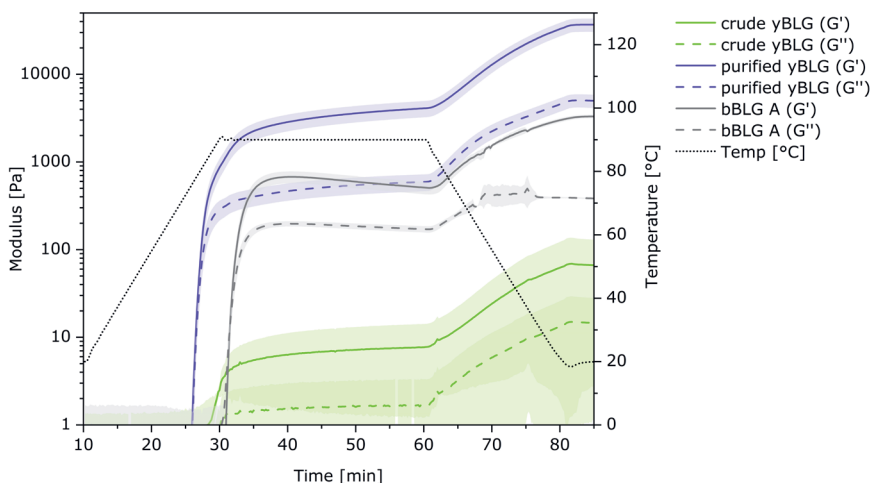
Figure 5.7. *Storage (G') and loss (G") moduli upon heating 15 wt% solutions of recombinant BLG from yeast before ('crude yBLG') and after purification ('purified yBLG').*

Table 5.5. *Gelation properties of various protein solutions (15 wt% total protein).*

	Gel point [min]	Final G' [Pa]	Critical strain [%]
bBLG A	31.7 ± 0.1	3,442 ± 146	5.2 ± 0.8
Crude yBLG	65.8 ± 5.4	88 ± 63	1.4 ± 0.4
Purified yBLG	26.7 ± 0.1	37,361 ± 6,209	2.9 ± 0.5

Gelation of purified yBLG occurred earlier and resulted in a much stronger gel, as compared to pure bovine BLG A, with an approximate 10-fold higher final G' (**Table 5.5**). The increase in the moduli was much more pronounced for purified yBLG than bBLG A during both heating and cooling (**Figure 5.7**). Although the gel of purified yBLG was stronger as compared to bBLG A, it was also more brittle during small deformation (i.e., lower critical strain; **Table 5.5**). Furthermore, the gel formed from purified yBLG was white, indicating a particulate network (Langton & Hermansson, 1992). In contrast, both isoforms of pure bBLG formed a transparent gel at pH 7.0, which is associated with a fine-stranded network (Langton & Hermansson, 1992). The purified yBLG gel exhibited strong strain stiffening during large deformation (i.e. at a shear strain of 101%; **Figure 5.8**). In contrast, bBLG A already started to yield at that strain (**Figure 5.8**).
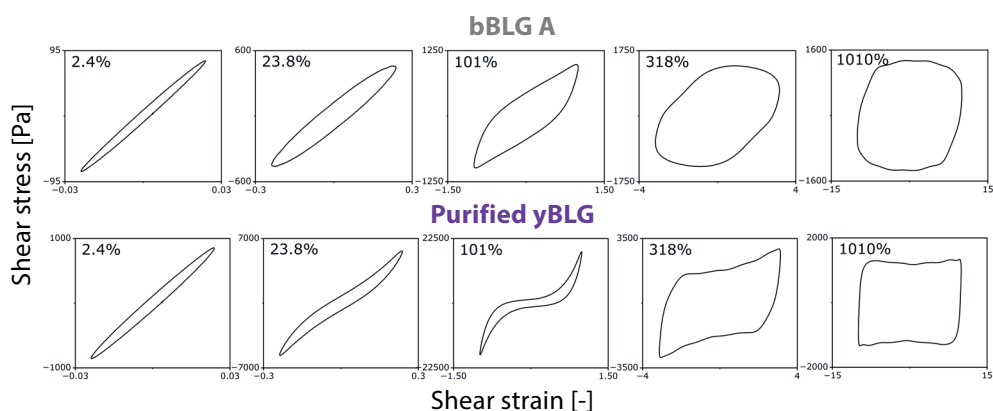
Figure 5.8. *Lissajous plots of heat-set bBLG A and purified yBLG gels (15 wt% protein; average of triplicate), plotting the shear stress and shear strain (for sinusoidal strain). The maximum strain amplitude is depicted in the upper left corner of the graphs.*

Some additional tests were performed with model systems to evaluate the impact of impurities that we know are similar to those present in purified yBLG. We combined pure bBLG A with mannan (from *Saccharomyces cerevisiae*) or hexametaphosphate (HMP). The added quantities of mannan or HMP corresponded to their content in purified yBLG. The results are depicted in **Supporting information 5.5.3**. Both compounds increased the final G′ of bBLG A by a factor of 4 and 15 in the presence of mannan or HMP, respectively. In addition, the gels were more ductile upon small deformation and the critical strains increased in the presence of either mannan or HMP (**Table S5.3**). Lastly, bBLG A with mannan added demonstrated stronger strain stiffening behaviour upon large deformation, but this was not observed in the presence of HMP (**Figure S5.2**).

The gelation of the model systems show that the poor gelation of crude yBLG is unlikely to be related to the presence of mannan, as the model system with added yeast mannan improved gelation (**Figure S5.1**). Instead, the remaining unidentified impurities in crude yBLG could have caused its poor gelation properties. The HMP in the purified yBLG is also expected to have accelerated gelation and increased the final G′ (**Table S5.3**). Nevertheless, gelation of purified yBLG resulted in a lower G′, as compared to the model system bBLG + HMP (difference of 8,344 Pa; **Table 5.5** and **Table S5.3**). Therefore, either the residual impurities in purified yBLG and/or the modified N-terminus interfered with the gelation. Furthermore, purified yBLG formed a more particulate gel network, as compared to the fine-stranded bBLG A (both with and without mannan or HMP). Reducing the electrostatic repulsion by adding ions or adjusting pH are reported to form particulate instead of fine-stranded networks (Langton & Hermansson, 1992). Although the purified yBLG is not expected to contain

many monovalent or divalent salts (due to dialysis), NaOH was added to neutralize the pH prior to gelation. The final concentration of Na^+ in the protein solutions was approximately 10 mM. This is relatively low and not expected to cause the white appearance. For example, it was reported that this shift in appearance of heat-set whey protein isolate was evident above NaCl additions of approximately 100 mM (Urbonaite et al., 2016). Alternatively, the N-terminal modification may have played a role, even though the additional charged amino acids would be expected to increase rather than decrease the overall electrostatic repulsion.

5.3.3. Intervention C: transformation into amyloid aggregates

Post-processing was performed to prepare anisotropic aggregates at pH 2.0 (amyloid fibrils) or pH 3.5 (amyloid-like aggregates). The pH was adjusted to 7.0 after preparation of the aggregates, excess ions were removed and the material was dried to obtain an easy-to-handle food ingredient. The aggregate morphology throughout this processing was visualized using transmission electron microscopy (TEM). The aggregates before and after processing are depicted in **Figure 5.9**, while the morphology for intermediate processing steps can be found in **Figure S5.3**. Amyloid-like aggregates mostly retained their shape and solubility (i.e., solutions remained clear; data not shown), while amyloid fibrils fragmented and aggregated (i.e., turbid sample and precipitation observed; data not shown). Both aggregation and fragmentation of amyloid fibrils have been previously reported (Mantovani et al., 2016). Precipitation appeared to have occurred primarily after the freezing step (data not shown), possibly due to further aggregation during concentration of the fibrils. We only considered the amyloid-like aggregates for further evaluation of the functional properties, since the amyloid fibrils were mostly destroyed and insoluble after processing.
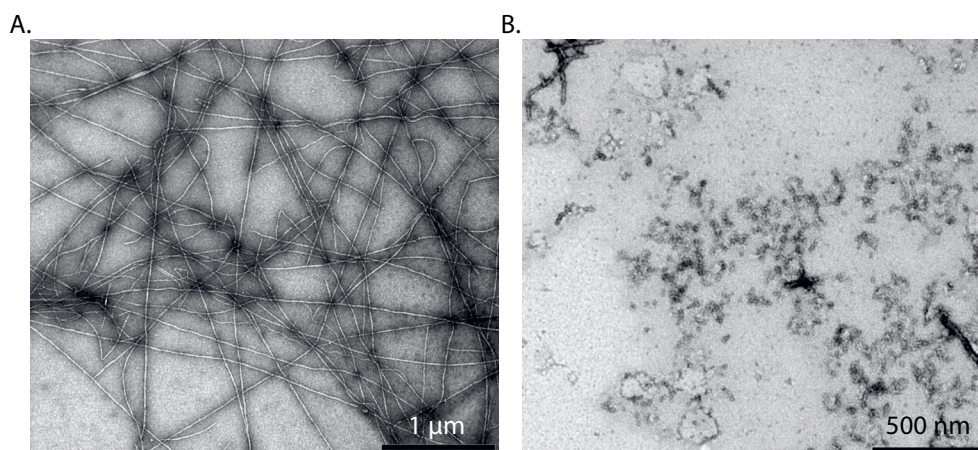
A.   B.

Figure 5.9. Morphology before (A, C) and after (B, D) processing. Protein concentration of the visualized samples were 5 and 10 mg mL^{-1} for amyloid fibrils (A, B) and amyloid-like aggregates (C, D), respectively.
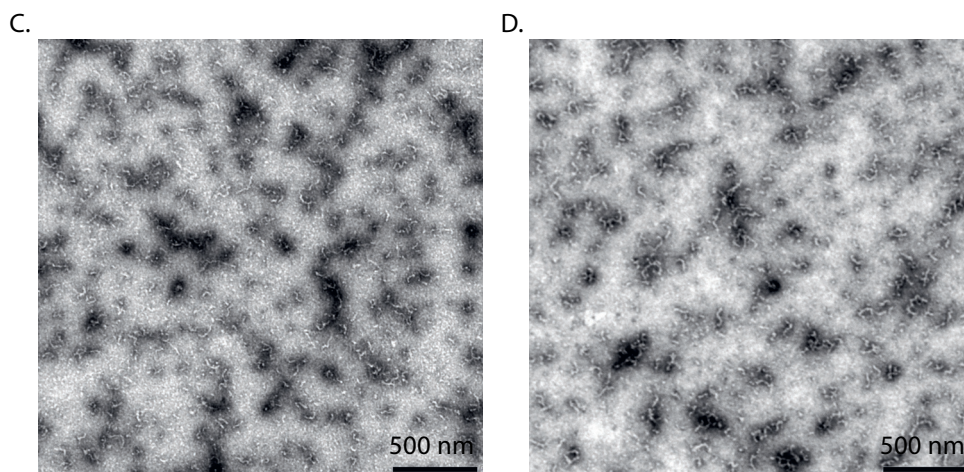
C.

D.

Figure 5.9. Continued.

5.3.3.1.   Impact of intervention C on foaming properties

Figure 5.10 shows the formation of foam from solutions containing native WPI or its amyloid-like aggregates, the resulting structure of the foam, and the foam collapse. The formation of foam was slightly faster and resulted in larger bubbles in the case of WPI amyloid-like aggregates, as compared to native WPI. This could be related to less drainage. The foam stabilized by WPI amyloid-like aggregates could have somewhat larger bubbles due to slower diffusion to the interface, as compared to native WPI (Davis & Foegeding, 2004; Rullier et al., 2008). Although small differences were noted, the structure of the foam was more or less similar. In contrast, the foam stability improved drastically when using amyloid-like aggregates instead of native WPI: a similar foam stability could be achieved with WPI amyloid-like aggregates using 4 – 10 times less protein (**Figure 5.10B**).

Dombrowski et al. (2016) demonstrated that the size of soluble (spherical) BLG aggregates positively correlated with their ability to stabilize foams. Schmitt et al. (2007) suggested that increased elongation of the WPI aggregate morphology could contribute to a thicker interfacial network. In addition, the non-aggregated material is also expected to improve foam properties, as reported for both BLG aggregates and amyloid fibrils (Lux et al., 2023; Rullier et al., 2008). Lux et al. (2023) suggested that this non-aggregated material acts as space fillers between aggregates. The shape and size of the WPI amyloid-like aggregates in the sample are not homogeneous (**Figure 5.9C**). It might very well be that the faster-diffusing small aggregates in the sample primarily stabilize the interface, while larger aggregates mostly counteract drainage in the thin liquid layer. Thus, WPI amyloid-like aggregates are superior foaming agents. Further investigations are necessary to confirm how the aggregate morphology contributes to the foam stability.
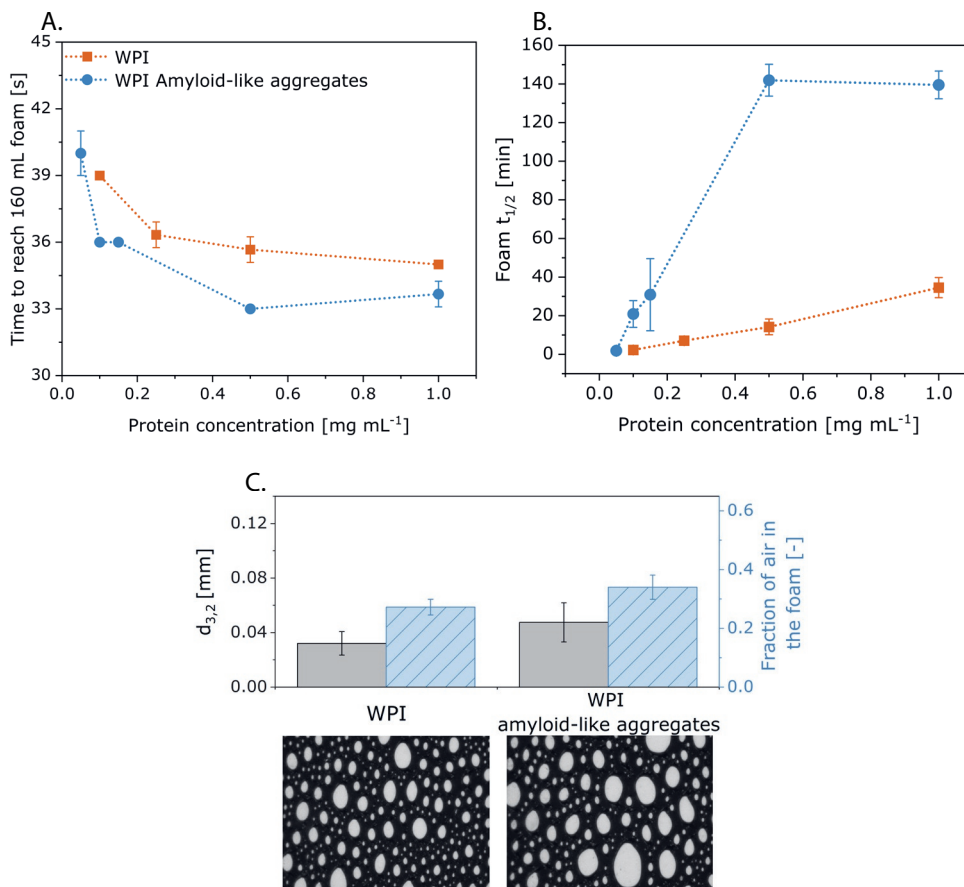
Figure 5.10. (**A**) *Time to reach 160 mL of foam volume when sparging (250 mL min^{-1}) solutions of WPI and WPI amyloid-like aggregates (WPI AA), and (**B**) the foam half-life time (t$_{1/2}$). Immediately after formation. (**C**) Immediately after formation of the foam from 1 mg mL^{-1} solutions, the Sauter mean diameter (d$_{3,2}$) of the bubbles and the fraction of air in the foam is shown, with corresponding pictures.*

5.3.3.2. Impact of intervention C on heat-set gelation

High concentration protein solutions (15 wt% protein) were prepared to subsequently evaluate the heat-set gelation. However, the solution containing WPI amyloid-like aggregates was highly viscous at this concentration (data not shown). This observation demonstrates the ability of these aggregates to increase the viscosity. Loveday et al. (2012) reported the formation of highly flexible amyloid aggregates (formed upon heating at pH 2.0 with CaCl2) that appear morphologically similar to our amyloid-like aggregates, and also reported enhanced viscosity. As it was challenging to obtain a homogenous and completely solubilized sample, instead we added amyloid-like

aggregates to a solution of native WPI (1:9, w/w; 15 wt% total protein) and investigated whether this improved its heat-set gelation. The main gelation properties are listed in **Table 5.6**, while the other results (moduli during gelling, LAOS) are depicted in **Supporting information 5.5.5**.

Table 5.6. *Gelation properties of various protein solutions (15 wt% total protein).*

	Gel point [min]	**Final G' [Pa]**	**Critical strain [%]**
WPI	32.6 ± 0.2	2,993 ± 327	6.3 ± 1.1
WPI + WPI amyloid-like aggregates (9:1, w/w)	34.5 ± 1.6	1,890 ± 935	6.9 ± 1.1

The addition of amyloid-like aggregates prior to heating had a negative impact of heat-set gelation: it resulted in slightly later gelation (~ 2 min), lower gel strength (-37%) and less ductile gel structure (**Table 5.6**; **Figure S5.5**). WPI gelation is reported to occur in two phases: primary aggregates first form and then associate into larger clusters (Mercade-Prieto & Gunasekaran, 2016). We suggest that WPI amyloid-like aggregates differ structurally from the primary aggregates formed by heating WPI at pH 7.0. Therefore, the WPI amyloid-like aggregates are unable to cross-link and participate in the gel network, while primary aggregates from (initially native) WPI are able to do so. Overall, the WPI amyloid-like aggregates are regarded unsuitable as heat-set gelling agents.

5.3.4. Comparison BLG ingredients

Consumers primarily observe the foaming and gelling properties of the protein ingredients in terms of foam stability and gel strength, respectively. We therefore use these two product characterizing parameters to summarize the impact of the interventions on the functionality range of BLG. The performance for the foam stability at the highest protein concentration (1 mg mL^{-1}) was compared, because bBLG B already showed relatively low foam stability at this concentration and should be further improved for application. An overview of the performances of the BLG ingredients is given in **Figure 5.11**, and is briefly discussed in the following.
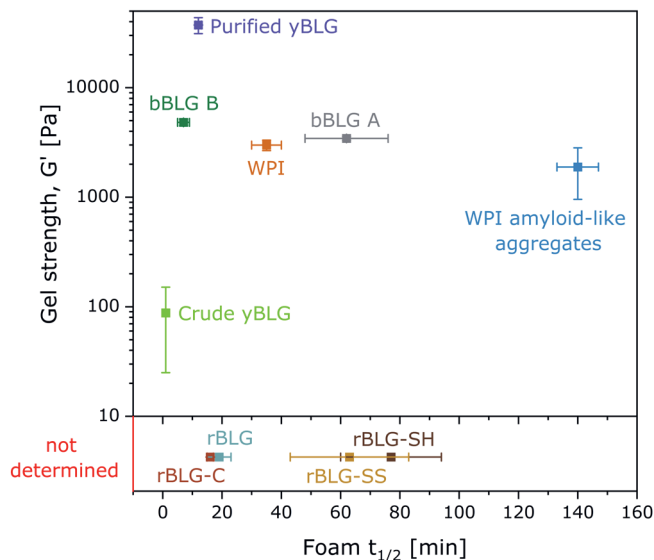
5

Figure 11. *Overview of the gelation (i.e. final gel strength, Pa) and foaming (i.e. foam $t_{1/2}$, min) properties of BLG ingredients used in this study. The gelation properties of recombinant BLG variants expressed from E. coli (rBLG, rBLG-SH, rBLG-SS and rBLG-C) were not investigated, and thereby indicated as 'not determined'.*

When using BLG as a foaming agent, minor differences in the amino acid sequence had major consequences for the final foam stability. The foam stability can be improved by almost a factor of 10 by choosing natural isoform A over B (**Figure 5.11**). Furthermore, improvements were observed when inducing cysteine mutations: in particular, substitutions of the free thiol (rBLG-SH; Cys121) and outer disulfide bond (rBLG-SS; Cys66–Cys160) improved the foam stability of bBLG B approximately by a factor of 10 times (**Figure 5.11**). Whether these mutations can also further improve foam stability of the natural isoform A remains to be determined. The N-terminal modification of yBLG most probably caused the inferior foam stability of purified yBLG, as compared to bBLG A (**Figure 5.11**). Nevertheless, the foam obtained with purified yBLG was almost twice as stable, as with native bBLG B (**Figure 5.11**). Purified yBLG can thus still be considered a functional foaming agent, even though a considerate amount of impurities is present (~ 33 wt% impurities). In contrast, crude yBLG was unable to stabilize foams (**Figure 5.11**), demonstrating the need for further purification (> 22 wt% protein). Finally, post-processing of WPI into amyloid-like aggregates resulted in superior foam stability, leading to almost four times more stable foam, as compared to native WPI (**Figure 5.11**). Future research could demonstrate whether such transformation on mesoscale outweighs the impact of minor molecular modifications (i.e. natural isoforms or cysteine mutations).

For the use of BLG as a gelling agent, also major differences between the natural isoforms were observed. About 40% higher gel strength was achieved with bBLG B than with bBLG A (***Figure 5.11***). A different isoform can be preferred when the gelation conditions are changed, as different heat-set gelation mechanisms were at play. For example, when salt is part of the formulation or a particular heating profile is used. In addition to the influence of molecular variation, impurities had major impact on gelation. Slight purification of up to ~ 22 wt% was not sufficient to allow proper gelation. After purification of up to ~ 67 wt%, the final G' upon heating was 10 times than that obtained with bBLG A. We thus conclude that purified yBLG is a suitable gelling agent. Finally, the addition of WPI amyloid-like aggregates to native WPI was not a suitable route to improve heat-induced gelation of native WPI, as the obtained gel strength was decreased by about a third (***Figure 5.11***). However, since high viscosity was observed prior to gelation and the WPI amyloid-like aggregates did not actively participate in the gel network, they can be used as thermostable viscosity enhancers.

5

5.4.   Conclusions

Three interventions in either the upstream production or further processing of (recombinant) BLG were considered as routes towards affordable recombinant BLG. Their potential was further evaluated based on the final functional properties of the BLG ingredient.

Intervention A included the selection of specific amino acid sequences for improved functional properties of recombinant BLG. Natural isoform A showed superior foaming (i.e., foam was 10 times more stable), while natural isoform B yielded stronger heat-set gels under the conditions applied (G' + 40% stronger). The substitution of cysteine by alanine in isoform B allowed a more effective stabilization of foams, in particular the substitution of only Cys121, or Cys66 and Cys160 (being up to 10 times more stable).

Intervention B simplified DSP in terms of purification. The removal of cellular material and low MW impurities (< 10 kDa) by centrifugation and filtration was not sufficient to obtain a functional ingredient. This material contained ~ 22 wt% and demonstrated poor gelling and foaming. Further purification of up to ~ 67 wt% was achieved by reversible precipitation using hexametaphosphate (HMP), while residual HMP remained (~ 1 wt%). The higher purity of yBLG and the introduction of HMP led to a stronger heat-set gel, with a G' that was 10 times higher as compared to bovine BLG, although the gel network seemed to be different. The foaming properties were in a similar range as compared to BLG B, but inferior to BLG A. The mild purification method thus has potential for future application, although identification of residual impurities is required.

Intervention C added post-processing to transform native whey protein (WPI) into functional aggregates. Amyloid fibrils are reported to have superior functionality, but we observed them to be instable upon processing at food-grade conditions and drying. In contrast, WPI amyloid-like aggregates were stable during processing and heating. These aggregates were excellent foaming agents, being able to stabilize foams up to four times longer than native WPI. Amyloid-like aggregation is thus promising for efficient application of recombinant proteins in foams. Future research should weigh such gains in functionality against the additional costs of the further processing required.

This explorative study indicates the strong dependence of protein functionality on the different interventions. Thus, for designing production processes for recombinant food proteins, one should consider gains in protein functionality (i.e., for efficient application), just as much as gains in protein purity and yield (i.e., for efficient production).

5.5. Supporting info

5.5.1. Charge and present of salt in natural BLG isoforms

The surface charge (i.e., zeta potential) of the BLG natural variants was determined, as listed in **Table S5.1**. The method can be found in **Chapter 2**. Besides the surface charge, the measured conductivities are shown, confirming similar salt content of the samples. Isoform A was found to be more negatively charged (**Table S5.1**), due to the different amino acid at position 64 where BLG A contains a negatively charged aspartic acid and BLG B a neutral glutamine (Basch & Timasheff, 1967).

Table S5.1. *Zetapotential and conductivity measurements of BLG solutions (1 mg mL^{-1} ultrapure water).*

	Zeta potential (mV)	Conductivity (µS cm^{-1})
bBLG A	-28.3 ± 4.2	23.17 ± 1.68
bBLG B	-18.3 ± 1.5	24.12 ± 0.99

5.5.2. Heat stability of the variants

The heat-induced unfolding was characterized using differential scanning calorimetry to identify differences in protein stability. The method can be found in **Chapter 7**. The enthalpy, onset and peak temperature for protein unfolding are listed in **Table S5.2**. For bovine BLG, the isoform B was found to be more heat stable than isoform A; unfolding required less energy and occured at a lower temperature (-4 °C). When adding amyloid-like aggregates to native WPI (ratio 1:9, w/w), this also lowered the enthalpy by 10% and did not change the onset or peak temperature. This demonstrates the heat-stability of the WPI amyloid-like aggregates. Lastly, recombinant expression of BLG led to a lower enthalpy for unfolding, which might be related to the modified N-terminus. Yet, the onset and peak temperature were increased, as carbohydrate impurities can stabilize protein folds.

Table S5.2. *Parameters for denaturation of BLG variants (15 protein w/w%).*

	Enthalpy [kJ mol^{-1}]	Onset temp. [°C]	Peak temp. [°C]
bBLG A	159 ± 4	65 ± 0	73 ± 0
bBLG B	171 ± 5	69 ± 0	75 ± 0
WPI	170 ± 5	64 ± 0	73 ± 0
WPI + WPI Amyloid-like aggregates (9:1, w/w)	154 ± 5	65 ± 1	74 ± 0
Crude yBLG A	128 ± 4	72 ± 0	80 ± 0
Purified yBLG A	146 ± 7	63 ± 0	72 ± 0

5.5.3. Rheology model systems: impact mannan and HMP

Mannan is a major impurity in the recombinant BLG material that is expressed from *Pichia pastoris*. A majority of the mannan can be removed through reversible and selective precipitation of the protein fraction by HMP. After removal of excess HMP, approximately 9 DM% of mannan and 1 DM% residual HMP is left, while the protein content is about 72% (**Chapter 3**). Pure mannan (from *Saccharomyces cerevisiae*; Sigma Aldrich) and HMP were added separately to pure bBLG A to see to what extent they influence its gelling behaviour. These impurities were added in the same quantity as present in yBLG, while the final protein content was set at 15 wt%. The gelling behaviour is shown in **Figure S5.1**, while the main parameters are listed in **Table S5.3**. The presence of mannan, but especially HMP, accelerated gelation and increased gel strength (**Figure S5.1** and **Table S5.3**).
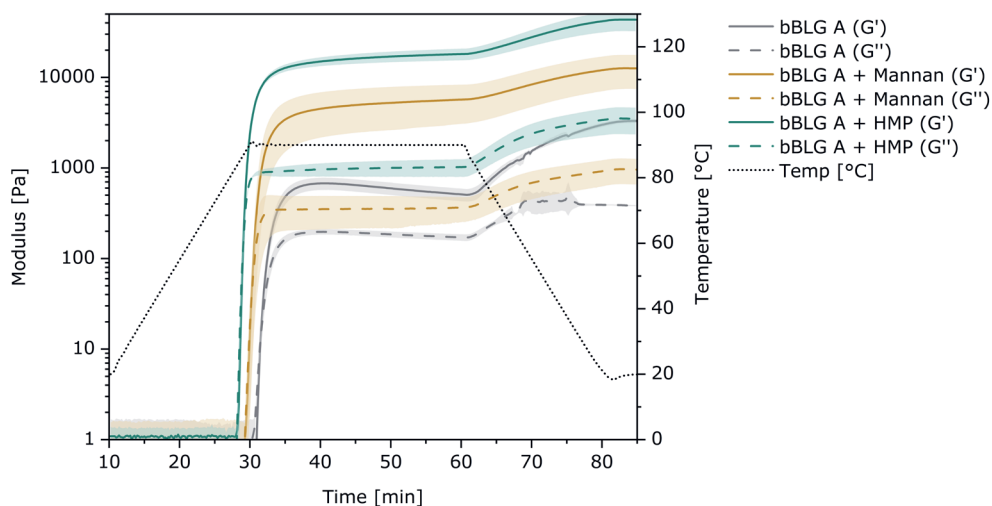
Figure S5.1. *Storage (G') and loss (G") moduli upon heating 15 wt% solutions of bBLG A; without or with added mannan (from Saccharomyces cerevisiae), or hexametaphosphate.*

Table S5.3. *Gelation properties of various protein solutions (15 wt% total protein).*

	Gel point [min]	Gel strength [Pa]	Critical strain [%]
bBLG A	31.7 ± 0.1	$3,442 \pm 146$	5.2 ± 0.8
bBLG A + Mannan	30.3 ± 0.6	$12,447 \pm 5,109$	18.4 ± 5.2
bBLG A + HMP	28.7 ± 0.1	$45,705 \pm 9,523$	22.5 ± 8.0

The behaviour upon large deformation is reflected in the Lissajous plots in *Figure S5.2*. *Figure 5.2* shows that the presence of mannan revealed an inverted sigmoidal shape of the Lissajous plot at 101%, indicating strain stiffening behaviour.
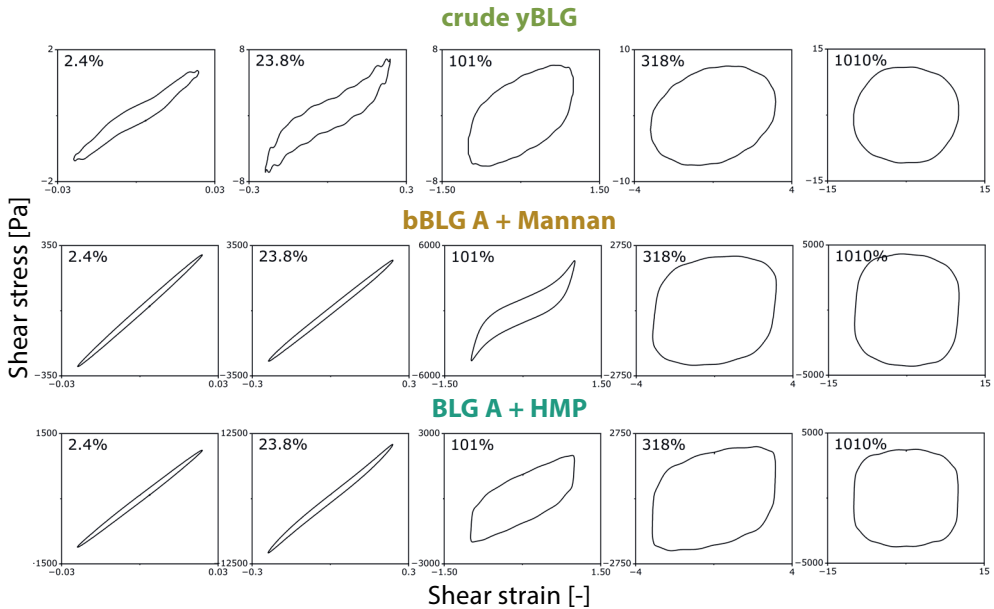

Figure S5.2. Lissajous plots of heat-set bBLG A gels (15 wt% total protein; average of triplicate); without or with added mannan (from Saccharomyces cerevisiae), or hexametaphosphate. The shear stress was plotted against the shear strain (for sinusoidal strain). The maximum strain amplitude is depicted in the upper left corner of the graphs.

5.5.4. Processing of WPI aggregates

After preparation of the amyloid fibrils and amyloid-like aggregates by heating for 5 hours at pH 2.0 and pH 3.5, respectively, the solutions were further processed to obtain an easy-to-handle ingredient. *Figure S5.3* shows the aggregate morphology (visualized with TEM) throughout the following processing steps: first, the pH was adjusted to pH 7.0, then the solution was dialyzed, after which it was frozen.
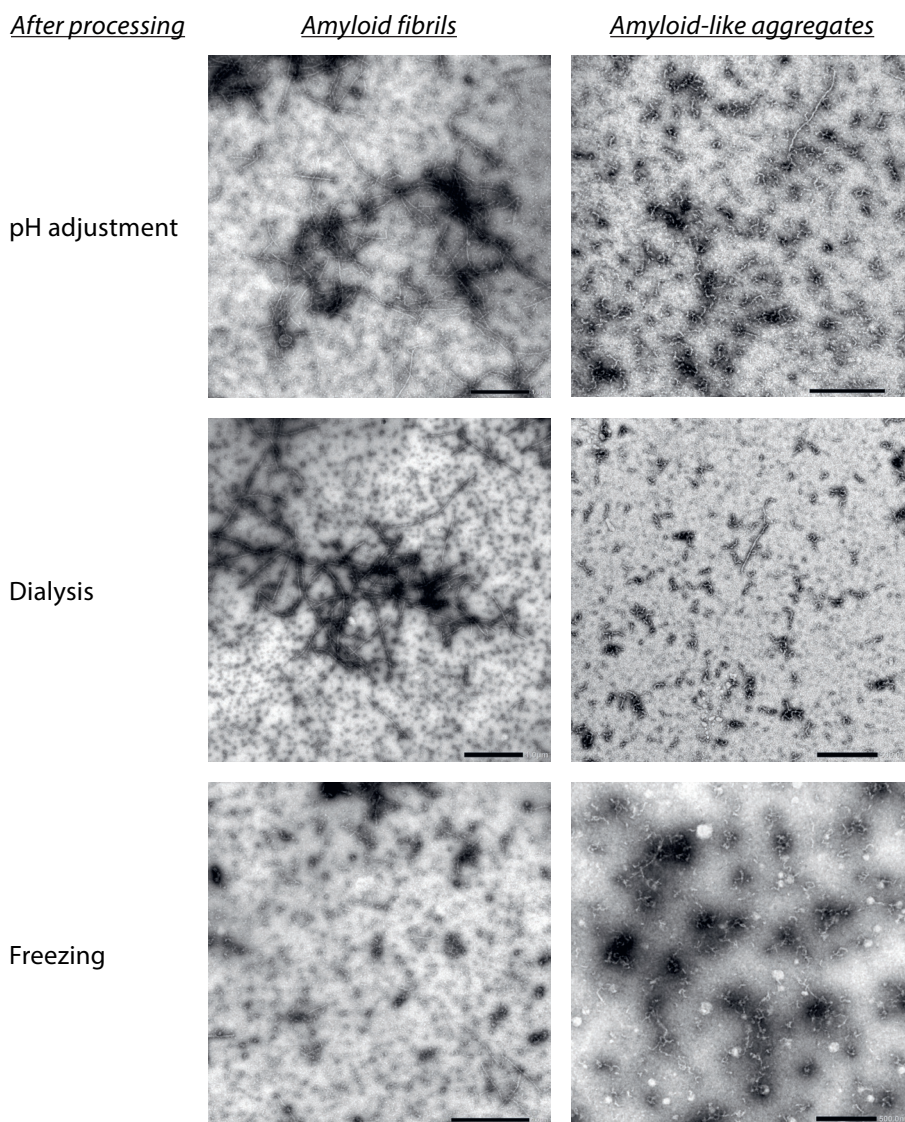
Figure S5.3. *Amyloid fibrils (prepared at pH 2.0) at a protein concentration of 10 mg mL^{-1}, with scale bars representing 1 µm. Amyloid-like aggregates (prepared at pH 3.5) at a protein concentration of 5 mg mL^{-1}, with scale bars representing 500 nm. Both shown after processing.*

5.5.5. Impact of amyloid-like aggregates on gelation

Amyloid-like WPI aggregates were added to native WPI in a ratio of 1:9 (w/w) with a final protein concentration of 15 wt%. The heat-set gelation of this solution and of native WPI is shown in **Figure S5.4**, while the gel breakdown behaviour is reflected in the Lissajous plots in **Figure S5.5**.
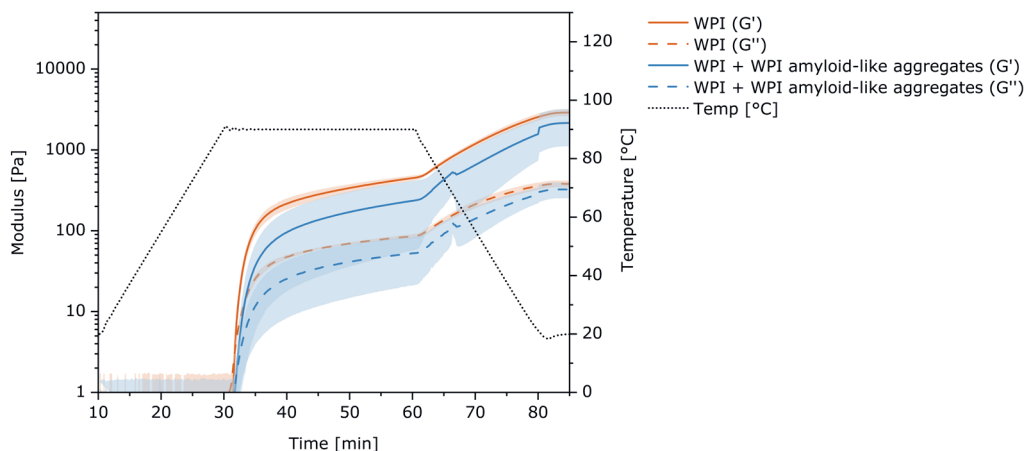
Figure S5.4. *Storage (G') and loss (G") moduli upon heating 15 wt% solutions of WPI and WPI with added amyloid-like WPI aggregates (9:1, w/w).*
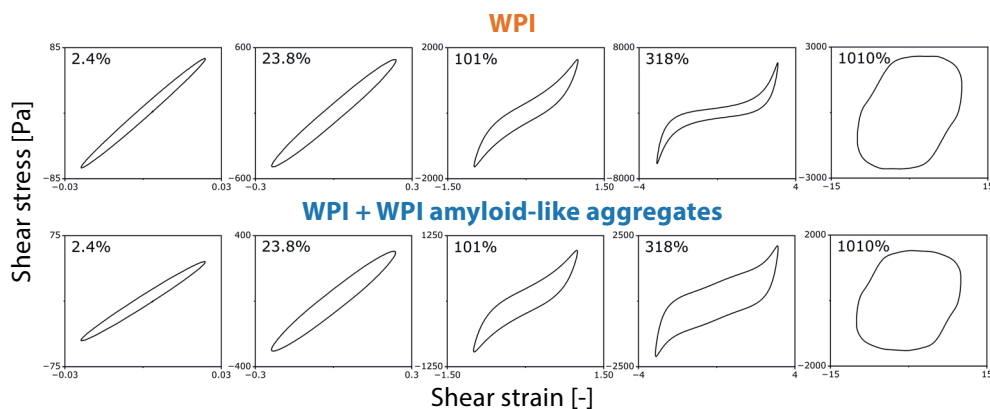
Figure S5.5. *Lissajous plots of heat-set gels from WPI with and without amyloid-like WPI aggregates (15 wt% total protein; average of triplicate). WPI amyloid-like aggregates were added to native WPI in a ratio of 9:1, w/w.*

Fibrillization of β-lactoglobulin at pH 2.0:

impact of cysteine substitution and disulfide bond reduction
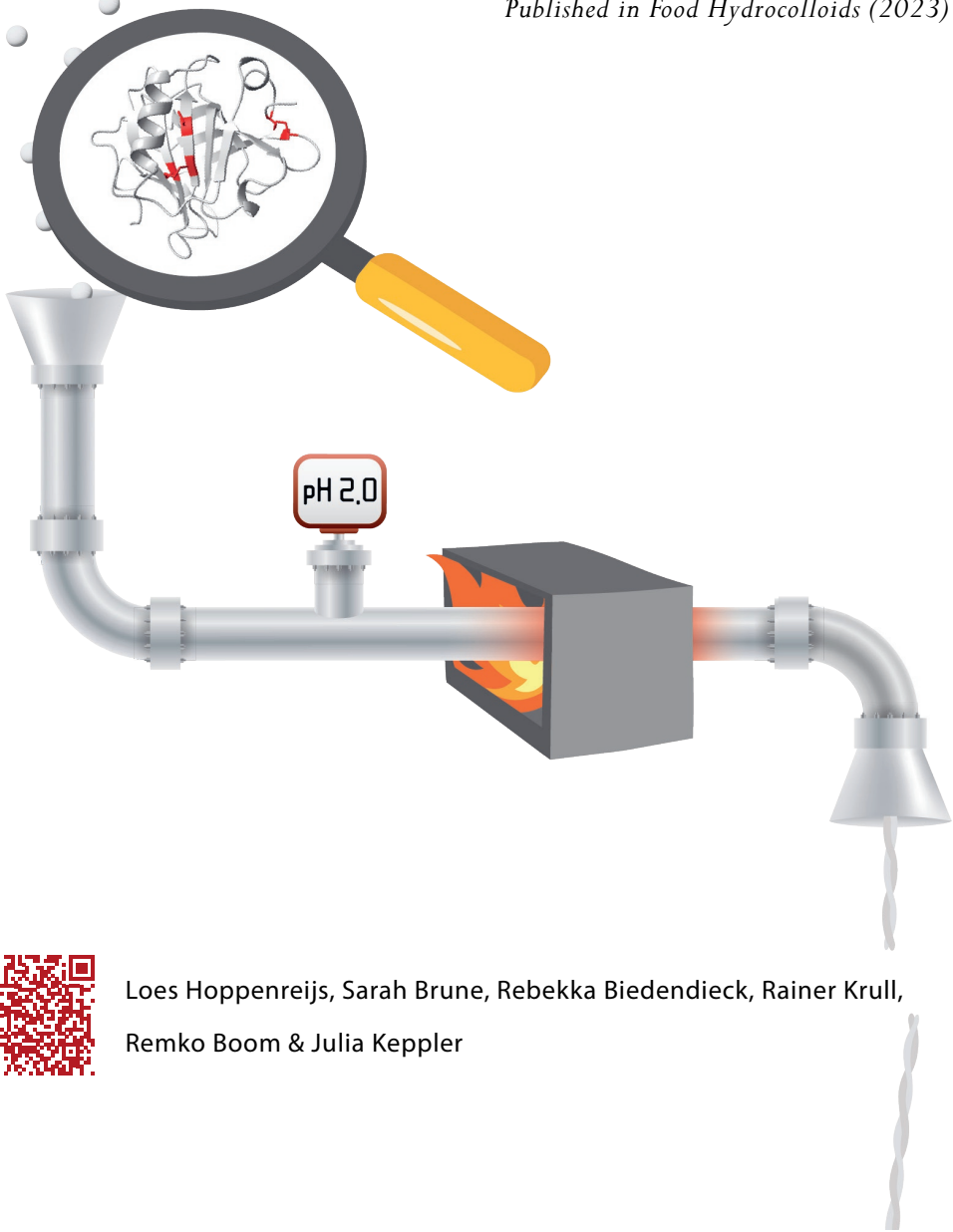
Loes Hoppenreijs, Sarah Brune, Rebekka Biedendieck, Rainer Krull,

Remko Boom & Julia Keppler

Fibrillization is a promising route to enhance protein functionality for food, while pre-fibrillar oligomers *in vivo* are suspected to be pathogenic. Here, the role of intramolecular disulfide bonds in fibrillization (80 °C, pH 2) of the major whey protein β-lactoglobulin (BLG) was studied. Different cysteine-modified variants were used for this investigation, removing one or both disulfide bonds in BLG.

Denaturation occurred but residual structure elements prevented aggregation of intact bovine BLG upon heating at pH 2.0 up to 1 h. Heating for longer caused acidic hydrolysis, which resulted in the release of peptides with enhanced aggregation tendency. Partial destabilization by removal of Cys66-Cys160 (by recombinant substitution) or both disulfide bonds (by chemical cleavage) was found to affect this hydrolysis rate, but only cleavage of both disulfide bonds accelerated the aggregation kinetics. No major impact on the fibril morphology was observed. In contrast, recombinant removal of both disulfide bonds led to complete structural disruption and instantaneous aggregation of intact BLG at pH 2 prior to heating. These small aggregates (10–50 nm) led to the formation of worm-like aggregates within 1 h of heating, which slowed down the acidic hydrolysis and inhibited further aggregation into fibrils.

We concluded that fibrillization can be accelerated by structural destabilization through disulfide bond cleavage, while complete destabilization can actually hinder it. These insights can be used for the production of functional protein aggregates, and possibly for avoiding pathogenic fibrillization of proteins.

Abstract

Abbreviations: amino acids, aa; bovine β-lactoglobulin, bBLG; circular dichroism, CD; differential scanning calorimetry, DSC; dithiothreitol, DTT; dynamic light scattering, DLS; Fourier-transform infrared spectroscopy, FTIR; high-performance size exclusion chromatography, HPSEC; recombinant β-lactoglobulin with substituted cysteine residues, rBLG-C; recombinant β-lactoglobulin with substituted outer disulfide bond, rBLG-SS; recombinant β-lactoglobulin, rBLG; thioflavin T, ThT; Transmission electron microscopy, TEM; tris(2-carboxyethyl)phosphine, TCEP.

6.1. Introduction

Taking examples from nature (Fowler et al., 2007), the transformation of food proteins into functional amyloid structures is gaining attention in the last decades. These linear aggregates, which are stabilised by intermolecular β-sheets, are a promising way to extend the properties of proteins for various material and food applications: e.g., as thickeners, emulsifiers, or carriers (Cao & Mezzenga, 2019; Jansens et al., 2019). In contrast, early stages of fibrillization of pathogenic proteins *in vivo* can cause neurodegenerative diseases (Caughey & Lansbury, 2003). Therefore, mechanistic understanding of amyloid aggregation under various environmental conditions is crucial to drive or control it.

β-lactoglobulin (BLG) is often used as a model protein, due to its excellent availability and well-characterised properties. BLG and many other globular proteins can form thin (2.6 nm), long (0.2–5 μm) and semi-flexible aggregates, called amyloid fibrils, under specific environmental conditions (Adamcik et al., 2010; Lambrecht et al., 2019). Usually this involves heating of a protein solution (1–3 mg mL^{-1}) at pH 2 for several hours (Cao & Mezzenga, 2019). Aggregation of intact protein is avoided at these incubation conditions, probably due to strong electrostatic repulsion (Loveday et al., 2011). However, acid-catalysed hydrolysis can release peptides that are able to subsequently assemble into intermolecular β-sheets, leading to the formation of fibrillar structures. Specific peptide regions are prone to this particular type of assembly, being mainly hydrophobic, low in charge and do not contain proline (Akkermans et al., 2008). Consequently, mostly N-terminal peptides (amino acids, aa; 1–33 and 1–52) are incorporated in BLG fibrils (***Figure 6.1***; Akkermans et al., 2008; Ye et al., 2018), although a minor fraction of C-terminal peptides is also included (VandenAkker et al., 2016). Such regions prone to fibrillization are also called aggregation 'hotspots' (de Groot et al., 2005).

According to VandenAkker et al. (2016), cysteine residues are preferably at the surface of amyloids, indicating that disulfide bonds may not play an active role in the stabilization of the intermolecular β-sheet core. Lux et al. (2021) concluded the same from experiments with spin-labelled cysteine residues. However, cysteines might have an indirect role in fibrillization, as intramolecular disulfide bonds are known to stabilize proteins (Mohan Reddy et al., 1988). It has not been yet reported whether these bonds affect the acidic hydrolysis rate, or the subsequent stages of fibrillization.

BLG contains five cysteine residues, of which three are located in a hotspot region (***Figure 6.1***). These three cysteines are located in the native hydrophobic core of BLG, in the form of a free thiol (Cys121) and a disulfide bond (Cys106-Cys119). Besides, two cysteines form a disulfide bond near the surface of BLG (Cys66-Cys160) and are located in non-hotspot regions. These covalent disulfide bonds restrict the conformational mobility of the protein chain. Thereby, they affect conformational changes in (re) folding pathways (Hattori et al., 2005) and stabilize native-like structures (Wiedemann

et al., 2020). Disulfides were shown to protect residual structures in BLG from unfolding, for example, even in 5 M urea at 37 °C (Hamada et al., 2009) and during heating up to 125 °C (de Wit, 2009).
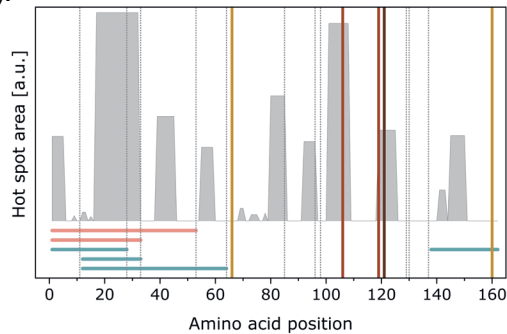

*Figure 6.1. Fibrillization tendency of the BLG sequence: peaks in the graph indicate 'hotspots' for fibril formation, according to amino acid sequence prediction with AGGRESCAN (Conchillo-Solé et al., 2007). The location of aspartic acid residues as possible cleavage sites are indicated with vertical dotted lines. The location of the outer and inner disulfide bonds (**Cys66-Cys160** and **Cys106-Cys119**, respectively) and the free thiol group (**Cys121**) are indicated with vertical solid lines. Horizontal lines below the graph indicate peptide sequences that are only found in fibril fraction (**pink**), or both in fibril and non-fibril fractions (**blue**) after isolation of fibrils with ultrafiltration (Akkermans et al., 2008; Ye et al., 2018).*

We have demonstrated In **Chapter 2** that these disulfide bonds can be either removed chemically (bBLG reduced) or recombinantly (rBLG-C) with different impact on its fold, as summarized in **Table 6.1**. In addition, recombinant production allows for specific removal of only the outer disulfide bond, while keeping the inner disulfide bond intact (rBLG-SS). In the current study, we study the impact of the disulfide bond removal through both approaches on subsequent stages of fibrillization, including (1) structural destabilization, (2) acidic hydrolysis, (3) assembly through intermolecular β-sheets, and (4) the aggregate morphology. The findings are used to identify factors that dominate the aggregation kinetics and the formation of a specific morphology. This information in turn is useful for development of functional protein aggregates, or avoiding pathogenic fibrillization.

Table 6.1. *Structural characteristics of BLG and its chemically or recombinantly modified variants, according to **Chapter 2**.*

Variant	Secondary structure [%]				Tertiary structure
	α-helix	β-sheet	Random coil	β-turn	
bBLG	16 ± 3	51 ± 3	24 ± 2	9 ± 2	Globular
bBLG reduced	13 ± 1	43 ± 1	39 ± 1	5 ± 1	Opened
rBLG	16 ± 1	51 ± 1	21 ± 1	12 ± 1	Globular
rBLG-SS	21 ± 1	35 ± 1	36 ± 1	8 ± 1	Slightly Opened
rBLG-C	29 ± 2	9 ± 3	57 ± 2	6 ± 2	Disordered

6.2.   Experimental section

Recombinant and bovine BLG (rBLG and bBLG, respectively) variants were produced as described **Chapter 2**. In short, *Escherichia coli* Origami B cells were transformed with a plasmid encoding recombinant β-lactoglobulin isoform B, which contains a Leu1Ala/Ile2Ser exchange to ensure cleavage of the N-terminal methionine (Loch et al., 2016). In addition, BLG variants were produced in which cysteine residues were exchanged with alanine residues, resulting in either removal of the outer SS bond Cys66-Cys160 (rBLG-SS), or all cysteine residues (rBLG-C). Variant rBLG-C was isolated from inclusion bodies, while rBLG and rBLG-SS were produced as soluble proteins.

According to **Chapter 2**, the corresponding *E. coli* strains were cultivated in LB medium in shake flasks and recombinant BLG production was induced with 500 µM iso-propyl-β-D-thiogalactopyranoside (IPTG, Sigma-Aldrich, Germany). Cells were harvested after 24 h and disrupted using sonication. The purification process of rBLG and rBLG-SS (present in soluble form in the supernatant) included ion exchange chromatography, ammonium sulfate precipitation, and desalting via size exclusion chromatography. Inclusion bodies containing rBLG-C were washed with triton to remove contaminating proteins and solubilized in 8 M urea. Refolding and purification of rBLG-C took place within one step via gravity flow ion exchange chromatography. Remaining salt was afterwards removed with dialysis. Also according to **Chapter 2**, bBLG was isolated from whey protein isolate and subsequently chemically reduced with tris(2-carboxyethyl) phosphine (TCEP) at pH < 3.5, after which the reducing agent was removed with dialysis. Finally, all protein variants were freeze-dried. A full reduction of both disulfide bonds was achieved (**Chapter 2**).

Protein solutions of 10 mg mL^{-1} were prepared and the pH was adjusted to 2.0, 3.5 and 7.0 using 2 M HCl or NaOH. Samples were kept overnight in the fridge. The spontaneous assembly prior to heating was analyzed with Thioflavin T (ThT) fluorescence and Fourier-transform infrared (FTIR) spectroscopy.

For aggregation experiments, BLG solutions (10 mg mL^{-1}) at pH 2 were aliquoted into volumes of 900 µL and incubated in an Eppendorf shaker at 80 °C while shaken at 350 rpm. Samples were taken after 0, 1, 3 and 5 h (independent duplicates) and were subsequently analyzed for the overall extent of the hydrolysis (high-performance size exclusion chromatography, HPSEC, after dissociation), relative intermolecular β-sheets (ThT fluorescence), and final morphology (transmission electron microscopy, TEM).

6.2.1.   Denaturation behaviour

The denaturation of the protein variants was analyzed with differential scanning calorimetry (DSC), similar to Rivera del Rio et al. (2022). Protein variants had to be analyzed at a concentration of 25 mg mL^{-1}, instead of 10 mg mL^1 used in other analyses,

due to low sensitivity (**Supporting information 6.6.4** provides more information). Unheated samples were analyzed at pH 2.0 in independent triplicate, using a DSC (TA instruments, USA). A high volume pan was filled with ~ 60 mg of protein solution (exact amount was noted to calculate the enthalpy) and subsequently sealed. An empty pan was prepared as a reference. The pan was heated up to 100 °C at a heating rate of 3.5 °C min^{-1} and then cooled to room temperature. A second heating/cooling cycle was used to check for complete denaturation. TRIOS software (TA Instruments) was used to determine the denaturation enthalpy (area under the endothermic peak, corrected for the protein content) and the onset temperature for denaturation.

6.2.2. Acidic hydrolysis by HPSEC

Independent duplicates of heated and unheated samples at pH 2.0 were dissociated and the protein size distribution was analyzed, using a method similar to Akkermans et al. (2008). A dissociating buffer was prepared in a 0.15 M Tris-HCl buffer at pH 8.0, including 8 M guanidine hydrochloride and 0.1 M dithiothreitol (DTT). The samples were diluted with this buffer in a ratio of 1:4 and incubated for at least one hour. The ThT fluorescence after dissociation of native BLG variants and mature fibrils confirmed complete dissociation (**Figure S6.1**). Dissociated protein samples were then analyzed on an Ultimate™ high performance liquid chromatography system (Thermo Scientific, USA) equipped with two subsequent size exclusion columns (TSKgel G2000 SWxl and TSKgel G3000 SWxl; both 7.8 mm I.D. x 30 cm, 5 μm; Tosoh Corporation, Japan). Isocratic elution was achieved using 30% acetonitrile (including 0.1% trifluoroacetic acid and 6 M urea) as a eluent at a flow rate of 1.5 mL min^{-1}. The protein was detected by UV detector (Thermo Scientific) at a wavelength of 214 nm. The retention was calibrated using proteins with different sizes: thyroglobulin, bovine blood serum albumin, β-lactoglobulin, α-lactalbumin, aprotin, bacitrin and phenylalanine (Sigma Aldrich, USA). All peaks were integrated for the dissociated BLG samples. Intact BLG eluted between 7.34–9.5 min, while protein or peptides < 10 kDa eluted between 9.5–13.95 min. Intact BLG was then expressed as a percentage of the total area of all peaks.

6.2.3. Intermolecular β-sheets by ThT fluorescence and FTIR analysis

The Thioflavin T (ThT) fluorescence was measured based on a method of Loveday et al. (2011). A 10 mM phosphate buffer containing 150 mM NaCl was prepared (pH 7.0) and ThT was added (56 μM). After stirring for about one hour the solution was filtered (Whatman 595 ½, GE Healthcare, USA). Fifty μL of protein solution (1 wt%) was transferred to a reaction tube and 4 mL ThT solution was added. The solution was vortexed and the fluorescence was measured exactly after one minute, using a fluorophotometer (RF6000, Shimadzu, Kyoto, Japan) with excitation and emission wavelengths of 440 and 482 nm, respectively. Ultrapure water was used as a blank and samples were measured in independent and dependent duplicates.

6

FTIR analysis was performed for all variants for the unheated samples to confirm the ThT results prior to heating, as well as after 1 h of heating, using a protocol from Heyn et al. (2019) with adjustments. Undiluted samples (1 wt%) were analyzed with a Confocheck Tensor 2 system (Bruker Optics, Ettlingen, Germany) equipped with a thermally controlled BioATR 2 unit (25 °C). Samples were transferred to the crystal, left to equilibrate for 2 min, and then analyzed using 64 scans with a resolution of 4 cm^{-1}. Ultrapure water was used as a control reference. The spectra were vector normalised in the amide I region (1700–1600 cm^{-1}) without further manipulation.

6.2.4. Aggregate morphology by TEM

Mature aggregates (5 h of heating) were visualised with TEM to check for major morphological changes, while BLG-C was analyzed after 0, 1, 3 and 5 h of heating. Samples were transferred on a 400 mesh copper grid (2 min), then washed with ultrapure water (5 s), and stained with 2% uranyl acetate (30 s). After drying, the samples were analyzed on a JEM-1400plus microscope (120 kV; Jeol, Tokyo, Japan).

6.3. Results

6.3.1. Self-assembly prior to heating

Two methods were used to analyse the intermolecular β-sheets prior to heating, ThT fluorescence and FTIR spectroscopy (**Figure 6.2**). ThT specifically binds with intermolecular β-sheets upon which its fluorescence is enhanced. As this is an indirect method for intermolecular β-sheet formation, FTIR spectroscopy was used to confirm the presence of intermolecular β-sheets at pH 2.0. The peptide bond vibrations absorb at a specific absorbance wavenumber, depending on its conformation. Intra- and intermolecular β-sheets can be distinguished, having absorbances between 1625–1640 and 1610–1628 cm^{-1}, respectively (Jackson & Mantsch, 1995).

All variants except rBLG-C showed already a relatively low ThT fluorescence (< 300 a.u.; blank had a fluorescence of 177 ± 8) at pH 2.0. However, no intermolecular β-sheets were evident from the FTIR spectra: the normalised spectra in the amide I were similar to bovine BLG with a typical absorption for intramolecular β-sheets around 1631 cm^{1} (**Figure 6.2**). Therefore, it is not likely that the ThT fluorescence prior to heating is due to aggregation. Instead, it is probably related to association of ThT with the native protein. This is supported by Rovnyagina et al (2020), who reported a correlation of BLG concentration with the ThT fluorescence. ThT does not usually bind to native globular proteins as their β-sheets are often too short (< 4 β-strands) and twisted (Biancalana & Koide, 2010). However, β-lactoglobulin contains a β-barrel that is relatively less twisted than open sheets (Páli & Marsh, 2001) and contains eight β-strands (Brownlow et al., 1997). Removal of the disulfide bond(s) in reduced bBLG

and rBLG-SS resulted in a slightly increased ThT fluorescence (1.3 and 2.2 times higher, respectively; *Figure 6.2A*). Opening of the tertiary structure in these variants (*Table 6.1*) may have facilitated entrance of ThT into the β-barrel and thus stimulated its association. However, these relative increases in ThT fluorescence are relatively low compared to the increases in ThT fluorescence obtained upon heating (4–9 times higher; *Figure 6.4B*).
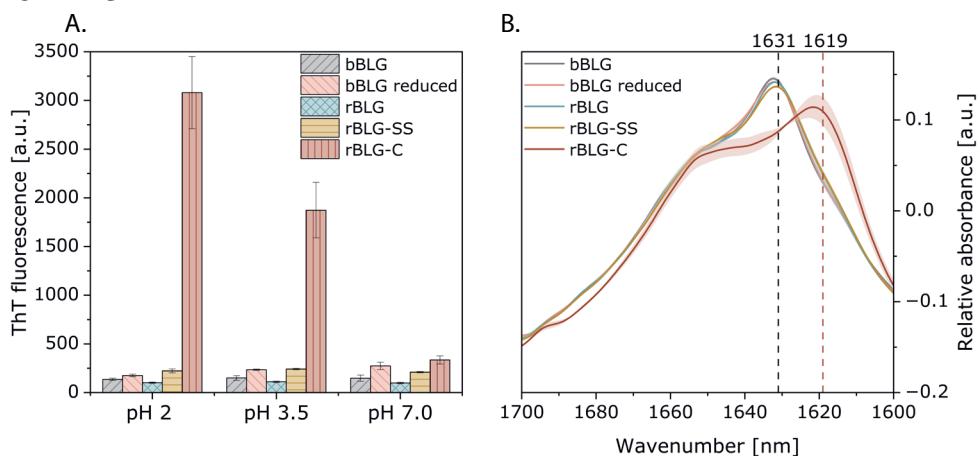

Figure 6.2. (**A**) Thioflavin T (ThT) fluorescence and (**B**) FTIR spectra of BLG variants prior to heating. The FTIR spectra were obtained at pH 2.0, highlighting the absorbance for intramolecular (1631 cm^{-1}) and intermolecular (1619 cm^{-1}) β-sheets. The peak wavenumber for these β-sheet was identified from the second derivative of the spectra.

Lastly, the removal of all cysteines led to an increased ThT fluorescence at acidic pH (i.e., almost 30 times higher than the wild-type rBLG; *Figure 6.2A*). The absorbance in the FTIR spectrum shifted from intra- to intermolecular β-sheets (i.e. from 1631 to 1619 cm^{-1}; *Figure 6.2B*). Therefore, it is concluded that rBLG-C self-assembled at acidic pH through intermolecular β-sheets. Additional analysis with dynamic light scattering (DLS) is shown in *Supporting information 6.6.2*, and showed that tiny aggregates were formed (10–50 nm) that were not visible with transmission electron microscopy (TEM; **Figure S6.2**). In contrast, rBLG-C was found to be mostly monomeric and dimeric at neutral pH (*Chapter 2*).

6.3.2. Impact of heating on aggregation mechanism

All variants were heated at a concentration of 10 mg mL^{-1} at 80 °C and pH 2. First, the breakdown of BLG will be described in terms of structure (DSC, FTIR) and acidic hydrolysis rate (decrease in intact BLG analyzed by HPSEC). These processes were expected to initiate intermolecular association through intermolecular β-sheets, which was analyzed with ThT fluorescence. Finally, the resulting morphology was visualised with TEM.

6.3.2.1. Breakdown of structure: protein denaturation

Protein denaturation is an endothermic reaction that can be quantified with differential scanning calorimetry (DSC). Thereby, DSC analysis was performed at pH 2 to observe differences in the denaturation behaviour of the variants. The analysis was performed with a higher protein concentration (25 mg mL^{-1}) due to low signal at lower concentrations, especially for destabilised variants that showed decreased enthalpies. We show the limited impact of the protein concentration (25 vs. 10 mg mL^{-1}) on the analysis in **Supporting information 6.6.3**. Early irreversible breakdown of the protein structure was also analyzed by the relative changes in the secondary structure, as detected with FTIR. FTIR analysis was only performed before and after 1 h of heating, as a mixture of peptide fractions and intact BLG exists during longer heating times due to acidic hydrolysis (**Figure 6.4A**).

The heat-induced unfolding of bBLG started at 72.9 ± 0.4 °C, with a peak temperature of 81.0 °C and a denaturation enthalpy of 182 ± 9 kJ mol^{-1}. Similarly, Heyn et al. (2020) reported an onset and peak temperature of 71.95 ± 0.1 and 84.32 ± 0.80, respectively, for 1 wt% BLG at pH 2.0. An endothermic peak was observed for both bBLG and rBLG during the subsequent second heating cycle, having an enthalpy of ~ 30 and ~ 50% as compared to the first run, respectively (**Figure S6.6**). The endothermic peak in the second heating cycle indicated that part of the unfolding was reversible and therefore the protein refolded upon cooling during the first cycle (after heating to 110 °C), or that part of the structure remained stable. Dave et al. (2013) reported a loss of secondary and tertiary structure within the first 10 min of heating at 80 °C and pH 2, while heating up to 1 h did not lead to a further disruption. Therefore, refolding of these structures upon cooling was more likely to have caused the endothermic peak around the same temperature during the second run. This was supported by the observation that heating at a slower rate did not resolve this peak (2 instead of 3.5 °C min^{-1}; **Figure S6.4**). DLS analysis of pre-heated bBLG samples (80 °C) demonstrated that this partial refolding only occurred after heating up to 3 h (**Figure S6.5**).

Chemically reducing the disulfide bonds in bBLG destabilized the structure: the onset temperature decreased to 58.1 °C. The peak temperature and enthalpy were not quantified, since the endothermic peak was not well-defined (**Figure S6.6**). Furthermore, no endothermic peak was observed during the second heating cycle. The relative change in secondary structure after 1 h of heating is shown in **Figure 6.3**. Further disruption of the intramolecular β-sheets (at ~ 1631 cm^{-1}) of the reduced BLG was observed upon heating than with native BLG (**Figure 6.3B**). Interestingly, the β-sheet structure was disrupted to a similar extent, as compared to the disordered recombinant variant without disulfide bonds (rBLG-C, pH 7.0; **Figure 6.3B**). However, the heated reduced BLG formed relatively more helical structural elements (~ 1654 cm^{-1}; Jackson & Mantsch, 1995).
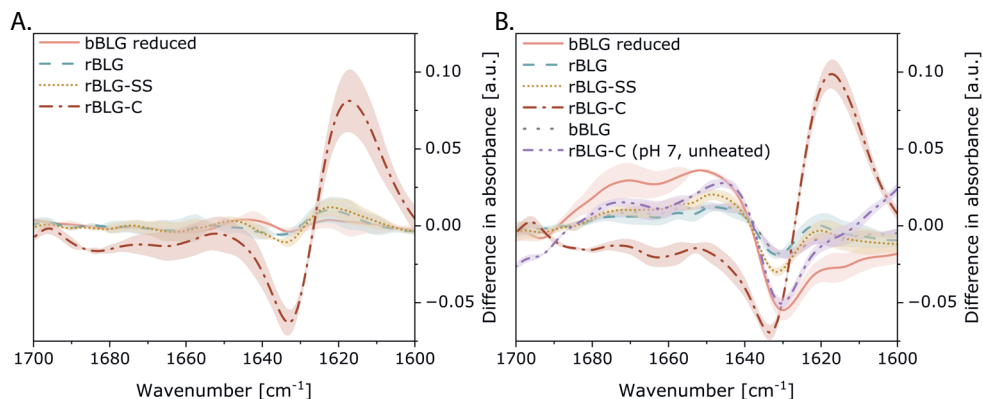
Figure 6.3. *The difference in the FTIR spectrum for different BLG variants (**A**) prior or (**B**) after 1 h of heating, as compared to bovine BLG (pH 2, unheated).*

Recombinant BLG (rBLG) showed a similar denaturation behaviour to bBLG, having an onset temperature of 73.1 ± 0.1 °C and enthalpy of 167 ± 27 kJ mol^{-1}. Recombinant removal of only the outer disulfide bond resulted in a destabilized variant (rBLG-SS); the onset temperature was 55.7 °C, with an unclear endothermic peak during the first heating cycle and no endothermic peak during the second heating cycle (**Figure S6.6**), similar to chemically reduced BLG. FTIR analysis revealed a slight decrease in intramolecular β-sheet structure, although not as much as in the variants lacking both disulfide bonds (i.e., rBLG-C and bBLG reduced; **Figure 6.3B**). As rBLG-C already had a disordered structure prior to heating (**Figure 6.3A**; **Table 6.1**), this variant showed no endothermic peak in both heating cycles (**Figure S6.6**).

6.3.2.2. Breakdown of peptide chain: acidic hydrolysis

The aggregated material was dissociated with guanidine hydrochloride and dithiothreitol to subsequently investigate the overall hydrolysis rate. Both heated and unheated samples had similar ThT fluorescence after dissociation, indicating complete dissociation (**Figure S6.1**). The dissociated aggregates and unassembled protein material was analyzed with HPSEC to determine the size distribution. bBLG was hydrolysed into fractions of peptides < 10 kDa and only these fractions are usually involved in fibrillization, irrespective of the heating time (Akkermans et al., 2008; Dave et al., 2013). Therefore, the decrease in intact BLG (18 kDa) and possibly large MW peptides (> 10 kDa) is shown in **Figure 6.4A**.
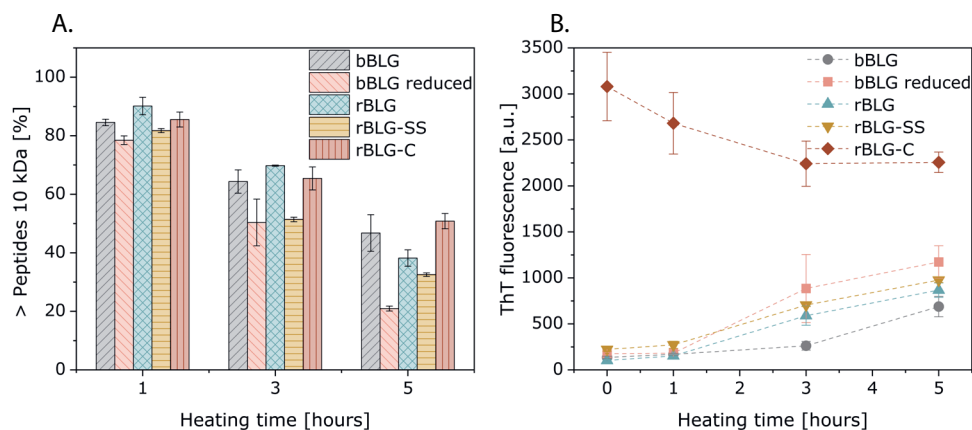
6

Figure 6.4. *The impact on heating time (80 °C, pH 2) on (**A**) protein and large peptide fraction (> 10 kDa) and (**B**) the ThT fluorescence as measure for the relative amount of intermolecular β-sheets.*

Both bBLG and rBLG are partly hydrolysed after 1 h and to a similar extent (**Figure 6.4A**). Removal of the outer disulfide bond in rBLG-SS and reduced bBLG led to an initially increased acidic hydrolysis (1–3 h; **Figure 6.4A**). However, rBLG-SS was hydrolysed to a similar extent as rBLG during extended heating times (5 h). In contrast, the reduced bBLG was further hydrolysed, as compared to both rBLG and bBLG. This indicates that additional cleavage of the outer disulfide bond accelerated acidic hydrolysis during initial heating, while the inner disulfide bond accelerated acidic hydrolysis during extended heating. rBLG-C showed a similar hydrolysis rate during early heating (1–3 h), but it was more resistant against acidic hydrolysis during extended heating (5 h).

6.3.2.3. Assembly through intermolecular β-sheets

The ThT fluorescence of the samples was utilised to observe the rate of intermolecular β-sheet formation, as shown in **Figure 6.4B**. Both rBLG and bBLG showed an increase in ThT fluorescence between 1–3 h of heating, while the increase was higher for the recombinant variant (+ 403% instead of + 93%). The ThT fluorescence was more comparable after 5 h of heating (500–1,000 a.u.). Recombinant removal of the outer disulfide bond in rBLG-SS had no major impact on the assembly rate. In contrast, chemical reduction accelerated the increase in ThT fluorescence between 1–3 h (+ 310%) and resulted in a higher ThT fluorescence after 5 h, as compared to bBLG (i.e., almost doubled).

6.3.2.4. Aggregate morphology

The morphology of the final aggregates (5 h, 80 °C, pH 2) was visualised with TEM as shown in *Figure 6.5* (*A–E*). Both bBLG and rBLG formed fibrillar aggregates, as well as the modified variants rBLG-SS and reduced bBLG. Some additional smaller spherical and worm-like aggregates were observed for rBLG-SS (*Figure 6.5D*). The recombinant substitution of all cysteine residues in rBLG-C yielded mostly worm-like aggregates, while some fibrils were observed (*Figure 6.5E*). Visualization of samples at earlier heating times revealed that worm-like aggregates already emerged after 1 h of heating, while at that time no fibrils were present yet (*Figure 6.5F*).
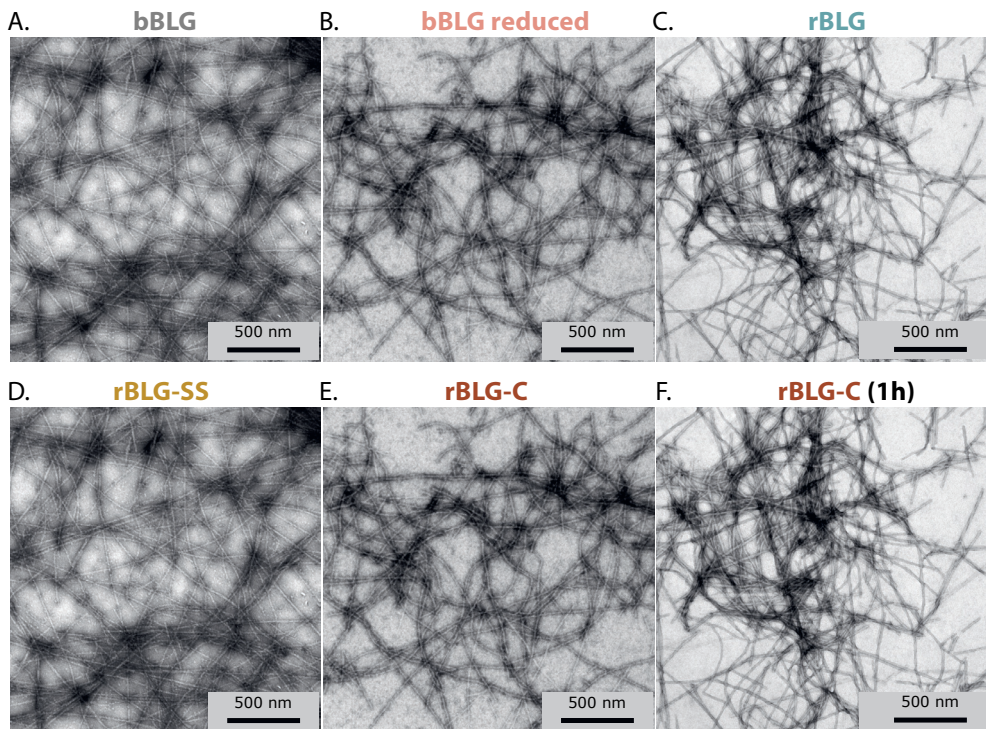
Figure 6.5. TEM picture of (*A–E*) mature fibrils from BLG variants (5 h, 80 °C, pH 2) and (E) aggregates formed after 1 h at 80 °C.

6.4. Discussion

Amyloid fibrils are built from stacked intermolecular β-sheets (Akkermans et al., 2008). Suitable building blocks need to be formed to allow subsequent assembly, which are formed by (1) structural destabilization and/or (2) acidic hydrolysis. The impact of disulfide bond removal (both chemically and recombinantly) on these two processes will be discussed further.

We will first discuss the structural changes prior and during short heating (< 1 h), after which acidic hydrolysis starts to play a role (> 1 h). Especially the impact of protein structure on the acidic hydrolysis rate is of main interest here. The time of assembly was established and compared to the extent of hydrolysis, as an indication of the type of building blocks (i.e., peptides or intact BLG). The type of aggregate building blocks was found to be crucial for the aggregate morphology, as will be finally evaluated.

6.4.1. Structural changes prior to heating

The FTIR spectra were similar for rBLG and bBLG at pH 2.0. This was expected, because their structures at pH 7.0 were already reported to be highly similar (Keppler et al., 2021). Also variants rBLG-SS and the chemically reduced bBLG showed a similar FTIR spectrum (**Figure 6.2B**), indicating an overall similar structure. Recombinant removal of the outer disulfide bond and chemical reduction of both disulfide bonds in bBLG both slightly disrupted the β-sheet structure, resulting in an opened but still conserved globular folding at pH 7.0 (**Chapter 2**). In contrast, elimination of both disulfide bonds through recombinant substitution of all cysteine residues (rBLG-C) resulted in a largely disordered secondary and tertiary structure at pH 7.0, lacking the typical β-sheet structure of BLG.

When moving to pH 2.0, the disordered structure of rBLG-C allowed the spontaneous formation of intermolecular β-sheets. This resulted in small aggregates (10–50 nm) that were not visible with TEM (**Supporting information 6.6.2**). This was not observed with the other variants, probably due to their (partial) globular fold (**Table 6.1**). Native BLG is reported to be remarkably stable at acidic pH (1.5–3.0; Kella & Kinsella, 1988), which was attributed to additional formation or rearrangements of hydrogen bonds after protonation of carboxyl groups. In addition, the loss of unfavourable electrostatic interaction might play a role. Thereby, it is hypothesized that BLG regions that are usually involved in strong intramolecular interactions at acidic pH, instead induce intermolecular interactions for the disordered variant rBLG-C.

The region 101–106 (KYLLFC) in BLG, in which Cys106 involved in the inner disulfide bond is located, is highly susceptible to β-sheet formation and might act as an initiator for fibrillization (Euston et al., 2007). This region is bound through the inner disulfide

bond (Cys106–Cys119) and lies inside the fold of native BLG, even upon heating in simulations up to 500 K (1 ns; Euston et al., 2007). Removal of the inner disulfide bond may therefore enhance aggregation in this region and possibly in other nearby regions. In combination with the disordered structure and enhanced interactions at pH 2.0, this can cause rBLG-C to form intermolecular β-sheets. The partially maintained globular fold in the chemically reduced bBLG, as well as in rBLG-SS (***Table 6.1***), avoids these proteins from forming these intermolecular associations.

6.4.2. Structural changes during short heating (< 1 h)

All BLG variants underwent structural changes within the first hour of heating at 80 °C, while the peptide backbone remained mostly intact (i.e. not hydrolysed; ***Figure 6.4A***). This was expected, as BLG has a denaturation temperature of ~ 80 °C (***Figure S6.6***). Covalent association under the applied conditions was not expected, because the number of free thiols remained constant (***Figure S6.3***). Especially covalent association is causes irreversible unfolding. Thereby, the denaturation of bBLG under the applied conditions was partially reversible up to even 3 h of heating (***Figure S6.5***). In contrast, *intra*molecular disulfide bonds can facilitate BLG folding. In ***Chapter 2*** it is shown that especially the inner disulfide bond was necessary to fold the β-barrel of BLG, while only about 70% of the β-sheet structure could form in the absence of only the outer disulfide bond (***Table 6.1***). Therefore, it is important to note that changes in the secondary structure, as will be described in the following, are the consequence of denaturation upon heating but also refolding upon cooling, prior to FTIR analysis. The latter being especially relevant in the variants that have intact disulfide bond(s) (***Chapter 2***). Besides, heat-induced denaturation of proteins in water does not lead to complete unfolding into random coil (Tanford, 1968). Instead, a minor amount of residual secondary structure remains/forms upon heating (de Wit, 2009). These residual structures are likely protected by native disulfides and possibly cause the additional endothermic peak in the thermogram of BLG at extreme temperatures (125–140 °C; De Wit, 2009).

After heating for one hour, the intramolecular β-sheet content of all BLG variants decreased, except in the already disordered rBLG-C (***Figure 6.3***). Removal of only the outer disulfide bond in rBLG-SS resulted in a further decrease in β-sheets, as compared to the wild-type, while removal of both disulfide bonds in bBLG by chemical reduction resulted in an even further decrease. This confirms that the removal of disulfide bonds caused structural destabilization and/or lowered the ability of BLG to refold. Even though the chemically reduced BLG was able to mostly maintain its secondary and tertiary structure prior to heating (***Table 6.1***), it is unlikely to refold after unfolding due to the absence of disulfide bonds (***Chapter 2***). Indeed, no endothermic peak was observed during the second heating/cooling cycle (***Figure S6.6***). Destabilization

6

resulted in a large disruption of the β-sheets, similar to the unheated and disordered rBLG-C (pH 7.0; unassembled; **Figure 6.4B**). Surprisingly, the structural disruption did not lead to intermolecular association, as was observed for rBLG-C at pH 2.0 prior to heating. The chemically reduced BLG variant formed α-helices upon disruption of the β-sheet structure, which was not the case for the already disrupted rBLG-C (**Figure 6.3B**). Hamada & Goto (1997) also demonstrated accumulation of non-native α-helical structure during unfolding of bovine BLG in guanidine hydrochloride (at pH 2.0). This increased helical structure in the chemically reduced BLG variant might have hindered the intermolecular assembly after 1 hour of heating. Similarly, Katou et al. (2002) have reported that the fibril formation of reduced β2-microglobulin was hindered due to its increased helical propensity, as compared to native β2-microglobulin.

Heating of all variants, except rBLG-C, reduced the intramolecular β-sheet structure and formed α-helical and/or disordered structural elements instead (**Figure 6.3B**). Dave et al. (2013) also reported a reduced β-sheet content and an increased α-helical content within the first hour of heating bBLG at 80 °C and pH 2.0. BLG is expected to contain mainly α-helices, according to sequence predictions especially the N-terminal half (Forge et al., 2000), but its tertiary structure stimulates β-sheet formation (Hamada et al., 1996). Thereby, breakdown of the tertiary structure upon heating can destabilize intramolecular β-sheets and transform them into disordered or helical structures. The enhanced conversion from β-sheets to α-helices in the chemically reduced variant is probably due to its lower heat stability, as it was also less evident (but to a lesser extent) for rBLG-SS. Partial folding in rBLG-SS was maintained through its remaining intramolecular disulfide bond. The cleavage of all disulfide bonds in the chemically reduced variant enhances its flexibility and opens the tertiary structure, which then allows the transformation from intramolecular β-sheets into α-helices. In contrast to other variants, rBLG-C did not show a decreased intramolecular β-sheet content upon the first hour of heating (**Figure 6.3**), as the intramolecular β-sheets were already disrupted prior to heating at pH 2.0. FTIR analysis showed a decrease in helical structure and more intermolecular β-sheets instead (**Figure 6.3**). The aggregation was confirmed with TEM, which could not detect aggregates prior to heating but demonstrated the formation of worm-like aggregates after 1 h of heating (**Figure 6.5**). Furthermore, the ThT fluorescence did not increase but instead decreased for rBLG-C, indicating that the association is different from a typical fibrillar structure (i.e., dense intermolecular β-sheet). Advanced stages of aggregation may cause declining ThT fluorescence due to local gelation and/or breakdown of the aggregates (Loveday et al., 2012).

Based on the structural changes for the different variants and their ability to aggregate prior to hydrolysis, as discussed above, we propose that two stages are necessary for the formation of intermolecular β-sheets of BLG at acidic pH: First, intramolecular

β-sheets transform into α-helical and random coil structures upon destabilization of the tertiary structure, as visible in the destabilised variant rBLG-SS. Also chemically reduced BLG demonstrated this behaviour, which was even accelerated due to its enhanced structural flexibility.

Subsequently, α-helix and random coil structures transform into intermolecular β-sheets, as observed for the mostly disordered variant rBLG-C. The other variants did not achieve this stage when heating up to 1 h, possibly due to residual structure elements. At later stages, aggregation was induced between specific peptides with enhanced aggregation propensity that were released through acidic hydrolysis.

6.4.3.   Acidic hydrolysis (> 1 h)

Intact BLG was hydrolyzed during extended heating (**Figure 6.4A**), resulting in the release of peptides. This backbone hydrolysis occurred after heating of BLG at 80 °C for 1–3 h, as also reported earlier for bBLG (Dave et al., 2013). Acidic hydrolysis almost exclusively cleaves aspartyl backbone bonds (Inglis, 1983). The carboxylic acid side chain of the aspartyl residues can attack the backbone carbonyl, leading to cyclization and subsequent backbone cleavage (Catak et al., 2008). The assembly and acidic hydrolysis occurred at the same time for both bBLG and rBLG (**Figure 6.4**). This is because acidic hydrolysis can release specific peptides over time that have enhanced aggregation propensity, mainly from the N-terminal side, which then aggregate into fibrils (Akkermans et al., 2008). rBLG assembled faster than bBLG, which might be related to the recombinant N-terminal substitution (Leu1Ala/Ile2Ser): both alanine- and serine-rich Aβ$_{(1-16)}$ peptides show enhanced fibrillization tendency (Mocanu et al., 2020).

Removal of disulfide bonds in the modified BLG variants (rBLG-SS and chemically reduced bBLG) accelerated the acidic hydrolysis rate (**Figure 6.4A**), as compared to rBLG and bBLG. This was possibly due to the more extensive unfolding of these variants, as discussed in **Section 6.4.1.2**. Residual structures might slow down acidic hydrolysis of rBLG and bBLG at 80 °C. For example, through its impact on the local molecular environment of the aspartyl residue, which will affect the pKa of the side chain and subsequently change the hydrolysis reaction rate. Intra- or intermolecular hydrophobic association may also hinder the reaction, as the cyclization is water-assisted (Catak et al., 2008). Removal of the exposed disulfide bond Cys66-Cys160 (in rBLG-SS and chemically reduced bBLG) will thereby accelerate the hydrolysis of the more exposed aspartic acid residues, observed as faster acidic hydrolysis during early stages of heating (1–3 h) in rBLG-SS and chemically reduced bBLG. The disulfide bond in the protein core of the reduced bBLG was also cleaved. This accelerates the acidic hydrolysis of the buried aspartic acid residues, which otherwise would only be cleaved when heated for 3–5 h. The variant rBLG-C already assembled prior to acidic

hydrolysis through intermolecular β-sheets. This slowed down the acidic hydrolysis of the aspartic acid residues in this hydrophobic region, which was observed as a slower hydrolysis rate during extended heating (5 h).

Whether the accelerated acidic hydrolysis of destabilised variants leads to more extensive aggregation depends on the type of peptides that are released. Only specific peptides are able to assemble through intermolecular β-sheets at pH 2.0 (Akkermans et al., 2008; Dave et al., 2013). The formation of intermolecular β-sheets will only be accelerated when these particular peptides are released more rapidly. Earlier work showed that mainly the N-terminal peptide (1–53) of bBLG forms aggregates under similar conditions (Akkermans et al., 2008; Dave et al., 2013). The aggregates included the C-terminal peptide (53–162), which is covalently linked to peptide 60–83 through Cys66–Cys160, to a lesser extent.

As the removal of Cys66-Cys160 did not accelerate the formation of intermolecular β-sheets, this bond is not expected to hinder fibrillization. In contrast, chemically reducing both disulfide bonds in bBLG increased the formation of intermolecular β-sheets. This indicates that the inner disulfide bond Cys106-Cys119 hindered fibrillization through (1) accelerating the release of the N-terminal peptide, and/or (2) enhancing the aggregation propensity of the peptide in which it is located (position 98–129; *Figure 6.1*). The latter explanation is more likely, because this disulfide bond is not located close to the N-terminus. Disulfide bonds are not expected to be directly involved in the stabilization of the intermolecular β-sheets of BLG fibrils, as cysteine residues are mainly found at the surface of BLG aggregates (VandenAkker et al., 2016). Besides, bioinformatics analysis of the primary sequence of BLG shows that the region 101–106 (KYLLFC) is highly susceptible to β-sheet formation (Euston et al., 2007). Cleaving of disulfide bonds might thus enhance the aggregation tendency of this region.

6.4.4. Aggregate building blocks and morphological consequences

The increase in intermolecular β-sheets for all variants, except rBLG-C, coincided with the moment that acidic hydrolysis became significant (i.e., after 1 h; *Figure 6.4*). Thereby, we expected that the aggregates formed from these variants mostly consisted of peptides. Even though there were differences in hydrolysis and assembly kinetics that might cause changes in the peptide building blocks, as mentioned before, no major morphological change was observed between the peptide-based fibrils (*Figure 6.5A–D*). The fibrillar shape of these variants could indicate that mostly peptides from the N-terminal region was involved in the aggregation (Akkermans et al., 2008). Earlier we discussed further incorporation of the C-terminal peptide (98-129) for the chemically reduced variant, but this then did not lead to a morphological shift (*Figure 6.5B*). In contrast, Ye et al. (2018) showed that further incorporation of

C-terminal peptide of BLG (aa 138–162) can cause worm-like morphology, as is the case when applying higher concentrations of BLG (> 40–60 mg mL[1] whey protein isolate).

Worm-like aggregates were visible in the TEM images, after heating rBLG-C for only 1 h (**Figure 6.5F**). Since the protein backbone started to hydrolyse only after 1 h (**Figure 6.3B**), the initial building blocks of the aggregates are expected to be mostly intact BLG. Likewise, tuning the aggregation conditions by addition of solvent (Gosal et al., 2002; Kayser et al., 2020) or glycine (Jaklin et al., 2022) allowed intact BLG to assemble at pH 2.0, resulting in worm-like shapes. These worm-like aggregates at pH 2.0 have a core structure that is similar to fibrils, but their surface contains mostly random/α-helical structural elements, while classical fibrils contain almost exclusively β-sheets (VandenAkker et al., 2016; Ye et al., 2018). Thereby, assembly of the hotspot regions in the core and exposure of the non-hotspot regions at the surface is thought to shape these worm-like aggregates. Aggregation of longer peptides or intact protein would involve multiple different hotspot regions and also inclusion of unassembled regions. This could avoid fibrillar and instead lead to worm-like morphology. This indicates that the formation of worm-like aggregates from intact BLG competed with fibrillization, as also shown earlier for the human disease protein β_2-microglobulin (Gosal et al., 2005). Extended heating of rBLG-C did not transform the worm-like aggregates into fibrils. However, the worm-like aggregates appeared to be stiffer after 5 h of heating, while minor fibrillar structures became visible (**Figure 6.5E**). We hypothesize that acidic hydrolysis caused these morphological changes, either transforming the morphology of existing aggregates (i.e., reduce flexibility) and/or form new ones (i.e., classical fibrillar structure). Housmans et al. (2022) also observed for ovalbumin that enzymatic hydrolysis resulted in a mixture of worm-like (also referred to as 'curly') or straight morphology. Worm-like aggregates contained undigested or partially digested protein with several hotspot regions, while further hydrolysis could separate these regions and allow for fibrillar morphology. In addition, unassembled structures at the surface of worm-like aggregates strain the intermolecular β-sheet structure and thereby can contribute to bending. Thereby, removal of the unassembled parts of worm-like rBLG-C aggregates by acidic hydrolysis also might have stimulated ordering of the β-sheets, with a stiffer morphology as a result.

6

6.5. Conclusions

We elucidated on the role of intramolecular disulfide bonds in fibrillization using cysteine-modified variants of the milk protein β-lactoglobulin. Disulfide bonds in bBLG and rBLG were removed through chemical cleavage or recombinant cysteine substitution, respectively. These variants were used to study the role of intramolecular disulfide bonds in heat-induced fibril formation at pH 2.0, in which intermolecular disulfide bonds do not form. Both approaches were compared, as it was earlier shown that they have different impact on BLG structure (**Chapter 2**).

The removal of one or both disulfide bonds reduced the stability of the β-sheet structure upon heating. The remaining secondary structures (i.e. β-sheets or α-helices) inhibited the intermolecular association up to 1 h of heating. During extended heating (1–3 h), acidic hydrolysis released peptides with enhanced aggregation tendency (Akkermans et al., 2008). The acidic hydrolysis rate depended on the protein structure. Removal of the exposed disulfide bond (Cys66-Cys160) in rBLG-SS accelerated early acidic hydrolysis (1–3 h), while additional cleaving of the inner disulfide bond (Cys106-Cys119) in the chemically reduced variant also accelerated acidic hydrolysis during extended heating (3–5 h). The additional cleavage of the inner disulfide bond accelerated intermolecular association, but still yielded fibrillar morphology. Thereby, it was shown that intramolecular disulfide bonds can hinder fibrillization, depending on their exact location. Targeting disulfide bonds can therefore be a strategy for the development of aggregated protein with enhanced functionality.

In contrast to rBLG-SS and the chemically reduced BLG, rBLG has a disordered structure that spontaneously assembled prior to heating at pH 2.0, forming tiny aggregates (10–50 nm). During heating, further aggregation of intact BLG led to aggregates with worm-like morphology. This aggregation inhibited acidic hydrolysis and partly suppressed fibrillization. Often it is reported that misfolding can induce fibrillization *in vivo*, but our results showed that misfolding induced by recombinant disulfide bond removal can actually stimulate intermolecular β-sheet formation, while at the same time hindering fibrillization.

We showed that disulfide bonds play a major role in the aggregation kinetics and morphology, through its impact on protein folding. The generated insights can potentially be used to identify conditions or modifications that stimulate fibrillization for the development of functional fibrils.

6.6. Supporting information

6.6.1. Thioflavin T fluorescence of dissociated fibrils for HPSEC analysis

HPSEC analysis was performed to analyze the size distributions of the protein and peptides in the heated samples. In order to include the building blocks of the aggregated material, dissociation of the aggregates was necessary. To achieve this, a dissociating buffer was prepared in a 0.15 Tris-HCl buffer (pH 8.0) that contained 8 M guanidine hydrochloride and 0.1 M dithiothreitol (DTT). Samples were diluted with this buffer in a ratio of 1:4 and incubated for at least one hour before analysis. The ThT fluorescence of the heated and unheated samples was determined prior to HPSEC analysis to ensure complete dissociation of the aggregates, as shown in *Figure S6.1*. As the ThT fluorescence of mature fibrils (24 h of heating) in the dissociation buffer are similar to the unheated samples, it is concluded that the dissociation buffer is suitable for complete dissociation of heated samples up to 24 h.
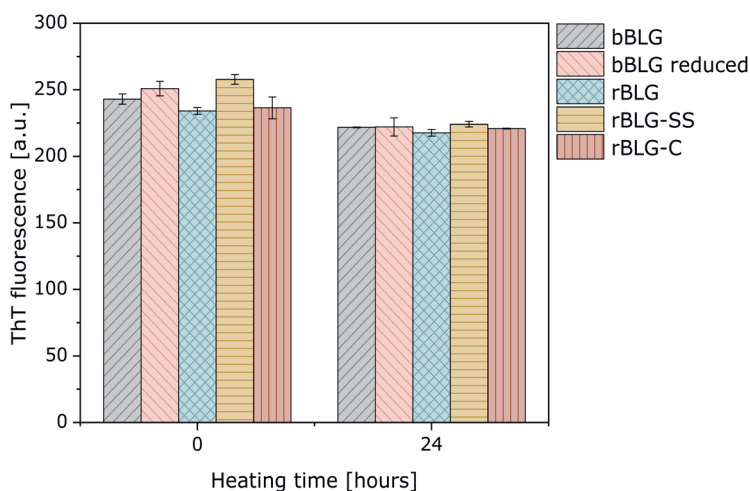

Figure S6.1. ThT fluorescence of unheated and heated BLG variants after dissociation in tris-HCl buffer (pH 8) containing 8 M guanidine hydrochloride and 0.1 M DTT.

6.6.2. Confirmation of spontaneous assembly rBLG-C

Since rBLG-C was shown to assemble prior to heating at pH 2, dynamic light scattering (DLS) was performed to check the size distribution (***Figure S6.2A***). Protein samples were diluted to 1 mg mL^{-1} for the DLS analysis and measured in a disposable folded capillary cell with the Zetasizer Nano ZS (Malvern instruments, UK). In addition, transmission electron microscopy (TEM) was performed to check the presence of visual aggregates (***Figure S6.2B***). The particle distribution with DLS shows an aggregate size between 10 – 50 nm, while no visual aggregates were seen in the TEM picture (***Figure S6.2B***).
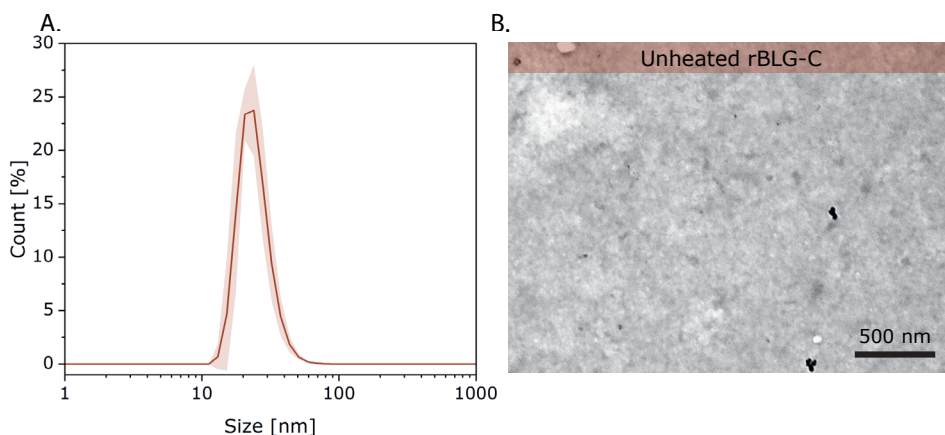
Figure S6.2. (A) *size distribution (diluted to 1 mg mL^{-1}) and* ***(B)*** *TEM image of rBLG-C after 1 day at pH 2 (10 mg mL^{-1}). The scale bar in the TEM picture represents 500 nm.*

6.6.3. Disulfide bond formation

The amount of free thiols were measured prior and after heating (1 – 5 hours), as shown in ***Figure S6.3***. If disulfide bonds are formed during heating, the amount of free thiols is expected to decrease. Since no major decrease is observed during the heat time frame analyzed, it is concluded that disulfide bond formation does not play a major role in the aggregation process under the conditions studied (pH 2 and 80 °C; 10 mg mL^{-1} BLG).
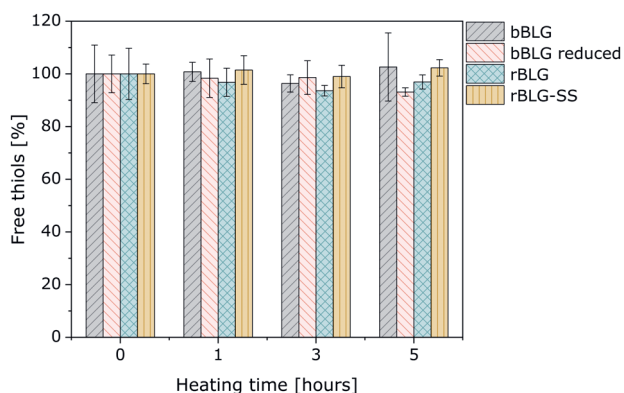
Figure S6.3. *Amount of free thiols during heating at 80 °C and pH 2, as compared to before heating.*

6.6.4. Additional DSC data

6.6.4.1. Preliminary experiments for set-up

Preliminary experiments were performed in which the ramp (2 vs 3.5 °C min⁻¹) and protein concentration (10 vs. 25 mg mL⁻¹) were varied, as shown in **Figure S6.4**. Using a ramp of 2 instead of 3.5 °C min⁻¹, it was tested whether the endothermic peak in the second run disappeared, but both showed this peak (having an enthalpy of 92 kJ mol and 73 kJ mol-1, respectively). Therefore, a ramp of 3.5 °C min⁻¹ was chosen for subsequent runs. When using a concentration of 10 mg mL⁻¹, the endothermic peak was in both the first and second run was difficult to quantify. The bovine BLG AB at a concentration of 10 had a lower enthalpy than the sample at 25 mg mL⁻¹, even though enthalpy values are in a similar range (~ 182 ± 8.6 and ~ 120 kJ mol⁻¹, respectively). Since quantification will be even less reliable for the destabilized variants, it was decided to measure the heat stability at the higher concentration.
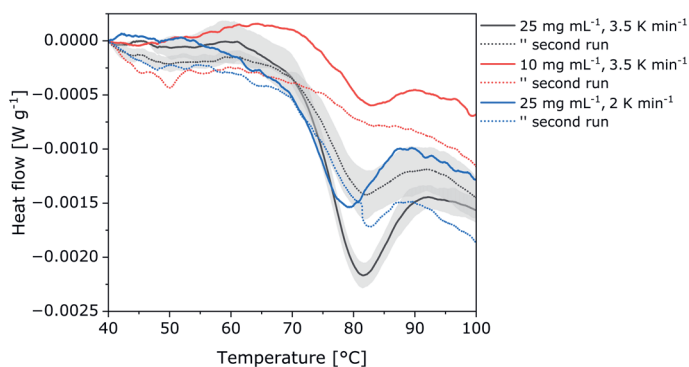

Figure S6.4. *Thermogram of bBLG AB upon first (solid line) and second (dotted line) heating/cooling cycle.*

6.6.4.2. Refolding of bBLG AB

The samples are exposed to two subsequent heating cycles during the DSC analysis, heating to 110 °C and then cooling to 20 °C. Bovine BLG AB still showed an endothermic peak during the second cycle. To observe how resistant the protein is against heating, samples (25 mg mL) were pre-heated at 80 °C and pH 2.0 and then analyzed with DSC. An endothermic peak was observed when heating up to 3 h of heating, as shown in **Figure S6.5**.
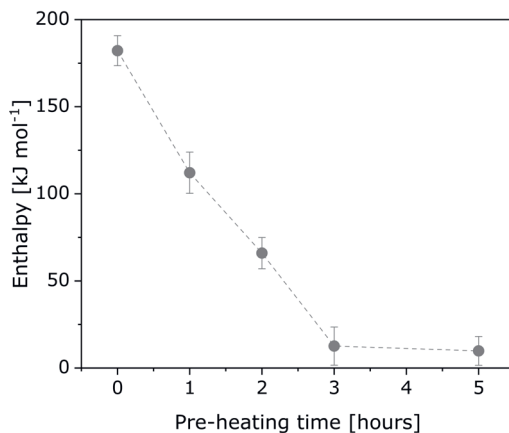

Figure S6.5. *Enthalpy of endothermic peak of bovine BLG AB in the first DSC run, either native or pre-heated (25 mg mL⁻¹; 80 °C at pH 2.0). Standard deviation is based on independent triplicates. Dotted line added to guide the eye.*
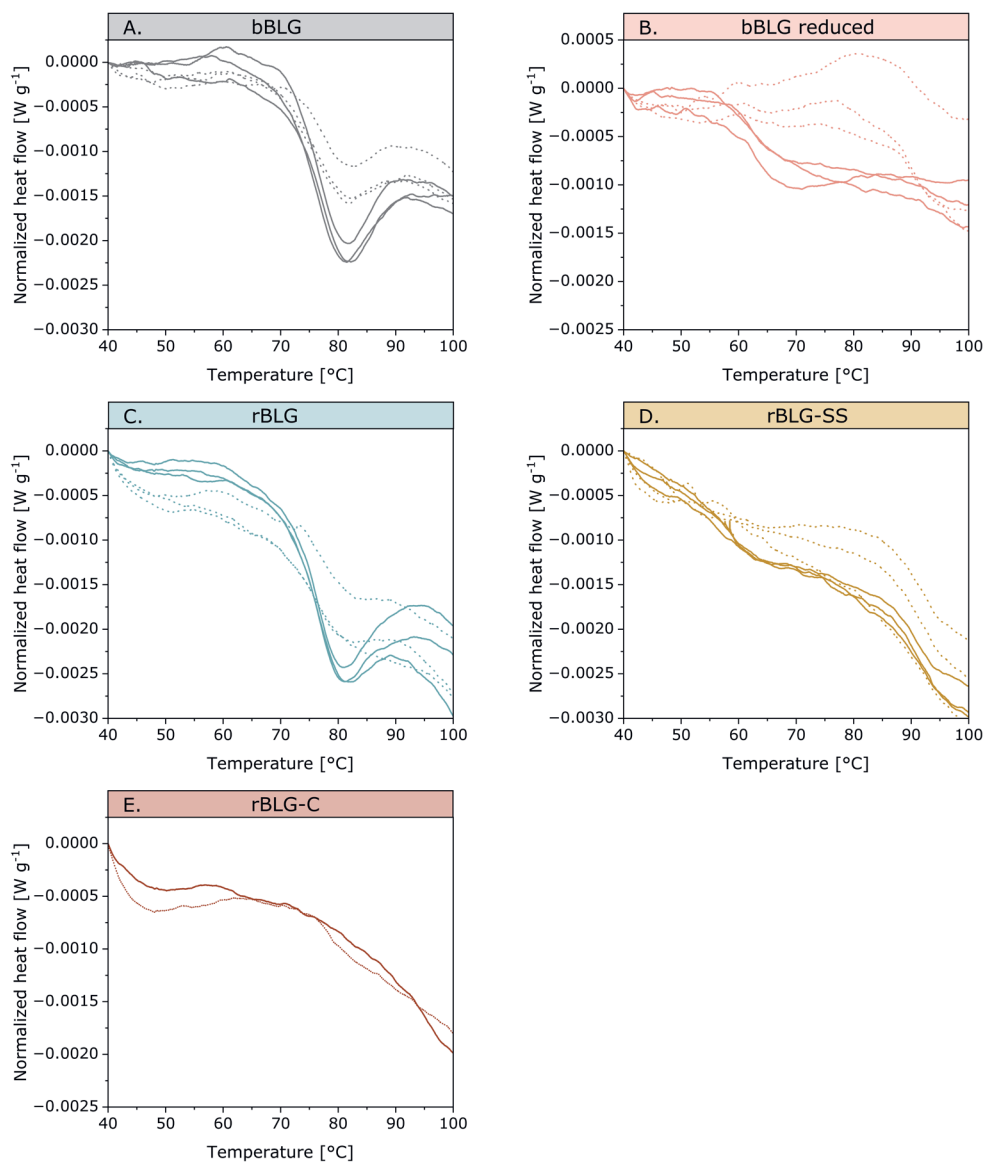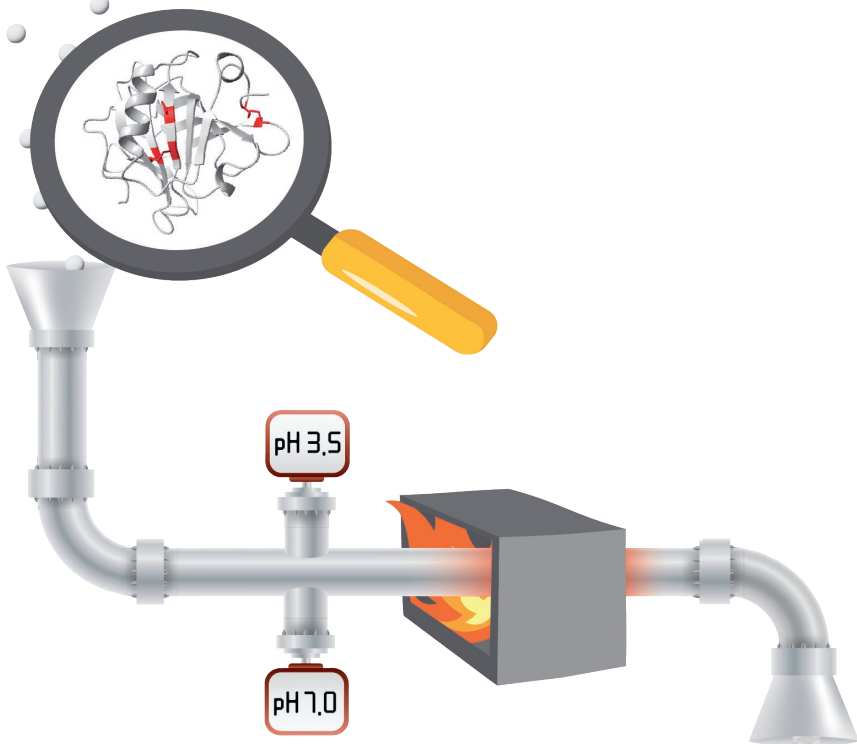
6.6.4.3. Thermograms of all BLG variants

Figure S6.6. *Thermogram upon heating of BLG variants (25 mg mL^{-1} at pH 2.0) from 20 to 110 ℃ with a rate of 3.5 ℃ min^{-1}: first (solid line) and subsequent second (dotted line) run.*

7

Amyloid-like aggregation of

β-lactoglobulin at pH 3.5 and 7.0:

is disulfide bond removal the key to fibrillization

Loes Hoppenreijs, Achim Overbeck, Sarah Brune, Rebekka Biedendieck, Arno Kwade, Rainer Krull, Remko Boom & Julia Keppler

Functional fibrils from globular proteins are usually formed by heating for several hours at pH 2.0, which induces acidic hydrolysis and consecutive self-association. The functional properties of these micro-metre-long anisotropic structures are promising for biodegradable biomaterials and food applications, but their stability at pH > 2.0 is low. The results presented here show that modified β-lactoglobulin can also form fibrils by heating at neutral pH without prior acidic hydrolysis; the key is removing covalent disulfide bonds. The aggregation behaviour of various recombinant β-lactoglobulin variants was systemically studied at pH 3.5 and 7.0. The suppression of intra- and intermolecular disulfide bonds by eliminating one to three out of the five cysteines makes the non-covalent interactions more prevalent and allows for structural rearrangement. This stimulated the linear growth of worm-like aggregates. Full elimination of all five cysteines led to the transformation of worm-like aggregates into actual fibril structures (several hundreds of nanometres long) at pH 7.0. This understanding of the role of cysteine in protein-protein interactions will help to identify proteins and protein modifications to form functional aggregates at neutral pH.

Abstract

Abbreviations: β-lactoglobulin, BLG; disulfide, SS; fourier transform infrared, FTIR; thiol, SH; recombinant β-lactoglobulin, rBLG; transmission electron microscopy, TEM.

7.1. Introduction

Many proteins are reported to form linear aggregates under specific conditions. They are either stabilized by intermolecular β-sheets that are densely (i.e. amyloid fibrils) or more loosely packed (i.e. amyloid-like aggregates; **Chapter 4**). Protein fibrils are reported to enhance the viscosity, gelling, foaming, emulsifying, antioxidant, and antimicrobial properties, and are useful for various material and food applications, such as biodegradable packaging films or techno-functional food ingredients (Adamcik & Mezzenga, 2012; Meng et al., 2022). Besides, amyloid-like aggregates are reported to entangle and thereby also show potential for specific applications, such as electrospinning towards textile fibres or edible encapsulants (**Chapter 4**).

The production of functional fibrils from globular proteins generally requires extreme incubation conditions, often heating for several hours at pH 2.0, as for example shown for β-lactoglobulin (BLG), α-lactalbumin, bovine serum albumin, lysozyme, hemoglobulin, and ferritin (Goers et al., 2002; Jayawardena et al., 2017; Jurado et al., 2019; Keppler et al., 2019; Rahimi Araghi & Dee, 2020; Usov et al., 2013). These conditions cause acidic hydrolysis and subsequent release of amyloidogenic peptide sequences. Specific peptides then assemble into protofilaments through stacking of intermolecular β-sheets. Individual protofilaments further entangle to form fibril bundles (Adamcik & Mezzenga, 2012). Amyloidogenic peptide sequences are often buried in the native protein core (Subedi et al., 2022), as they are hydrophobic and low in charge (Akkermans et al., 2008), and thus are not directly available for intermolecular interaction.

Globular proteins often form spherical aggregates instead of fibrils upon heating at neutral pH. However, previous studies have shown that fibrillar structures can be formed at neutral pH, when reducing disulfide (SS) bonds and subsequently carboxymethylating released thiol groups (SH) prior to aggregation. This was shown for BLG upon incubation with urea (Hamada et al., 2009), as well as for α-lactalbumin and ovalbumin upon heating (Goers et al., 2002; Tanaka et al., 2011). The working hypothesis is that SS bonds hinder fibril formation of globular proteins by hiding the amyloidogenic sequences within the molecular structure, and counteracting conformational changes. A systematic approach that links the location and number of SS bonds to the amyloid aggregation capacity is yet missing.

In this study, recombinant BLG expression was performed to produce different BLG variants in which specific SS bonds or SH are removed, instead of chemically modifying all cysteines. The tendency of these particular cysteine-modified variants to form fibrils is then evaluated. Different aggregation pH conditions were applied (3.5 and 7.0) to vary the contribution of covalent and non-covalent associations. These

findings will be valuable for future selection of proteins and protein modifications for the production of engineered functional protein fibrils. We investigated the globular milk protein bovine BLG, since it is the most extensively studied food protein and is widely used in the food industry. BLG contains a free SH (Cys121) and SS bond (Cys106–Cys119) that are buried in its hydrophobic core. The other SS bond (Cys66–Cys160) is located at the surface of BLG. Recombinant BLG mutants were investigated with either missing a SH (rBLG-SH), missing the outer SS (rBLG-SS) or missing all cysteine residues (rBLG-C). In these variants, corresponding cysteine residues were changed against alanine residues (**Chapter 2**).

7

7.2. Experimental section

7.2.1. Preparation of recombinant variants

During production of the recombinant BLG (natural variant B), the N-terminal was modified (Leu1Ala/Ile2Ser) in order to ensure complete cleavage of Met (Loch et al., 2016). This slight modification in the recombinant wild-type did not have major impact on the secondary and primary structure and physicochemical properties, as compared to bovine BLG (Keppler et al., 2020). Therefore, this wild-type ('rBLG') was used as a control instead of bovine BLG. Various cysteine residues were exchanged against alanine residues, according to **Chapter 2**, to eliminate either only the free thiol group (rBLG-SH), the outer disulfide bond (rBLG-SS) or all cysteine residues (rBLG-C) was achieved (**Table 7.1**).

Table 7.1. *Recombinant BLG variants produced and used in this study.*

Abbreviation	Symbol	Description	Mutation
rBLG	▲	BLG isoform B with modified N-terminal	Leu1Ala/Ile2Ser
rBLG-SH	◄	rBLG missing free thiol group	Leu1Ala/Ile2Ser + Cys121Ala
rBLG-SS	▼	rBLG missing outer disulfide bond	Leu1Ala/Ile2Ser + Cys66Ala + Cys106Ala
rBLG-C	◆	rBLG missing all cysteine residues	Leu1Ala/Ile2Ser + all Cys (66, 106, 119, 121, 160) with Ala

7.2.2. Heat stability (Differential scanning calorimetry)

The heat stability of the proteins was evaluated using differential scanning calorimetry (DSC; TA instruments, USA). About 65 mg of protein solution (50 mg mL^{-1}) was weighed in a high volume pan (TA instruments) and sealed. The temperature was increased up to 100 °C using a rate of 3.5 °C min^{-1}, after which it was cooled back to room temperature. Then a second heating/cooling cycle was performed to check whether the protein was fully denatured during the first cycle. The enthalpy and onset for unfolding were determined using the TRIOS software (TA Instruments). The enthalpy was determined based on the area under the endothermic peak, which was corrected for the protein content of the solution.

7.2.3. Aggregation

Protein solutions were prepared (10 mg mL^{-1}) in ultrapure water and the pH was adjusted to 2.0, 3.5, and 7 using 2 M NaOH or HCl, and stored overnight in the fridge. The next day, samples were aliquoted into volumes of 900 μL and incubated in an

Eppendorf shaker at 80 °C, while shaken at 350 rpm, in independent duplicates. Samples were taken after 10 min, 1 h, 3 h, 5 h, and 24 h, placed on ice, and stored in the fridge before analysis. All analyses were performed within two weeks.

7.2.4. Disulfide bond formation (Ellman's assay)

The SS bond formation was evaluated using Ellman's assay under denaturing conditions with slight modifications (Ellman, 1959). A 100 mM phosphate buffer with 6 M guanidine hydrochloride was prepared (pH 8.0) and Ellman's reagent (5,5'-Dithiobis (2-nitrobenzoic acid)) was prepared in the buffer (0.2 wt%). The protein solution (150 µL; 10 mg mL^{-1}), 1.5 mL sodium phosphate buffer and 30 µL reagent were combined and mixed with a vortex. The absorbance was measured at 412 nm after approximately 15 min, using a spectrophotometer (DR6000, Hach, Germany). *L*-cysteine in 1 mM HCl was used for calibration (70–710 µM). The free thiol group content was corrected for the amount of protein in the sample (mol/mol), which was determined based on the dry weight and purities (**Chapter 2**). Subsequently, the change in SH content was calculated relative to the amount prior heating. The time at which 50% of the thiol was consumed ($t_{1/2}$) was calculated by assuming first-order kinetics.

7.2.5. Secondary structure (Fourier Transform Infrared Spectroscopy)

The secondary structure of the BLG variants and their aggregates were determined with Fourier Infra-Red Spectroscopy (FTIR), using a Confocheck Tensor 2 system (Bruker Optics, Ettlingen, Germany) equipped with a thermally controlled BioATR 2 unit at 25 °C. The system was continuously flushed with nitrogen. The sample was left on the crystal for exactly 2 min prior to each measurement. Spectra were obtained against ultrapure water, using 64 scans and a resolution of 4 cm^{-1}.

Data analysis was performed in OPUS (Bruker Optics, Ettlingen, Germany). Spectra were vector normalized in the amide I region (1700–1600 cm^{-1}), cut (2200–1000 cm^{-1}) and baseline corrected (concave rubberband correction with 10 iterations and 64 baseline points, excluding CO_2 bands). The second derivative was then calculated using nine smoothening points. The minima in the second derivative of the FTIR spectra of unheated BLG were used to identify the wavenumber at which the absorbance for α-helix and intramolecular β-sheets was highest. It has been shown that the absorbance maxima for β-sheets are protein specific (Zandomeneghi et al., 2009). Therefore, the peak absorbances for intra- and intermolecular β-sheets were identified for each BLG variant at the corresponding pH values.

7.2.6. Aggregate morphology (Transmission Electron Microscopy)

Aggregates were visualized using transmission electron microscopy (TEM). Grids were coated with carbon using a carbon coater (K950K, EMITech inc., USA) to allow better

7

adhesion of the specimen. Five µL of sample was placed on a 400 mesh copper grid (Wageningen Electron Microscopy Center, the Netherlands) for 2 min. The fluid was then removed using a filter paper. Similarly, ultrapure water and subsequent staining solution containing 2% uranyl acetate (Wageningen Electron Microscopy Center) was added and removed after 5 and 30 s, respectively. Samples were analyzed with a JEM-1400Plus microscope (120 kV; Jeol, Japan).

7.2.7. Aggregate morphology (Atomic Force Microscopy)

The aggregate morphology was determined using atomic force microscopy (AFM) imaging, similar to Heyn et al. (2019). Imaging requires immobilization of the aggregates on a smooth substrate. The aggregate samples were diluted with milli-Q of the appropriate pH value to obtain a suitable surface coverage. The diluted sample (10 µL) was applied to freshly split mica substrate and incubated in air for 2 min. This was followed by three washes with 200 µL ultrapure water to remove unattached aggregates. The sample was dried in air for at least 15 min before transferring it to the AFM.

The surface topography was determined with a Nanowizard 3 (JPK, Bruker, Germany) in AC mode. The high resolution Probe SHR-300 supersharp (Budget Sensors, Bulgaria) with a force constant of 40 N m^{-1}, a resonance frequency of 300 kHz and a tip radius of 1 nm was used at a scanning frequency was between 0.5 and 1 Hz. Data analysis was initially performed using JPK Data Processing software (JPK, Bruker). Polynomial surface subtraction and polynomial line fit were applied to each image.

To determine the height and width of fibrils and worm-like aggregates, 10 cross-sections perpendicular to the aggregate section were exported from JPK Data Processing software for both species of 20 specimens each. A Gaussian function was then applied to each cross-section using a Python script to obtain a smooth baseline. The full width at half maximum of the function is taken as the width of the aggregate, the height of the function as the aggregate height.

The lengths of fibrils and worm-like aggregates were determined using two approaches. Firstly, both species were measured by manual tracing with ImageJ (distribution Fiji; National Institutes of Health, USA). Secondly, images were analyzed using the ImageJ plugin FibrilJ (Sokolov et al., 2017). The automatic evaluation by FibrilJ only produced appropriate results when the aggregates were separated. This was the case at a dilution of 1:24 for our samples.

7.2.8. Statistical analysis

A bivariate correlation analysis was performed to identify significant correlations between the changes in secondary structure. A two-tailed test was performed to obtain the Pearson's correlation coefficients (r). The software IBM SPSS Statistics (version 25.0.0.2) was used to perform this analysis.

7.3. Results and discussion

First, the native secondary structure and heat stability of the different recombinant variants rBLG, rBLG-SH, rBLG-SS and rBLG-C (***Table 7.1***) will be discussed. Further characterization of these variants can be found in ***Chapter 2***. The aggregation of the variants was evaluated at acidic (pH 3.5) and neutral pH conditions (pH 7.0) at 80 °C, in terms of covalent (i.e., SS bonds) and non-covalent (i.e., α-helix and β-sheet) association. The impact of these changes on the resulting morphology after 24 h of heating will be described as well. Lastly, a general mechanism is proposed for the role of the SS bonds in aggregation under these conditions.

7.3.1. Structure and heat stability

The secondary structure and the heat stability of the BLG variants were analyzed with fourier-transform infrared spectroscopy (FTIR) and differential scanning calorimetry (DSC), respectively. Relative differences in the heat stability were identified by performing DSC experiments only at neutral pH, due to limitations in the amount of recombinant protein available. Recombinant exchange of cysteine(s) by alanine residue(s) led to (slight) disruption of the intramolecular β-sheet structure and decreased the heat stability for all variants, as will be discussed in the following.

The substitution of only the free thiol group (rBLG-SH) led to a minor decrease in enthalpy (from 224 ± 34 to 228 ± 38 kJ mol^{-1}), while lowering the onset temperature for denaturation from 82.5 ± 0.7 to 77.2 ± 1.4 °C. Similarly, Yagi et al. (2003) also found a slight decrease in enthalpy for urea-induced unfolding of recombinant BLG with the Cys121Ala substitution (from 172 ± 5 to 151 ± 5 kJ mol^{-1}). Burova et al. (1998) showed that the SH group is not directly involved in stabilization of the tertiary structure, as it is too distant from neighbouring groups to form hydrogen bonds. Therefore, the introduction of an alanine residue and not necessarily the removal of cysteine residue is expected to mainly cause this destabilization. Similarly, chemical modifications of the SH are reported to destabilize BLG mainly by the introduction of bulky modifying groups rather than elimination of the SH group (Burova et al., 1998; Hoffmann & Van Mil, 1997; Sakai et al., 2000). FTIR analysis also showed a slight decrease in intramolecular β-sheet structure in rBLG-SH as compared to rBLG at both pH 3.5 and 7.0 (***Figure S7.2A*** and ***Figure S7.2B***).

Intramolecular SS bonds stabilize the tertiary structure of proteins (Mitra & Sarkar, 2022), having a bond dissociation enthalpy of 167 kJ mol^{-1} (Petsko & Ringe, 2004). Therefore, removal of the outer SS bond in rBLG-SS led to a reduction in the enthalpy from 244 ± 34 to 205 ± 32 kJ mol^{-1}, while also lowering the peak temperature by from 82.5 ± 0.7 to 64.2 ± 0.2 °C. Complete elimination of both SS bonds in rBLG-C led to disappearance of the endothermic peak (data not shown), which indicates unfolding

prior to heating. The inner SS bond facilitates the folding of the BLG core, and its absence in rBLG-C results in an unfolded structure (**Chapter 2**). This is also evident in the FTIR spectra (**Figure S7.2**) as a shift towards random coil structures (1640–1648 cm^{-1}) (Kavanagh et al., 2000).

7.3.2. Aggregation

7.3.2.1. Covalent interactions

Proteins that have an available free thiol (SH) group can undergo SH oxidation and SH/SS exchange reactions upon heating, which results in the formation of intermolecular SS bonds (Nagy, 2013). Therefore, the SH content was analyzed as an indirect indication for the relative tendency of the variants to form intermolecular SS bonds. As variants rBLG-SH and rBLG-C do not contain SH groups (**Table S7.1**), they will not be further discussed in this section.

The variants rBLG and rBLG-SS contained 0.90 ± 0.07 and 1.08 ± 0.05 SH groups (mol mol^{-1}), respectively. The SH content decreased upon heating at both pH 3.5 and 7.0 (**Figure 7.1**), confirming the formation of SS-bonds. The heating time at which 50% of SH has reacted ($t_{1/2}$) was longer at pH 3.5 than at pH 7.0 (i.e., 2.1 h compared to 0.3 h for rBLG). The enhanced reactivity of SH at higher pH is due the larger nucleophilicity upon deprotonation (0.7 and 18.2% S$^-$ at pH 3.5 and 7.0, respectively; the calculation for this is given in **Supporting information 7.5.1**).

The decrease in SH content upon heating for rBLG-SS was compared to rBLG to study the impact of the removal of the outer SS bond on the formation kinetics of intermolecular SS bonds. As expected, the SH reactivity was decreased in rBLG-SS as compared to rBLG: $t_{1/2}$ was increased from 0.3 to 1.8 h (pH 7.0), or from 2.1 to 17.8 h (pH 3.5). Removal of one of the two SS bonds approximately halved the loss in SH upon heating at pH 3.5 (**Figure S7.1**). This indicates that both SS bonds are equally reactive under the applied conditions. Earlier studies of bovine BLG showed that mainly the outer SS bond was involved in intermolecular interactions during early aggregation (< 0.5 h), as it is surface exposed (Creamer et al., 2004; Livney & Dalgleish, 2004; Surroca et al., 2002). However, during extended heating times applied here (≥ 1 h), the selectivity of the involved SS bonds towards SH/SS exchange reactions was decreased due to a better accessibility of the inner SS bond through further unfolding. In addition, the remaining SS bond in rBLG-SS was exposed at lower temperatures, due to its lowered heat stability. Thereby, the SS bond formation was not limited by the accessibility of the SH group and SS bonds anymore, but depended more on the amount of intramolecular SS bonds.
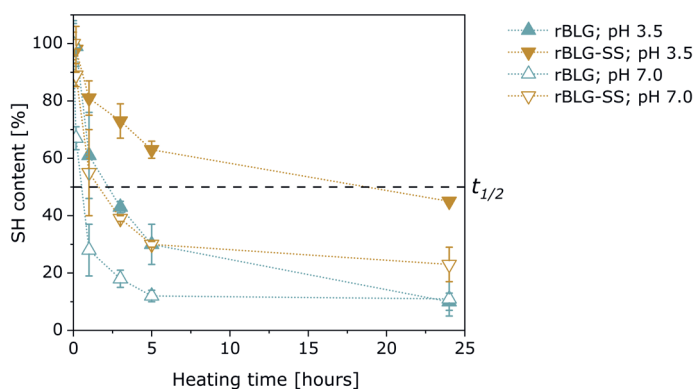
Figure 7.1. *The free thiol group (SH) content of rBLG and rBLG-SS upon heating at pH 3.5 or pH 7.0. A dashed reference line is added for value at which SH content has decreased by 50% ($t_{1/2}$). Values are relative to the sample prior to heating and measured in independent and dependent duplicates.*

The removal of the outer SS bond in rBLG-SS also decreased the SH reactivity at pH 7.0, but to a lesser extent than at pH 3.5. Almost a complete depletion of SH groups was observed after 24 h of heating of rBLG, both at pH 3.5 and pH 7.0 (9.8 ± 2.8% and 10.9 ± 6.0%, respectively). Depletion and accessibility of SH groups thus becomes the limiting factor of SS bond formation at pH 7.0, instead of the number of SS bonds available.

7.3.2.2. Non-covalent interactions

Besides the covalent interactions, the change in non-covalent interactions was also measured during 24 h of heating. Stretching vibrations of C=O and C-N groups of the peptide backbone absorb infrared light at a specific wavenumber in the amide I region of the FTIR spectrum (1600–1700 cm^{-1}). The protein conformation can shift the specific wavelength that shows maximum absorbance ('peak wavenumber'), which thus allows us to follow conformational changes. Peak wavenumbers for α-helix, intramolecular β-sheet, and intermolecular β-sheet conformations were identified for all BLG variants (***Table S7.2***). All variants showed similar peak wavenumbers for the corresponding secondary structures, confirming similar hydrogen bonding, except the peak for intramolecular β-sheets in rBLG-C. The latter was shifted to larger wavenumbers (from 1628 to 1632 cm^{-1} and 1636 cm^{-1} at pH 3.5 and 7.0, respectively), which may indicate weaker hydrogen bonding due to topological or packing constraints (Shivu et al., 2013). The peak wavenumber was used to determine the relative changes in the conformation upon heating for all variants, by plotting the difference in absorbance at this wavenumber relative to the unheated samples (***Figure 7.2***). In addition, a multivariate analysis was performed to identify correlations between changes in particular conformations. The Pearson's correlation coefficients are listed in ***Table***

7.2. Besides, the presence of intermolecular β-sheets was confirmed for all variants by showing that the Thioflavin T fluorescence increased by approximately a factor of ten after heating for five hours (***Figure S7.3***). Thioflavin T fluorescence is generally regarded as an indication for stacked β-sheet assemblies (Krebs et al., 2005).

Table 7.2. *Pearson's correlation for the changes between specific secondary structures: intra- and intermolecular β-sheet, and α-helix structures. Values are in grey if not significant.*

	Variable 1	***Intra*mol. β-sheet**	***Intra*mol. β-sheet**	***Inter*mol. β-sheet**
	Variable 2	***Inter*mol. β-sheet**	α-helix	α-helix
pH 3.5	**rBLG**	-.437	.523	-.907*
	rBLG-SS	-.188	.252	-.983**
	rBLG-SH	-.163	-.004	-.890*
	rBLG-C	.533	-.390	-.976**
pH 7.0	**rBLG**	-.650	.997**	-.684
	rBLG-SS	-.991**	.940**	-.918**
	rBLG-SH	-.375	.827*	-.477
	rBLG-C	-.964**	.964**	-.961**

* Correlation is significant at the 0.05 level (2-tailed).

* Correlation is significant at the 0.01 level (2-tailed).

The relative absorbance for intramolecular β-sheets did not decrease after heating of rBLG-C and rBLG-SH at pH 3.5 (***Figure 7.2C***). The slight increase in relative absorbance for intramolecular β-sheets could have been caused by overlap with the peak for intermolecular β-sheets in the FTIR spectra. Thus, the variants in which SS bond formation was impossible, the intramolecular β-sheet structure was found to be mostly stable. The decrease in relative absorbance for intramolecular β-sheets in rBLG and to a lesser extent in rBLG-SS can in turn be explained by the disruption through intermolecular SS bond formation. Similarly, Jayat et al. (2004) reported irreversible heat-induced aggregation of rBLG, while a variant without free thiol (Cys121Ser) remained monomeric.

Interestingly, the heat-induced formation of intermolecular β-sheets significantly correlated with a decrease in α-helix structures, and not with the decrease of intramolecular β-sheets, at pH 3.5 for all variants (***Table 7.2***). Alpha-helices are widely reported to be able to transform towards intermolecular β-sheet structures. BLG is expected to predominantly consist of α-helices, according to structure predictions, but its native structure actually consists mostly of β-sheets (Hamada et al., 1995). Forge et al. (2000) reported the core β-sheet is expanded during folding by non-native α-helices that are transformed to β-sheets, due to forces stabilizing the tertiary structure. The α-helix to β-sheet transition has been universally observed in a broad range of protein filaments rich in α-helices (Qin & Buehler, 2010).
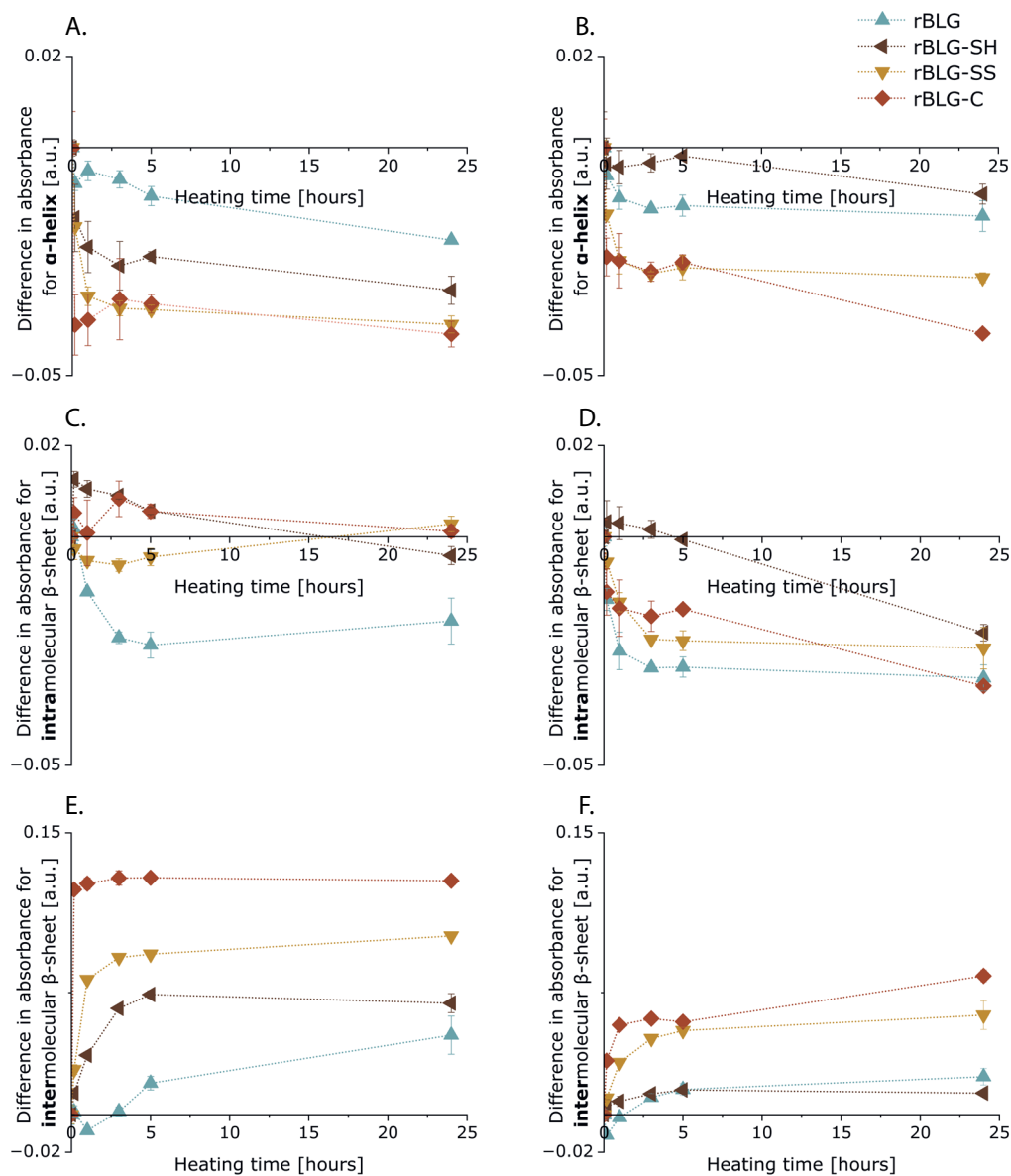
Figure 7.2. *Relative changes in (**A, B**) α-helix, (**C, D**) intramolecular β-sheet and (**E, F**) intermolecular β-sheet content of BLG variants upon heating (80°C) at pH 3.5 (left graphs) or pH 7.0 (right graphs).*

The α-helix to β-sheet transition upon heating could be enhanced when removing the outer SS bond: rBLG-SS and especially rBLG-C showed a faster and stronger increase in the relative absorbance for intermolecular β-sheets at the expense of α-helices at pH 3.5 (**Figure 7.2A** and **Figure 7.2E**, respectively). In addition, the maximum relative absorbance for the intermolecular β-sheets at pH 3.5 was higher in rBLG-C than rBLG-SS, even though the decrease in relative absorbance for α-helices was similar. The decreased heat stability of rBLG-C accelerated these conformational changes. In addition, opening of the polypeptide chain through SS removal could also expose more aggregation-prone regions. The inner SS bond connects regions that are predicted to have high aggregation propensity, while the regions connected by the outer SS bond are expected to have low aggregation propensity (**Figure 7.3**). Similarly, Euston et al. (2007) reported the high amyloidogenic potential of the sequence KYLLFC (101–106) in BLG. They discussed that Cys106 may repress the non-covalent association of this peptide region in native BLG through the formed inner SS bond. Thereby, the removal of this inner SS bond in rBLG-C may enhance its aggregation. Besides, the β-sheet content in rBLG-C already decreased prior to heating (**Figure S7.2**). Assembly of these peptide sequences will thus lead to a relative higher absorbance for intermolecular β-sheets. For the same reason, the increase in relative absorbance for intermolecular β-sheets was enhanced at pH 7.0, when removing the intramolecular SS bonds (**Figure 7.2F**).

The increase in relative absorbance for intermolecular β-sheet at pH 7.0 was lower than that at pH 3.5 for all variants (**Figure 7.2E** and **Figure 7.2F**). In addition, the intramolecular β-sheet structure was disrupted upon heating of rBLG-C and rBLG-SH at neutral pH, and not at acidic pH. Both observations can be explained by the pH dependence of the stability of β-sheet: destabilization of (intra- and intermolecular) β-sheets is induced at higher pH due to repulsing deprotonated carboxyl groups (Xing et al., 2018). As a result, the relative absorbance for intermolecular β-sheets upon heating of rBLG-SS and rBLG-C correlates with the decreased relative absorbance for both α-helices and intramolecular β-sheets at pH 7.0 (**Table 7.2**).

At neutral pH, the increase in relative absorbance for intermolecular β-sheets did not correlate with the decrease in relative absorbance for α-helix structure, for variants containing both native intramolecular SS bonds (rBLG and rBLG-SH; **Table 7.2**). The decrease in relative absorbance for α-helices in these variants in fact was limited, especially for rBLG-SH (**Figure 7.2B**). This indicates that intramolecular SS bonds preserved the α-helix structure at neutral pH. Xing et al. (2018) reported that amyloid-derived dipeptide assemblies tend to form an α-helical structure at neutral pH. Deprotonation of the carboxyl groups resulted in intramolecular hydrogen bonding, which facilitated the formation of α-helices. The α-helices are further stabilized by intramolecular SS bonds by inducing conformation strains and thereby trap the molecular conformations (Croguennec et al., 2004).
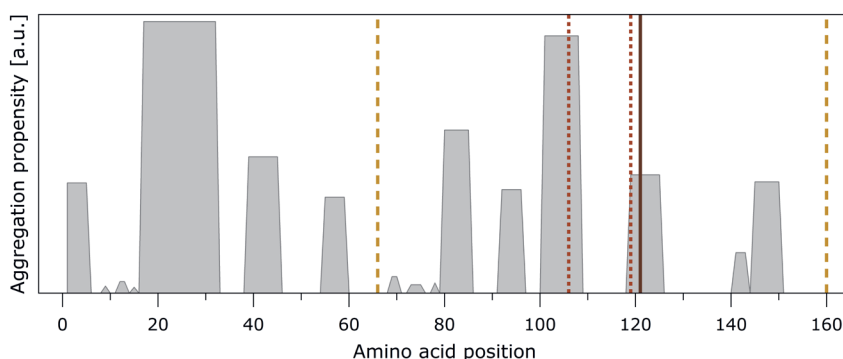
Figure 7.3. *Relative aggregation propensity of particular regions in the amino acid sequence of rBLG, predicted according to de Groot et al. (2005). Positions for the free thiol group (▬), outer SS bond (**- -**) and inner SS bond (•••) are highlighted.*

In contrast, intermolecular SS bonds can force deformations that disrupt secondary structures. Thereby, the relative absorbance for intramolecular β-sheet content in rBLG decreased faster and further than in rBLG-SH, both at pH 3.5 and pH 7.0 (***Figure 7.2B*** and ***Figure 7.2D***). This was also the case for α-helices at pH 7.0, but not at pH 3.5 (***Figure 7.2A*** and ***Figure 7.2C***). The formation of intermolecular SS bonds in rBLG was less at pH 3.5 as compared to pH 7.0, and thereby the further decrease in α-helices in rBLG-SH than in rBLG might be related to the heat stability rather than SS bond formation.

The enhanced preservation of the α-helix structure rBLG-SH at pH 7.0 limited its transformation into intermolecular β-sheets, as compared to pH 3.5 (***Figure 7.2F***). The ability of α-helices to be transformed to β-sheets depends on the stability of the helix: Dong et al. (1998) showed that incubation of BLG with trifluoroethanol destabilizes α-helices and that gradually transform into intermolecular β-sheets, while this did not occur for proteins that predominantly have α-helices in their native structure. Qin & Buehler (2010) also reported that during the initial stage of the α-helix to β-sheet transformation, structural defects in the α-helices allowed for unfolded turns. Hydrophobic interactions are then enhanced in these unfolded turns that 'squeeze' the turns into a β-sheet conformation.

7.3.3. Aggregate morphology

Transmission Electron Microscopy (TEM) was used to identify major changes in the shape of the aggregates after 24 hours of heating. All variants appeared to be worm-like at pH 3.5 (***Figure S7.4***), similar to bovine BLG at this pH (***Chapter 4***) and indicating no impact of the modification. Aggregation of rBLG at pH 7.0 resulted in relatively shorter aggregates than those obtained at pH 3.5 (***Figure 7.4***). Li et al. (2022) reported

that initially small, covalently linked aggregates are formed when heating BLG at pH 7.0. These then form the building blocks of larger aggregates, which are associated by non-covalent interactions. Almeida et al. (2012) reported that covalent SS bonds can participate in the stabilization of parallel β-sheets, but can also terminate their progressive growth through the SS bond position. Therefore, the intermolecular SS bonds in rBLG at pH 7.0 (**Figure 7.1**), as compared to the limited intermolecular bond formation at pH 3.5, may hinder the formation of longer aggregates. This is also in line with the longer aggregates that were observed at pH 7.0, when the formation of SS bonds was limited through the removal of the outer SS bond or the SH group. To our knowledge, this has not been reported yet.

Additional removal of inner SS bond in rBLG-C led to the heat-induced formation of fibrils (several hundred nanometres long), besides the long worm-like aggregates (**Figure 7.4D** and **Figure 4E**). The formation of these fibrils occurred between 5 and 24 h of heating, while they were not yet evident after 5 h of heating (**Supporting information 7.7.4**). rBLG-C after 24 hours of heating was also analyzed with atomic force microscopy to obtain more details about these mixed morphologies (**Figure 4F**; **Supporting information 7.7.5**). The worm-like aggregates in this sample had a height of 2.02 ± 1.53 nm, which is similar to native monomeric BLG (~ 2 nm; Daniela et al., 2010) and is thinner than solvent-induced worm-like aggregates (2.7 ± 0.5 nm). The fibrils were found to be thicker (2.64 ± 1.73 nm). Similarly, BLG fibrils formed at pH 2 are shown to be approximately 3 nm and consist of linear protofilaments twisted in a periodic structure (Daniela et al., 2010; Gosal et al., 2004).

The aggregate length was challenging to quantify. On the one hand, low magnifications resulted in low resolution, especially of thin worm-like aggregates. On the other hand, higher magnifications led to incomplete visualization of aggregates at the edge of the image. Only considering the aggregates that are completely visualized within the images (**Figure S7.6**), analysis of the aggregates at a dilution of 1:7.5 indicate that worm-like aggregates were longer than the fibrils (643 ± 385 nm compared to 235 ± 87 nm), as well as more abundant (1:2). Classical fibrils formed at pH 2.0 are generally longer, ranging in length from several hundreds of nm to μm (Daniela et al., 2010; Gosal et al., 2004).

Further dilutions were analyzed to check whether overlap of aggregates at low dilutions (1:7.5) were problematic for length quantification. Surprisingly, worm-like aggregates were disappearing at higher dilutions (1:24; **Figure S7.5**), while fibrils remained. Manual annotation and analysis by FibrilJ of aggregates at this dilution (**Figure S7.7**) showed a fibril length of 244 ± 103 nm and 229 ± 108 nm, respectively. This is in a similar range as compared to the lower dilution (1:7.5; ~ 250 nm), indicating that the analysis of these fibrillar structures is not dilution dependent, in contrast to the fraction of worm-like aggregates.
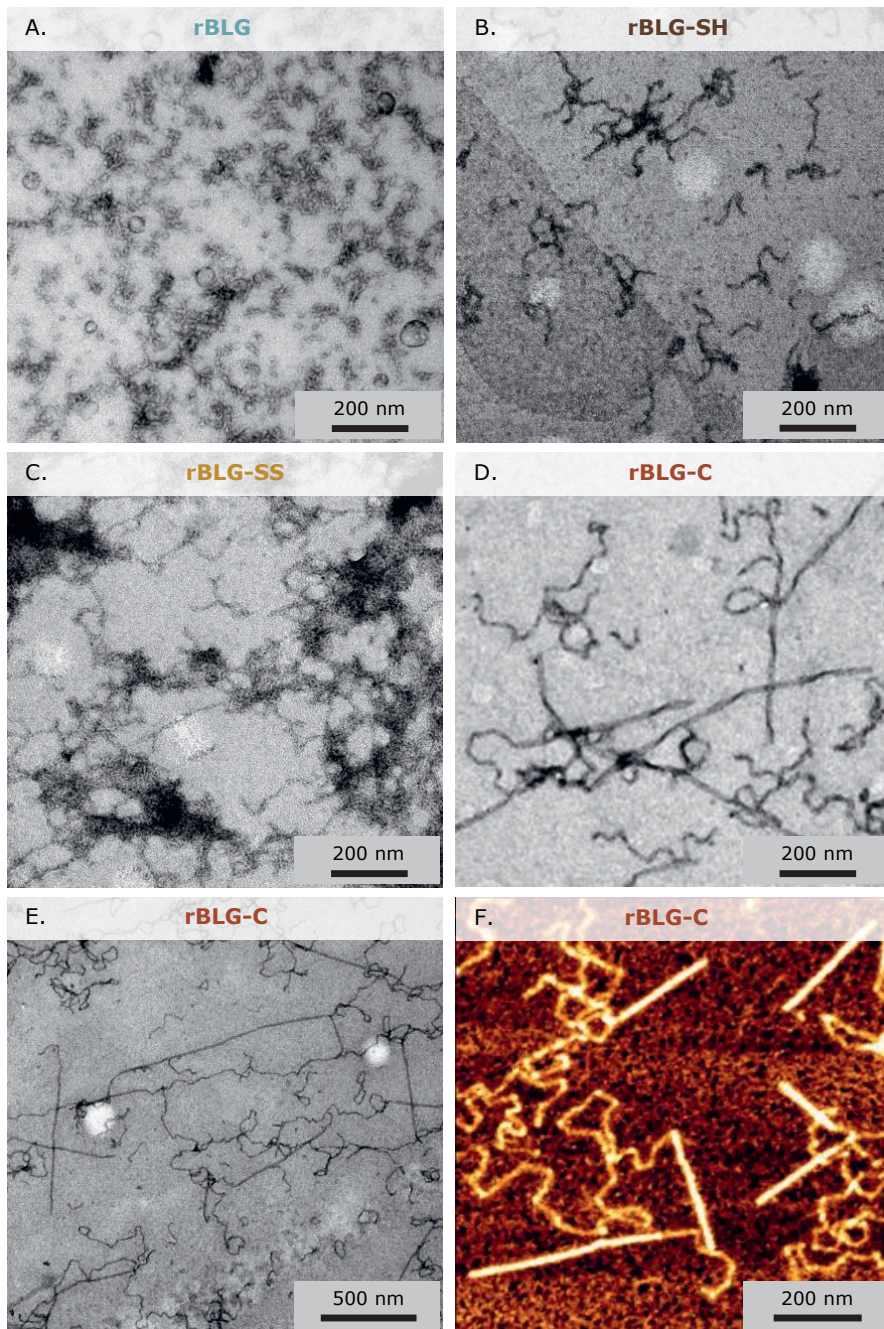
Figure 7.4. *TEM images of aggregates after heating of corresponding BLG variants at 80 °C for 24 hours at pH 7.0: (**A**) rBLG, (**B**) rBLG-SH, (**C**) rBLG-SS, (**D** and **E**) rBLG-C. The latter sample was also analyzed with (**F**) AFM.*

The dissociation of worm-like aggregates upon dilution is not probable, as both aggregates are expected to be stable in water. Instead, worm-like aggregates might attach poorly to the mica substrate and thereby are possibly washed away during sample preparation, or swept away by the cantilever tip during the analysis (Lea et al., 1992). This is not the case for fibrils, as they attach better to mica than oligomers (Green et al., 2004; VandenAkker et al., 2016). Multiple entanglement points of worm-like aggregates might avoid their removal at higher protein concentrations.

The morphological shift from worm-like to fibrillar is also reported before under different conditions. Van den Akker et al. (2011) showed that structural differences could explain these morphological differences between aggregates: They prepared worm-like aggregates (7.0 wt% BLG) and fibrils (3.0 wt% BLG), both at pH 2.0, and found that α-helices were more evident in worm-like aggregates and β-sheets in the fibrils. In our study, the relative amount of intermolecular β-sheets increased between 5 and 24 hours of heating of rBLG-C at pH 7.0 (*Figure 7.2F*), so structural differences could explain the shift in morphology. However, aggregates formed at pH 3.5 seem to contain relatively even more intermolecular β-sheets, while having a worm-like morphology (*Figure 7.2E*). Therefore, it is more likely that the morphological shift from worm-like to straight aggregates observed at pH 7.0 was related to the formation of higher-order assemblies, as will be discussed next.

Straight fibrils consist of twisted protofilaments with a pitch of about 200 nm, as can be observed in *Figure 7.4D* as dark shades within in the aggregate. Adamcik and Mezzenga (Adamcik & Mezzenga, 2012) showed that BLG fibrils produced at pH 2.0 also compose of twisted protofilaments during prolonged heating, and the length of the pitch reveals the amount of protofilaments in the nanofibril. Thereby it is likely that for rBLG-C, the morphological shift occurred due to assembling of protofilaments. It has been reported earlier that an increase in the contour length of protofilaments enhances their alignment, which allows for attraction and cross-over upon very short-range length scales. The driving force of this association could be of the Lennard-Jones type, or through hydrophobic interactions along the protofilaments (Bolisetty et al., 2011). As mentioned earlier, the linear growth of the individual aggregates (i.e., protofilaments) was enhanced upon elimination of cysteine residues. Thereby, the enhanced non-covalent interactions and subsequently longer aggregates from rBLG-C might allow for alignment and assembly of (initially worm-shaped) protofilaments. Further assembly of protofilaments will reduce their flexibility and could induce a morphological shift from individual worm-like aggregates into straight nanofibril bundles, which would also explain the increased thickness of fibrils as compared to worm-like aggregates observed earlier. The pH conditions have an impact on the assembly of protofilaments, only stimulating bundling of protofilaments at pH 7.0 and not pH 3.5. The pH-dependence of supramolecular assembly has also been

reported for β-amyloid peptide (10–35), which forms individual protofilaments at pH 3.7 and pairs of protofilaments or higher order bundles at pH 7.4 (Antzutkin et al., 2002). This was attributed to pH-dependent side chain charges at the interface of the protofilaments. Lastly, the enhanced inter-protofilament association at pH 7.0 could also be due to different structural properties of the protofilaments (i.e., less intra- and intermolecular β-sheets, more α-helical structure; ***Figure 7.2***).

7.3.4. General mechanisms

In the following, the proposed mechanism for the heat-induced formation of engineered functional BLG fibrils upon elimination of covalent bonds at neutral pH will be summarized. In addition, it will be discussed whether the role of cysteine residues in BLG assembly could be extrapolated to other proteins as well, for example, those forming pathogenic fibrils (e.g., related to Alzheimer disease or Parkinson) or natural functional fibrils (e.g., biofilms of bacteria).

Worm-like aggregates were formed from intact BLG during initial stages of heating (< 5 h of heating at 80 °C). Elimination of the intramolecular SS bonds destabilized the secondary structures of BLG. In turn, this enhanced flexibility accelerated the α-helix to β-sheet transition. Removal of the additional inner SS bond also exposed amyloidogenic regions. Recently, Mitra & Sarkar (2022) concluded in their review that removal of intramolecular SS bonds induces disordering of the structure and thereby stimulates pathogenic fibrillization of several proteins, including insulin, superoxide dismutase, amyloid β, and α-synuclein. The same principle was also shown for natural functional bacterial fibrils formed by CsgA (Balistreri et al., 2020): the introduction of an engineered intramolecular SS bond 'locked' the structure and thereby hindered β-sheet formation, while its reduction resulted in amyloid formation similar to the wild-type within hours. While there seems to be a common hindering effect of intramolecular SS bonds on fibril formation, there are no clear indications in literature whether proteins with a low amount of intramolecular SS bonds would be a favoured choice for engineering fibrils. Therefore, this needs further investigation.

Intermolecular SS bonds were found to enhance or suppress β-sheet formation, depending on the aggregation conditions. Either way, supressing SS bond formation in the cysteine-modified BLG resulted in longer aggregates. The impact of intermolecular SS bonds on fibrillization in general is more debatable than for intramolecular SS bonds. Intermolecular SS bonds allow for close proximity of peptide chains and thereby can stimulate oligomerization, as reported for proteins associated with amyloid disorders, like prion proteins and transthyretin, although the impact on the aggregate shape (i.e., worm-like aggregates or straight fibrils) was not considered (Mitra & Sarkar, 2022). It should be noted that the β-sheet intensity or concentration is often taken as a measure of fibrillization, but this does not necessarily coincide with

7

fibrillar aggregate shape. For example, covalent dimerization of pathogenic amyloid β also resulted in accelerated formation of β-sheet structure and Thioflavin T reactivity upon further aggregation, even though the morphology of the formed aggregates were in fact much shorter and worm-like as compared to the wild-type (Yamaguchi et al., 2010). Authors emphasize that intermolecular SS bonds can accelerate kinetics, but thereby might also activate different aggregation pathways. It is probable that the impact of intermolecular SS bonds on the aggregation pathways is highly dependent on the protein sequence and the location of the introduced intermolecular SS bond. It could enhance association of amyloidogenic peptide sequences when inducing close proximity of these regions. In contrast, it could also trap oligomers in a conformation that is not favourable for fibril formation, when non-amyloidogenic sequences are involved. Suk et al. (2010) produced α-synuclein variants in which intermolecular SS bonds were recombinantly introduced. Depending on the location of the SS bonds, fibril formation was enhanced or an amorphous aggregation pathway was followed instead. Besides, intermolecular SS bonds can stabilize small pre-amyloid oligomers, as shown for FapC in bacterial biofilm (Bleem et al., 2018). The cysteine residues were located in non-amyloidogenic regions of the protein, and their removal did not affect the fibril formation. Both cysteine residues in FapC are located close to the C-terminus (304 and 307; total of 316 amino acids) and thereby the conformational restraint is expected to be limited. Thus, it is recommended to screen not only for amyloid sequences, but also for the location of cysteine residues, in order to select functional proteins for the artificial formation of fibrils. Although this would need to be substantiated by further studies.

Lastly, it is proposed that (functional) fibrils could be engineered from individual worm-like aggregates at neutral pH. Even though alignment and assembly of worm-like aggregates has not been reported yet, this behaviour is very common for BLG fibrils at pH 2.0: individual strands tend to align and assemble, depending on their contour length and flexibility (i.e., stimulated when longer and more rigid) and on the interactions between the strands (Bolisetty et al., 2011). Thereby, short and flexible worm-like aggregates usually do not align (**Chapter 4**). Enhancing the aggregate length (e.g., through protein selection or modification to eliminate cysteines) and tuning the aggregation conditions (to stimulate association of strands) could thereby be a promising strategy for the production of engineered functional fibrils at neutral pH.

7.4. Conclusions

Recombinant variants of a protein can be used to understand the contribution of covalent and non-covalent interactions during aggregation, and the impact on aggregation kinetics and resulting morphology, as we showed for BLG. Intermolecular disulfide bonds (SS) disrupt the secondary structure, while intramolecular SS stabilize it. Beta-sheets are more stable at acidic pH, due to protonation of carboxyl groups, and are partially preserved upon heating. However, intermolecular SS destabilize β-sheets at both acidic and neutral pH, as well as α-helices. Unstable α-helices transform into intermolecular β-sheets. As α-helices are less stable and β-sheets more stable at pH 3.5 as compared to pH 7.0, this conversion was enhanced. Removal of intramolecular SS accelerated and enhanced conformation changes. Increasing the relative contribution of non-covalent interactions (either by cysteine removal or by pH) enhanced linear growth of aggregates. Full elimination of covalent association even allowed for the transformation of worm-like aggregates into fibril structures at pH 7.0, possibly by alignment and entanglement. For future production of engineered fibrils, one should therefore consider proteins that contain amyloidogenic protein sequences that are not constrained by SS bonds, while at the same time, the aggregation conditions should stimulate rearrangements.

7

7.5. Supporting information

7.5.1. Free thiol groups

The thiol content (SH) prior and after heating of rBLG-SH and rBLG-C are listed in **Table S7.1**. These variants were not expected to contain thiols, which was confirmed by the initial low values (< 0.1) that did not decrease upon heating.

Table S7.1. *Thiol content of BLG variants prior and after heating for 24 hours at 80 °C, at pH 3.5 and 7.0.*

	pH 3.5		pH 7.0	
Variant	Native	Heated	Native	Heated
rBLG	0.83 ± 0.06	0.08 ± 0.02	0.90 ± 0.07	0.10 ± 0.05
rBLG-SH	0.06 ± 0.03	0.07 ± 0.01	0.10 ± 0.06	0.09 ± 0.05
rBLG-SS	1.03 ± 0.04	0.47 ± 0.01	1.08 ± 0.05	0.24 ± 0.06
rBLG-C	0.02 ± 0.01	0.14 ± 0.07	0.02 ± 0.01	0.06 ± 0.04

The other variants, rBLG-SS and rBLG contained about one free thiol group, which decreased upon heating (**Table S7.1**). The decrease in SH content of rBLG-SS was calculated relative to the decreased SH content in rBLG, as shown in **Figure S7.1**.
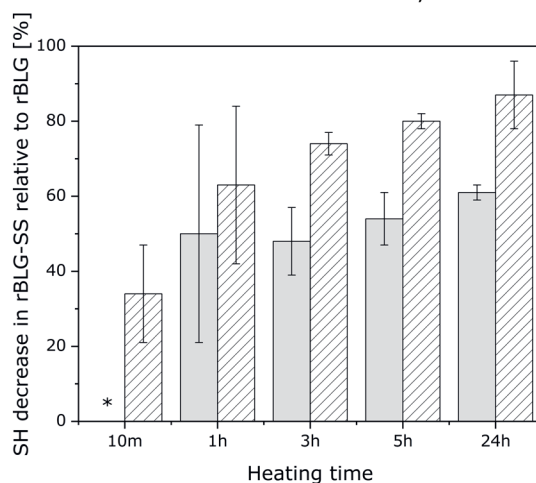

Figure S7.1. *Decrease in SH content of rBLG-SS relative to the decrease in rBLG at pH 3.5 (solid grey) and pH 7.0 (white with stripes). Values were not depicted when the decrease in SH was lower than 2% (*).*

The enhanced reactivity of the free thiol group upon an increase in pH was due to deprotonation. Thiols are deprotonated depending on the pH, according to the Henderson-Hasselbalch equation (Poole, 2015):

$$pH = pK_a + log_{10}\left(\frac{[S^-]}{[SH]}\right)$$ **[Eq. S7.1]**

A pKa of an 'unperturbed' cysteine residue was assumed, which is ~ 8.5, although it can be lowered due to the protein environment. The amount of deprotonated SH (S⁻) was calculated to be 0.7 and 18.2% for pH 3.5 and pH 7.0, respectively, using this equation and pKa.

7.5.2. FTIR peak wavenumbers and second derivatives

Changes in the secondary structures were identified from the FTIR spectra. Peak wavenumbers were identified as minima in the second derivative (**Figure S7.2**) and are listed in **Table S7.2**. Native structures (α-helices and intramolecular β-sheets) were identified from unheated samples, while the peak wavenumber for intermolecular β-sheets was identified from heated samples (24 hours, 80 °C). Peaks were annotated according to Kavanagh, Clark & Ross-Murphy (2000): α-helices (1648–1658 cm⁻¹), intramolecular β-sheets (1620–1640 cm⁻¹) and intermolecular β-sheets (1610–1620 cm⁻¹).
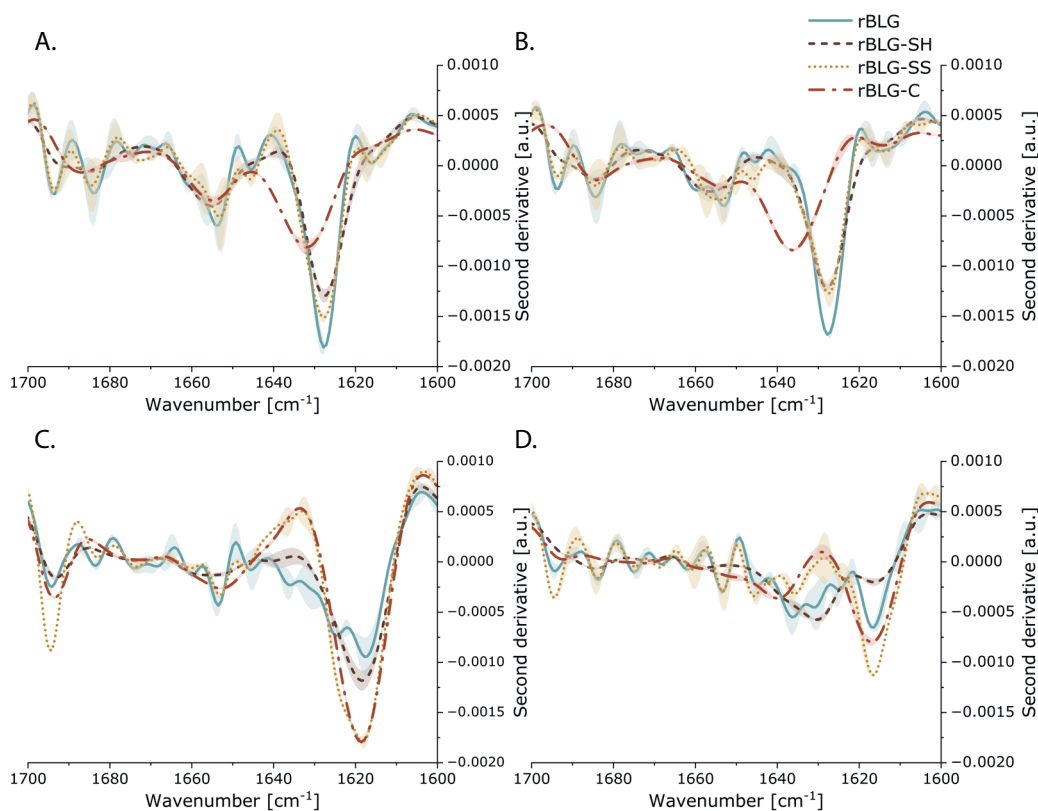

Figure S7.2. *Second derivative of FTIR spectra of BLG variants at pH 3.5 (left; **A** and **C**) and pH 7.0 (right; **B** and **D**) prior (upper; **A** and **B**) or after (lower; **C** and **D**) heating for 24 h at 80 °C.*

Table S7.2. *Peak wavenumbers (cm^{-1}) identified for intramolecular β-sheets ('intra'), intermolecular β-sheets ('inter') and α-helices ('helix').*

Variant	pH 3.5			pH 7.0		
	intra	inter	helix	intra	inter	helix
rBLG	1628	1617	1654	1628	1616	1653
rBLG-SH	1628	1618	1654	1628	1616	1656
rBLG-SS	1628	1619	1654	1628	1616	1653
rBLG-C	1632	1619	1655	1636	1617	1653

7.5.3. ThT fluorescence

Thioflavin T (ThT) is a substance that binds to specific β-sheet structures and fluoresces after doing so. Its mode of action was well described in Krebs, Bromley & Donald (2005). Side chains on the side of the β-sheets form neat rows, and thereby between every row of side chains so-called 'channels' are formed. These channels thereby run perpendicular to the strands. ThT binds within these channels (of at least five assembling strands) and is thereby closely surrounded by the side chains. This physical confinement of the side chains causes the ThT to assume a flat conformation, which greatly enhances it fluorescence. Thereby, the ThT fluorescence is not only depending on the size, but also the structure of the β-sheet. Besides FTIR analysis, we have also tested the ThT fluorescence of native and heated protein variants (5 h, 80 °C) to confirm the presence of β-sheets.

All variants showed enhanced ThT fluorescence after 5 hours of heating (**Figure S7.3**). All samples have higher fluorescence when they contain more β-sheet structures according to FTIR, except for rBLG-C (**Figure 7.2E** and **Figure 7.2F**). The aggregated structure of rBLG-C seemed to be less reactive towards ThT as compared to rBLG-SS, even though it contains more β-sheets according to FTIR analysis.
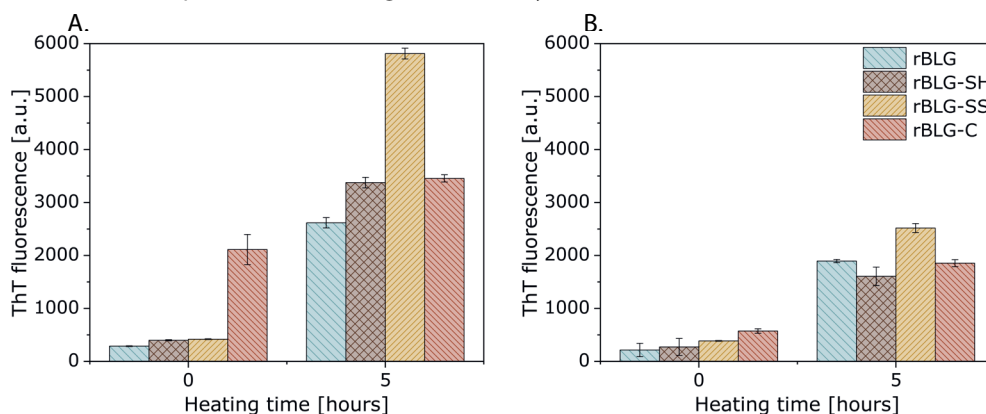
Figure S7.3. *ThT fluorescence of recombinant BLG variants at (A) pH 3.5 or (B) pH 7.0.*

Method: The ThT fluorescence was measured based on a method of Loveday et al. (2012). A 10 mM phosphate buffer containing 150 mM NaCl was prepared (pH 7.0). ThT was added (56 µM) and after stirring for about one hour the solution was filtered (Whatman 54, Sigma Aldrich). Fifty µL of protein solution (1 wt% BLG) transferred to a reaction tube and 4 mL ThT solution was added. The solution was vortexed and the fluorescence was measured exactly after 1 min, using a fluorophotometer (RF6000, Shimadzu, Japan) with an excitation and emission wavelength of 440 and 482 nm, respectively. Water was used as a blank and samples were measured in independent and dependent duplicates.

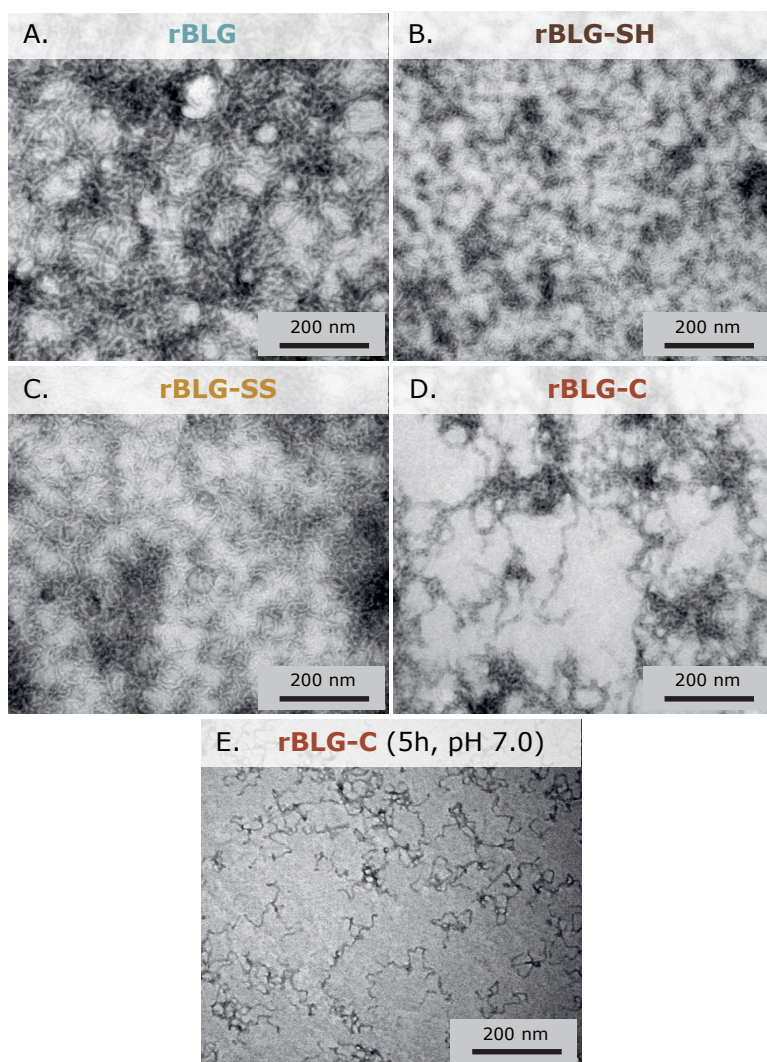### 7.5.4. TEM images for heated samples at pH 3.5

Figure S7.4. *TEM images of aggregates after heating of (**A**) rBLG, (**B**) rBLG-SH and (**C**) rBLG-SS at 80 °C for 24 h at pH 3.5. Variant rBLG-C was also heated (**D**) under these conditions and (**E**) at 80 °C for 5 h at pH 7.0.*

7.5.5. Additional analysis of mixed morphology by Atomic Force Microscopy

Two types of aggregates were observed with the TEM analysis of rBLG-C after 24 hours of heating at 80 °C and pH 7.0: (1) worm-like aggregates and (2) fibrillar aggregates. This samples was further characterized with atomic force microscopy. It became clear that further diluting the sample resulted in disappearance of the worm-like fraction, as shown in *Figure S7.5*. Ten cross-sections were made for 20 aggregates for both morphologies. The aggregate thickness was derived from the mathematical description after applying a gaussian-fit. The results are listed in *Table S7.3*.
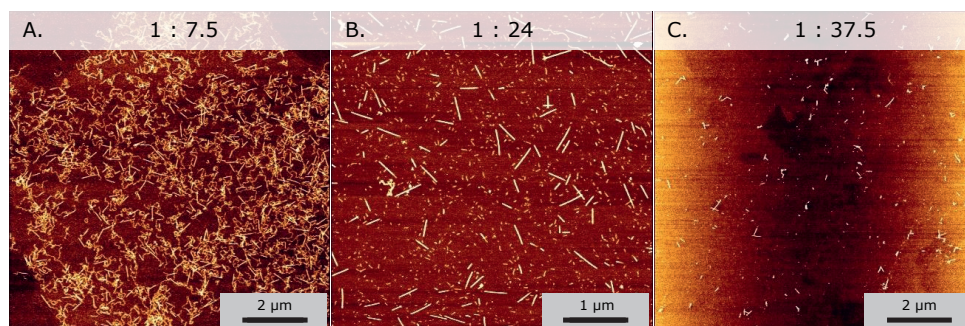

Figure S7.5. *AFM analysis of diluted samples of rBLG-C after heating at 80 °C and pH 7.0 for 24 hours: (**A**) 1:7.5, (**B**) 1:24, and (**C**) 1:37.5.*

Table S7.3. *Thickness (nm) of different type of aggregates found in rBLG-C when heated at 80 °C and pH 7.0. Analysis is based on 20 aggregates with 10 cross-sections.*

Type	Mean	Median	Minimum	Maximum
Worm-like aggregates	2.02 ± 1.53	1.53	0.55	5.54
Fibrils	2.64 ± 1.73	1.51	1.18	6.1

Analysis of the aggregate length was challenging due to low resolution (at low magnification) or incomplete visualization (at high magnification). An estimation of the aggregate length could be based on images with high magnification and only aggregates that were completely visualized (*Figure S7.6*). Based on these images, a manual estimation of the aggregate length was determined to be 250 and 620 nm for fibrils and worm-like aggregates, respectively. Aggregates were found to be more worm-like than fibrillar at this dilution (1:2), even though it should be considered that the fraction of visualized worm-like aggregates is dilution-dependent (*Figure S7.5*). Since overlap of aggregates could have an impact on the analysis, as annotation of individual aggregates is difficult, higher dilutions were tested (1:24). Even though the worm-like fraction was removed at this condition, the fibrils did not and thereby their length was determined (based on images *Figure S7.7*). This was performed both manually and

computationally (by FibrilJ), as listed in **Table S7.4**. Inly aggregates were considered that were fully depicted for manual analysis (i.e., not cut-off at the edge of the image), as well as analysis with FibrilJ (described as 'corrected' in **Table S7.4**). In addition, the analysis with FibrilJ was done for all aggregates. The corrected length with FibrilJ gave a similar value as the manually determined length, while the aggregate length is shorter when considering the aggregates that are cut-off at the edge (**Table S7.4**).
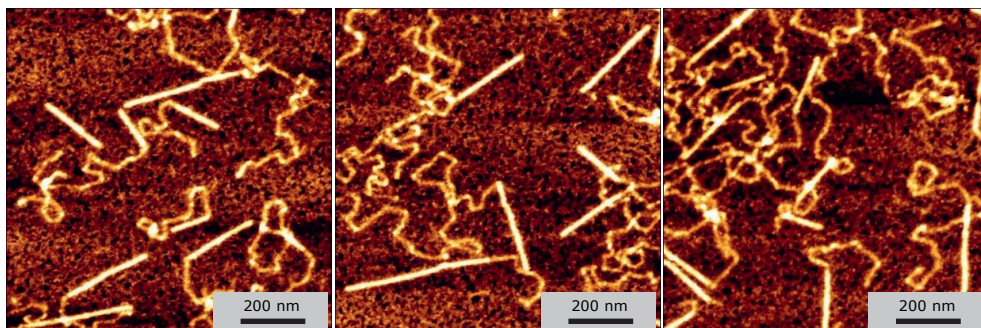

Figure S7.6. *Images that were used to quantify the aggregate length of both worm-like aggregates and fibrils (dilution 1:7.5).*
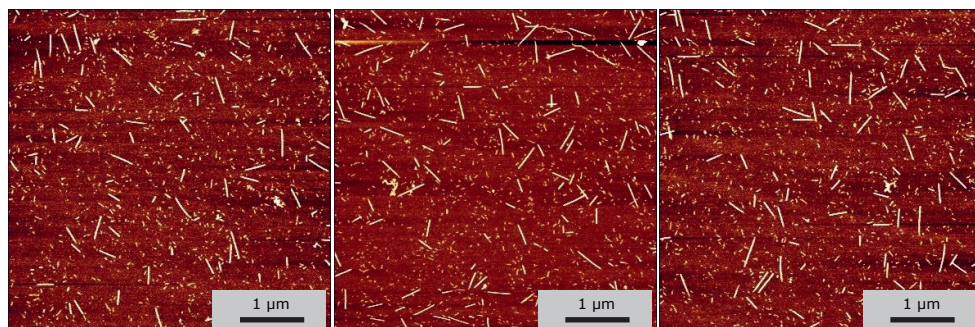

Figure S7.7. *Images that were used to quantify the aggregate length of fibrils (dilution 1:24) both manually or computationally (with FibrilJ).*

Table S7.4. *Aggregate length [nm] determined manually or computationally with FibrilJ. The latter method was applied to all aggregates, or was corrected to only consider the aggregates that were completely visualized (i.e., not cut-off at the edge of the image).*

Method	N total	Mean	Median	Maximum	Minimum
Manually	266	244 ± 103	231	566	71
FibrilJ	373	178 ± 122	153	639	31
FibrilJ corrected	266	229 ± 108	216	639	72

8

General discussion

8.1. This thesis

Precision fermentation using recombinant micro-organisms has traditionally been utilized to produce enzymes or pharmaceuticals. This technique is currently gaining attention for the production of recombinant animal-based protein ingredients, which have an application in food formulations. The production process should be re-designed for this particular purpose to enable both efficient production and application. This thesis therefore aimed to develop design strategies for the production process of recombinant bovine β-lactoglobulin (BLG) to be used as a food ingredient.

This thesis considered three main interventions in the production process. Simplification of the downstream purification process was considered to allow efficient production of recombinant proteins (***Intervention B***; ***Section 8.2***). Furthermore, efficient application may include the reduction of the amount of protein required to create high quality foods, which can be achieved by improving the techno-functional properties of BLG (i.e., functionalization; ***Section 8.3***). Functionalization on a molecular scale could be achieved by particular changes in the primary structure of BLG during upstream production (***Intervention A***; ***Section 8.3.1)***. Besides, functionalization on a meso-scale may be achieved through post-processing; this thesis studied amyloid aggregation in particular for this purpose (***Intervention C***; ***Section 8.3.2***).

Here, the above-mentioned interventions in the production process of recombinant food proteins are further evaluated from different perspectives (***Figure 8.1***). For each intervention, the relevant knowledge gap(s) are recited and the findings of this thesis that help to fill these gaps are summarized. Several considerations that are relevant for industrial food application are then discussed from different perspectives. Finally, an outlook is given that highlights the key elements to be taken into account when designing a production process of recombinant food proteins for food formulations.
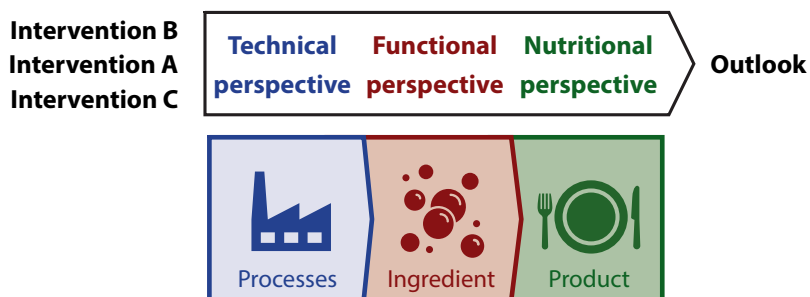

Figure 8.1. *An overview of the general discussion of the interventions (explained in the text above) from different perspectives.*

8.2. **Intervention B**: simplification of the purification process

Traditional purification of recombinant proteins usually includes chromatographic methods, which can be relatively expensive and challenging to scale. Purification generally improves functional properties of recombinant protein ingredients but at the cost of production yield. Thus, simple and scalable purification methods are required for the production of affordable recombinant food proteins. It is currently not clear to what extent purification is required to obtain a functional ingredient (***Knowledge gap 2***).

Key findings for the knowledge gaps: In this thesis, the purification of secreted recombinant BLG produced by *Pichia pastoris* has been investigated as a case for demonstration. A rough protein fraction was obtained after clarification of the cell broth by centrifugation and subsequent removal of small MW impurities by filtration of the cell-free supernatant. ***Chapter 5*** demonstrated that this fraction with a protein purity of 24–26 wt% has poor foaming and (heat-set) gelation properties, and thus further purification was required for these functionalities. In contrast, ***Chapter 3*** showed that it is a suitable emulsifying agent. ***Chapter 3*** also showed that purification up to 72 wt% protein could be achieved with traditional ion exchange chromatography (IEX), but also with an alternative purification method based on complexation. Purification with IEX is based on reversible charge-driven adsorption of the protein to the resin beads in the column, while most impurities run through. A similar mechanism was utilized in the alternative purification method, being based on reversible ionic complexation of BLG by hexametaphosphate (HMP), and only requiring relatively simple processing steps (i.e., centrifugation and filtration). First trials with caseinate demonstrated that this method was also suitable to purify other proteins. ***Chapter 5*** demonstrated that purification to this extent was sufficient to enable adequate foaming and superior gelling properties of recombinant yeast-based BLG , as compared to bovine BLG. Residual HMP left in the protein concentrate (~ 1 wt%) in fact contributed to the gelation.

The HMP-aided purification yielded similar BLG purity to purification with IEX, but introduced small amounts of (food-grade) HMP in the final ingredient. ***Section 8.2.1*** will discuss alternative precipitation agents that can be utilized and the techno-functional consequence of such process-related compounds. Besides, other alternative purification methods with potential for cost-effective purification of recombinant proteins will be suggested. A protein purity of 67–72 wt% was obtained after purification with IEX, as well as with the alternative purification method, leaving approximately 30 wt% of residual impurities in the final ingredient. ***Section 8.2.2*** will raise potential issues for application of this less purified recombinant protein from a nutritional point of view. Lastly, an outlook will be given in ***Section 8.2.3***.

8.2.1. Techno-functional perspective (intervention B)

The precipitation agent HMP is an inorganic polyanion, having a high density of negative charges and an extended configuration that allows cross-linking. Other food-grade polyanions are polysaccharides with charged side groups, which can potentially be used as alternative precipitation agents. Examples of food-grade polyanions that are already reported to interact with WPI are carrageenan (highly sulfated polysaccharides; Stone & Nickerson, 2012), alginate (Fioramonti et al., 2014), and pectin (Du et al., 2022). One could speculate that with this precipitation strategy, a strongly protein-bound impurity (e.g., acidic mannan) is substituted with the polyanion that interacts even stronger with the protein. Removal of the latter may thus be even more challenging. Those polyanions can remain in the final ingredient, as long as they are food grade and do not have negative consequences for the application. Particular polyanions can even improve functional properties for specific applications; this is exemplified by the better gelation properties of the recombinant BLG when purified with HMP, shown in **Chapter 5**. Adding polyanions could therefore even be a potential functionalization strategy. For example, carrageenan is a common gelation agent for milk-based desserts (Mleko et al., 1991), alginate-WPI gels allow the slow release of encapsulated components (Wichchukit et al., 2013), while pectin-WPI complexes can increase heat stability in food beverages (Wagoner & Foegeding, 2017).

The presence of polyanions can also have negative consequences for particular applications, for example, reducing the protein solubility at acidic pH. Other alternative purification methods should thus be explored as well. Liquid-liquid extraction of the cell broth is suggested for mild (intermediate) purification of pharmaceutical proteins (dos Santos et al., 2018). The protein fraction is (selectively) extracted from the cell broth by using an immiscible liquid, usually organic solvents. This extraction could even be implemented during fermentation, instead of after it, to improve productivity of the fermentation (Chaichol & Weeranoppanant, 2023). Ethanol/salt solutions were reported to efficiently partition recombinant protein that was secreted using *P. pastoris*, although the protein purity and configuration was not reported (Dong et al., 2012). Ionic liquids and deep eutectic solvents are suggested as alternatives to organic solvents, since they are more suitable for industrial application, being generally less hazardous and more environmentally friendly (Bowen et al., 2022). Canales et al. (2009) reported efficient purification of a recombinant protein (*Aedes albopictus* akirin) secreted from *P. pastoris* using liquid-liquid extraction. The authors induced ionic liquid-based partitioning during fermentation (i.e., by 38% polyethylene glycol 4000/12% salts) and obtained a protein purity of > 85% with relatively simple separation techniques (i.e., centrifugation and filtration). This two-phase system however caused cells and proteins to partition to the same phase and is thereby not suited for extractive fermentation. Another example for the potential of ionic liquids was reported by Čížová et al. (2017), who demonstrated

efficient separation of mannan-protein mixtures using the ionic liquid mixture 1-butyl-3-methylimidazolium bromide/dipotassium phosphate.

8.2.2. Nutritional perspective (intervention B)

Less extensive purification leaves residual impurities in the final recombinant protein ingredient, which in turn may have nutritional consequences that should be taken into consideration. Identification of those impurities is essential before their application in foods, in particular to assess potential food safety risks. Besides, such impurities can cause off-flavours and off-taste, and thus the sensorial impact should also be evaluated. Even though the identity of a large fraction of the impurities is currently unknown, we can trace back the safety risks of components in the growth medium, and safety issues regarding the yeast itself, as further discussed below.

P. pastoris is considered as a 'generally regarded as safe' (GRAS) organism, being a nontoxigenic and non-pathogenic microbial fermentation yeast. The standard procedure for cultivation (Invitrogen, 2014) includes using a growth medium that contains basal salts media (phosphoric acid, calcium sulfate, potassium sulfate, magnesium sulfate, potassium hydroxide, glycerol and water) and PTM1 salts (manganese sulfate, cupric sulfate, sodium iodide, sodium molybdate, boric acid, cobalt chloride, zinc chloride, ferrous sulfate, biotin, sulfuric acid and water). Most of those compounds also have GRAS status and thus are considered safe to use as food additives, except the compounds listed in *Table 8.1*. Still no considerable risks are expected for these compounds, as they are widely used as dietary supplements and their potential content in the final product is expected to be relatively low (*Table 8.1*). Besides these different salts, substrates have to be added to the growth medium. Methanol is often used as the energy and carbon source for the metabolism of *P. pastoris*, as it is a methylotrophic yeast. Moreover, its metabolism generates toxic by-products that are sequestered by the native alcohol oxidase (AOX). High amounts of AOX are usually produced due to the low enzyme activity (Invitrogen, 2014). The promoter that regulates the expression of the encoding gene of this enzyme (mostly AOX1) is therefore generally utilized for high-level production of the recombinant protein of interest. This promotor is strongly induced by methanol and thus results in high yields for the production of the recombinant target protein (up to 30% of the total soluble protein in the cells; Invitrogen, 2014). Methanol-induced production of recombinant food proteins is not desired, as methanol is flammable, volatile, and most of all, quite toxic. However, methanol is also used in the food industry for extraction purposes, which is allowed as long as the final residual methanol is < 10 mg kg^{-1} foodstuff (The European parliament and the council of the European Union, 2009). Therefore, the content of residual methanol should be examined after purification. Other promoters may also be considered for expression, but this generally lowers the production yield (García-Ortega et al., 2019).

8

Table 8.1. *Compounds in the growth medium of P. pastoris that do not have GRAS status, the tolerable upper intake level (UL) for human intake, and the content in the final product when not metabolized or removed during purification.*

Compounds	UL[1] (mg day^{-1})	Max. content in final product[1] (mg g^{-1} protein)
Manganese sulfate	30.2	0.015
Sodium iodide	1.2	0.006
Sodium molybdate	3.6	< 0.000
Boric acid	122	< 0.000

[1]For adolescents. Values reported by Institute of Medicine (2001) and German Federal Institute for Risk Assessment (2021).

[2]Assuming no metabolism by *P. pastoris*, no removal during purification, and a production yield of 1 g BLG L^{-1} cell culture.

P. pastoris can be grown on other carbon sources than methanol, usually being glycerol. A major drawback is that the metabolism pathway of glycerol results in the release of molecules that repress the AOX production. Shen et al. (2016) demonstrated that this release of repression signals can be circumvented when directly using a metabolite of glycerol as the growth medium (in this case dihydroxyacetone, DHA; being non-toxic). Besides, the strain was reconstructed to enable the use of the AOX1 promoter in this new growth medium. Even though the production of the recombinant target protein was successful, the production yield was lower than that of the traditional methanol-induced system (decreased by 40–50%).

Another consideration is the presence of recombinant DNA. Products that contain whole genetically modified organisms (GMOs) are strictly regulated. In contrast, recombinant proteins can be secreted by a genetically modified micro-organism (GMM; i.e., modified *P. pastoris*), while the protein and GMM can then be separated during downstream processing (DSP). Thus, the final product thus does not contain GMM cells. However, traces of recombinant DNA may be released (e.g. during cell lysis), which can pose regulatory issues. Lensch et al. (2022) challenged the regulatory relevance of recombinant proteins, marking the differences between GMO and products from GMM. The degradation of any traces of DNA starts already during processing prior to consumption and continues in the gastrointestinal tract after ingestion. Furthermore, it is highly unlikely that traces of DNA (fragments) can cause any form of antimicrobial resistance. Additional DSP can be considered to specifically degrade DNA prior to consumption if complete elimination of the DNA is required, but extreme conditions (e.g. boiling at pH 2.0; Bitskinashvili et al., 2018) or employing enzymes (DNases from GMM origin) have consequences for the nativity (and techno-functional properties) of the protein and the DSP costs.

8.2.3. Outlook for food application (intervention B)

Recombinant food proteins can become more affordable when less extensive purification is required and when cost-effective and scalable purification methods are applied. When designing the DSP for recombinant food proteins, it should be considered what purity is at least required to obtain a functional ingredient that is safe to consume. While simplification of the purification process can contribute to a cost-effective production process, such gains should be weighed against the changes in the value of the ingredient (in terms of protein yield, purity and functional properties). Either additional purification steps or alternative purification method are required in case the process- or production-related components reduce the functionality or would compromise the safety of the final ingredient.

8.3. Efficient application – functionalization strategies

This thesis proposed to functionalize recombinant proteins for their application in food formulations, which in turn enables the creation of the same types of food with a lower protein content. This may be achieved through molecular and/or mesoscale modification of the proteins. The relevant knowledge gaps, key findings and further considerations of these functionalization strategies will be further discussed in **Section 8.3.1** and **Section 8.3.2**, respectively. Here, a brief discussion is first raised about the nutritional consequences of functionalization strategies in general.

Lowered protein intake may cause adverse health effects. Recommendations of the Food and Agriculture Organization (FAO) of the United Nations showed that a healthy diet should include a daily digestible protein intake of about 0.75 g kg^{-1} of bodyweight, which equals about 50 g of protein (assuming an average adult weighing 70 kg). In **Figure 8.2**, the average protein intake is depicted for high-income countries (**Figure 8.2A**), as well as for low- and middle-income countries (**Figure 8.2B**). Protein is generally overconsumed in the high-income countries, while the fraction of animal-based protein consumption is quite high. Lowering the animal-based protein content in food formulations in high-income countries is therefore regarded as an acceptable strategy from a nutritional point of view. These low-protein products however may be less suited for lower-income countries and particular vulnerable groups (e.g. elderly; Brownie, 2006).
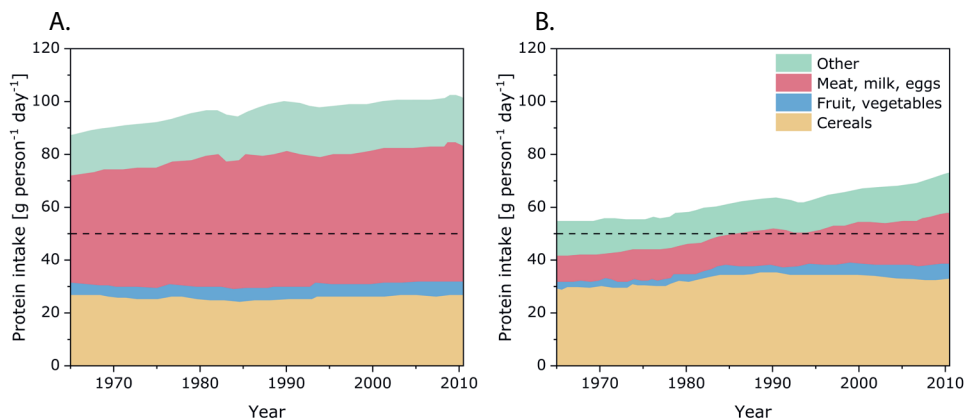
8

Figure 8.2. *Protein intake per capita in (**A**) high- and (**B**) low/middle-income countries (between 1965–2010). Figure is reproduced using the data obtained by the Food and Agriculture Organization of the United Nations (2017). The reference line indicates the recommended intake of digestible protein (assuming an average adult weighing 70 kg).*

8.3.1. **Intervention A**: molecular-scale functionalization

The production of recombinant proteins through precision fermentation allows substitution of specific amino acids in a given protein to optimize its properties for particular applications, but it is currently unknown which substitutions in BLG would improve its techno-functional properties (**Knowledge gap 1**). Besides, it is unclear how far the functionality range of recombinant BLG could be extended by such an intervention (**Knowledge gap 3**).

Key findings for the knowledge gaps: Specific cysteines in recombinantly produced BLG were substituted by alanine to potentially functionalize the protein through molecular modification. First, **Chapter 2** demonstrated that different cysteines in BLG can be targeted to change its fold to different extents. Exchange of the free thiol (Cys121Ala) did not affect the protein fold to a significant extent, but could change its ability to form intermolecular disulfide bonds during processing and application. Exchange of the cysteines involved in the outer disulfide bond (Cys60Ala–Cys160Ala) opened the globular fold, while partially disrupting the secondary structure, resulting in a partially destabilized BLG variant. Finally, substitution of all cysteines yielded a disordered variant that spontaneously aggregated at acidic pH. **Chapter 5** further evaluated the impact of such molecular changes on the ability to stabilize the air-water interface in foams. While complete disorder of the globular structure improved the foamability in the protein-depleted regime, the partial destabilized variant mostly improved the stability of the foam (up to 10 times). In particular the latter is suggested to be beneficial for application. The gelation properties are expected to be mostly impaired by the removal of cysteines.

Such amino acid exchanges in the primary sequence of recombinant proteins can have consequences for the production process, as will be discussed in **Section 8.3.1.1**. **Section 8.3.1.2** will discuss the relevance of other amino acid exchanges to alter functional properties, and **Section 8.3.1.3** will describe potential consequences of such targeted exchanges for nutrition and health. Lastly, an outlook for the optimization of the primary structure for food application will be given in **Section 8.3.1.4**.

8.3.1.1. Technical perspective (intervention A)

Single amino acids can be substituted in a given protein to improve its functional properties, but this can also affect upstream production and/or downstream processes. The conformation of yeast-based recombinant proteins influences the secretion of the protein; Katakura et al. (1999) demonstrated that the secretion of BLG by *Saccharomyces cerevisiae* was accelerated by a factor of six when implementing a single Trp19Tyr mutation. This variant had an improved folding ability, yielded a slightly less stable but probably similar structure to the wild-type (Katakura et al., 1999). Variants that included the exchanges Trp19Phe or Trp19Ala failed to fold, leading to reduced secretion levels (Katakura et al., 1999). These results suggest that slightly less stable recombinant BLG variants might be easier to fold, increasing the yeast-based secretion rate, while complete destabilized variants hinder secretion.

Single amino acid exchanges in the primary sequence of BLG can also have benefits for downstream processing. Covalent aggregation of BLG has been identified as a major cause for membrane fouling during both ultra- and microfiltration of whey proteins. Steinhauer et al. (2015) showed that the flux of BLG solution (2.2 wt%) through a microfiltration membrane decreased within minutes, while it was unaffected when the free thiol was blocked with NEM. Thus, the Cys121Ala exchange could potentially reduce membrane fouling, as it disables intermolecular disulfide bond formation (**Chapter 7**).

8.3.1.2. Functional perspective (intervention A)

Exchanges of single amino acid residues can enhance techno-functional properties, while still obtaining native-like structure. Lee et al. (1994) demonstrated that the introduction of additional cysteine residues (Arg40Cys/Phe82Cys; distant from Cys121) improved the gelation properties of BLG. The gelation temperature was decreased from 85 to 70 °C, while this variant demonstrated a five-fold higher gel strength after heating at 90 °C. Further studies that induce single exchanges to enhance techno-functional properties are unfortunately lacking. Random screening of the potential of point mutations is undesired, especially because of the relatively large amount of expensive recombinant protein required for functionality studies. Alternatively, predictive modelling can be used to identify particular amino acid

8

substitutions that could improve functional properties. Molecular dynamics (MD) simulations are suitable to predict the impact of single exchanges on protein folding, but accurate prediction of *in vivo* folding remains challenging (Rizzuti & Daggett, 2013). In addition, models are required to predict the impact of molecular changes on subsequent functional behaviour. For example, Delahaije et al. (2015) proposed a model that describes the relationship between the molecular properties of a protein and its ability to form emulsions. This model suggested the importance of particular physicochemical properties, such as high surface hydrophobicity and charge, for efficient emulsification.

Some studies reported BLG variants with single substituted amino acids that still assumed a native-like structure (**Table 8.2**). Those BLG variants were not constructed to improve its techno-functional properties, but to better understand the behaviour of bovine BLG (Jayat et al., 2004; Sakurai & Goto, 2002), to change ligand-binding (Bonarek et al., 2020), and/or to alter its immunogenicity (Kazem-Farzandi et al., 2015; Taheri-Kafrani et al., 2015; Yoshida et al., 2022). These variants have a native-like structure, but changed physicochemical properties may be beneficial for food application. **Table 8.2** highlights local changes in physicochemical properties, based on the properties of the single amino acids that were exchanged. Although those local changes can be used as a first indication for potential differences, the actual surface physicochemical properties that determine functionality will depend highly on the protein fold and stability.

Table 8.2. *Amino acid (AA) substitutions in recombinant BLG that still results in a native-like fold, according to [a]Sakurai et al. (2002), [b]Katakura et al. (1999), [c]Bonarek et al. (2020), [d]Taheri-Kafrani (2015), [e]Kazem-Farzandi et al. (2015), [f]Jayat et al. (2004), [g]Yoshida et al. (2022). Changes in protein stability are indicated when mention in the referred study. Besides, changes in relatively hydrophobicity and charge are listed, taking into account the nature of the particular amino acids involved in the substitution. Relative hydrophobicity was quantified according to Monera et al. (1995), assuming neutral pH.*

Position	original AA	AA for substitution	Thermostability	Δ relative hydrophobicity	Δ charge
4[a]	Arg	Asp	n.d.	↓ (41)	↓
4[a]	Arg	Asp	n.d.	↓ (41)	↓
19[b]	Trp	Tyr	↓	↓ (34)	–
33[a]	Asp	Arg	n.d.	↑ (41)	↑
39[c]	Leu	Tyr	↑	↓ (34)	–
69[d]	Lys	Asn	n.d.	↓ (5)	↓
86[e]	Ala	Gln	n.d.	↓ (42)	–
92[c]	Val	Phe	unchanged	↑ (24)	–

Table 8.2. *continued.*

Position	original AA	AA for substitution	Thermostability	Δ relative hydrophobicity	Δ charge
92[c]	Val	Tyr	↓	↓ (13)	–
107[c]	Met	Leu	↑	↑ (23)	–
121[f]	Cys	Ser	↓	↓ (54)	–
126[g]	Pro	Ala	n.d.	↑ (87)	–
128[g]	Val	Asp	n.d.	↓ (131)	↓
129[g]	Asp	Ala	n.d.	↑ (96)	–

8.3.1.3. Nutritional perspective (intervention A)

Nine amino acids cannot be anabolized by the human body and should be provided through the diet. These are referred to as essential amino acids (His, Ile, Leu, Lys, Met, Phe, Thr, Trp, and Val), and are all present in whey proteins. Substitution of such amino acids can thus reduce the nutritional value of recombinant protein, while their addition to the recombinant protein sequence can improve its nutritional value. Besides its nutritional value as such, BLG has gained much attention for encapsulation, protection and controlled release of bioactive compounds, for example drugs or vitamins, which can bind in its hydrophobic pocket (i.e., calyx; Simões et al., 2020). Amino acids in the calyx can be substituted to influence the affinity for binding those bioactive compounds (Bonarek et al., 2020). Furthermore, amino acid substitution in recombinant proteins can have consequences for their allergenicity, and may pose a suitable approach to destroy epitopes and reduce the allergenicity of BLG (Kazem-Farzandi et al., 2015; Taheri-Kafrani et al., 2015; Yoshida et al., 2022). Conventional enzymatic digestion is the most common method to reduce protein allergenicity, but this also hydrolyzes bioactive peptides (Yukalo et al., 2022) and induces bitterness (Spellman et al., 2009). Amino acid substitution in recombinant BLG could be useful to overcome these disadvantages; specific cleavage sites can be introduced in the amino acid sequence to allow targeted enzymatic hydrolysis to maintain bioactive peptides, or stimulate digestion of BLG.

8.3.1.4. Outlook for food application (intervention A)

It is clear that single or multiple amino acid substitutions can be used to improve techno- and bio-functionality for food application. With such molecular design of recombinant proteins, particular attention should be given to food safety of the designed protein. While particular substitutions can improve bio-functionality, it can also cause adverse effects. For example, the new peptide sequence may introduce new epitopes causing allergenicity or inducing toxicity (Liu et al., 2020). Such potential risks should obviously be carefully evaluated.

8

Protein engineering has been widely accepted to produce, for example, enzymes for industrial applications (Kaur & Sharma, 2006) or therapeutics in pharmaceutical applications (Murphy, 1996). Yet, its application for the production of major food components might raise ethical concerns. As an alternative to introducing amino acid substitutions that are not available in nature, one could also make use of the variation in particular acid sequences that are available in nature. For example, instead of removing the free thiol from bovine BLG (Cys121Ala) as proposed in **Chapter 2**, one could use equine BLG (genetic variant I; Godovac-Zimmerman et al., 1985) or porcine BLG (Bell et al., 1981) that both naturally lack this free thiol.

8.3.2. **Intervention C**: meso-scale functionalization

Classical fibrillization of BLG is a functionalization route that requires extensive processing. Intrinsic protein characteristics and extrinsic conditions can stimulate fibrillization. In turn, these intrinsic and extrinsic features can be controlled through upstream protein modification, DSP and post-processing. It is currently unknown which particular amino acid exchanges (in upstream production) and/or processing conditions (applied during DSP and/or post-processing) can stimulate fibrillization of recombinant proteins (**knowledge gap 4**). Besides, it is unclear how far the functionality range of recombinant BLG could be extended by such interventions (**knowledge gap 3**).

Key findings for the knowledge gaps: **Chapter 4** summarizes post-processing conditions that can induce amyloid aggregation. Two major types of amyloid aggregates are described for BLG, as shown in **Figure 8.3** and **Figure 8.4**:

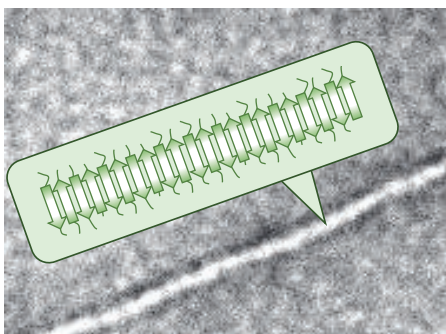| Amyloid Fibrils	Amyloid-like aggregates

***Figure 8.3.** Long and semi-flexible amyloid fibrils are formed by aggregation of specific short amyloid-prone peptides. Classical fibrillization is often described to occur upon heating at pH 2.0 for several hours.*
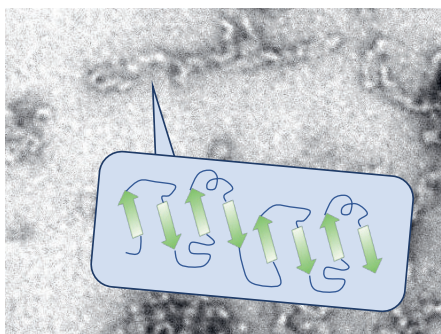
***Figure 8.4.** Shorter and more flexible amyloid-like aggregates are formed from less specifically assembled intact or longer peptide sequences. These aggregates are often described to form upon heating at pH 3.5 and 7.0.*

Chapter 5 showed the instability of amyloid fibrils upon pH adjustment, ion removal, freezing and drying. In contrast, amyloid-like aggregates were able to withstand these processing steps. Furthermore, amyloid-like aggregates had an improved ability to stabilize of air-water interfaces in foams (i.e., being up to 4 times more stable), as compared to native whey protein. Precision fermentation can be used as a tool to adjust the primary sequence of BLG to further improve these two types of aggregates (*Figure 8.3* and *Figure 8.4*) for industrial application. *Chapter 2* demonstrated that targeting different cysteine residues can yield BLG variants with different structures and stabilities. *Chapter 6* showed that partial destabilization cannot accelerate fibrillization at classical amyloid fibrillization conditions (i.e., heating at pH 2.0). Complete destabilization by recombinant substitution of all cysteines accelerated aggregation kinetics, but resulted in random spherical aggregates instead of fibrils. Alternatively, *Chapter 7* investigated the impact of cysteine substition on the aggregation mechanism under relatively milder conditions: heating at pH 3.5 and 7.0. Hindering disulfide bond formation by substitution of Cys121, as well as reducing intramolecular disulfide bonds by substitution of Cys66–Cys160, increased the aggregate length upon incubation. Complete destabilization allowed for formation of fibrillar aggregates at pH 7.0 during extended heating times (5–24 h). The functional properties of such aggregates is yet to be determined.

While a combination of upstream interventions (i.e., cysteine substition) and post-processing conditions (pH 7.0) led to the formation of fibrillar aggregates, extended heating times were still required for fibrillization (5–24 h). Efficient formation of amyloid aggregates for food application may be achieved by alternative production and processing strategies, which will be discussed in *Section 8.3.2.1*. Besides, one should also consider the nutritional consequences when using aggregation as a functionalization tool, which will be discussed in *Section 8.3.2.2*. Finally, an outlook for application will be given in *Section 8.3.2.3*.

8.3.2.1. Techno-functional perspective (intervention C)

8.3.2.1.1. Selection of the primary sequence to stimulate amyloid aggregation

The first step of classical fibrillization includes the hydrolysis of the protein to release particular fibril building blocks, which were identified as mainly being the N-terminal peptide sequences (1–33 or 1–53). In theory, precision fermentation would allow the production of these fibril building blocks directly, thus not requiring processing to induce hydrolysis, and making better use of the raw material. Therefore, Brune, Biedendieck & Krull (project partners at Braunschweig University) have tried to directly produce the recombinant N-terminal sequence 1–53 (from BLG) with E. coli. Overall, the production of N-terminal peptides as fibril building blocks was found to be challenging, as will be discussed in the following.

As a first approach, the peptide sequence was complemented with a glutathione S-transferase (GST) tag for the purification, similar to the method described in **Chapter 3**. However, none or very low amounts of the peptide were produced (data not shown). Next, a natural hydroxylamine cleavage site was inserted next to the N-terminal peptide sequence (position 54/55) in rBLG-C. Besides, the C-terminus of the remaining peptide sequence was fused to a His-tag to allow its subsequent chromatographic removal. This new variant was produced as inclusion bodies. An overview of this approach can be found in **Figure 8.5A**. Both the production and cleavage were successful, but further DSP was troublesome: a large fraction of the His-tagged C-terminus peptides did not bind to the column (immobilized metal chelate affinity chromatography), resulting in incomplete removal. Lastly, just the N-terminal peptide (1–53) was produced with a C-terminal His-tag for purification. To allow subsequent removal of this His-tag, a hydroxylamine cleavage site was inserted (**Figure 8.5B**). The peptide production and purification was successful, but the peptide immediately precipitated after inducing cleavage of the His-tag. This demonstrated that the tendency of the peptide to aggregate is too high after removal of the His-tag, impeding the controlled formation of amyloid fibrils or amyloid-like aggregates. Thus, direct production of the N-terminal peptide does not look as a promising route for production of fibrils for food application.
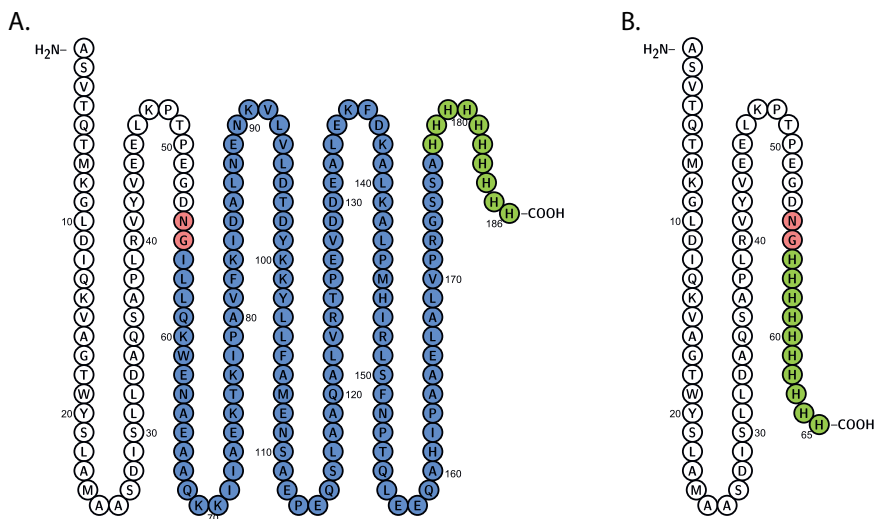

Figure 8.5. *Two approaches for the recombinant production of the N-terminal peptide. The N-terminal peptide sequence is shown in white, while additional peptide sequences that should be removed are coloured. The natural hydroxylamine cleavage site is shown in red, the His-tag in green and the C-terminal peptide in blue. Graphic created using Protter (Omasits et al., 2015).*

Alternative protein sequences can be considered instead of changing the BLG sequence to drive fibrillar aggregation. For example, Bahraminejad et al. (2022) demonstrated the formation of well-defined fibrils from the disordered milk protein β-casein, in particular the camel orthologue (compared to bovine and goat), upon heating at pH 7.0 and 65 °C. It also assembled at 37 °C yielding smaller worm-like aggregates. The *in vivo* production of such proteins in a host might pose problems, as also observed for the N-terminal peptide of BLG, as described before. Besides, they most likely cause the formation of inclusion bodies, which can be undesired when aiming to secrete the protein. A potential approach could be to extend the protein with an N-terminal sequence that counteracts aggregation. For example, peptide extensions with high charge were already demonstrated to counteract *in vivo* aggregation (Zhang et al., 2004). Moreover, Lin-Cereghino et al. (2013) suggest a positive impact on protein secretion by including polar and charged residues within the signal peptide. So, particular signal peptides might hinder aggregation (Akkermans et al., 2008), while stimulating secretion. In that sense, non-amyloidogenic regions play an important role in the controlled formation of amyloids.

8.3.2.1.2. Impact of DSP-related impurities on amyloid aggregation

Section 8.2 suggested alternative DSP for cost-effective production of recombinant BLG, but residual HMP was introduced (~ 1 wt%) during purification that may affect the aggregation behaviour of the protein. Zhang et al. (2019) demonstrated that polyphosphates can actually stimulate amyloid formation, even at neutral pH, as was shown for β2-microglobulin. They found that either fibrillar or amorphous aggregation can be induced, depending on the polyphosphate concentration and chain-length. Thereby, we further investigated the impact of residual HMP on the aggregation kinetics and morphology of BLG. Heat-set aggregation was performed for 10 mg mL^{-1} bBLG AB solutions with approximately 1 wt% HMP (similar content that is achieved after purification process in ***Chapter 3***). BLG solutions with NaCl were used as a control. The kinetics were determined using ThT (method in ***Chapter 6***). HMP did not affect the aggregation kinetics at neutral pH (***Figure 8.6B***), probably since both the protein and HMP have similar charge, but accelerated aggregation at pH 2.0 (***Figure 8.6A***). In the latter case, a precipitate was observed and TEM analysis (method in ***Chapter 6***) demonstrated aggregates with amorphous instead of fibrillar morphology (***Figure 8.7***). Thus, HMP does not stimulate fibril formation under those conditions. If fibril formation is important for efficient application of recombinant BLG, the suggested alternative purification method in ***Chapter 3*** is not suitable, or additional purification is required to remove HMP.
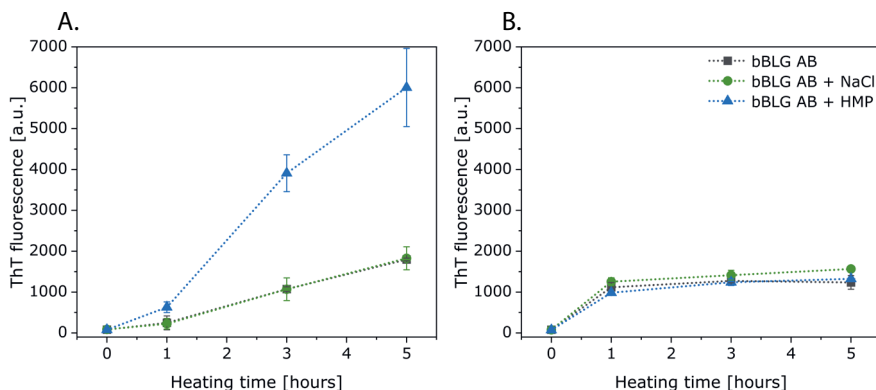
Figure 8.6. *Aggregation kinetics of 10 mg mL^{-1} BLG solutions upon heat-set aggregation (80 °C) at (**A**) pH 2.0 or (**B**) pH 7.0, in the presence of HMP or NaCl (~ 1 wt%).*
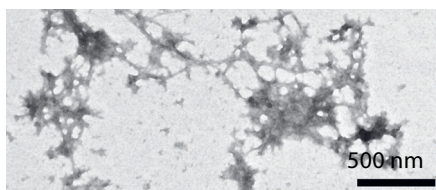

Figure 8.7. *TEM image of bBLG AB + HMP after 5 hours of heating.*

8.3.2.1.3. Post-processing conditions to stimulate amyloid aggregation

A major drawback of BLG amyloid fibrils is their limited application range, as they are not stable at common formulation and processing conditions (**Chapter 5**). Disintegration of fibrils upon an increase in pH has been demonstrated also for other peptides. Picotti et al. (2007) reported that a particular fragment of horse heart apomyoglobulin is highly prone to form fibrils at pH 2.0, but those fall apart when increasing the pH to 8.3, and then can reform when adjusting the pH back to 2.0. They suggest that particular acidic residues that are deprotonated at higher pH cause this disintegration, while re-protonation at acidic pH causes them to form again (Asp and Glu). These acidic residues make up about 13% of the sequence of the main building block of the BLG fibrils (peptide 1–53: Asp on position 11, 28, 33 and 53; Glu on position 44, 45 and 51) and might cause the pH-instability of BLG fibrils. Alternatively, intact BLG can form amyloid-like structures at higher pH (e.g., pH 3.5 and 7.0) that are more suited for application. Besides, point mutations can be induced to drive the formation of longer and more rigid amyloid-like aggregates upon heating at neutral pH, as exemplified in **Chapter 7**.

8.3.2.2. Nutritional perspective (intervention C)

There have been ongoing discussions regarding the potential health consequences of incorporating amyloid fibrils into food, as these structures have been reported

to play a role in the *in vivo* development of neurodegenerative diseases. Bateman et al. (2010) demonstrated that BLG amyloid fibrils are easily digestible by pepsin, being completely digested within 2 min. Also Xu et al. (2023) demonstrated no conformational differences after digestion of amyloid fibrils and their monomer counterparts, both for BLG and lysozyme.

Fibril fragments that may survive the digestion prior to adsorption might potentially seed new (pathogenic) fibrillar structures *in vivo*. Rahman et al. (2023) investigated such cross-seeding of the pathogenic amyloid-β (Aβ) peptide by 16 types of food fibrils, but none of them accelerated the aggregation of Aβ. Xu et al. (2023) showed that the digested food amyloids were equally safe to ingest as the monomeric counterparts; based on experiments with *in vitro* exposure to human cell lines, as well as *in vivo* studies with mouse models. BLG fibrils are therefore regarded suitable for human consumption. However, effects on digestion and *in vitro* fibrillization should be carefully considered when designing the protein sequence to stimulate fibrillization during post-processing of recombinant proteins/peptides.

Lastly, amino acid degradation could potentially occur during the preparation of fibrils by a long and severe heat treatment, which in turn may release toxic oxidation products. However, oxidation reactions are slower at acidic pH than at neutral or alkaline pH. Keppler et al. (2019) investigated the oxidation of BLG during formation of amyloid fibrils or amyloid-like aggregates when heating at pH 2.0 and 3.5, respectively, at 90 °C. Oxidation was only marginally up to 5 h of heating, as measured by specific markers (i.e., carbonyls, N-formylkynurenine, and dityrosine). The risk for oxidation by-products can be lowered by changing aggregation conditions.

8.3.2.3. Outlook for food application (intervention C)

The formation of functional aggregates may well be a feasible functionalization strategy, but the production and process should be specifically designed for efficient and scalable aggregation and application. The high aspect ratio of aggregates is often related to its favourable functional properties, but the role of aggregate length and flexibility should be further related to the exact functionalities required for particular food applications. Specific amino acid sequences should be selected that do not aggregate *in vivo*, and that can be relatively easily triggered to form fibrils through post-processing conditions, for example, through biological (e.g., enzymes), physical (e.g., shearing), and/or chemical (e.g., solvents) processing. Moreover, the fibril production and application pH can be aligned to ensure the stability of the aggregates. Aggregate morphology can be steered through the choice in amino acid sequence, as well as post-processing conditions. Finally, the functionality gain of the functional aggregates should outweigh the additional post-processing that was required for their formation.

8.4. Conclusions

Recombinant food proteins give us the unprecedented freedom to obtain better functionality and nutrition without the need for animal slaughter. Conventional precision fermentation processes are not developed for the production of protein ingredients to be used as major constituents of food products. These processes should thus be adapted to facilitate large-scale production of affordable food proteins. For this purpose, the aim of this thesis was to develop protein and processing design strategies for recombinant β-lactoglobulin. Extensive purification or complete retention of the native structure (primary to higher order levels) are not required for food application, as generally is the case with traditionally produced recombinant proteins (e.g., enzymes or pharmaceuticals). Thus, the functionality of recombinant food proteins should be taken into account for the development of such design strategies.

During the protein design in the upstream production, single or multiple amino acid exchanges can enhance the techno- and bio-functionality for food applications. Although, careful attention must be given to the safety of the designed protein, as specific substitutions may lead to adverse effects such as allergenicity or toxicity. Its use for production of foods may also raise ethical concerns, even though protein engineering is widely accepted in industrial and pharmaceutical contexts. It may well be that regulatory authorities and the public at large will embrace these techniques as soon as the benefits become obvious. Alternatively, the genetic variation present in nature can be utilized.

Downstream processing with less extensive purification contributes to cost-reduction and improves scalability, but the balance between financial gains and changes in the value of the produced protein ingredient (considering yield, purity, and functional properties) is crucial. Additional purification steps or alternative methods are required when the process- or production-related impurities compromise the quality of the ingredient to an unacceptable extent or cause a food safety risk.

Further post-processing steps may increase the value of the protein. Here, functionalization of the protein through amyloid aggregation was considered. Specific design considerations are required to allow efficient formation and application of these aggregates. Aggregate morphology is a result of the amino acid sequence (selected upstream), impurities (process- and production-related), as well as the post-processing conditions applied. The aggregate stability upon further food processing and resulting application conditions should also be regarded. Finally, the increased protein ingredient value (by increased techno-functionality) should outweigh the additional processing costs.

This thesis has explored the impact of protein and/or process design strategies on the techno-functionality of BLG. However, this protein-to-application approach should be reversed into application-driven production process design, because it is impractical to screen for the functional impact of all possible design strategies. The intended application of the protein ingredient should be assessed first. Particular application types (e.g., creation of an emulsion, foam, or gel) demand distinct techno-functional properties, which may be differently affected by the protein purity or structure. Besides, it is important to consider the targeted consumer group to identify the nutritional requirements. This thorough upfront evaluation of the techno- and bio-functional requirements of the recombinant protein might in the future be translated to design the desired recombinant protein and associated production processes by predictive modelling or machine learning.

Innovative production processes are required for large-scale production of affordable recombinant food proteins. The concepts introduced in this thesis serve as an initial framework. Advancing these concepts holds promise for producing animal-based protein ingredients for food that has all the sensory attributes of our traditional foods, without using animals in the process.

8

References

Adamcik, J., & Mezzenga, R. (**2011**). Adjustable twisting periodic pitch of amyloid fibrils. Soft Matter, 7(11), 5437-5443.

Adamcik, J., & Mezzenga, R. (**2012**). Study of amyloid fibrils via atomic force microscopy. Current Opinion in Colloid & Interface Science, 17(6), 369-376.

Adamcik, J., & Mezzenga, R. (**2018**). Amyloid polymorphism in the protein folding and aggregation energy landscape. Angewandte Chemie International Edition, 57(28), 8370-8382.

Adamcik, J., Jung, J. M., Flakowski, J., De Los Rios, P., Dietler, G., & Mezzenga, R. (**2010**). Understanding amyloid aggregation by statistical analysis of atomic force microscopy images. Nature nanotechnology, 5(6), 423-428.

Agyei, D., Ongkudon, C. M., Wei, C. Y., Chan, A. S., & Danquah, M. K. (**2016**). Bioprocess challenges to the isolation and purification of bioactive peptides. Food and Bioproducts Processing, 98, 244-256.

Ahmad, M., Hirz, M., Pichler, H., & Schwab, H. (**2014**). Protein expression in *Pichia pastoris*: recent achievements and perspectives for heterologous protein production. Applied microbiology and biotechnology, 98, 5301-5317.

Akkermans, C. (**2008**). Protein fibrillization: preparation, mechanism and application. Wageningen University and Research.

Akkermans, C., Van der Goot, A. J., Venema, P., Gruppen, H., Vereijken, J. M., Van der Linden, E., & Boom, R. M. (**2007**). Micrometer-sized fibrillar protein aggregates from soy glycinin and soy protein isolate. Journal of Agricultural and Food Chemistry, 55(24), 9877-9882.

Akkermans, C., van der Goot, A. J., Venema, P., van der Linden, E., & Boom, R. M. (**2008**). Formation of fibrillar whey protein aggregates: Influence of heat and shear treatment, and resulting rheology. Food Hydrocolloids, 22(7), 1315-1325.

Akkermans, C., Venema, P., Rogers, S. S., van der Goot, A. J., Boom, R. M., & van der Linden, E. (**2006**). Shear pulses nucleate fibril aggregation. Food Biophysics, 1, 144-150.

Akkermans, C., Venema, P., van der Goot, A. J., Boom, R. M., & van der Linden, E. (**2008**). Enzyme-induced formation of β-lactoglobulin fibrils by AspN endoproteinase. Food Biophysics, 3, 390-394.

Akkermans, C., Venema, P., van der Goot, A. J., Gruppen, H., Bakx, E. J., Boom, R. M., & van der Linden, E. (**2008**). Peptides are building blocks of heat-induced fibrillar protein aggregates of β-lactoglobulin formed at pH 2. Biomacromolecules, 9(5), 1474-1479.

Alavi, F., Momen, S., Emam-Djomeh, Z., Salami, M., & Moosavi-Movahedi, A. A. (**2018**). Radical cross-linked whey protein aggregates as building blocks of non-heated cold-set gels. Food Hydrocolloids, 81, 429-441.

Albani, J. R., Vogelaer, J., Bretesche, L., & Kmiecik, D. (**2014**). Tryptophan 19 residue is the origin of bovine β-lactoglobulin fluorescence. Journal of pharmaceutical and biomedical analysis, 91, 144-150.

Almeida, A. M., Li, R., & Gellman, S. H. (**2012**). Parallel β-sheet secondary structure is stabilized and terminated by interstrand disulfide cross-linking. Journal of the American Chemical Society, 134(1), 75-78.

Alomirah, H. F., & Alli, I. (**2004**). Separation and characterization of β-lactoglobulin and α-lactalbumin from whey and whey protein preparations. International Dairy Journal, 14(5), 411-419.

Al-Shabib, N. A., Khan, J. M., Malik, A., Alsenaidy, A. M., Alsenaidy, M. A., Husain, F. M., ... & Khan, R. H. (**2018**). Negatively charged food additive dye "Allura Red" rapidly induces SDS-soluble amyloid fibril in beta-lactoglobulin protein. International journal of biological macromolecules, 107, 1706-1716.

Al-Shabib, N. A., Khan, J. M., Malik, A., Sen, P., Alsenaidy, M. A., Husain, F. M., ... & Shahzad, S. A. (**2019**). A quercetin-based flavanoid (rutin) reverses amyloid fibrillization in β-lactoglobulin at pH 2.0 and 358 K. Spectrochimica Acta Part A: Molecular and Biomolecular Spectroscopy, 214, 40-48.

Amundson, C. H., Watanawanichakorn, S., & Hill Jr, C. G. (**1982**). Production of enriched protein fractions of β-lactoglobulin and α-lactalbumin from cheese whey. Journal of food Processing and Préservation, 6(2), 55-71.

Antonets, K. S., Belousov, M. V., Sulatskaya, A. I., Belousova, M. E., Kosolapova, A. O., Sulatsky, M. I., ... & Nizhnikov, A. A. (**2020**). Accumulation of storage proteins in plant seeds is mediated by amyloid formation. PLoS Biology, 18(7), e3000564.

Antoniou, J., Liu, F., Majeed, H., Qi, J., Yokoyama, W., & Zhong, F. (**2015**). Physicochemical and morphological properties of size-controlled chitosan–tripolyphosphate nanoparticles. Colloids and Surfaces A: Physicochemical and Engineering Aspects, 465, 137-146.

Antzutkin, O. N., Leapman, R. D., Balbach, J. J., & Tycko, R. (**2002**). Supramolecular structural constraints on Alzheimer's β-amyloid fibrils from electron microscopy and solid-state nuclear magnetic resonance. Biochemistry, 41(51), 15436-15450.

Arnaudov, L. N., de Vries, R., Ippel, H., & van Mierlo, C. P. (**2003**). Multiple steps during the formation of β-lactoglobulin fibrils. Biomacromolecules, 4(6), 1614-1622.

Avelar, Z., Vicente, A. A., Saraiva, J. A., & Rodrigues, R. M. (**2021**). The role of emergent processing technologies in tailoring plant protein functionality: New insights. Trends in Food Science & Technology, 113, 219-231.

Azevedo, A. M., Rosa, P. A., Ferreira, I. F., & Aires-Barros, M. R. (**2009**). Chromatography-free recovery of biopharmaceuticals through aqueous two-phase processing. Trends in biotechnology, 27(4), 240-247.

Baca-Bocanegra, B., Martínez-Lapuente, L., Nogales-Bueno, J., Hernández-Hierro, J. M., & Ferrer-Gallego, R. (**2022**). Feasibility study on the use of ATR-FTIR spectroscopy as a tool for the estimation of wine polysaccharides. Carbohydrate Polymers, 287, 119365.

Bagnani, M., Nyström, G., De Michele, C., & Mezzenga, R. (**2018**). Amyloid fibrils length controls shape and structure of nematic and cholesteric tactoids. Acs Nano, 13(1), 591-600.

Bahraminejad, E., Paliwal, D., Sunde, M., Holt, C., Carver, J. A., & Thorn, D. C. (**2022**). Amyloid fibril formation by αS1-and β-casein implies that fibril formation is a general property of casein proteins. Biochimica et Biophysica Acta (BBA)-Proteins and Proteomics, 1870(11-12), 140854.

Balistreri, A., Kahana, E., Janakiraman, S., & Chapman, M. R. (**2020**). Tuning functional amyloid formation through disulfide engineering. Frontiers in Microbiology, 11, 944.

Barth, A. (**2007**). Infrared spectroscopy of proteins. Biochimica et Biophysica Acta (BBA)-Bioenergetics, 1767(9), 1073-1101.

Basch, J. J., & Timasheff, S. N. (**1967**). Hydrogen ion equilibria of the genetic variants of bovine β-lactoglobulin. Archives of Biochemistry and Biophysics, 118(1), 37-47.

Bell, K., McKenzie, H. A., & Shaw, D. C. (**1981**). Porcine β-lactoglobulin A and C: Occurrence, isolation and chemical properties. Molecular and Cellular Biochemistry, 35, 103-111.

Berton, C., Genot, C., & Ropers, M. H. (**2011**). Quantification of unadsorbed protein and surfactant emulsifiers in oil-in-water emulsions. Journal of colloid and interface science, 354(2), 739-748.

Biancalana, M., & Koide, S. (**2010**). Molecular mechanism of Thioflavin-T binding to amyloid fibrils. Biochimica et Biophysica Acta (BBA)-Proteins and Proteomics, 1804(7), 1405-1412.

Bitskinashvili, K., Gabriadze, I., Kutateladze, T., Vishnepolsky, B., Mikeladze, D., & Datukishvili, N. (**2018**). Effects of thermal-acid treatment on degradation and amplification of wheat and maize DNA. Journal of Food & Nutrition Research, 57(3).

Bleem, A., Christiansen, G., Madsen, D. J., Maric, H., Strømgaard, K., Bryers, J. D., ... & Otzen, D. E. (**2018**). Protein engineering reveals mechanisms of functional amyloid formation in Pseudomonas aeruginosa biofilms. Journal of molecular biology, 430(20), 3751-3763.

Böhm, M., Bäuml, C. A., Hardes, K., Steinmetzer, T., Roeser, D., Schaub, Y., ... & Imhof, D. (**2014**). Novel insights into structure and function of factor XIIIa-inhibitor tridegin. Journal of Medicinal Chemistry, 57(24), 10355-10365.

Bolder, S. G., Hendrickx, H., Sagis, L. M., & van der Linden, E. (**2006**). Fibril assemblies in aqueous whey protein mixtures. Journal of agricultural and food chemistry, 54(12), 4229-4234.

Bolder, S. G., Sagis, L. M., Venema, P., & van der Linden, E. (**2007**). Effect of stirring and seeding on whey protein fibril formation. Journal of agricultural and food chemistry, 55(14), 5661-5669.

Bolder, S. G., Vasbinder, A. J., Sagis, L. M., & van der Linden, E. (**2007**). Heat-induced whey protein isolate fibrils: Conversion, hydrolysis, and disulfide bond formation. International dairy journal, 17(7), 846-853.

Bolisetty, S., Adamcik, J., & Mezzenga, R. (**2011**). Snapshots of fibrillization and aggregation kinetics in multistranded amyloid β-lactoglobulin fibrils. Soft Matter, 7(2), 493-499.

Bolisetty, S., Harnau, L., Jung, J. M., & Mezzenga, R. (**2012**). Gelation, phase behavior, and dynamics of β-lactoglobulin amyloid fibrils at varying concentrations and ionic strengths. Biomacromolecules, 13(10), 3241-3252.

Bonarek, P., Loch, J. I., Tworzydło, M., Cooper, D. R., Milto, K., Wróbel, P., ... & Lewiński, K. (**2020**). Structure-based design approach to rational site-directed mutagenesis of β-lactoglobulin. Journal of Structural Biology, 210(2), 107493.

Bos, M. A., & Van Vliet, T. (**2001**). Interfacial rheological properties of adsorbed protein layers and surfactants: a review. Advances in colloid and interface science, 91(3), 437-471.

Bowen, H., Durrani, R., Delavault, A., Durand, E., Chenyu, J., Yiyang, L., ... & Fei, G. (**2022**). Application of deep eutectic solvents in protein extraction and purification. Frontiers in Chemistry, 10, 912411.

Bretthauer, R. K., & Castellino, F. J. (**1999**). Glycosylation of *Pichia pastoris*-derived proteins. Biotechnology and applied biochemistry, 30(3), 193-200.

Brownie, S. (**2006**). Why are elderly individuals at risk of nutritional deficiency?. International journal of nursing practice, 12(2), 110-118.

Brownlow, S., Cabral, J. H. M., Cooper, R., Flower, D. R., Yewdall, S. J., Polikarpov, I., ... & Sawyer, L. (**1997**). Bovine β-lactoglobulin at 1.8 Å resolution—still an enigmatic lipocalin. Structure, 5(4), 481-495.

Brune, S. E., Hoppenreijs, L. J., Kühl, T., Lautenbach, V., Walter, J., Peukert, W., ... & Biedendieck, R. (**2023**). Precision fermentation as a route to modify β-lactoglobulin structure through substitution of specific cysteine residues. International Dairy Journal, 147, 105772.

Burova, T. V., Choiset, Y., Tran, V., & Haertlé, T. (**1998**). Role of free Cys121 in stabilization of bovine beta-lactoglobulin B. Protein engineering, 11(11), 1065-1073.

Canales, M., Ballesteros, C., Moreno-Cid, J. A., Espinosa, A. M., Villar, M., & de la Fuente, J. (**2009**). Extractive bioconversion to produce the Aedes albopictus akirin in an aqueous two-phase system supporting *Pichia pastoris* growth and protein secretion. Biochemical engineering journal, 46(2), 105-114.

Cao, Y., & Mezzenga, R. (**2019**). Food protein amyloid fibrils: Origin, structure, formation, characterization, applications and health implications. Advances in colloid and interface science, 269, 334-356.

Catak, S., Monard, G., Aviyente, V., & Ruiz-López, M. F. (**2008**). Computational study on nonenzymatic peptide bond cleavage at asparagine and aspartic acid. The Journal of Physical Chemistry A, 112(37), 8752-8761.

Caughey, B., & Lansbury Jr, P. T. (**2003**). Protofibrils, pores, fibrils, and neurodegeneration: separating the responsible protein aggregates from the innocent bystanders. Annual review of neuroscience, 26(1), 267-298.

Chaichol, P., & Weeranoppanant, N. (**2023**). Advances in in-situ and in-line liquid-liquid extraction for bioprocess intensification. Reaction Chemistry & Engineering.

Chatani, E., Lee, Y. H., Yagi, H., Yoshimura, Y., Naiki, H., & Goto, Y. (**2009**). Ultrasonication-dependent production and breakdown lead to minimum-sized amyloid fibrils. Proceedings of the National Academy of Sciences, 106(27), 11119-11124.

Cheignon, C., Tomas, M., Bonnefont-Rousselot, D., Faller, P., Hureau, C., & Collin, F. (**2018**). Oxidative stress and the amyloid beta peptide in Alzheimer's disease. Redox biology, 14, 450-464.

Chen, D., Fang, F., Federici, E., Campanella, O., & Jones, O. G. (**2020**). Rheology, microstructure and phase behavior of potato starch-protein fibril mixed gel. Carbohydrate polymers, 239, 116247.

Chen, D., Narayanan, N., Federici, E., Yang, Z., Zuo, X., Gao, J., ... & Jones, O. G. (**2020**). Electrospinning induced orientation of protein fibrils. Biomacromolecules, 21(7), 2772-2785.

Chlup, P. H., Conery, J., & Stewart, G. G. (**2007**). Detection of mannan from *Saccharomyces cerevisiae* by flow cytometry. Journal of the American Society of Brewing Chemists, 65(3), 151-156.

Čížová, A., Korcová, J., Farkaš, P., & Bystrický, S. (**2017**). Efficient separation of mannan–protein mixtures by ionic liquid aqueous two-phase system, comparison with lectin affinity purification. International Journal of Biological Macromolecules, 98, 314-318.

Conchillo-Solé, O., de Groot, N. S., Avilés, F. X., Vendrell, J., Daura, X., & Ventura, S. (**2007**). AGGRESCAN: a server for the prediction and evaluation of" hot spots" of aggregation in polypeptides. BMC bioinformatics, 8, 1-17.

Creamer, L. K., Bienvenue, A., Nilsson, H., Paulsson, M., van Wanroij, M., Lowe, E. K., ... & Jiménez-Flores, R. (**2004**). Heat-induced redistribution of disulfide bonds in milk proteins. 1. Bovine β-lactoglobulin. Journal of Agricultural and Food Chemistry, 52(25), 7660-7668.

Creamer, L. K., Loveday, S. M., & Sawyer, L. (**2011**). Milk proteins | β-lactoglobulin.

Creamer, L. K., Nilsson, H. C., Paulsson, M. A., Coker, C. J., Hill, J. P., & Jimenez-Flores, R. (**2004**). Effect of genetic variation on the tryptic hydrolysis of bovine β-lactoglobulin A, B, and C. Journal of Dairy Science, 87(12), 4023-4032.

Croguennec, T., Mollé, D., Mehra, R., & Bouhallab, S. (**2004**). Spectroscopic characterization of heat-induced nonnative β-lactoglobulin monomers. Protein Science, 13(5), 1340-1346.

Croguennec, T., Renault, A., Bouhallab, S., & Pezennec, S. (**2006**). Interfacial and foaming properties of sulfydryl-modified bovine β-lactoglobulin. Journal of Colloid and Interface Science, 302(1), 32-39.

Da Silva Pinto, M., Bouhallab, S., De Carvalho, A. F., Henry, G., Putaux, J. L., & Leonil, J. (**2012**). Glucose slows down the heat-induced aggregation of β-lactoglobulin at neutral pH. Journal of agricultural and food chemistry, 60(1), 214-219.

Dairy Global Nutrition. (**2019**). Dairy Price Trends. https://dairyglobalnutrition.org/Price-and-Supply-Trends/Dairy-Price-Trends.

Dave, A. C., Loveday, S. M., Anema, S. G., Jameson, G. B., & Singh, H. (**2014**). Glycation as a tool to probe the mechanism of β-lactoglobulin nanofibril self-assembly. Journal of Agricultural and Food Chemistry, 62(14), 3269-3278.

Dave, A. C., Loveday, S. M., Anema, S. G., Jameson, G. B., & Singh, H. (**2014**). Modulating β-lactoglobulin nanofibril self-assembly at pH 2 using glycerol and sorbitol. Biomacromolecules, 15(1), 95-103.

Dave, A. C., Loveday, S. M., Anema, S. G., Loo, T. S., Norris, G. E., Jameson, G. B., & Singh, H. (**2013**). β-Lactoglobulin self-assembly: Structural changes in early stages and disulfide bonding in fibrils. Journal of Agricultural and Food Chemistry, 61(32), 7817-7828.

Davies, M. J. (**2005**). The oxidative environment and protein damage. Biochimica et Biophysica Acta (BBA)-Proteins and Proteomics, 1703(2), 93-109.

Davies, M. J. (**2016**). Protein oxidation and peroxidation. Biochemical journal, 473(7), 805-825.

Davis, J. P., & Foegeding, E. A. (**2004**). Foaming and interfacial properties of polymerized whey protein isolate. Journal of Food Science, 69(5), C404-C410.

Day, L. (**2013**). Proteins from land plants–potential resources for human nutrition and food security. Trends in Food Science & Technology, 32(1), 25-42.

De Groot, N. S., Pallarés, I., Avilés, F. X., Vendrell, J., & Ventura, S. (**2005**). Prediction of" hot spots" of aggregation in disease-linked polypeptides. BMC Structural Biology, 5, 1-15.

de Kort, E., Minor, M., Snoeren, T., van Hooijdonk, T., & van der Linden, E. (**2011**). Effect of calcium chelators on physical changes in casein micelles in concentrated micellar casein solutions. International Dairy Journal, 21(12), 907-913.

De Wit, J. N. (**2009**). Thermal behaviour of bovine β-lactoglobulin at temperatures up to 150 C. A review. Trends in Food Science & Technology, 20(1), 27-34.

Deepankumar, K., Lim, C., Polte, I., Zappone, B., Labate, C., De Santo, M. P., ... & Miserez, A. (**2020**). Supramolecular β-sheet suckerin–based underwater adhesives. Advanced Functional Materials, 30(16), 1907534.

Delahaije, R. J., & Wierenga, P. A. (**2022**). Hydrophobicity Enhances the Formation of Protein-Stabilized Foams. Molecules, 27(7), 2358.

R

Delahaije, R. J., Gruppen, H., Giuseppin, M. L., & Wierenga, P. A. (**2015**). Towards predicting the stability of protein-stabilized emulsions. Advances in Colloid and Interface Science, 219, 1-9.

Denton, H., Smith, M., Husi, H., Uhrin, D., Barlow, P. N., Batt, C. A., & Sawyer, L. (**1998**). Isotopically Labeled Bovine β-Lactoglobulin for NMR Studies Expressed in*Pichia pastoris*. Protein expression and purification, 14(1), 97-103.

Dombrowski, J., Johler, F., Warncke, M., & Kulozik, U. (**2016**). Correlation between bulk characteristics of aggregated β-lactoglobulin and its surface and foaming properties. Food Hydrocolloids, 61, 318-328.

Dong, A., Matsuura, J., Allison, S. D., Chrisman, E., Manning, M. C., & Carpenter, J. F. (**1996**). Infrared and circular dichroism spectroscopic characterization of structural differences between β-lactoglobulin A and B. Biochemistry, 35(5), 1450-1457.

Dong, A., Matsuura, J., Manning, M. C., & Carpenter, J. F. (**1998**). Intermolecular β-sheet results from trifluoroethanol-induced nonnative α-helical structure in β-sheet predominant proteins: Infrared and circular dichroism spectroscopic study. Archives of biochemistry and biophysics, 355(2), 275-281.

Dong, Y., Zhang, F., Wang, Z., Du, L., Hao, A., Jiang, B., ... & Xiu, Z. (**2012**). Extraction and purification of recombinant human serum albumin from *Pichia pastoris* broths using aqueous two-phase system combined with hydrophobic interaction chromatography. Journal of Chromatography A, 1245, 143-149.

dos Santos, N. V., de Carvalho Santos-Ebinuma, V., Pessoa Junior, A., & Pereira, J. F. B. (**2018**). Liquid–liquid extraction of biopharmaceuticals from fermented broth: trends and future prospects. Journal of Chemical Technology & Biotechnology, 93(7), 1845-1863.

Du, Q., Zhou, L., Lyu, F., Liu, J., & Ding, Y. (**2022**). The complex of whey protein and pectin: Interactions, functional properties and applications in food colloidal systems–A review. Colloids and Surfaces B: Biointerfaces, 210, 112253.

Dunstan, D. E., Hamilton-Brown, P., Asimakis, P., Ducker, W., & Bertolini, J. (**2009**). Shear-induced structure and mechanics of β-lactoglobulin amyloid fibrils. Soft Matter, 5(24), 5020-5028.

Dupuis, J. H., Cheung, L. K., Newman, L., Dee, D. R., & Yada, R. Y. (**2023**). Precision cellular agriculture: The future role of recombinantly expressed protein as food. Comprehensive Reviews in Food Science and Food Safety, 22(2), 882-912.

Ellman, G. L. (**1959**). Tissue sulfhydryl groups. Archives of biochemistry and biophysics, 82(1), 70-77.

Elofsson, U. M., Paulsson, M. A., Sellers, P., & Arnebrant, T. (**1996**). Adsorption during heat treatment related to the thermal unfolding/aggregation of β-lactoglobulins A and B. Journal of Colloid and Interface Science, 183(2), 408-415.

Euston, S. R., Hirst, R. L., & Hill, J. P. (**1999**). The emulsifying properties of β-lactoglobulin genetic variants A, B and C. Colloids and surfaces B: Biointerfaces, 12(3-6), 193-202.

Euston, S. R., Ur-Rehman, S., & Costello, G. (**2007**). Denaturation and aggregation of β-lactoglobulin—a preliminary molecular dynamics study. Food Hydrocolloids, 21(7), 1081-1091.

Farinha, I., Baptista, S., Reis, M. A., & Freitas, F. (**2022**). Influence of Dissolved Oxygen Level on Chitin–Glucan Complex and Mannans Production by the Yeast *Pichia pastoris*. Life, 12(2), 161.

Farrell Jr, H. M., Jimenez-Flores, R., Bleck, G. T., Brown, E. M., Butler, J. E., Creamer, L. K., ... & Swaisgood, H. E. (**2004**). Nomenclature of the proteins of cows' milk—Sixth revision. Journal of dairy science, 87(6), 1641-1674.

Fioramonti, S. A., Perez, A. A., Aríngoli, E. E., Rubiolo, A. C., & Santiago, L. G. (**2014**). Design and characterization of soluble biopolymer complexes produced by electrostatic self-assembly of a whey protein isolate and sodium alginate. Food Hydrocolloids, 35, 129-136.

Foegeding, E. A. (**2015**). Food protein functionality - a new model. Journal of food science, 80(12), C2670-C2677.

Foegeding, E. A., Davis, J. P., Doucet, D., & McGuffey, M. K. (**2002**). Advances in modifying and understanding whey protein functionality. Trends in Food Science & Technology, 13(5), 151-159.

Foegeding, E. A., Luck, P. J., & Davis, J. P. (**2006**). Factors determining the physical properties of protein foams. Food hydrocolloids, 20(2-3), 284-292.

Forge, V., Hoshino, M., Kuwata, K., Arai, M., Kuwajima, K., Batt, C. A., & Goto, Y. (**2000**). Is folding of β-lactoglobulin non-hierarchic? Intermediate with native-like β-sheet and non-native α-helix. Journal of molecular biology, 296(4), 1039-1051.

Fowler, D. M., Koulov, A. V., Balch, W. E., & Kelly, J. W. (**2007**). Functional amyloid–from bacteria to humans. Trends in biochemical sciences, 32(5), 217-224.

Francis, D. M., & Page, R. (**2010**). Strategies to optimize protein expression in *E. coli*. Current protocols in protein science, 61(1), 5-24.

Gao, Y. Z., Xu, H. H., Ju, T. T., & Zhao, X. H. (**2013**). The effect of limited proteolysis by different proteases on the formation of whey protein fibrils. Journal of Dairy Science, 96(12), 7383-7392.

García-Ortega, X., Cámara, E., Ferrer, P., Albiol, J., Montesinos-Seguí, J. L., & Valero, F. (**2019**). Rational development of bioprocess engineering strategies for recombinant protein production in *Pichia pastoris* (Komagataella phaffii) using the methanol-free GAP promoter. Where do we stand?. New biotechnology, 53, 24-34.

Gasymov, O. K., Abduragimov, A. R., & Glasgow, B. J. (**2011**). The conserved disulfide bond of human tear lipocalin modulates conformation and lipid binding in a ligand selective manner. Biochimica et Biophysica Acta (BBA)-Proteins and Proteomics, 1814(5), 671-683.

German Federal Institute for Risk Assessment (BfR). (**2021**). Proposed maximum levels for the addition of iodine to foods including food supplements. www.bfr.bund.de

Ghadami, S. A., Khodarahmi, R., Ghobadi, S., Ghasemi, M., & Pirmoradi, S. (**2011**). Amyloid fibril formation by native and modified bovine β-lactoglobulins proceeds through unfolded form of proteins: A comparative study. Biophysical Chemistry, 159(2-3), 311-320.

Giovani, G., Canuti, V., & Rosi, I. (**2010**). Effect of yeast strain and fermentation conditions on the release of cell wall polysaccharides. International journal of food microbiology, 137(2-3), 303-307.

Godovac-Zimmerman, J. Conti, A., Liberatori, J. & Braunitzer, G. (**1985**). The amino-acid sequence of β-lactoglobulin II from horse colostrum (Equus caballus, Perissodactyla): β-lactoglobulins are retinol-binding proteins.

Goers, J., Permyakov, S. E., Permyakov, E. A., Uversky, V. N., & Fink, A. L. (**2002**). Conformational prerequisites for α-lactalbumin fibrillization. Biochemistry, 41(41), 12546-12551.

Goldschmidt, L., Teng, P. K., Riek, R., & Eisenberg, D. (**2010**). Identifying the amylome, proteins capable of forming amyloid-like fibrils. Proceedings of the National Academy of Sciences, 107(8), 3487-3492.

Gorji, E. G., Rocchi, E., Schleining, G., Bender-Bojalil, D., Furtmüller, P. G., Piazza, L., ... & Toca-Herrera, J. L. (**2015**). Characterization of resveratrol–milk protein interaction. Journal of food engineering, 167, 217-225.

Gosal, W. S., Clark, A. H., & Ross-Murphy, S. B. (2004). Fibrillar β-lactoglobulin gels: Part 1. Fibril formation and structure. Biomacromolecules, 5(6), 2408-2419.

Gosal, W. S., Clark, A. H., Pudney, P. D., & Ross-Murphy, S. B. (**2002**). Novel amyloid fibrillar networks derived from a globular protein: β-lactoglobulin. Langmuir, 18(19), 7174-7181.

Gosal, W. S., Morten, I. J., Hewitt, E. W., Smith, D. A., Thomson, N. H., & Radford, S. E. (**2005**). Competing pathways determine fibril morphology in the self-assembly of β2-microglobulin into amyloid. Journal of molecular biology, 351(4), 850-864.

Green, J. D., Kreplak, L., Goldsbury, C., Blatter, X. L., Stolz, M., Cooper, G. S., ... & Aebi, U. (**2004**). Atomic force microscopy reveals defects within mica supported lipid bilayers induced by the amyloidogenic human amylin peptide. Journal of molecular biology, 342(3), 877-887.

Gregersen, N., Bolund, L., & Bross, P. (**2005**). Protein misfolding, aggregation, and degradation in disease. Molecular biotechnology, 31, 141-150.

Greving, I., Cai, M., Vollrath, F., & Schniepp, H. C. (**2012**). Shear-induced self-assembly of native silk proteins into fibrils studied by atomic force microscopy. Biomacromolecules, 13(3), 676-682.

Grossmann, L., & McClements, D. J. (**2021**). The science of plant-based foods: Approaches to create nutritious and sustainable plant-based cheese analogs. Trends in Food Science & Technology, 118, 207-229.

Guetouache, M., Guessas, B., & Medjekal, S. (**2014**). Composition and nutritional value of raw milk. J Issues Biol Sci Pharm Res, 2350, 1588.

Gupta, S. K., & Shukla, P. (**2017**). Sophisticated cloning, fermentation, and purification technologies for an enhanced therapeutic protein production: a review. Frontiers in pharmacology, 8, 419.

Hamada, D., & Dobson, C. M. (**2002**). A kinetic study of β-lactoglobulin amyloid fibril formation promoted by urea. Protein Science, 11(10), 2417-2426.

Hamada, D., & Goto, Y. (**1997**). The equilibrium intermediate of β-lactoglobulin with non-native α-helical structure. Journal of molecular biology, 269(4), 479-487.

Hamada, D., Kuroda, Y., Tanaka, T., & Goto, Y. (**1995**). High helical propensity of the peptide fragments derived from β-lactoglobulin, a predominantly β-sheet protein. Journal of molecular biology, 254(4), 737-746.

Hamada, D., Segawa, S. I., & Goto, Y. (**1996**). Non-native α-helical intermediate in the refolding of β-lactoglobulin, a predominantly β-sheet protein. Nature structural biology, 3(10), 868-873.

Hamada, D, Tanaka, T., Tartaglia, G. G., Pawar, A., Vendruscolo, M., Kawamura, M., ... & Dobson, C. M. (**2009**). Competition between folding, native-state dimerisation and amyloid aggregation in β-lactoglobulin. Journal of molecular biology, 386(3), 878-890.

Hamaguchi, T., Ono, K., Murase, A., & Yamada, M. (**2009**). Phenolic compounds prevent Alzheimer's pathology through different effects on the amyloid-β aggregation pathway. The American journal of pathology, 175(6), 2557-2565.

Hattori, M., Hiramatsu, K., Kurata, T., Nishiura, M., Takahashi, K., Ametani, A., & Kaminogawa, S. (**2005**). Complete refolding of bovine β-lactoglobulin requires disulfide bond formation under strict conditions. Biochimica et Biophysica Acta (BBA)-Proteins and Proteomics, 1752(2), 154-165.

Haug, I. J., Skar, H. M., Vegarud, G. E., Langsrud, T., & Draget, K. I. (**2009**). Electrostatic effects on β-lactoglobulin transitions during heat denaturation as studied by differential scanning calorimetry. Food Hydrocolloids, 23(8), 2287-2293.

Heldt, C. L., Zhang, S., & Belfort, G. (**2011**). Asymmetric amyloid fibril elongation: A new perspective on a symmetric world. Proteins: Structure, Function, and Bioinformatics, 79(1), 92-98.

Hellwig, M. (**2019**). The chemistry of protein oxidation in food. Angewandte Chemie International Edition, 58(47), 16742-16763.

Hendriks, C. L., & Van Vliet, L. J. (**2001**). DIPimage user manual: a scientific image processing toolbox.

Hettiarachchi, C. A., Melton, L. D., McGillivray, D. J., Loveday, S. M., Gerrard, J. A., & Williams, M. A. (**2016**). β-Lactoglobulin nanofibrils can be assembled into nanotapes via site-specific interactions with pectin. Soft matter, 12(3), 756-768.

Heyn, T. (**2020**). Influence of process factors on the formation and fragmentation of amyloid and amyloid-like aggregates from beta-lactoglobulin (Doctoral dissertation).

Heyn, T. R., Garamus, V. M., Neumann, H. R., Uttinger, M. J., Guckeisen, T., Heuer, M., ... & Keppler, J. K. (**2019**). Influence of the polydispersity of pH 2 and pH 3.5 beta-lactoglobulin amyloid fibril solutions on analytical methods. European Polymer Journal, 120, 109211.

Heyn, T. R., Mayer, J., Neumann, H. R., Selhuber-Unkel, C., Kwade, A., Schwarz, K., & Keppler, J. K. (**2020**). The threshold of amyloid aggregation of beta-lactoglobulin: Relevant factor combinations. Journal of Food Engineering, 283, 110005.

Heyn, T. R., Uttinger, M. J., Kwade, A., Peukert, W., Keppler, J. K., & Schwarz, K. (**2021**). Whey protein (amyloid)-aggregates in oil-water systems: The process-related comminution effect. Journal of Food Engineering, 311, 110730.

Hidalgo, J., Kruseman, J., & Bohren, H. U. (**1973**). Recovery of whey proteins with sodium hexametaphosphate. Journal of Dairy Science, 56(8), 988-993.

Hinderink, E. B., Münch, K., Sagis, L., Schroën, K., & Berton-Carabin, C. C. (**2019**). Synergistic stabilisation of emulsions by blends of dairy and soluble pea proteins: Contribution of the interfacial composition. Food Hydrocolloids, 97, 105206.

Hoffmann, M. A., & van Mil, P. J. (**1997**). Heat-induced aggregation of β-lactoglobulin: role of the free thiol group and disulfide bonds. Journal of Agricultural and Food Chemistry, 45(8), 2942-2948.

Hoppenreijs, L. J. G., Annibal, A., Vreeke, G. J. C., Boom, R. M., & Keppler, J. K. (**2024**). Food proteins from yeast-based precision fermentation: Simple purification of recombinant β-lactoglobulin using polyphosphate. Food Research International, 176, 113801.

Hoppenreijs, L. J. G., Fitzner, L., Ruhmlieb, T., Heyn, T. R., Schild, K., Van der Goot, A. J., ... & Keppler, J. K. (**2022**). Engineering amyloid and amyloid-like morphologies of β-lactoglobulin. Food Hydrocolloids, 124, 107301.

Hoppenreijs, L. J., Brune, S. E., Biedendieck, R., Krull, R., Boom, R. M., & Keppler, J. K. (**2023**). Fibrillization of β-lactoglobulin at pH 2.0: Impact of cysteine substitution and disulfide bond reduction. Food Hydrocolloids, 141, 108727.

Hoppenreijs, L. J., Overbeck, A., Brune, S. E., Biedendieck, R., Kwade, A., Krull, R., ... & Keppler, J. K. (**2023**). Amyloid-like aggregation of recombinant β-lactoglobulin at pH 3.5 and 7.0: Is disulfide bond removal the key to fibrillization?. International Journal of Biological Macromolecules, 242, 124855.

Housmans, J. A., Houben, B., Monge-Morera, M., Asvestas, D., Nguyen, H. H., Tsaka, G., ... & Schymkowitz, J. (**2022**). Investigating the sequence determinants of the curling of amyloid fibrils using ovalbumin as a case study. Biomacromolecules, 23(9), 3779-3797.

Hu, B., Shen, Y., Adamcik, J., Fischer, P., Schneider, M., Loessner, M. J., & Mezzenga, R. (**2018**). Polyphenol-binding amyloid fibrils self-assemble into reversible hydrogels with antibacterial activity. ACS nano, 12(4), 3385-3396.

Huang, X. L., Catignani, G. L., Foegeding, E. A., & Swaisgood, H. E. (**1994**). Comparison of the Gelation Properties of. beta.-Lactoglobulin Genetic Variants A and B. Journal of Agricultural and Food Chemistry, 42(5), 1064-1067.

Humblet-Hua, N. P. K., van der Linden, E., & Sagis, L. M. (**2012**). Microcapsules with protein fibril reinforced shells: effect of fibril properties on mechanical strength of the shell. Journal of agricultural and food chemistry, 60(37), 9502-9511.

Humblet-Hua, N. P. K., van der Linden, E., & Sagis, L. M. (**2013**). Surface rheological properties of liquid–liquid interfaces stabilized by protein fibrillar aggregates and protein–polysaccharide complexes. Soft Matter, 9(7), 2154-2165.

Imre, T., Zsila, F., & Szabó, P. T. (**2003**). Electrospray mass spectrometric investigation of the binding of cis-parinaric acid to bovine beta-lactoglobulin and study of the ligand-binding site of the protein using limited proteolysis. Rapid communications in mass spectrometry, 17(22), 2464-2470.

Inglis, A. S. (**1967**). Cleavage at aspartic acid. In Methods in enzymology, 11, 255-263. Academic Press.

Institute of Medicine. (**2001**). Dietary Reference Intakes for Vitamin A, Vitamin K, Arsenic, Boron, Chromium, Copper, Iodine, Iron, Manganese, Molybdenum, Nickel, Silicon, Vanadium, and Zinc. In Dietary Reference Intakes for Vitamin A, Vitamin K, Arsenic, Boron, Chromium, Copper, Iodine, Iron, Manganese, Molybdenum, Nickel, Silicon, Vanadium, and Zinc. National Academies Press.

Intergovernmental Panel on Climate Change. (**2019**). In Climate Change and Land. IPCC Special Report on Climate Change, Desertification, Land Degradation, Sustainable Land Management, Food Security, and Greenhouse Gas Fluxes in Terrestrial Ecosystems. Cambridge University Press.

Invernizzi, G., Annoni, E., Natalello, A., Doglia, S. M., & Lotti, M. (**2008**). *In vivo* aggregation of bovine β-lactoglobulin is affected by Cys at position 121. Protein expression and purification, 62(1), 111-115.

Invitrogen. (**2014**). User guide: Pichia expression kit for expression of recombinant proteins in *Pichia pastoris*.

Ipsen, R., & Otte, J. (**2004**). The relation between protein structure, interfacial rheology and foam formation for various milk proteins. Annu. Trans. Nord. Rheol. Soc, 21, 143-178.

Ipsen, R., Otte, J., Sharma, R., Nielsen, A., Hansen, L. G., & Qvist, K. B. (**2001**). Effect of limited hydrolysis on the interfacial rheology and foaming properties of β-lactoglobulin A. Colloids and Surfaces B: Biointerfaces, 21(1-3), 173-178.

Jackson, M., & Mantsch, H. H. (**1995**). The use and misuse of FTIR spectroscopy in the determination of protein structure. Critical reviews in biochemistry and molecular biology, 30(2), 95-120.

Jahic, M., Veide, A., Charoenrat, T., Teeri, T., & Enfors, S. O. (**2006**). Process technology for production and recovery of heterologous proteins with *Pichia pastoris*. Biotechnology progress, 22(6), 1465-1473.

R

Jaklin, M., Hritz, J., & Hribar-Lee, B. (**2022**). A new fibrillization mechanism of β-lactoglobulin in glycine solutions. International journal of biological macromolecules, 216, 414-425.

Jansens, K. J., Rombouts, I., Grootaert, C., Brijs, K., Van Camp, J., Van der Meeren, P., ... & Delcour, J. A. (**2019**). Rational design of amyloid-like fibrillary structures for tailoring food protein techno-functionality and their potential health implications. Comprehensive Reviews in Food Science and Food Safety, 18(1), 84-105.

Jayat, D., Gaudin, J. C., Chobert, J. M., Burova, T. V., Holt, C., McNae, I., ... & Haertlé, T. (**2004**). A recombinant C121S mutant of bovine β-lactoglobulin is more susceptible to peptic digestion and to denaturation by reducing agents and heating. Biochemistry, 43(20), 6312-6321.

Jayawardena, N., Kaur, M., Nair, S., Malmstrom, J., Goldstone, D., Negron, L., ... & Domigan, L. J. (**2017**). Amyloid fibrils from hemoglobin. Biomolecules, 7(2), 37.

Jordens, S., Adamcik, J., Amar-Yuli, I., & Mezzenga, R. (**2011**). Disassembly and reassembly of amyloid fibrils in Water– Ethanol mixtures. Biomacromolecules, 12(1), 187-193.

Jordens, S., Isa, L., Usov, I., & Mezzenga, R. (2013). Non-equilibrium nature of two-dimensional isotropic and nematic coexistence in amyloid fibrils at liquid interfaces. Nature communications, 4(1), 1917.

Jordens, S., Riley, E. E., Usov, I., Isa, L., Olmsted, P. D., & Mezzenga, R. (**2014**). Adsorption at liquid interfaces induces amyloid fibril bending and ring formation. ACS nano, 8(11), 11071-11079.

Jovanović, S., Barać, M., & Maćej, O. (**2005**). Whey proteins-properties and possibility of application. Mljekarstvo, 55(3), 215-233.

Jung, J. M., Gunes, D. Z., & Mezzenga, R. (**2010**). Interfacial activity and interfacial shear rheology of native β-lactoglobulin monomers and their heat-induced fibers. Langmuir, 26(19), 15366-15375.

Jung, J. M., Savin, G., Pouzot, M., Schmitt, C., & Mezzenga, R. (**2008**). Structure of heat-induced β-lactoglobulin aggregates and their complexes with sodium-dodecyl sulfate. Biomacromolecules, 9(9), 2477-2486.

Jurado, R., Adamcik, J., López-Haro, M., González-Vera, J. A., Ruiz-Arias, A., Sánchez-Ferrer, A., ... & Gálvez, N. (**2018**). Apoferritin protein amyloid fibrils with tunable chirality and polymorphism. Journal of the American Chemical Society, 141(4), 1606-1613.

Kalidas, C., Joshi, L., & Batt, C. (**2001**). Characterization of glycosylated variants of β-lactoglobulin expressed in *Pichia pastoris*. Protein Engineering, 14(3), 201-207.

Kamada, A., Mittal, N., Söderberg, L. D., Ingverud, T., Ohm, W., Roth, S. V., ... & Lendel, C. (**2017**). Flow-assisted assembly of nanostructured protein microfibers. Proceedings of the National Academy of Sciences, 114(6), 1232-1237.

Kar, S. R., Kingsbury, J. S., Lewis, M. S., Laue, T. M., & Schuck, P. (**2000**). Analysis of transport experiments using pseudo-absorbance data. Analytical Biochemistry, 285(1), 135-142.

Karbasi, M., Sánchez-Ferrer, A., Adamcik, J., Askari, G., Madadlou, A., & Mezzenga, R. (**2021**). Covalent β-lactoglobulin-maltodextrin amyloid fibril conjugate prepared by the Maillard reaction. Food chemistry, 342, 128388.

Karlsson, J. O., & Röös, E. (**2019**). Resource-efficient use of land and animals—environmental impacts of food systems based on organic cropping and avoided food-feed competition. Land Use Policy, 85, 63-72.

Katakura, Y., Ametani, A., Totsuka, M., Nagafuchi, S. Y., & Kaminogawa, S. (**1999**). Accelerated secretion of mutant β-lactoglobulin in *Saccharomyces cerevisiae* resulting from a single amino acid substitution. Biochimica et Biophysica Acta (BBA)-Protein Structure and Molecular Enzymology, 1432(2), 302-312.

Katou, H., Kanno, T., Hoshino, M., Hagihara, Y., Tanaka, H., Kawai, T., ... & Goto, Y. (**2002**). The role of disulfide bond in the amyloidogenic state of β2-microglobulin studied by heteronuclear NMR. Protein science, 11(9), 2218-2229.

Kaur, J., & Sharma, R. (**2006**). Directed evolution: an approach to engineer enzymes. Critical reviews in biotechnology, 26(3), 165-199.

Kavanagh, G. M., Clark, A. H., & Ross-Murphy, S. B. (**2000**). Heat-induced gelation of globular proteins: part 3. Molecular studies on low pH β-lactoglobulin gels. International Journal of Biological Macromolecules, 28(1), 41-50.

Kayser, J. J., Arnold, P., Steffen-Heins, A., Schwarz, K., & Keppler, J. K. (**2020**). Functional ethanol-induced fibrils: Influence of solvents and temperature on amyloid-like aggregation of beta-lactoglobulin. Journal of Food Engineering, 270, 109764.

Kazem-Farzandi, N., Taheri-Kafrani, A., & Haertlé, T. (**2015**). β-lactoglobulin mutation Ala86Gln improves its ligand binding and reduces its immunoreactivity. International journal of biological macromolecules, 81, 340-348.

Kella, N. K. D., & Kinsella, J. E. (**1988**). Enhanced thermodynamic stability of β-lactoglobulin at low pH. A possible mechanism. Biochemical Journal, 255(1), 113-118.

Kella, N. K., Yang, S. T., & Kinsella, J. E. (**1989**). Effect of disulfide bond cleavage on structural and interfacial properties of whey proteins. Journal of Agricultural and Food Chemistry, 37(5), 1203-1210.

Keppler, J. K., Heyn, T. R., Meissner, P. M., Schrader, K., & Schwarz, K. (**2019**). Protein oxidation during temperature-induced amyloid aggregation of beta-lactoglobulin. Food Chemistry, 289, 223-231.

Keppler, J. K., Heyse, A., Scheidler, E., Uttinger, M. J., Fitzner, L., Jandt, U., ... & Biedendieck, R. (**2021**). Towards recombinantly produced milk proteins: Physicochemical and emulsifying properties of engineered whey protein beta-lactoglobulin variants. Food Hydrocolloids, 110, 106132.

Khan, J. M., Qadeer, A., Chaturvedi, S. K., Ahmad, E., Abdul Rehman, S. A., Gourinath, S., & Khan, R. H. (2012). SDS can be utilized as an amyloid inducer: a case study on diverse proteins. PloS one, 7(1), e29694.

Kielkopf, C. L., Bauer, W., & Urbatsch, I. L. (**2021**). Expression of cloned genes in *Pichia pastoris* using the methanol-inducible promoter AOX1. Cold Spring Harbor Protocols, 2021(1), pdb-prot102160.

Kim, T. R., Goto, Y., Hirota, N., Kuwata, K., Denton, H., Wu, S. Y., ... & Batt, C. A. (**1997**). High-level expression of bovine beta-lactoglobulin in *Pichia pastoris* and characterization of its physical properties. Protein engineering, 10(11), 1339-1345.

Kleiner-Grote, G. R., Risse, J. M., & Friehs, K. (**2018**). Secretion of recombinant proteins from *E. coli*. Engineering in Life Sciences, 18(8), 532-550.

Knowles, T. P., & Mezzenga, R. (**2016**). Amyloid fibrils as building blocks for natural and artificial functional materials. Advanced materials, 28(31), 6546-6561.

Knowles, T. P., Oppenheim, T. W., Buell, A. K., Chirgadze, D. Y., & Welland, M. E. (**2010**). Nanostructured films from hierarchical self-assembly of amyloidogenic proteins. Nature nanotechnology, 5(3), 204-207.

Kong, F., Kang, S., Zhang, J., Jiang, L., Liu, Y., Yang, M., ... & Yue, X. (**2022**). The non-covalent interactions between whey protein and various food functional ingredients. Food Chemistry, 394, 133455.

Kosters, H. A., Wierenga, P. A., & Gruppen, H. (**2010**). SELDI-TOF-MS as a rapid tool to study food related protein–peptide interactions. Food Hydrocolloids, 24(6-7), 667-673.

Krachmarova, E., Ivanov, I., & Nacheva, G. (**2020**). Nucleic acids in inclusion bodies obtained from *E. coli* cells expressing human interferon-gamma. Microbial Cell Factories, 19(1), 1-9.

Krátký, Z., Biely, P., & Bauer, Š. (**1975**). Wall mannan of *Saccharomyces cerevisiae*: Metabolic stability and release into growth medium. Biochimica et Biophysica Acta (BBA)-General Subjects, 404(1), 1-6.

Krebs, M. R., Bromley, E. H., & Donald, A. M. (**2005**). The binding of thioflavin-T to amyloid fibrils: localisation and implications. Journal of structural biology, 149(1), 30-37.

Kroes-Nijboer, A., Venema, P., & van der Linden, E. (**2012**). Fibrillar structures in food. Food & function, 3(3), 221-227.

Kunaschk, M., Schmalz, V., Dietrich, N., Dittmar, T., & Worch, E. (**2015**). Novel regeneration method for phosphate loaded granular ferric (hydr) oxide–A contribution to phosphorus recycling. Water research, 71, 219-226.

Kuncheva, M., Pavlova, K., Panchev, I., & Dobreva, S. (**2007**). Emulsifying power of mannan and glucomannan produced by yeasts. International Journal of Cosmetic Science, 29(5), 377-384.

Lajnaf, R., Picart-Palmade, L., Attia, H., Marchesseau, S., & Ayadi, M. A. (**2022**). Foaming and air-water interfacial properties of camel milk proteins compared to bovine milk proteins. Food Hydrocolloids, 126, 107470.

Lambrecht, M. A., Jansens, K. J., Rombouts, I., Brijs, K., Rousseau, F., Schymkowitz, J., & Delcour, J. A. (**2019**). Conditions governing food protein amyloid fibril formation. Part II: Milk and legume proteins. Comprehensive Reviews in Food Science and Food Safety, 18(4), 1277-1291.

Langton, M., & Hermansson, A. M. (**1992**). Fine-stranded and particulate gels of β-lactoglobulin and whey protein at varying pH. Food Hydrocolloids, 5(6), 523-539.

Lara, C., Adamcik, J., Jordens, S., & Mezzenga, R. (**2011**). General self-assembly mechanism converting hydrolyzed globular proteins into giant multistranded amyloid ribbons. Biomacromolecules, 12(5), 1868-1875.

Lautenbach, V., Hosseinpour, S., & Peukert, W. (**2021**). Isoelectric point of proteins at hydrophobic interfaces. Frontiers in Chemistry, 9, 712978.

Lea, A. S., Pungor, A., Hlady, V., Andrade, J. D., Herron, J. N., & Voss Jr, E. W. (**1992**). Manipulation of proteins on mica by atomic force microscopy. Langmuir, 8(1), 68-73.

Lee, G., Lee, W., Lee, H., Lee, C. Y., Eom, K., & Kwon, T. (**2015**). Self-assembled amyloid fibrils with controllable conformational heterogeneity. Scientific Reports, 5(1), 16220.

Lee, J. S., Um, E., Park, J. K., & Park, C. B. (**2008**). Microfluidic self-assembly of insulin monomers into amyloid fibrils on a solid surface. Langmuir, 24(14), 7068-7071.

Lee, S. P., Kim, D. S., Watkins, S., & Batt, C. A. (**1994**). Reducing whey syneresis in yogurt by the addition of a thermolabile variant of β-lactoglobulin. Bioscience, biotechnology, and biochemistry, 58(2), 309-313.

Lensch, A., Duwenig, E., Dederer, H. G., Kärenlampi, S. O., Custers, R., Borg, A., & Wyss, M. (**2022**). Recombinant DNA in fermentation products is of no regulatory relevance. Food Control, 141, 109170.

Li, C., Engholm-Keller, K., & Lund, M. N. (**2022**). Site-Specific Characterization of Heat-Induced Disulfide Rearrangement in Beta-Lactoglobulin by Liquid Chromatography–Mass Spectrometry. Journal of agricultural and food chemistry, 70(3), 847-856.

Lin-Cereghino, G. P., Stark, C. M., Kim, D., Chang, J., Shaheen, N., Poerwanto, H., ... & Lin-Cereghino, J. (**2013**). The effect of α-mating factor secretion signal mutations on recombinant protein expression in *Pichia pastoris*. Gene, 519(2), 311-317.

Linder, T. (**2023**). Beyond Agriculture: How Microorganisms Can Revolutionize Global Food Production. ACS food science & technology, 3(7), 1144-1152.

Lindmark Månsson, H. (**2008**). Fatty acids in bovine milk fat. Food & nutrition research, 52(1), 1821.

Liu, G., & Zhong, Q. (**2013**). Dispersible and thermal stable nanofibrils derived from glycated whey protein. Biomacromolecules, 14(7), 2146-2153.

Liu, G., Li, W., Qin, X., & Zhong, Q. (**2021**). Flexible protein nanofibrils fabricated in aqueous ethanol: Physical characteristics and properties of forming emulsions of conjugated linolenic acid. Food Hydrocolloids, 114, 106573.

Liu, H. C., Chen, W. L., & Mao, S. J. T. (**2007**). Antioxidant nature of bovine milk β-lactoglobulin. Journal of dairy science, 90(2), 547-555.

Liu, P., O'mara, B. W., Warrack, B. M., Wu, W., Huang, Y., Zhang, Y., ... & Russell, R. J. (**2010**). A tris (2-carboxyethyl) phosphine (TCEP) related cleavage on cysteine-containing proteins. Journal of the American Society for Mass Spectrometry, 21, 837-844.

Livney, Y. D., & Dalgleish, D. G. (**2004**). Specificity of disulfide bond formation during thermal aggregation in solutions of β-lactoglobulin B and κ-casein A. Journal of agricultural and food chemistry, 52(17), 5527-5532.

Loch, J. I., Bonarek, P., Tworzydło, M., Polit, A., Hawro, B., Łach, A., ... & Lewiński, K. (**2016**). Engineered β-lactoglobulin produced in *E. coli*: purification, biophysical and structural characterisation. Molecular Biotechnology, 58, 605-618.

Loveday, S. M., & Gunning, A. P. (**2018**). Nanomechanics of pectin-linked β-lactoglobulin nanofibril bundles. Biomacromolecules, 19(7), 2834-2840.

Loveday, S. M., Anema, S. G., & Singh, H. (**2017**). β-Lactoglobulin nanofibrils: The long and the short of it. International Dairy Journal, 67, 35-45.

Loveday, S. M., Su, J., Rao, M. A., Anema, S. G., & Singh, H. (**2012**). Whey protein nanofibrils: Kinetic, rheological and morphological effects of group IA and IIA cations. International dairy journal, 26(2), 133-140.

Loveday, S. M., Wang, X. L., Rao, M. A., Anema, S. G., & Singh, H. (**2011**). Effect of pH, NaCl, CaCl2 and temperature on self-assembly of β-lactoglobulin into nanofibrils: A central composite design study. Journal of agricultural and food chemistry, 59(15), 8467-8474.

Loveday, S. M., Wang, X. L., Rao, M. A., Anema, S. G., & Singh, H. (**2012**). β-Lactoglobulin nanofibrils: Effect of temperature on fibril formation kinetics, fibril morphology and the rheological properties of fibril dispersions. Food Hydrocolloids, 27(1), 242-249.

Loveday, S. M., Wang, X. L., Rao, M. A., Anema, S. G., Creamer, L. K., & Singh, H. (**2010**). Tuning the properties of β-lactoglobulin nanofibrils with pH, NaCl and CaCl2. International Dairy Journal, 20(9), 571-579.

Lux, J., Azarkh, M., Fitzner, L., Keppler, J. K., Schwarz, K., Drescher, M., & Steffen-Heins, A. (**2021**). Amyloid aggregation of spin-labeled β-lactoglobulin. Part II: Identification of spin-labeled protein and peptide sequences after amyloid aggregation. Food Hydrocolloids, 112, 106174.

Lux, J., Kieserling, H., Koop, J., Drusch, S., Schwarz, K., Keppler, J. K., & Steffen-Heins, A. (**2023**). Identification of an optimized ratio of amyloid and non-amyloid fractions in engineered fibril solutions from whey protein isolate for improved foaming. Colloids and Surfaces A: Physicochemical and Engineering Aspects, 660, 130849.

Ma, B., Zhang, F., Liu, Y., Xie, J., & Wang, X. (**2017**). Resveratrol induces the conversion from amyloid to amorphous aggregation of β-lactoglobulin. Protein and Peptide Letters, 24(12), 1113-1119.

Macchi, F., Hoffmann, S. V., Carlsen, M., Vad, B., Imparato, A., Rischel, C., & Otzen, D. E. (**2011**). Mechanical stress affects glucagon fibrillization kinetics and fibril structure. Langmuir, 27(20), 12539-12549.

Mackie, A. R., Husband, F. A., Holt, C., & Wilde, P. J. (**1999**). Adsorption of β-Lactoglobulin variants A and B to the air–water interface. International journal of food science & technology, 34(5-6), 509-516.

Mahadevan, K., & Farmer, L. (**2006**). Key odor impact compounds in three yeast extract pastes. Journal of Agricultural and Food Chemistry, 54(19), 7242-7250.

Mahmoudi, N., Mehalebi, S., Nicolai, T., Durand, D., & Riaublanc, A. (**2007**). Light-scattering study of the structure of aggregates and gels formed by heat-denatured whey protein isolate and β-lactoglobulin at neutral pH. Journal of Agricultural and Food Chemistry, 55(8), 3104-3111.

Mailliart, P., & Ribadeau-Dumas, B. (**1988**). Preparation of β-lactoglobulin and p-lactoglobulin-free proteins from whey retentate by NaCl salting out at low pH. Journal of Food Science, 53(3), 743-745.

Maity, S., Pal, S., Sardar, S., Sepay, N., Parvej, H., Begum, S., ... & Halder, U. C. (**2018**). Inhibition of amyloid fibril formation of β-lactoglobulin by natural and synthetic curcuminoids. New Journal of Chemistry, 42(23), 19260-19271.

Maity, S., Sepay, N., Pal, S., Sardar, S., Parvej, H., Pal, S., ... & Halder, U. C. (**2021**). Modulation of amyloid fibrillization of bovine β-lactoglobulin by selective methionine oxidation. RSC advances, 11(19), 11192-11203.

Makarava, N., & Baskakov, I. V. (**2008**). The same primary structure of the prion protein yields two distinct self-propagating states. Journal of Biological Chemistry, 283(23), 15988-15996.

Manderson, G. A. (**1998**). The effect of heat on the structure and aggregation behaviour of bovine b-lactoglobulins A, B and C. Doctoral dissertation, PhD thesis, Massey University, Palmerston North, New Zealand.

Mantovani, R. A., de Figueiredo Furtado, G., Netto, F. M., & Cunha, R. L. (**2018**). Assessing the potential of whey protein fibril as emulsifier. Journal of Food Engineering, 223, 99-108.

Mantovani, R. A., Fattori, J., Michelon, M., & Cunha, R. L. (**2016**). Formation and pH-stability of whey protein fibrils in the presence of lecithin. Food Hydrocolloids, 60, 288-298.

Martell, A. E., & Smith, R. M. (**1974**). Critical stability constants (Vol. 1, p. 135). New York: Plenum press.

Martin, A. H., Grolle, K., Bos, M. A., Stuart, M. A. C., & van Vliet, T. (**2002**). Network forming properties of various proteins adsorbed at the air/water interface in relation to foam stability. Journal of Colloid and Interface Science, 254(1), 175-183.

Mattick, C. S. (**2018**). Cellular agriculture: the coming revolution in food production. Bulletin of the Atomic Scientists, 74(1), 32-35.

R

McClements, D. J. (**2006**). Non-covalent interactions between proteins and polysaccharides. Biotechnology advances, 24(6), 621-625.

McSwiney, M., Singh, H., Campanella, O., & Creamer, L. K. (**1994**). Thermal gelation and denaturation of bovine β-lactoglobulins A and B. Journal of Dairy Research, 61(2), 221-232.

Melachouris, N. (**1972**). Interactions of. beta.-lactoglobulin with polyphosphates. Journal of Agricultural and Food Chemistry, 20(4), 798-802.

Melina, V., Craig, W., & Levin, S. (**2016**). Position of the Academy of Nutrition and Dietetics: vegetarian diets. Journal of the Academy of Nutrition and Dietetics, 116(12), 1970-1980.

Meng, Y., Wei, Z., & Xue, C. (**2022**). Protein fibrils from different food sources: A review of fibrillization conditions, properties, applications and research trends. Trends in Food Science & Technology, 121, 59-75.

Mercade-Prieto, R., & Gunasekaran, S. (**2016**). Gelation and Thickening with Globular Proteins at Low Temperatures. Novel Food Processing: Effects on Rheological and Functional Properties, 46, 147.

Mirmoghtadaie, L., Aliabadi, S. S., & Hosseini, S. M. (**2016**). Recent approaches in physical modification of protein functionality. Food chemistry, 199, 619-627.

Mitra, A., & Sarkar, N. (**2022**). The role of intra and inter-molecular disulfide bonds in modulating amyloidogenesis: A review. Archives of Biochemistry and Biophysics, 716, 109113.

Mleko, S., Li-Chan, E. C. Y., & Pikus, S. (**1997**). Interactions of κ-carrageenan with whey proteins in gels formed at different pH. Food Research International, 30(6), 427-433.

Mocanu, C. S., Jureschi, M., & Drochioiu, G. (**2020**). Aluminium binding to modified amyloid-β peptides: Implications for alzheimer's disease. Molecules, 25(19), 4536.

Mohammadian, M., Salami, M., Momen, S., Alavi, F., Emam-Djomeh, Z., & Moosavi-Movahedi, A. A. (**2019**). Enhancing the aqueous solubility of curcumin at acidic condition through the complexation with whey protein nanofibrils. Food Hydrocolloids, 87, 902-914.

Mohanty, D. P., Mohapatra, S., Misra, S., & Sahu, D. P. (**2016**). Milk derived bioactive peptides and their impact on human health–A review. Saudi journal of biological sciences, 23(5), 577-583.

Monera, O. D., Sereda, T. J., Zhou, N. E., Kay, C. M., & Hodges, R. S. (**1995**). Relationship of sidechain hydrophobicity and α-helical propensity on the stability of the single-stranded amphipathic α-helix. Journal of peptide science: an official publication of the European Peptide Society, 1(5), 319-329.

Monge-Morera, M., Lambrecht, M. A., Deleu, L. J., Gallardo, R., Louros, N. N., De Vleeschouwer, M., ... & Delcour, J. A. (**2020**). Processing induced changes in food proteins: Amyloid formation during boiling of hen egg white. Biomacromolecules, 21(6), 2218-2228.

Monge-Morera, M., Lambrecht, M. A., Deleu, L. J., Louros, N. N., Rousseau, F., Schymkowitz, J., & Delcour, J. A. (**2021**). Heating wheat gluten promotes the formation of amyloid-like fibrils. ACS omega, 6(3), 1823-1833.

Moores, B., Drolle, E., Attwood, S. J., Simons, J., & Leonenko, Z. (**2011**). Effect of surfaces on amyloid fibril formation. PLoS One, 6(10), e25954.

Mottet, A., de Haan, C., Falcucci, A., Tempio, G., Opio, C., & Gerber, P. (**2017**). Livestock: On our plates or eating at our table? A new analysis of the feed/food debate. Global food security, 14, 1-8.

Munialo, C. D., Martin, A. H., Van Der Linden, E., & De Jongh, H. H. (**2014**). Fibril formation from pea protein and subsequent gel formation. Journal of Agricultural and Food Chemistry, 62(11), 2418-2427.

Murphy, J. R. (**1996**). Protein engineering and design for drug delivery. Current opinion in structural biology, 6(4), 541-545.

Nagy, P. (**2013**). Kinetics and mechanisms of thiol–disulfide exchange covering direct substitution and thiol oxidation-mediated pathways. Antioxidants & redox signaling, 18(13), 1623-1641.

Navarra, G., Tinti, A., Di Foggia, M., Leone, M., Militello, V., & Torreggiani, A. (**2014**). Metal ions modulate thermal aggregation of beta-lactoglobulin: A joint chemical and physical characterization. Journal of Inorganic Biochemistry, 137, 64-73.

Nerome, S., Onishi, M., Saito, D., Mizobuchi, A., Ando, T., Daira, Y., ... & Azuma, M. (**2020**). Cell surface changes that advance the application of using yeast as a food emulsifier. Food chemistry, 315, 126264.

Nicorescu, I., Riaublanc, A., Loisel, C., Vial, C., Djelveh, G., Cuvelier, G., & Legrand, J. (**2009**). Impact of protein self-assemblages on foam properties. Food research international, 42(10), 1434-1445.

Nicoud, L., Lazzari, S., Balderas Barragán, D., & Morbidelli, M. (**2015**). Fragmentation of amyloid fibrils occurs in preferential positions depending on the environmental conditions. The Journal of Physical Chemistry B, 119(13), 4644-4652.

Nielsen, B. T., Singh, H., & Latham, J. M. (**1996**). Aggregation of bovine β-lactoglobulins A and B on heating at 75 C. International Dairy Journal, 6(5), 519-527.

Noyes, A., Godavarti, R., Titchener-Hooker, N., Coffman, J., & Mukhopadhyay, T. (**2014**). Quantitative high throughput analytics to support polysaccharide production process development. Vaccine, 32(24), 2819-2828.

Oboroceanu, D., Wang, L., Brodkorb, A., Magner, E., & Auty, M. A. (**2010**). Characterization of β-lactoglobulin fibrillar assembly using atomic force microscopy, polyacrylamide gel electrophoresis, and in situ Fourier transform infrared spectroscopy. Journal of Agricultural and Food Chemistry, 58(6), 3667-3673.

Oboroceanu, D., Wang, L., Magner, E., & Auty, M. A. (**2014**). Fibrillization of whey proteins improves foaming capacity and foam stability at low protein concentrations. Journal of Food Engineering, 121, 102-111.

Ohtomo, H., Fujiwara, K., & Ikeguchi, M. (**2012**). Important role of methionine 145 in dimerization of bovine β-lactoglobulin. The journal of biochemistry, 151(3), 329-334.

Olsen, K., Orlien, V., & Skibsted, L. H. (**2022**). Pressure denaturation of β-lactoglobulin: Volume changes for genetic A and B variants. International Dairy Journal, 133, 105416.

Omasits, U., Ahrens, C. H., Müller, S., & Wollscheid, B. (**2014**). Protter: interactive protein feature visualization and integration with experimental proteomic data. Bioinformatics, 30(6), 884-886.

Onwulata, C., & Huth, P. (**2009**). Whey processing, functionality and health benefits (Vol. 82). John Wiley & Sons.

Ow, S. Y., Bekard, I., & Dunstan, D. E. (**2018**). Effect of natural biopolymers on amyloid fibril formation and morphology. International journal of biological macromolecules, 106, 30-38.

Páli, T., & Marsh, D. (**2001**). Tilt, twist, and coiling in β-barrel membrane proteins: relation to infrared dichroism. Biophysical Journal, 80(6), 2789-2797.

Pandeirada, C. O., Merkx, D. W., Janssen, H. G., Westphal, Y., & Schols, H. A. (**2021**). TEMPO/NaClO2/NaOCl oxidation of arabinoxylans. Carbohydrate Polymers, 259, 117781.

Pelroy, G. A., & Spinelli, J. (**1971**). Availability of amino acids in sarcoplasmic fish proteins complexed with sodium hexametaphosphate. Journal of Food Science, 36(1), 144-146.

Peng, D., Yang, J., Li, J., Tang, C., & Li, B. (**2017**). Foams stabilized by β-lactoglobulin amyloid fibrils: Effect of pH. Journal of agricultural and food chemistry, 65(48), 10658-10665.

Peng, J., Calabrese, V., Geurtz, J., Velikov, K. P., Venema, P., & van der Linden, E. (**2019**). Composite gels containing whey protein fibrils and bacterial cellulose microfibrils. Journal of food science, 84(5), 1094-1103.

Perna, M., & Hewlings, S. (**2022**). Saturated fatty acid chain length and risk of cardiovascular disease: a systematic review. Nutrients, 15(1), 30.

Perriman, A. W., Henderson, M. J., Holt, S. A., & White, J. W. (**2007**). Effect of the air– water interface on the stability of β-Lactoglobulin. The Journal of Physical Chemistry B, 111(48), 13527-13537.

Peternel, Š., Grdadolnik, J., Gaberc-Porekar, V., & Komel, R. (**2008**). Engineering inclusion bodies for non denaturing extraction of functional proteins. Microbial cell factories, 7, 1-9.

Petkova, A. T., Leapman, R. D., Guo, Z., Yau, W. M., Mattson, M. P., & Tycko, R. (**2005**). Self-propagating, molecular-level polymorphism in Alzheimer's ß-amyloid fibrils. Science, 307(5707), 262-265.

Petsko, G. A., & Ringe, D. (**2004**). Protein structure and function. New Science Press.

Pettersen, E. F., Goddard, T. D., Huang, C. C., Meng, E. C., Couch, G. S., Croll, T. I., ... & Ferrin, T. E. (**2021**). UCSF ChimeraX: Structure visualization for researchers, educators, and developers. Protein Science, 30(1), 70-82.

Phillips, L. G., Hawks, S. E., & German, J. B. (**1995**). Structural Characteristics and foaming properties of. beta.-lactoglobulin: effects of shear rate and temperature. Journal of Agricultural and Food Chemistry, 43(3), 613-619.

R

Picotti, P., De Franceschi, G., Frare, E., Spolaore, B., Zambonin, M., Chiti, F., ... & Fontana, A. (**2007**). Amyloid fibril formation and disaggregation of fragment 1-29 of apomyoglobin: insights into the effect of pH on protein fibrillogenesis. Journal of molecular biology, 367(5), 1237-1245.

Poole, L. B. (**2015**). The basics of thiols and cysteines in redox biology and chemistry. Free Radical Biology and Medicine, 80, 148-157.

Porat, Y., Abramowitz, A., & Gazit, E. (**2006**). Inhibition of amyloid fibril formation by polyphenols: structural similarity and aromatic interactions as a common inhibition mechanism. Chemical biology & drug design, 67(1), 27-37.

Priemel, T., Degtyar, E., Dean, M. N., & Harrington, M. J. (**2017**). Rapid self-assembly of complex biomolecular architectures during mussel byssus biofabrication. Nature communications, 8(1), 14539.

Qi, X. L., Holt, C., McNulty, D., Clarke, D. T., Brownlow, S., & Jones, G. R. (**1997**). Effect of temperature on the secondary structure of β-lactoglobulin at pH 6.7, as determined by CD and IR spectroscopy: a test of the molten globule hypothesis. Biochemical Journal, 324(1), 341-346.

Qin, B. Y., Bewley, M. C., Creamer, L. K., Baker, E. N., & Jameson, G. B. (**1999**). Functional implications of structural differences between variants A and B of bovine β-lactoglobulin. Protein Science, 8(1), 75-83.

Qin, M., Zhang, J., & Wang, W. (**2006**). Effects of disulfide bonds on folding behavior and mechanism of the β-sheet protein tendamistat. Biophysical journal, 90(1), 272-286.

Qin, Z., & Buehler, M. J. (**2010**). Molecular dynamics simulation of the α-helix to β-sheet transition in coiled protein filaments: Evidence for a critical filament length scale. Physical Review Letters, 104(19), 198304.

Radovan, D., Smirnovas, V., & Winter, R. (**2008**). Effect of pressure on islet amyloid polypeptide aggregation: revealing the polymorphic nature of the fibrillization process. Biochemistry, 47(24), 6352-6360.

Rahaman, T., Vasiljevic, T., & Ramchandran, L. (**2015**). Conformational changes of β-lactoglobulin induced by shear, heat, and pH—Effects on antigenicity. Journal of dairy science, 98(7), 4255-4265.

Rahimi Araghi, L., & Dee, D. R. (**2020**). Cross-species and cross-polymorph seeding of lysozyme amyloid reveals a dominant polymorph. Frontiers in molecular biosciences, 7, 206.

Rahman, M. M., Pires, R. S., Herneke, A., Gowda, V., Langton, M., Biverstål, H., & Lendel, C. (**2023**). Food protein-derived amyloids do not accelerate amyloid β aggregation. Scientific Reports, 13(1), 985.

Rashchi, F., & Finch, J. A. (**2000**). Polyphosphates: a review their chemistry and application with particular reference to mineral processing. Minerals Engineering, 13(10-11), 1019-1035.

Rasouli, M., Abbasi, S., Azarikia, F., & Ettelaie, R. (**2020**). On the heat stability of whey protein: Effect of sodium hexametaphosphate. International Journal of Dairy Technology, 73(1), 46-56.

Ratledge, C., & Kristiansen, B. (**2006**). Basic biotechnology. Cambridge University Press.

Reddy, I. M., Kella, N. K., & Kinsella, J. E. (**1988**). Structural and conformational basis of the resistance of. beta.-lactoglobulin to peptic and chymotryptic digestion. Journal of agricultural and food chemistry, 36(4), 737-741.

Rivera del Rio, A., Möller, A. C., Boom, R. M., & Janssen, A. E. (**2022**). *In vitro* gastro-small intestinal digestion of conventional and mildly processed pea protein ingredients. Food Chemistry, 387, 132894.

Rizzuti, B., & Daggett, V. (**2013**). Using simulations to provide the framework for experimental protein folding studies. Archives of biochemistry and biophysics, 531(1-2), 128-135.

Robinson, T. E., Arkinstall, L. A., Cox, S. C., & Grover, L. M. (**2022**). Determining the structure of hexametaphosphate by titration and 31P-NMR spectroscopy. Comments on Inorganic Chemistry, 42(1), 47-59.

Rovnyagina, N. R., Budylin, G. S., Vainer, Y. G., Tikhonova, T. N., Vasin, S. L., Yakovlev, A. A., ... & Shirshin, E. A. (**2020**). Fluorescence lifetime and intensity of thioflavin T as reporters of different fibrillization stages: Insights obtained from fluorescence up-conversion and particle size distribution measurements. International Journal of Molecular Sciences, 21(17), 6169.

Rudge, S. R., & Ladisch, M. R. (**2020**). Industrial challenges of recombinant proteins. Current Applications of Pharmaceutical Biotechnology, 1-22.

Rullier, B., Novales, B., & Axelos, M. A. (**2008**). Effect of protein aggregates on foaming properties of β-lactoglobulin. Colloids and Surfaces A: Physicochemical and Engineering Aspects, 330(2-3), 96-102.

Sakai, K., Sakurai, K., Sakai, M., Hoshino, M., & Goto, Y. (**2000**). Conformation and stability of thiol-modified bovine β lactoglobulin. Protein Science, 9(9), 1719-1729.

Sakurai, K., & Goto, Y. (**2002**). Manipulating monomer-dimer equilibrium of bovine β-lactoglobulin by amino acid substitution. Journal of Biological Chemistry, 277(28), 25735-25740.

Saraswat, M., Musante, L., Ravidá, A., Shortt, B., Byrne, B., & Holthofer, H. (**2013**). Preparative purification of recombinant proteins: current status and future trends. BioMed research international, 2013.

Schleeger, M., Deckert-Gaudig, T., Deckert, V., Velikov, K. P., Koenderink, G., & Bonn, M. (**2013**). Amyloids: from molecular structure to mechanical properties. Polymer, 54(10), 2473-2488.

Schmitt, C., Bovay, C., Rouvet, M., Shojaei-Rami, S., & Kolodziejczyk, E. (**2007**). Whey protein soluble aggregates from heating with NaCl: physicochemical, interfacial, and foaming properties. Langmuir, 23(8), 4155-4166.

Scholz-Ahrens, K. E., Ahrens, F., & Barth, C. A. (**2020**). Nutritional and health attributes of milk and milk imitations. European journal of nutrition, 59, 19-34.

Schuck, P. (**2000**). Size-distribution analysis of macromolecules by sedimentation velocity ultracentrifugation and lamm equation modeling. Biophysical journal, 78(3), 1606-1619.

Seetharam, R., & Sharma, S. K. (**1991**). Purification and analysis of recombinant proteins (Vol. 12). CRC Press.

Serfert, Y., Lamprecht, C., Tan, C. P., Keppler, J. K., Appel, E., Rossier-Miranda, F. J., ... & Schwarz, K. (**2014**). Characterisation and use of β-lactoglobulin fibrils for microencapsulation of lipophilic ingredients and oxidative stability thereof. Journal of Food Engineering, 143, 53-61.

Shang, J., Ritian, J., Yang, W., Teng, X., Sun, H., Zhang, F., ... & Liu, N. (**2023**). The effect of different edible fungal polysaccharides on the stability of whey protein isolate solution near isoelectric point. International Journal of Food Science & Technology, 58(3), 1150-1161.

Sharma, S., Kumar, P., Betzel, C., & Singh, T. P. (**2001**). Structure and function of proteins involved in milk allergies. Journal of Chromatography B: Biomedical Sciences and Applications, 756(1-2), 183-187.

Shen, W., Xue, Y., Liu, Y., Kong, C., Wang, X., Huang, M., ... & Zhou, M. (**2016**). A novel methanol-free Pichia pastoris system for recombinant protein expression. Microbial cell factories, 15, 1-11.

Shen, Y., Posavec, L., Bolisetty, S., Hilty, F. M., Nyström, G., Kohlbrecher, J., ... & Mezzenga, R. (**2017**). Amyloid fibril systems reduce, stabilize and deliver bioavailable nanosized iron. Nature nanotechnology, 12(7), 642-647.

Shiraki, K., Nishikawa, K., & Goto, Y. (**1995**). Trifluoroethanol-induced stabilization of the α-helical structure of β-lactoglobulin: implication for non-hierarchical protein folding. Journal of molecular biology, 245(2), 180-194.

Shivu, B., Seshadri, S., Li, J., Oberg, K. A., Uversky, V. N., & Fink, A. L. (**2013**). Distinct β-sheet structure in protein aggregates determined by ATR–FTIR spectroscopy. Biochemistry, 52(31), 5176-5183.

Simões, L. S., Abrunhosa, L., Vicente, A. A., & Ramos, O. L. (**2020**). Suitability of β-lactoglobulin micro-and nanostructures for loading and release of bioactive compounds. Food Hydrocolloids, 101, 105492.

Singh, S., Singh, G., & Arya, S. K. (**2018**). Mannans: An overview of properties and application in food products. International Journal of Biological Macromolecules, 119, 79-95.

Smith, C. A. (**1988**). Estimation of Sedimentation Coefficients and Frictional Ratios of Globular Proteins. Biochemical education, 16(2), 104-6.

Smith, K. B., Fernandez-Rodriguez, M. Á., Isa, L., & Mezzenga, R. (**2019**). Creating gradients of amyloid fibrils from the liquid–liquid interface. Soft matter, 15(42), 8437-8440.

Sneideris, T., Milto, K., & Smirnovas, V. (**2015**). Polymorphism of amyloid-like fibrils can be defined by the concentration of seeds. PeerJ, 3, e1207.

Sokolov, P. A., Belousov, M. V., Bondarev, S. A., Zhouravleva, G. A., & Kasyanenko, N. A. (**2017**). FibrilJ: ImageJ plugin for fibrils' diameter and persistence length determination. Computer Physics Communications, 214, 199-206.

R

Spellman, D., O'cuinn, G., & FitzGerald, R. J. (**2009**). Bitterness in Bacillus proteinase hydrolysates of whey proteins. Food Chemistry, 114(2), 440-446.

Steinhauer, T., Marx, M., Bogendörfer, K., & Kulozik, U. (**2015**). Membrane fouling during ultra-and microfiltration of whey and whey proteins at different environmental conditions: The role of aggregated whey proteins as fouling initiators. Journal of Membrane Science, 489, 20-27.

Stone, A. K., & Nickerson, M. T. (**2012**). Formation and functionality of whey protein isolate–(kappa-, iota-, and lambda-type) carrageenan electrostatic complexes. Food Hydrocolloids, 27(2), 271-277.

Storm, C., Pastore, J. J., MacKintosh, F. C., Lubensky, T. C., & Janmey, P. A. (**2005**). Nonlinear elasticity in biological gels. Nature, 435(7039), 191-194.

Stumpe, M. C., & Grubmüller, H. (**2007**). Interaction of urea with amino acids: implications for urea-induced protein denaturation. Journal of the American Chemical Society, 129(51), 16126-16131.

Subedi, S., Sasidharan, S., Nag, N., Saudagar, P., & Tripathi, T. (**2022**). Amyloid cross-seeding: Mechanism, implication, and inhibition. Molecules, 27(6), 1776.

Suk, J. E., Lokappa, S. B., & Ulmer, T. S. (**2010**). The clustering and spatial arrangement of β-sheet sequence, but not order, govern α-synuclein fibrillogenesis. Biochemistry, 49(7), 1533-1540.

Surroca, Y., Haverkamp, J., & Heck, A. J. R. (**2002**). Towards the understanding of molecular mechanisms in the early stages of heat-induced aggregation of β-lactoglobulin AB. Journal of Chromatography A, 970(1-2), 275-285.

Taheri-Kafrani, A., Koupaie, N. T., & Haertlé, T. (**2015**). β-Lactoglobulin mutant Lys69Asn has attenuated IgE and increased retinol binding activity. Journal of Biotechnology, 212, 181-188.

Tanaka, N., Morimoto, Y., Noguchi, Y., Tada, T., Waku, T., Kunugi, S., ... & Takahashi, N. (**2011**). The mechanism of fibril formation of a non-inhibitory serpin ovalbumin revealed by the identification of amyloidogenic core regions. Journal of Biological Chemistry, 286(7), 5884-5894.

Tanford, C. (**1968**). Protein denaturation. Advances in protein chemistry, 23, 121-282.

The European parliament and the council of the European Union. (**2009**). Directive 2009/32/EC on the approximation of the laws of the Member States on extraction solvents used in the production of foodstuffs and food ingredients. Official Journal of the European Union.

Thompson, L. U., Allum-Poon, P., & Procope, C. (**1976**). Isolation of rapeseed protein using sodium hexametaphosphate. Canadian Institute of Food Science and Technology Journal, 9(1), 15-19.

Tomadoni, B., Capello, C., Valencia, G. A., & Gutiérrez, T. J. (**2020**). Self-assembled proteins for food applications: A review. Trends in Food Science & Technology, 101, 1-16.

Tomasula, P. M., Yee, W. C. F., Tomasula, P. M., & Yee, W. C. F. (**2001**). Enriched fractions of alpha-lactoglobumin and beta-lactoglobulin from whey protein concentrate using carbox dioxide. Functional properties in aqueous solution. Journal of food processing and preservation, 25(4), 267-282.

Trinh, N. T. M., Thuoc, T. L., & Thao, D. T. P. (**2021**). Production of recombinant human G-CSF from non-classical inclusion bodies in *Escherichia coli*. Brazilian Journal of Microbiology, 52, 541-546.

United Nations Environment Programme. (**2016**). Food systems and natural resources.

Urbonaite, V., Van der Kaaij, S., De Jongh, H. H. J., Scholten, E., Ako, K., Van der Linden, E., & Pouvreau, L. (**2016**). Relation between gel stiffness and water holding for coarse and fine-stranded protein gels. Food Hydrocolloids, 56, 334-343.

Usov, I., Adamcik, J., & Mezzenga, R. (**2013**). Polymorphism in bovine serum albumin fibrils: morphology and statistical analysis. Faraday Discussions, 166, 151-162.

Uttinger, M. J., Heyn, T. R., Jandt, U., Wawra, S. E., Winzer, B., Keppler, J. K., & Peukert, W. (**2020**). Measurement of length distribution of beta-lactoglobulin fibrils by multiwavelength analytical ultracentrifugation. European Biophysics Journal, 49, 745-760.

Van Zanten, H. H. E., Simon, W., Van Selm, B., Wacker, J., Maindl, T. I., Frehner, A., ... & Herrero, M. (**2023**). Circularity in Europe strengthens the sustainability of the global food system. Nature Food, 1-11.

VandenAkker, C. C., Engel, M. F., Velikov, K. P., Bonn, M., & Koenderink, G. H. (**2011**). Morphology and persistence length of amyloid fibrils are correlated to peptide molecular structure. Journal of the American Chemical Society, 133(45), 18030-18033.

VandenAkker, C. C., Schleeger, M., Bruinen, A. L., Deckert-Gaudig, T., Velikov, K. P., Heeren, R. M., ... & Koenderink, G. H. (**2016**). Multimodal spectroscopic study of amyloid fibril polymorphism. The Journal of Physical Chemistry B, 120(34), 8809-8817.

Veerman, C., Baptist, H., Sagis, L. M., & van der Linden, E. (**2003**). A new multistep Ca2+-induced cold gelation process for β-lactoglobulin. Journal of agricultural and food chemistry, 51(13), 3880-3885.

Veerman, C., Sagis, L. M., & van der Linden, E. (**2003**). Gels at extremely low weight fractions formed by irreversible self-assembly of proteins. Macromolecular Bioscience, 3(5), 243-247.

Vermasvuori, R. (**2009**). Production of recombinant proteins and monoclonal antibodies-Techno-enonomical evaluation of the production methods.

Vetri, V., & Foderà, V. (**2015**). The route to protein aggregate superstructures: Particulates and amyloid-like spherulites. FEBS letters, 589(19), 2448-2463.

Villa, C., Costa, J., Oliveira, M. B. P., & Mafra, I. (**2018**). Bovine milk allergens: A comprehensive review. Comprehensive Reviews in Food Science and Food Safety, 17(1), 137-164.

Vinogradov, E., Petersen, B. O., & Duus, J. Ø. (**2000**). Isolation and characterization of non-labeled and 13C-labeled mannans from *Pichia pastoris* yeast. Carbohydrate research, 325(3), 216-221.

Vivian, J. T., & Callis, P. R. (**2001**). Mechanisms of tryptophan fluorescence shifts in proteins. Biophysical journal, 80(5), 2093-2109.

Vreeke, G. J., Lubbers, W., Vincken, J. P., & Wierenga, P. A. (**2022**). A method to identify and quantify the complete peptide composition in protein hydrolysates. Analytica Chimica Acta, 1201, 339616.

Vreeke, G. J., Vincken, J. P., & Wierenga, P. A. (**2023**). The path of proteolysis by bovine chymotrypsin. Food Research International, 165, 112485.

Wagoner, T. B., & Foegeding, E. A. (**2017**). Whey protein–pectin soluble complexes for beverage applications. Food Hydrocolloids, 63, 130-138.

Wang, W., Nema, S., & Teagarden, D. (**2010**). Protein aggregation—Pathways and influencing factors. International journal of pharmaceutics, 390(2), 89-99.

Watanabe, M., Sato, S., & Saito, H. (**1975**). The mechanism of the hydrolysis of condensed phosphates. II. The mechanism of the degradation of long-chain polyphosphates. Bulletin of the Chemical Society of Japan, 48(3), 896-898.

Wei, G., Su, Z., Reynolds, N. P., Arosio, P., Hamley, I. W., Gazit, E., & Mezzenga, R. (**2017**). Self-assembling peptide and protein amyloids: from structure to tailored function in nanotechnology. Chemical Society Reviews, 46(15), 4661-4708.

Wei, Z., & Huang, Q. (**2019**). Modulation of formation, physicochemical properties, and digestion of ovotransferrin nanofibrils with covalent or non-covalent bound gallic acid. Journal of agricultural and food chemistry, 67(35), 9907-9915.

Wei, Z., & Huang, Q. (**2020**). Impact of covalent or non-covalent bound epigallocatechin-3-gallate (EGCG) on assembly, physicochemical characteristics and digestion of ovotransferrin fibrils. Food Hydrocolloids, 98, 105314.

Wichchukit, S., Oztop, M. H., McCarthy, M. J., & McCarthy, K. L. (**2013**). Whey protein/alginate beads as carriers of a bioactive component. Food Hydrocolloids, 33(1), 66-73.

Wiedemann, C., Kumar, A., Lang, A., & Ohlenschläger, O. (**2020**). Cysteines and disulfide bonds as structure-forming units: insights from different domains of life and the potential for characterization by NMR. Frontiers in Chemistry, 8, 280.

Wilce, M. C., Aguilar, M. I., & Hearn, M. T. (**1995**). Physicochemical basis of amino acid hydrophobicity scales: evaluation of four new scales of amino acid hydrophobicity coefficients derived from RP-HPLC of peptides. Analytical chemistry, 67(7), 1210-1219.

Wilson, C., Quarrie, L., Allan, G. J., Flint, D. J., Sawyer, L., & Holt, C. (**1999**). Expression of recombinant wild-type and mutant β-Lactoglobulins in the yeast *Pichia pastoris*. International journal of food science & technology, 34(5-6), 445-450.

Wu, X., & Narsimhan, G. (**2008**). Characterization of secondary and tertiary conformational changes of β-lactoglobulin adsorbed on silica nanoparticle surfaces. Langmuir, 24(9), 4989-4998.

R

Xing, R., Yuan, C., Li, S., Song, J., Li, J., & Yan, X. (**2018**). Charge-Induced Secondary Structure Transformation of Amyloid-Derived Dipeptide Assemblies from β-Sheet to α-Helix. Angewandte Chemie International Edition, 57(6), 1537-1542.

Xu, D., Zhou, J., Soon, W. L., Kutzli, I., Molière, A., Diedrich, S., ... & Mezzenga, R. (**2023**). Food amyloid fibrils are safe nutrition ingredients based on in-vitro and in-vivo assessment. Nature Communications, 14(1), 6806.

Yagi, M., Sakurai, K., Kalidas, C., Batt, C. A., & Goto, Y. (**2003**). Reversible unfolding of bovine β-lactoglobulin mutants without a free thiol group. Journal of Biological Chemistry, 278(47), 47009-47015.

Yamada, Y., Nakagawa, K., Yajima, T., Saito, K., Tokushima, A., Fujiwara, K., & Ikeguchi, M. (**2006**). Structural and thermodynamic consequences of removal of a conserved disulfide bond from equine β-lactoglobulin. Proteins: Structure, Function, and Bioinformatics, 63(3), 595-602.

Yamaguchi, T., Yagi, H., Goto, Y., Matsuzaki, K., & Hoshino, M. (**2010**). A disulfide-linked amyloid-β peptide dimer forms a protofibril-like oligomer through a distinct pathway from amyloid fibril formation. Biochemistry, 49(33), 7100-7107.

Ye, X., Hedenqvist, M. S., Langton, M., & Lendel, C. (**2018**). On the role of peptide hydrolysis for fibrillization kinetics and amyloid fibril morphology. RSC advances, 8(13), 6915-6924.

Yoshida, K., Vogtt, K., Izaola, Z., Russina, M., Yamaguchi, T., & Bellissent-Funel, M. C. (**2012**). Alcohol induced structural and dynamic changes in β-lactoglobulin in aqueous solution: A neutron scattering study. Biochimica et Biophysica Acta (BBA)-Proteins and Proteomics, 1824(3), 502-510.

Yoshida, T., Kume, C., Sachi, A., Yuyama, F., Tomiyama, N., Kodama, R., ... & Hattori, M. (**2022**). Reduced immunogenicity of β-lactoglobulin by single amino acid substitution. Cytotechnology, 74(6), 623-634.

Yukalo, V., Datsyshyn, K., & Turkina, V. (**2022**). Low-allergenic hydrolysates of whey proteins with natural bioactive peptides. Food Science & Technology (2073-8684), 16(1).

Zahrl, R. J., Peña, D. A., Mattanovich, D., & Gasser, B. (**2017**). Systems biotechnology for protein production in *Pichia pastoris*. FEMS yeast research, 17(7), fox068.

Zandomeneghi, G., Krebs, M. R., McCammon, M. G., & Fändrich, M. (**2004**). FTIR reveals structural differences between native β-sheet proteins and amyloid fibrils. Protein science, 13(12), 3314-3321.

Zappone, B., De Santo, M. P., Labate, C., Rizzuti, B., & Guzzi, R. (**2013**). Catalytic activity of copper ions in the amyloid fibrillization of β-lactoglobulin. Soft Matter, 9(8), 2412-2419.

Zhang, G., Zhao, J., Lin, G., Guo, Y., Li, D., & Wu, Y. (**2022**). Effects of Protein-Chelated Zinc Combined with Mannan-Rich Fraction to Replace High-Dose Zinc Oxide on Growth Performance, Nutrient Digestibility, and Intestinal Health in Weaned Piglets. Animals, 12(23), 3407.

Zhang, L., & Schmit, J. D. (**2017**). Theory of amyloid fibril nucleation from folded proteins. Israel journal of chemistry, 57(7-8), 738-749.

Zhang, P., Moretti, M., Allione, M., Tian, Y., Ordonez-Loza, J., Altamura, D., ... & Di Fabrizio, E. (**2020**). A droplet reactor on a super-hydrophobic surface allows control and characterization of amyloid fibril growth. Communications Biology, 3(1), 457.

Zhang, Y. B., Howitt, J., McCorkle, S., Lawrence, P., Springer, K., & Freimuth, P. (**2004**). Protein aggregation during overexpression limited by peptide extensions with large net negative charge. Protein expression and purification, 36(2), 207-216.

Zhang, Y., Wright, E., & Zhong, Q. (**2013**). Effects of pH on the molecular binding between β-lactoglobulin and bixin. Journal of agricultural and food chemistry, 61(4), 947-954.

Zhao, D., Zhang, X., Xu, D., Su, G., Li, B., & Li, C. (**2020**). Heat-induced amyloid-like aggregation of β-lactoglobulin affected by glycation by α-dicarbonyl compounds in a model study. Journal of the Science of Food and Agriculture, 100(2), 607-613.

Zhu, M., Souillac, P. O., Ionescu-Zanetti, C., Carter, S. A., & Fink, A. L. (**2002**). Surface-catalyzed amyloid fibril formation. Journal of Biological Chemistry, 277(52), 50914-50922.

R

Summary

Precision fermentation has traditionally been used to produce enzymes or pharmaceuticals that are challenging to isolate from natural sources. This technique has recently gained attention for the large-scale production of animal proteins to be used in food formulations. It is important for this new application that the produced protein is affordable, food-grade and exhibits techno-functional properties. The production process needs to be re-designed for these purposes. Several interventions in the production process were explored in this thesis, using the major whey protein β-lactoglobulin (BLG) as a case for demonstration.

Intervention A included amino acid exchanges during upstream production, aiming to functionalize recombinant BLG on a molecular scale. Functionalization can ensure efficient application, allowing lower protein content (from a techno-functional point of view) in food formulations. **Chapter 2** demonstrated the structural consequences of exchanging specific cysteines with alanine in recombinant BLG. A partially destabilized BLG variant with a maintained globular fold was obtained when targeting the disulfide bond exposed at the surface of the globular fold. In contrast, complete destabilization occurred when substituting all cysteines. Such variants were expected to extend the functional range of BLG during food application.

Intervention B included less extensive purification during downstream processing, aiming to reduce costs and improve yield, while still yielding a functional ingredient. For yeast-based secreted recombinant BLG, **Chapter 3** presented a relatively simple precipitation-based purification method. The purified material had a BLG content of ~ 72 wt% and contained residuals of the precipitation agent (hexametaphosphate; ~ 1 wt%). This method shows potential as a cost-effective and scalable alternative to conventional extensive chromatographic purification, but further research is required to confirm.

Intervention C included additional post-processing, aiming to functionalize recombinant BLG through meso-scale modification. This modification particularly focused on the formation of amyloid aggregates. **Chapter 4** reviewed the post-processing conditions that can be applied to transform BLG into amyloid aggregates. Peptide-based amyloid fibrils can be formed from BLG via extreme conditions, often heating at pH 2.0 for several hours. In particular the high aspect ratio of amyloid fibrils enabled their functional behaviour. Alternatively, shorter and more flexible amyloid-like aggregates can form relatively quickly through assembly of intact BLG (for example, upon heating at pH 3.5 and 7.0). These aggregates are less suited than amyloid fibrils to form space-spanning networks due to their lower aspect ratio, but have an increased tendency to entangle due to their flexibility.

While the above mentioned interventions demonstrate that different recombinant BLG ingredients can be produced, **Chapter 5** further evaluated their functional properties (i.e., foaming and gelation). Intervention A specifically included natural (isoforms A and B) or cysteine substitutions. Those substitutions had a major impact on the foaming properties, in some cases being able to increase the foam stability up to 10 times. The natural isoforms also demonstrated different heat-set gelation, while cysteine substitutions were not expected to improve gelation. Intervention B specifically included mild purification of yeast-based secreted BLG. Purification up to ~ 25 wt% did not yield a functional foaming or gelling agent, while further purification up to ~ 70 wt% enabled those functional properties. Lastly, intervention C specifically included aggregation of whey protein into amyloid aggregates; amyloid-like aggregates or amyloid fibrils. Amyloid fibrils were instable upon processing to the application conditions (i.e., pH neutralization, desalting and drying). In contrast, amyloid-like aggregates maintained their morphology and solubility, and demonstrated improved foaming properties (up to 10 times more stable foam), while being heat-resistant.

A combination of molecular and meso-scale modification (intervention A and intervention C, respectively) was investigated to stimulate the formation of functional amyloid fibrils. **Chapter 6** demonstrated that cysteine substitutions affected the acidic hydrolysis rate upon heating at pH 2.0, but did not accelerate fibril formation significantly. In contrast to amyloid fibrils, amyloid-like aggregates were more stable upon processing but had a lower aspect ratio. **Chapter 7** demonstrated that cysteine substitutions can be used to alter the aggregate morphology upon heating at pH 3.5 and 7.0. Disulfide bond suppression by cysteine substitution generally increased the aspect ratio. Besides, stiff and long fibrillar aggregates formed when heating recombinant BLG lacking all cysteines at pH 7.0. Those aggregates may be promising for application, due to their high aspect ratio and varying flexibility.

Chapter 8 further evaluated the potential of the proposed interventions from a technological, functional, and nutritional point of view. Intervention A (either natural or induced point mutations) can improve techno- and/or bio-functional properties, but may also pose risks for adverse health effects, which should be carefully evaluated. While intervention B can simplify the downstream process, the identity and quantity of remaining impurities should be evaluated for food safety. Lastly, intervention C can improve functional properties, but molecular and post-processing design should be aligned to allow efficient formation and stability of those aggregates. The consequences of the molecular design for *in vivo* digestion and toxicity should be carefully considered.

This thesis exemplifies that both the recombinant protein itself (intervention A), and the subsequent processing steps (intervention B and intervention C) can be designed specifically for the application of recombinant protein ingredients in food formulations. For the protein and processing design, the purpose of this new food application should be taken into account, including the techno-functional but also nutritional consequences of the design.

Appendices

Acknowledgements

Science is like Wonderland: full of distractions, but persistence leads to discovery. Colleagues, friends, and family have guided and supported me in this journey. Their support, encouragement, and/or expertise has helped me to reach my final destination: this thesis that I am extremely proud of. I wasn't able to complete this journey without them:

First and foremost, **Julia** and **Remko**, it was a pleasure to work with you and to learn from you. I am grateful for the opportunity you gave me, and for your commitment and enthusiasm throughout my project. You really made me feel part of a team that worked together to a shared goal. **Julia**, you always encouraged me to pursuit any aspects of the project that I liked. You could always bring order to my chaos with your calm guidance and expertise. Whenever questions or struggles arose, you made time to solve them together. No matter how busy you were. I really appreciate your way of supervision and this was exactly what I needed. **Remko**, when my enthusiasm tended to drive me into a tunnel vision, you pulled me out. You asked the right questions and taught me to place findings into a larger perspective. This often led to interesting and most of all fun brainstorm sessions, which gave me energy to continue the journey. Besides, **Marie**, I also want to thank you for sparking my enthusiasm for research prior to my PhD. You gave me the confidence to acknowledge myself as an independent researcher. If it wasn't for you, I don't know if I would have had the courage to even start this journey.

Collaborations can only accelerate scientific research when the people involved are committed; and that definitely applied to you, **Sarah**, **Rebekka**, and **Rainer**. Thanks a lot for providing me with the recombinant proteins that I needed, but also for taking the time to give advice from a biotechnology point of view. You all played an important role in my PhD. **Sarah**, I also appreciate your openness and kindness; you made me feel welcome to ask anything.

Furthermore, I received a lot of help and support through other collaborations. Of course, my partners in crime at Kiel: **Laura**, **Therese**, **Kerstin**, **Timon**, **Anja**, and **Karin** – I enjoyed the discussions with fellow BLG-enthusiasts. Besides, thank you for the warm welcome when I visited Kiel.

Naast mijn collega's en vrienden, heeft mijn familie natuurlijk ook een grote rol gespeeld. **Pap**, als iemand weet hoe je hard moet werken dan ben jij het wel. Dit blijft mij inspireren, bedankt hiervoor. **Mam**, jij bent toch wel mijn grootste fan, dankje voor je steun. **Tom**, ondanks dat je niet het onderzoek in bent gegaan, ben je toch van nature wel een onderzoeker. Jouw kritische blik en nieuwsgierigheid daagt mij vaak genoeg uit om mijn standpunt tot in de puntjes te verdedigen, bedankt voor deze voorbereiding op mijn PhD verdediging. **Bente** en **Puck**, jullie vragen regelmatig hoe het met me is, dit waardeer ik heel erg. Zoals opa zou zeggen: bedankt voor de belangstelling. En natuurlijk **Erik**, hoewel jij pas halverwege mijn PhD om het hoekje kwam kijken, kan ik je niet meer wegdenken. Elke dag ben je weer geïnteresseerd over hoe het was op mijn werk en wat me bezig houdt. Ik vind het ontzettend lief dat je altijd aandachtig luistert, terwijl ik weet dat ik de helft van mijn verhalen véél te ingewikkeld maak. Je begrijpt me en ik kan me geen betere steun wensen.

Everybody, thank you for all of this and more.

About the author

Loes J. G. Hoppenreijs was born on the 27th of February in 1995 (Elst, The Netherlands). She attended Isendoorn College, in Warnsveld, where she obtained her VWO diploma and international baccalaureate certificate, with a major in both *Nature & Health* and *Nature & Technology*.

In 2013, Loes started the bachelor Food Technology at Wageningen University, with a minor in Nutrition and Health. For her bachelor thesis, she investigated the impact of solvent conditions on protein adsorption at Food Process Engineering department at the Wageningen University & Research (WUR). After obtaining her bachelor diploma, Loes continued with the master Food Technology at the WUR, specializing in both *Ingredient Functionality* and *Product Design*. For her first master thesis, she studied the impact of water addition on the heat-set formation of protein oleogels at the Food Physics department at the WUR. After that, she did her master internship at the Food Innovation Centre of CSIRO (Werribee, Australia), where she explored several methods for protein extraction from broccoli leaves. When she came back in the Netherlands, she performed her second master thesis, studying the impact of temperature, oxygen partial pressure, and the presence of antioxidants on the lipid oxidation mechanism in oil blends. This work was executed at the Food Chemistry and Food Process Engineering departments at the WUR, and was performed in collaboration with Danone Nutricia (Utrecht, the Netherlands).

After obtaining her master diploma, Loes continued the work that she did for her second master thesis during a one-year project at the Food Chemistry department at the WUR, under the supervision of Dr Marie Hennebelle. After that, she did the research that is described in this thesis, under the supervision of Dr Julia Keppler and Prof. Dr Remko Boom. This work was performed at the Food Process Engeering department at the WUR.

Publications

This thesis

Loes Hoppenreijs, Laura Fitzner, Therese Ruhmlieb, Timon Heyn, Kerstin Schild, Atze-Jan van der Goot, Remko Boom, Anja Steffen-Heins, Karin Schwarz & Julia Keppler (**2022**). Engineering amyloid and amyloid-like morphologies of β-lactoglobulin. *Food Hydrocolloids*, 124.

Sarah Brune[1], **Loes Hoppenreijs**[1], Toni Kühl, Vanessa Lautenbach, Johannes Walter, Wolfgang Peukert, Karin Schwarz, Diana Imhof, Remko Boom, Rainer Krull, Julia Keppler & Rebekka Biedendieck (**2023**). Precision fermentation as a route to modify β-lactoglobulin structure through substitution of specific cysteine residues. *International Dairy Journal*, 147.

Loes Hoppenreijs, Achim Overbeck, Sarah Brune, Rebekka Biedendieck, Arno Kwade, Remko Boom & Julia Keppler (**2023**). Amyloid-like aggregation of recombinant β-lactoglobulin at pH 3.5 and 7.0: Is disulfide bond removal the key to fibrillization? *International Journal of Biological Macromolecules*, 242.

Loes Hoppenreijs, Sarah Brune, Rebekka Biedendieck, Rainer Krull, Remko Boom & Julia Keppler (**2023**). Fibrillization of β-lactoglobulin at pH 2.0: Impact of cysteine substitution and disulfide bond reduction. *Food Hydrocolloids*, 141.

Loes Hoppenreijs, Andrea Annibal, Gijs Vreeke, Remko Boom & Julia Keppler (**2024**). Food proteins from yeast-based precision fermentation: simple purification of recombinant β-lactoglobulin using polyphosphate. *Food Research International*, 176.

Loes Hoppenreijs, Sarah Brune, Rebekka Biedendieck, Rainer Krull, Remko Boom, Julia Keppler (**2024**). Exploring functionality gain for (recombinant) β-lactoglobulin through production and processing interventions. *Food and Bioprocess Technology*.

Other

Loes Hoppenreijs, Claire Berton-Carabin, Arend Dubbelboer & Marie Hennebelle (**2021**). Evaluation of oxygen partial pressure, temperature and stripping of antioxidants for accelerated shelf-life testing of oil blends using ^{1}H NMR. *Food Research International*, 147.

Loes Hoppenreijs & Andrea Annibal (**2023**). Process. Australian Provisional Patent Application 2023901257 filed on Apr 28, 2023.

---

[1]Equal authorship

Completed training activities

Discipline specific activities

Courses

Rheology: the do's and don'ts (VLAG, NL)	2020
Food proteins: significance, reactions and modifications (University of Copenhagen, VLAG, NL)	2020
TEM training (WEMC, NL)	2020
Dairy protein biochemistry (VLAG, NL)	2022
Han sur Lesse winterschool (WUR, TU Delft, NL)	2022
The protein transition course: diverse perspectives (PE&RC, NL)	2023

Conferences

12th NIZO Dairy conference (NIZO, NL)	2021
13th NIZO Dairy conference (NIZO, NL)	2023
4th International conference on engineering future food (AIDIC, IT)	2023

Other

Yearly project meeting with all project partners (DFG project, DE)	2020 - 2023

General courses

VLAG PhD week (VLAG, NL)	2020
Popular science writing (WASS, NL)	2021
Brain-friendly working (WGS, NL)	2021
Supervising bachelor and master thesis students (ESD, NL)	2021
Adobe InDesign (WGS, NL)	2023
Career perspectives (WGS, NL)	2023

Other activities

Preparation of research proposal (FPE, WUR)	2020
FPE group meetings (FPE, WUR)	2020 - 2024
Biweekly DFG fibril meeting (DFG, DE)	2020 - 2023
Organizing PhD trip Singapore (FPE, WUR)	2022
PhD trip Singapore (FPE, WUR)	2022
Participating in a short documentary of VPRO tegenlicht	2023
PhD trip England (FPE, WUR)	2024

About the cover

The cover of this thesis illustrates an alternative route for future β-lactoglobulin production, including the upstream production by micro-organisms, downstream processing, and post-processing.

The upstream production is illustrated on the front of the cover. The microscope highlights the investigations performed in this thesis, studying two production hosts (*Chapter 5*). The hosts that are illustrated are *Escherichia coli* (*Chapter 2*; in red) and *Pichia pastoris* (*Chapter 3*; in green).

Furthermore, the back of the cover represents further processing (*Chapter 4, 6 and 7*) that is depicted as the industrial pipes. Two different type of aggregates are illustrated as final BLG ingredients: being either long and stiff fibrils (*Chapter 6*) or short and flexible amyloid-like aggregates (*Chapter 7*).